On Limits of Multi-Antenna Wireless Communications in Spatially Selective Channels

Tony Steven Pollock

B.E.(Hons 1) (Canterbury)
B.Sc. (Otago)

July 2003

A thesis submitted for the degree of Doctor of Philosophy
of The Australian National University

Department of Telecommunications Engineering
Research School of Information Sciences and Engineering
The Australian National University

Declaration

The contents of this thesis are the results of original research and have not been submitted for a higher degree to any other university or institution.

Much of the work in this thesis has been published or has been submitted for publication as journal papers or conference proceedings. These papers are:

1. T.S. Pollock, T.D. Abhayapala, and R.A. Kennedy, "Fundamental limits of constrained array capacity," in *Australian Communications Theory Workshop*, Melbourne, Australia, 2003, pp. 7–12.

2. R.A. Kennedy, T.D. Abhayapala, and T.S. Pollock, "Modeling multipath scattering environments using generalized Herglotz wave functions," in *Australian Communications Theory Workshop*, Canberra, Australia, 2003, pp. 87–92.

3. T.S. Pollock, T.D. Abhayapala, and R.A. Kennedy, "Introducing space into space-time MIMO capacity calculations: A new closed form upper bound," in *International Conference on Telecommunications*, Papeete, Tahiti, 2003, pp. 1536–1541.

4. T.S. Pollock, T.D. Abhayapala, and R.A. Kennedy, "Antenna saturation effects on dense array MIMO capacity," in *International Conference on Acoustics, Speech and Signal Processing*, Hong Kong, 2003, vol. IV, pp. 361–364.

5. R.A. Kennedy, T.D. Abhayapala, and T.S. Pollock, "Generalized Herglotz wave functions for modeling wireless nearfield multipath scattering environments," in *International Conference on Acoustics, Speech, and Signal Processing*, Hong Kong, 2003, vol. IV, pp. 660–663.

6. T.S. Pollock, T.D. Abhayapala, and R.A. Kennedy, "Antenna saturation effects on MIMO capacity," in *International Conference on Communications*, Anchorage, Alaska, 2003.

7. T.D. Abhayapala, T.S. Pollock, and R.A. Kennedy, "Novel 3D spatial wireless channel model," in *IEEE Vehicular Technology Conference (Fall)*, Orlando, Florida, USA, 2003, (to appear).

8. T.D. Abhayapala, T.S. Pollock, and R.A. Kennedy, "Spatial decomposition of MIMO wireless channels," in *International Symposium on Signal Processing and its Applications*, Paris, France, 2003.

9. T.S. Pollock, T.D. Abhayapala, and R.A. Kennedy, "Intrinsic capacity of spatially constrained multiple antenna systems in general scattering environments," in *IEEE Transactions on Communications* (to be submitted).

10. T.S. Pollock, T.D. Abhayapala, and R.A. Kennedy, "Spatial limits to MIMO capacity in general scattering environments," in *7th International Symposium on DSP for Communication Systems*, Coolangatta, Australia, 2003, (submitted June 2003).

11. T.S. Pollock, T.D. Abhayapala, and R.A. Kennedy, "MIMO capacity saturation of dense UCAs," *IEEE Signal Processing Letters*, (submitted July 2003).

12. T.S. Pollock, T.D. Abhayapala, and R.A. Kennedy, "Introducing space into MIMO capacity calculations," *Journal on Telecommunications Systems*, 2004, (invited paper - to appear).

The research represented in this thesis has been performed jointly with Professor Rodney A. Kennedy and Dr Thushara D. Abhayapala. The substantial majority of this work is my own.

Tony Steven Pollock
The Australian National University
July 2003

To
Kirstie

by all appearances, I am one person, but in reality I am two

Acknowledgements

The real voyage of discovery consists not in seeing new land
but in seeing with new eyes - Marcel Proust

I would like to expresses my deepest gratitude to my supervisors Dr. Thushara Abhayapala and Prof. Rod Kennedy, who showed me the world through their eyes for 3 years, and taught me how to use mine. Thushara for his many technical contributions and insights, Rod for his ability to see the big picture in every problem, and both for their wonderful humour, friendship and guidance.

I would also like to thank Prof. Robert Williamson and Prof. Zhi Ding for many fruitful discussions during the early stages of my research. Although no results from these interactions became part of this thesis, the experience was invaluable and their energy and enthusiasm was infectious.

To my fellow TelEng students and staff, thank you for tolerating my bizarre sense of humour for the past few years. In particular Dino, and more recently Michael, whom with which conversations on everything and anything but the contents of my thesis kept me sane.

My family; Mum, Dad, Kirsty, and Nana Jo thank you for letting me grow to be the best I can be. For their love and patience, along with their tolerance when I was 'fiddling' with household appliances in the name of science, without which the inquisitive mind I have today would not exist.

Lastly, I want to express my love and gratitude to my wife Kirstie, who has supported and encouraged me in pursuing my dreams, and has always been there to make sure they become realities.

Abstract

Multiple-Input Multiple-Output (MIMO) communications systems using multi-antenna arrays simultaneously during transmission and reception have generated significant interest in recent years. Theoretical work in the mid 1990's showed the potential for significant capacity increases in wireless channels via spatial multiplexing with sparse antenna arrays and rich scattering environments. However, in reality the capacity is significantly reduced when the antennas are placed close together, or the scattering environment is sparse, causing the signals received by different antennas to become correlated, corresponding to a reduction of the effective number of sub-channels between transmit and receive antennas.

By introducing the previously ignored spatial aspects, namely the antenna array geometry and the scattering environment, into a novel channel model new bounds and fundamental limitations to MIMO capacity are derived for spatially constrained, or spatially selective, channels. A theoretically derived capacity saturation point is shown to exist for spatially selective MIMO channels, at which there is no capacity growth with increasing numbers of antennas. Furthermore, it is shown that this saturation point is dependent on the shape, size and orientation of the spatial volumes containing the antenna arrays along with the properties of the scattering environment.

This result leads to the definition of an intrinsic capacity between separate spatial volumes in a continuous scattering environment, which is an upper limit to communication between the volumes that can not be increased with increasing numbers of antennas within. It is shown that there exists a fundamental limit to the information theoretic capacity between two continuous volumes in space, where using antenna arrays is simply one choice of implementation of a more general spatial signal processing underlying all wireless communication systems.

Notation and Symbols

AWGN	additive white Gaussian noise
BER	bit error rate
CDF	cumulative distribution function
CSI	channel state information
UCA	uniform circular array
UGA	uniform grid array
ULA	uniform linear array
MISO	multiple-input single-ouput
MIMO	multiple-input multiple-output
SISO	single-input single-output
SIMO	single-input multiple-output
SNR	signal-to-noise ratio
SDOF	spacial degrees of freedom
$\lceil \cdot \rceil$	ceiling operator
$\lfloor \cdot \rfloor$	floor operator
$\overline{f(\cdot)}$	complex conjugate of scalar or function f
$\boldsymbol{A}^\dagger$	complex conjugate transpose of matrix or vector $\boldsymbol{A}$
$\lvert\boldsymbol{A}\rvert$	determinant of matrix $\boldsymbol{A}$
$\lVert\boldsymbol{a}\rVert$	euclidian norm of vector $\boldsymbol{a}$
$E_X\{\cdot\}$	Expectation operator over random process X
$\delta(i-j)$	Kronecker delta
$\langle \cdot, \cdot \rangle$	inner product
$\boldsymbol{a}'$	transpose of matrix or vector $\boldsymbol{a}$
η	signal-to-noise ratio (SNR)
$\mathbb{S}^1$	1 sphere (unit circle)
$\mathbb{S}^2$	2 sphere (unit sphere)
$\boldsymbol{I}_n$	$n \times n$ identity matrix
$\mathbf{1}_n$	$n \times n$ matrix of ones

Contents

List of Figures

Chapter 1

Introduction

1.1 Motivation and Background

Since the end of the 19th century, when Marconi and Hertz demonstrated the feasibility of radio transmissions, mankind has endeavored to fulfill the dream of flawless wireless multimedia telecommunications, enabling people to communicate with anyone or anything, anywhere, at any time, using a range of multimedia services. Naturally, the provision of these services requires a further quantum leap in a range of enabling technologies from the current state-of-the-art, such as the well-known mobile phone.

To meet these demands the most significant hurdle facing wireless mobile communications is that of increasing capacity; the measure of how much information can be transmitted and received with a negligible probability of error. High performance wireless communication systems are impeded by random channel noise, intersymbol interference (ISI) and signal fading due to multipath effects. External factors such as multi-user interference (MUI) and co-channel interference (CCI) also contribute to an overall lowering of system capacity.

Trying to increase the capacity or data rate by simply transmitting more power is extremely costly. This is due to the logarithmic relationship between the capacity of a wireless link and the signal-to-noise ratio (SNR) at the receiver [1]. A more effective way of improving the data rate is to increase the signal bandwidth, along with the transmitted power. However, with the frequency spectrum being rapidly allocated, it is a scarce and very expensive resource at the frequencies of interest, where propagation conditions are favorable[1]. Moreover, increasing the

[1]At this time, and into the foreseeable future, radio propagation and equipment costs restrict mobile system to the 1-5GHz range.

signal bandwidth beyond the coherence bandwidth of the wireless channel results in frequency selectivity. Although well-established techniques such as equalization and orthogonal frequency-division multiplexing (OFDM) can address this issue, their complexity grows rapidly with signal bandwidth.

A significant advancement for increasing capacity performance has been the development of *smart antennas*, which consist of an antenna array combined with signal processing in both space and time. The use of spatial processing introduces a new degree of freedom, offering enormous potential to improve performance including range extension; capacity enhancement; higher data rates; and better bit error rate performance [2,3]. Traditionally, the use of antenna arrays in mobile communications was limited to the base station, simply due to size and cost considerations. The basic objective of those arrays, before interference suppression and other signal processing advances were considered, was to provide spatial diversity against fading [4]. Signal fading, arising from multipath propagation caused by scattering, has always been regarded as an impairment that has to be mitigated. However, a recent successful application of smart antennas at both the transmit and the receive ends of the communications link have shown that multipath interference can not only be mitigated, but actually exploited to establish multiple parallel channels operating simultaneously and in the same frequency band [5–7]. This multiple-input multiple-output (MIMO) system provides much higher data rates without requiring additional power or bandwidth over the single antenna case. A little known yet earlier version of this outstanding result was also presented in [8] for application to broadcast digital TV. However, the first results hinting at the capacity gains of MIMO were published by J. Winters in [9].

The large spectral efficiencies achieved with MIMO systems are only valid under certain channel conditions. MIMO systems were originally derived for the independent and identically distributed (i.i.d.) flat Rayleigh fading channels corresponding to a rich scattering environment and sufficiently spaced antennas. For a single-user system with n_{T} transmit and n_{R} receive antennas, independent transmission paths from each transmit antenna to each receive antenna provides approximately $\min(n_{\mathrm{T}}, n_{\mathrm{R}})$ separate channels, and hence the capacity scales linearly with $\min(n_{\mathrm{T}}, n_{\mathrm{R}})$ relative to a system with just one transmit and one receive antenna. This linear capacity scaling requires a scattering environment and antenna placement such that the matrix of channel gains between transmit and receive antenna pairs has full rank and independent entries, along with perfect knowledge of these

gains at the receiver[2].

This thesis is primarily concerned with whether the outstanding capacity gains predicted by Foschini [5] and Telatar [7] can be obtained in more realistic operating scenarios. In particular, this thesis concentrates on the limits of MIMO capacity in more physically realistic situations, such as when the antennas are placed in a constrained region of space and when there exists a non-rich scattering environment, along with what specific gains result from adding more antennas. As would be expected, the overall effect of increasing the density of antennas, or reducing the number of scatterers, is to correlate the channel gains leading to a reduction of channel capacity from that of the ideal i.i.d. case, therefore we begin with this chapter exploring the i.i.d. case in some detail.

The remainder of this chapter introduces the difficulties of communicating through a wireless environment and gives the possible gains achievable using multiple antenna systems in ideal scattering environments. This chapter serves as a introduction to the concepts involved in MIMO systems and provides an overview of the research to date, therefore the MIMO erudite reader may wish to proceed directly to Chapter 2. For a more extensive introduction on MIMO systems, the reader is referred to the recently published tutorials [11] and [12], which provide an excellent introduction into the current state of MIMO research.

1.2 Wireless Communication Channels

The wireless channel places fundamental limitations on the performance of wireless communications systems. The transmission path between the transmitter and the receiver ranges from simple line-of-sight to complex environments with obstruction from mountains, foliage, and man-made objects such as buildings. Unlike fixed or wired channels which are stationary and predictable, wireless channels exhibit an extremely random nature and are often difficult to characterize and analyze. Notwithstanding the environmental factors mentioned above, any motion of the transmitter or receiver also severely impacts on the performance of the communications system.

The mechanisms behind electromagnetic wave propagation through the wireless channel are wide and varied, however, they can generally be attributed to reflection, diffraction, and scattering. More often than not, wireless communications

[2]Perfect knowledge of channel gains at both the transmitter and receiver gives an increase in the slope of the linear scaling [10].

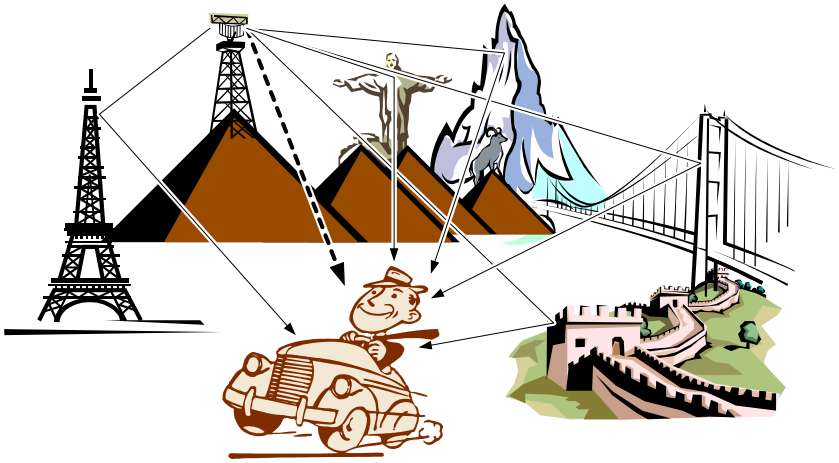

Figure 1.1: Multipath Scattering Environment. (reprinted with permission from Dino Miniutti ©2002.)

systems operate in urban areas with no line-of-sight propagation, and the presence of buildings cause severe diffraction losses. Due to multiple reflections from various objects, the electromagnetic waves propagate along various paths of differing lengths. The presence of several paths by which a signal can travel along between transmitter and receiver is known as *multipath propagation*. A simplified pictorial of the multipath environment is shown in Fig. 1.1. At the receiver, the incoming waves arrive from many different directions with different propagation delays. The signal received at any point in space may consist of a large number of plane waves with random distributed amplitudes, phases, and angles of arrival. The received signal will typically be a superposition of these many multipath components thereby creating a rapid fluctuation in signal strength at the receiver, known as *multipath fading*. An example of a fading signal is shown in Fig. 1.2 (a) for a single stationary antenna receiver. Here the rapid changes are clearly visible and the signal power drops over 40dB in some fades.

If the objects in the channel are stationary and static, and any motion is due only to the receiver, then the fading is purely a spatial phenomenon. These spatial variations in the received signal of a moving receiver appear as temporal fading as the receiver moves through the multipath field. Due to the constructive and destructive effects of the multiple components at various positions in space, a moving receiver may encounter many fades over a small distance, or if moving fast

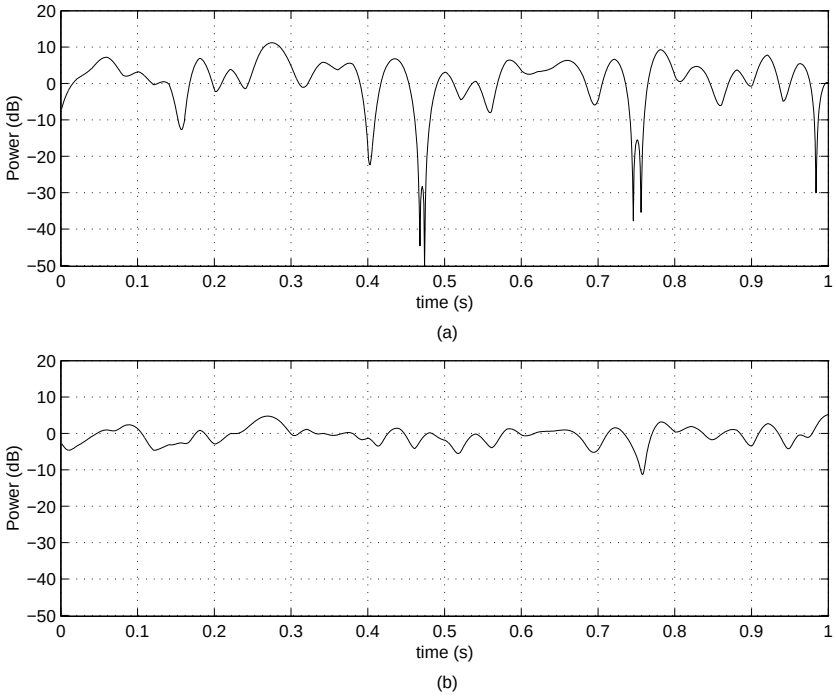

Figure 1.2: Example of a Rayleigh fading channel. (a) Signal power as a function of time for a single receive antenna. (b) Signal power as a function of time for two receive antenna with maximum ratio diversity combining .

enough, over a small period of time. A typical variation in received signal power is shown in Fig. 1.3 over a small $3\lambda \times 3\lambda$ region in space. In this example we see rapid variations in received power over just fractions of a wavelength, representing a commonly experienced scenario amongst cell-phone users where small head movements can have a significant impact on reception.

1.2.1 Diversity

The traditional approach to mitigate fading effects is to simply allow for deep fades by increasing the transmit power. However, this simple approach leads to a majority of the time transmitting multiple times the actual required power for reliable communication, therefore causing high power consumption and considerable user interference.

A more recent and successful scheme to overcome the effects of signal fading is that of exploiting channel diversity. The principle idea is for the receiver to obtain several independent copies of the signal of interest transmitted over independently fading channels, thus the probability that all the signal components will fade simultaneously is considerably reduced. For successful exploitation of diversity schemes

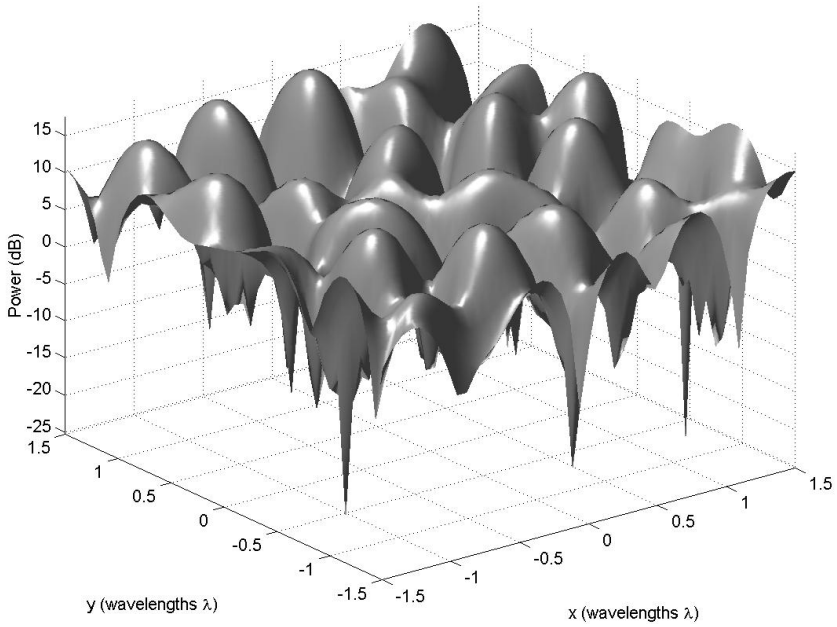

Figure 1.3: Example of spatial fading. Signal power over a $3\lambda \times 3\lambda$ region in a multipath scattering environment.

in fading channels the different received branches must, on average, exhibit low mutual correlation, that is, while one signal experiences a deep fade the others should not. Several different schemes for obtaining several replicas of the signal have been proposed:

Time diversity: Time diversity repeatedly transmits information at time spacings that exceed the coherence time of the channel, where the coherence time is the minimum time separation between independent channel fades. Time diversity provides multiple repetitions of the signal to the receiver with independent fading conditions. Interleaving, forward error control (FEC), and automatic repeat request (ARQ) are often used to exploit time diversity. More recently, RAKE receivers for spread spectrum CDMA are being utilized, where the multipath channel provides redundancy in the transmitted signals. Although simple, time diversity has a significant drawback in the inherent delay due to the time spreading.

Frequency diversity: Frequency diversity simply transmits information on more than one carrier frequency. Provided the frequencies are separated by more than the coherence bandwidth of the channel they will not experience the same fades [13]. The coherence bandwidth of the channel is the minimum frequency separation between independent fades and is inversely proportional to

the delay spread in the channel. Frequency diversity can be utilized through spread spectrum techniques or through interleaving and FEC techniques in combination with multicarrier modulation [14]. Frequency diversity techniques do however use much more expensive frequency spectrum and require a separate transmitter for each carrier.

Polarization diversity: With the increase in mobile services, vertically polarized whip antennas are becoming obsolete due to problems with hand-tilting of the receiver. This recent change has increased interest in utilizing polarization diversity at the base station. Polarization diversity consists of transmitting information over two orthogonally polarized antennas. Measured horizontal and vertical polarization paths between a mobile and a base station have been shown to be uncorrelated [15], while providing only two diversity branches it does allow the antennas to be co-located.

Space diversity: One of the oldest techniques, and with a recent resurgence in interest, space diversity is a strong contender for many wireless mobile communication systems. As we have seen, in the presence of multipath the received power-level is a random function of the user location and at times experiences fading. By using spatially separated multiple antennas we can reduce the probability of losing the signal by combining the antenna signals in order to increase the received average power. For example, the spatial fading shown in Fig. 1.3 reveals that if two antennas are separated by a fraction of a wavelength, one may be at a null while the other is on a peak of the received signal strength. An example of diversity combining is shown in Fig. 1.2 (b), where a combination technique known as Maximum Ratio Combining (MRC) [16, 17] is used for a two receive antenna system. MRC is the optimal technique in the sense that the received signal-to-noise (SNR) ratio is maximized. The value of diversity combining is evident, the use of multiple antennas reduces the signal fluctuations and eliminates the deep fades in the example shown, hence the performance of the system will be greatly improved. This is particularly important for high performance systems, where almost all the transmission errors occur due to the fades.

This thesis is mostly concerned with spatial diversity, in particular the performance improvement, with respect to channel capacity, that can be achieved when multiple antennas are used. The use of multiple antennas at the receiver, known as *receive diversity*, is a well understood and studied subject [16]. However, with

the decreasing size of wireless mobile receivers, the employment of multiple antennas at the receiver is becoming more difficult. With this limitation in mind, there has been a recent surge in research focusing on the use of multiple antennas at the transmitter, or *transmit diversity* [18–22]. In the case of transmitter knowledge of the channel, transmit diversity involves transmission over multiple antennas such that the signals from the individual antennas arrive in phase at the receiver antenna. If the channel is not known at the transmitter, transmit diversity is a more complicated process involving methods such as space-time coding which codes information across antennas (space) and time. The basic idea of transmit diversity without channel information is to transmit the information with different preprocessing (coding, modulation, delay, etc.) from different antennas such that the receiver can combine the received signals to obtain diversity.

While receive diversity simply needs multiple antennas with independent fading, transmit diversity requires special modulation/coding schemes in order to be effective. Receive diversity also provides an array gain effect, where the total received SNR is increased due to antenna combining, whereas transmit diversity does not when the the channel is unknown at the transmitter and the total transmit power is fixed (typical scenario).

Whilst spatial diversity protects the communication system from the effects of fading when multiple antennas are used at either the transmitter or receiver, significant capacity increases can be achieved by using multiple antennas at both ends of the link [7, 23]. The use of multiple transmit and receive antennas to increase capacity is known as *spatial multiplexing*, and when employed in rich scattering environments it can create multiple data pipes within the same frequency band to yield a linear (in the number of antennas) increase in capacity. Spatial multiplexing operates by breaking up the symbol stream into several parallel streams which are then transmitted simultaneously within the same frequency band. At the receiver, information from each transmit antenna has a unique spatial signature due to multipath propagation, which is exploited to separate the individual data streams. With the increase in capacity obtained at no extra bandwidth or power consumption, it is an attractive solution to the capacity demands of next generation wireless systems.

1.3 Fundamental Limits to Wireless Communication Systems

As mentioned above, the use of multiple antennas at both ends of the link offer significant capacity gains over single antenna systems, or transmit/receive diversity systems. In this section we detail the capacity aspects of spatial diversity and spatial multiplexing systems and demonstrate the outstanding capacity gains achievable. A more detailed derivation and analysis of MIMO capacity is covered in Section 1.4.

1.3.1 MIMO Fading Channel Model

The principle objective of a channel model in communications is to relate the received signal to the transmitted signal. Let $x(t)$ represent the baseband signal to be transmitted at time t, then the received signal $y(t)$ at a stationary receiver is given by the convolution of the channel impulse response, $h(\tau, t)$, and $x(t)$ as

$$y(t) = \int_{-\infty}^{\infty} h(\tau, t)x(t-\tau)d\tau + n(t), \tag{1.1}$$

assuming additive white Gaussian noise (AWGN) at the receiver, given by $n(t)$. Noise models other than AWGN can also be considered [16, 24], however, this thesis will restrict its attention to AWGN. Here we assume the channel impulse response $h(\tau, t)$ is a function of both time t, and delay τ of the channel.

For a multiple-input multiple-output (MIMO) communication system shown in Fig. 1.4 with n_{T} transmit antennas and n_{R} receive antennas, the channel impulse response can be described by a $n_{\mathrm{R}} \times n_{\mathrm{T}}$ matrix $\boldsymbol{H}(\tau, t)$, where element $\boldsymbol{H}(\tau, t)|_{r,s}$ is the impulse response of the channel from transmitter s to receiver r. Let $\boldsymbol{x}(t) = [x_1(t), x_2(t), \ldots, x_{n_{\mathrm{T}}}(t)]'$ be the $n_{\mathrm{T}} \times 1$ vector of transmitted signals, where $[\cdot]'$ denotes the vector transpose, then (1.1) can be written as

$$\boldsymbol{y}(t) = \int_{-\infty}^{\infty} \boldsymbol{H}(\tau, t)\boldsymbol{x}(t-\tau)d\tau + \boldsymbol{n}(t), \tag{1.2}$$

where $\boldsymbol{y}(t) = [y_1(t), y_2(t), \ldots, y_{n_{\mathrm{R}}}(t)]'$ is the $n_{\mathrm{R}} \times 1$ vector of received signals and $\boldsymbol{n}(t)$ is the $n_{\mathrm{R}} \times 1$ noise vector.

Although the continuous channel representation given by (1.2) is natural from an electromagnetic wave propagation point of view, understanding digital communications is facilitated by a discrete time representation. Consider the sampling of

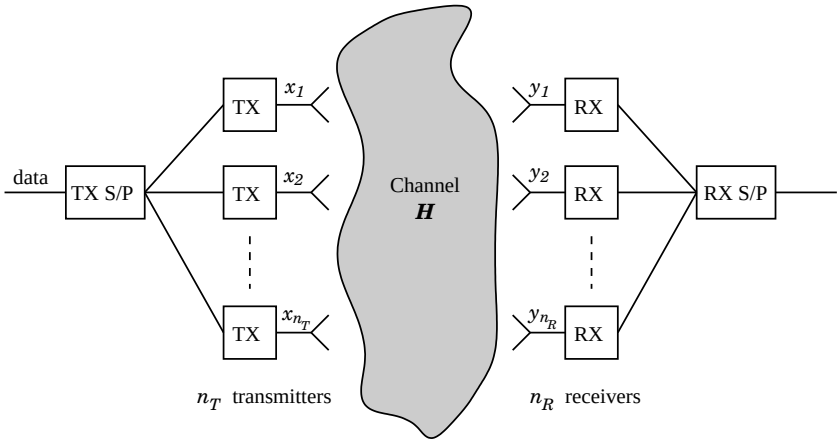

Figure 1.4: A MIMO wireless transmission system with n_{T} transmit antennas and n_{R} receive antennas. The transmit and receive signal processing (S/P) includes coding, modulation, mapping, etc. and may be realized jointly or separately.

the received signal at $t = nT$ with period T, then letting $y(n) = y(nT)$ we have

$$y(n) = \sum_{k=-\infty}^{\infty} \boldsymbol{H}(k,n)\boldsymbol{x}(n-k) + \boldsymbol{n}(n). \tag{1.3}$$

In this thesis, only narrowband frequency-flat systems will be studied, frequency selective fading channel models and capacity results can be found in [6, 25, 26]. In narrowband systems, where there is negligible delay τ, we may simplify the model to

$$\boldsymbol{y} = \boldsymbol{H}\boldsymbol{x} + \boldsymbol{n}, \tag{1.4}$$

where, for simplicity, the time index n has also been dropped. The channel matrix in (1.4) is now the $n_{\mathrm{R}} \times n_{\mathrm{T}}$ matrix

$$\boldsymbol{H} = \begin{bmatrix} h_{11} & h_{12} & \cdots & h_{1n_{\mathrm{T}}} \\ h_{21} & h_{22} & & \\ \vdots & & \ddots & \vdots \\ h_{n_{\mathrm{R}}1} & & \cdots & h_{n_{\mathrm{R}}n_{\mathrm{T}}} \end{bmatrix}, \tag{1.5}$$

with elements $\boldsymbol{H}|_{r,t} = h_{rt}$ representing the complex channel gain between the t-th transmit antenna and the r-th receive antenna, assumed constant over a symbol period.

1.3.2 Channel Capacity

The analysis of information theoretic channel capacity gives very useful, although often idealistic, bounds on the maximum information transfer rate realizable between two points of a communication link. Furthermore, the theoretical capacity allows analysis of the effects on the transmission rate of the system setup and channel model, along with providing a benchmark for real system implementation and design of transmitter and receiver algorithms.

In this thesis we consider only an isolated single-user link limited only by thermal noise. In comparison to a real system, this would correspond to an extreme case where the entire bandwidth is allocated to an individual user, and that no other users be active anywhere in the system or that their interference is perfectly suppressed. Therefore, under these unrealistic conditions, the single-user analysis presented provides an upper bound which is rarely attainable.

Consider a multiple-input multiple-output (MIMO) wireless communication system shown in Fig. 1.4 with n_{T} transmit and n_{R} receive antennas and channel model given by (1.4). For channel matrix $\boldsymbol{H}$ with random independent complex elements, it was shown in [7, 23] that the capacity is given by

$$C = \log \left| \boldsymbol{I}_{n_{\mathrm{R}}} + \frac{\eta}{n_{\mathrm{T}}} \boldsymbol{H}\boldsymbol{H}^{\dagger} \right|, \tag{1.6}$$

where η is the average SNR at any receive antenna, $\dagger$ is the complex conjugate transpose, and perfect channel information is known at the receiver and none at the transmitter. Variants of channel information knowledge is further explored in Section 1.4. Throughout this thesis logarithms are assumed base 2 and the capacity (1.6) is therefore in bits/s/Hz.

Note that the above capacity formulation differs from the definition of Shannon [27]. Here, we consider a random channel model represented by a stochastic channel matrix $\boldsymbol{H}$, hence the capacity given by (1.6) is also random and represents an instantaneous capacity for a particular realization of $\boldsymbol{H}$. With the capacity defined as a random variable, it is necessary to consider how to best characterize it. Two simple summaries are often used: *ergodic capacity* [7, 28] and the *outage capacity* [5, 29, 30].

Ergodic Capacity

The average or *ergodic capacity* is the average of all occurrences of C and is defined as

$$C_{\text{erg}} \triangleq E_{\boldsymbol{H}}\{C\} = E_{\boldsymbol{H}}\left\{\log\left|\boldsymbol{I}_{n_{\text{R}}} + \frac{\eta}{n_{\text{T}}}\boldsymbol{H}\boldsymbol{H}^{\dagger}\right|\right\}, \tag{1.7}$$

where $E_{\boldsymbol{H}}\{\cdot\}$ is the expectation over all possible channel realizations $\boldsymbol{H}$. The ergodic capacity gives information on the average data rate offered by the link and gives a useful measure of the possible performance for a randomly fading channel.

Outage Capacity

Another measure of channel capacity that is frequently used is *outage capacity*. The outage capacity C_{out} is defined as the data rate that can be guaranteed with a high level of certainty. If the channel capacity falls below the outage capacity, there is no possibility that the transmitted block of information can be decoded with no errors, whichever coding scheme is employed. Let p be the outage threshold (say 1% or 0.01), then define the outage capacity $C_{\text{out},p}$ for which

$$\text{Prob}\{C \leq C_{\text{out},p}\} = p. \tag{1.8}$$

The outage capacities are often presented in the form of a Cumulative Distribution Function (CDF), for example see Fig. 1.5.

1.3.3 Single-Input Single-Output (SISO) System

Consider a single channel corrupted by additive white Gaussian noise (AWGN). Denote the normalized (unit power) random complex Gaussian amplitude of the channel as h_{11}, assumed constant over the symbol interval, then the channel capacity (1.6) becomes a random quantity given by

$$C = \log\left(1 + \eta\left|h_{11}\right|^2\right). \tag{1.9}$$

The cumulative distribution of this 1×1 'no diversity' (one transmit and one receive antenna) system is shown in Fig. 1.5. Notice that for this SISO system, the outage capacity $C_{\text{out},1\%}$ is approximately zero (bottom of curve), indicating the capacity can become very small at certain times due to fading. In fact, although the ergodic capacity is around 2.5 bps/Hz (top of curve), the instantaneous capacity will be

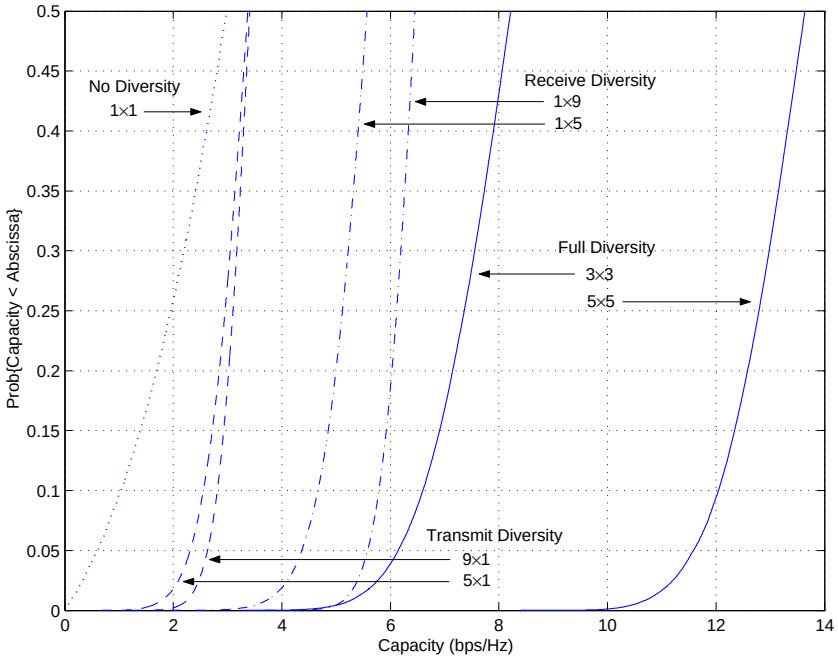

Figure 1.5: Cumulative Distribution Function (CDF) of the channel capacity for different numbers of transmit and receive antennas for an i.i.d. Rayleigh fading environment with SNR of 10dB. For each curve, the values at the top and bottom of the vertical scale gives an indication of the ergodic and outage capacities respectively.

below 1 bps/Hz for 10% of the time. It is evident from (1.9) that for high SNRs a 3dB increase in η gives an increase in capacity of one bps/Hz, as can be seen in Fig. 1.6, where the ergodic capacity of the SISO system is shown for increasing SNR.

1.3.4 Spatial Diversity Systems

Given a single transmit antenna and a set of n_{R} antennas at the receiver (SIMO system), the channel is now described by a column vector of independent elements $\boldsymbol{h} = [h_{11}, h_{21}, \ldots, h_{n_{\mathrm{R}}1}]'$, where h_{r1} is the channel gain from the transmitter to the r-th receive antenna. The random channel capacity (1.6) is then given by

$$C = \log \left| \boldsymbol{I}_{n_{\mathrm{R}}} + \eta \boldsymbol{h}\boldsymbol{h}^{\dagger} \right| \tag{1.10a}$$

$$= \log \left(1 + \eta \boldsymbol{h}^{\dagger}\boldsymbol{h}\right) \tag{1.10b}$$

$$= \log \left(1 + \eta \sum_{r=1}^{n_{\mathrm{R}}} |h_{r1}|^2\right), \tag{1.10c}$$

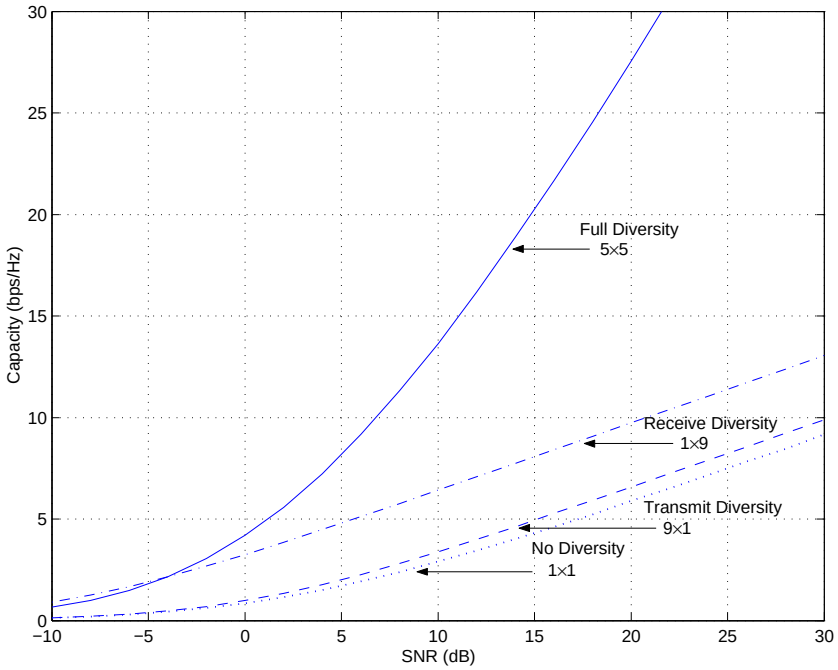

Figure 1.6: Ergodic channel capacity with increasing SNR for different numbers of transmit and receive antennas for an i.i.d. Rayleigh fading environment.

where (1.10b) follows from the reciprocity of (1.6), that is, as $|\boldsymbol{I} + \boldsymbol{AB}| = |\boldsymbol{I} + \boldsymbol{BA}|$ the channel capacity (1.6) is invariant under the transformation $\boldsymbol{H} \rightarrow \boldsymbol{H}^{\dagger}$. It can be seen in Fig. 1.5 that receiver diversity increases both the outage and ergodic capacity compared to the SISO system for 5 and 9 receive antennas. The use of multiple receive antennas reduces fading, however, due to the logarithmic increase in capacity with increasing receive antennas, the higher SNR of the combined antennas quickly gives limited returns. The increase in ergodic capacity is also limited with increasing SNR, as can be seen in Fig. 1.6, due to the logarithmic relationship.

Consider also a system employing transmit diversity. Using n_{T} transmit antennas gives a multiple-input single-output (MISO) system with the channel described by a row vector $\boldsymbol{h} = [h_{11}, h_{12}, \ldots, h_{1n_{\mathrm{T}}}]$, where h_{1s} is the channel gain from the s-th transmit antenna to the receive antenna. The random capacity (1.6) can be expressed as

$$C = \log\left(1 + \frac{\eta}{n_{\mathrm{T}}}\boldsymbol{h}\boldsymbol{h}^{\dagger}\right) \tag{1.11a}$$

$$= \log\left(1 + \frac{\eta}{n_{\mathrm{T}}}\sum_{t=1}^{n_{\mathrm{T}}}|h_{1t}|^2\right), \tag{1.11b}$$

where the normalization factor $1/n_{\mathrm{T}}$ ensures a fixed total transmitter power. It

is important to note here there is no array gain, unlike the receive diversity case where the total received SNR is increased due to antenna combining. In this case the outage capacity is improved (see Fig. 1.5) but not the ergodic capacity which remains approximately the same as the no diversity case.

1.3.5 Multiple-Input Multiple-Output (MIMO) System

Now consider a full diversity system shown in Fig. 1.4, where multiple antennas are used at both ends of the link. A MIMO system consisting of n_{T} transmit and n_{R} receive antennas with independent channel gains has capacity given by (1.6), and is shown in Fig. 1.5 for the 3×3 and 5×5 cases. The enormous gains of MIMO systems are apparent, both in ergodic and outage capacity. It is important to note that all the plots in Fig. 1.5 have the same transmit power and bandwidth, therefore the significant gains of MIMO comes only at a cost of increased transmitter and receiver complexity due to the processing of the multiple antennas.

To indicate the potential performance of MIMO systems consider the special case of $n_{\mathrm{T}} = n_{\mathrm{R}}$. Then, for a large number of antennas, by the law of large numbers $\boldsymbol{H}\boldsymbol{H}^{\dagger}/n_{\mathrm{T}} \to \boldsymbol{I}_{n_{\mathrm{R}}}$, the ergodic capacity increases linearly with n_{R};

$$C_{\mathrm{erg}} = n_{\mathrm{R}} \log(1+\eta). \tag{1.12}$$

In general, the capacity grows linearly with the smallest number of antennas, $\min(n_{\mathrm{T}}, n_{\mathrm{R}})$, hinting at the significant capacity gains of MIMO systems. Moreover, the capacity growth does not saturate as long as additional uncorrelated antennas can be incorporated into the arrays. In Fig. 1.6 we see that the use of multiple antennas at both ends of the link provides much better performance for a fixed SNR than those systems employing multiple antennas at one end of the link only. In fact, for $n_{\mathrm{T}} = n_{\mathrm{R}}$, and the special case of $\boldsymbol{H} = \boldsymbol{I}_{n_{\mathrm{R}}}$ we have

$$C_{\mathrm{erg}} = n_{\mathrm{R}} \log\left(1 + \frac{\eta}{n_{\mathrm{R}}}\right) \to \frac{\eta}{\ln(2)}, \quad \text{as } n_{\mathrm{R}} \to \infty, \tag{1.13}$$

which, unlike the SISO or diversity cases, shows the capacity scaling linearly, rather than logarithmically, with increasing SNR. In fact, for large SNR the MIMO system achieves an increase of almost n_{R} bps/Hz for every 3dB increase in SNR, compared one bps/Hz for a 3dB increase in SNR for the SISO case.

1.4 Capacity of MIMO systems

The underlying mathematical nature of MIMO, where data is transmitted over a matrix rather than a vector channel, creates new and enormous opportunities beyond just the added diversity or array gain benefits. This section provides a detailed derivation and analysis of the capacity of a matrix channel, and sets the scene for what follows in the rest of this thesis.

Consider the transmission of n_{T} signals $\boldsymbol{x} \in \mathbb{C}^{n_{\mathrm{T}}}$ over a linear matrix channel with AWGN given by the complex baseband vector notation (1.4), where the noise components $\boldsymbol{n}$ are statistically independent with $E\left\{\boldsymbol{n}\boldsymbol{n}^{\dagger}\right\} = \sigma^2 \boldsymbol{I}_{n_{\mathrm{R}}}$, and have identical power at each of the n_{R} antenna outputs. The transmitted signals are assumed to be of fixed narrow bandwidth, with total transmitted power constrained to P_{T}, regardless of the number of transmit antennas, equivalently,

$$E\left\{\boldsymbol{x}^{\dagger}\boldsymbol{x}\right\} = \mathrm{tr}\left(\boldsymbol{\Phi}_{\boldsymbol{x}}\right) \leq P_{\mathrm{T}}, \tag{1.14}$$

where $\boldsymbol{\Phi}_{\boldsymbol{x}} = E\left\{\boldsymbol{x}\boldsymbol{x}^{\dagger}\right\}$ is the covariance matrix of the transmitted signal vector $\boldsymbol{x}$, and $\mathrm{tr}(\cdot)$ is the trace of the matrix.

The classical results in [5, 7] used an ideal MIMO environment where there is rich scattering and enough separation between the antennas at the transmitter and at the receiver such that the fades for each transmitting-receiving pair are independent. This model is satisfied by assuming each element of the random channel matrix $\boldsymbol{H}$ is independent and has uniform phase and Rayleigh magnitude. Therefore, the elements of the channel matrix are modelled by i.i.d. complex Gaussian with zero mean and unit variance. Except where otherwise indicated, it is assumed the realization of $\boldsymbol{H}$ is known at the receiver.

1.4.1 Channel Capacity

It is important to note that the information theoretic capacity is an upper limit on the possible error-free bit rate, and this limit can only be approached in practice with high complexity. In real system implementation, the achievable bit rate is limited due to coding, detection, constellation size, etc., therefore any practical system can only achieve a bit rate (at some desired small BER) that is typically a fraction of capacity.

The capacity is defined as the maximum of the average mutual information $I(\boldsymbol{x};\boldsymbol{y})$ between the input and the output of the channel with respect to all possible

transmitter statistical distributions $p(\boldsymbol{x})$ [1]:

$$C = \max_{p(\boldsymbol{x}):\mathrm{tr}(\boldsymbol{\Phi}_{\boldsymbol{x}})\leq P_{\mathrm{T}}} I(\boldsymbol{x};\boldsymbol{y}). \tag{1.15}$$

Here the mutual information between transmitted and received signals is given by

$$\begin{aligned} I(\boldsymbol{x};\boldsymbol{y}) &= \mathcal{H}(\boldsymbol{y}) - \mathcal{H}(\boldsymbol{y}|\boldsymbol{x}) && \text{(1.16a)}\\ &= \mathcal{H}(\boldsymbol{y}) - \mathcal{H}\left(\boldsymbol{H}\boldsymbol{x}+\boldsymbol{n}|\boldsymbol{x}\right) && \text{(1.16b)}\\ &= \mathcal{H}(\boldsymbol{y}) - \mathcal{H}\left(\boldsymbol{n}|\boldsymbol{x}\right) && \text{(1.16c)}\\ &= \mathcal{H}(\boldsymbol{y}) - \mathcal{H}\left(\boldsymbol{n}\right), && \text{(1.16d)} \end{aligned}$$

where $\mathcal{H}(\cdot)$ is the entropy of a random variable, and gives a measure of uncertainty. It is assumed that the transmitted signals $\boldsymbol{x}$ and the noise $\boldsymbol{n}$ are independent. From (1.16d) maximizing $I(\boldsymbol{x};\boldsymbol{y})$ is equivalent to maximizing $\mathcal{H}(\boldsymbol{y})$, which occurs when $\boldsymbol{y}$ is circularly symmetric complex Gaussian, which is the case when $\boldsymbol{x}$ is circularly symmetric complex Gaussian, and is equal to $\mathcal{H}(\boldsymbol{y}) = \log|\pi e\boldsymbol{\Phi}_{\boldsymbol{y}}|$, with covariance matrix $\boldsymbol{\Phi}_{\boldsymbol{y}} = E\left\{\boldsymbol{y}\boldsymbol{y}^{\dagger}\right\}$ [7]. In this case the mutual information is given by

$$\begin{aligned} I(\boldsymbol{x};\boldsymbol{y}) &= \log|\pi e\boldsymbol{\Phi}_{\boldsymbol{y}}| - \log|\pi e\boldsymbol{\Phi}_{\boldsymbol{n}}| && \text{(1.17a)}\\ &= \log\left|\frac{1}{\sigma^2}\boldsymbol{\Phi}_{\boldsymbol{y}}\right| && \text{(1.17b)}\\ &= \log\left|\boldsymbol{I}_{n_{\mathrm{R}}} + \frac{1}{\sigma^2}\boldsymbol{H}\boldsymbol{\Phi}_{\boldsymbol{x}}\boldsymbol{H}^{\dagger}\right|. && \text{(1.17c)} \end{aligned}$$

Define

$$C(\boldsymbol{\Phi}_{\boldsymbol{x}}) \triangleq \log\left|\boldsymbol{I}_{n_{\mathrm{R}}} + \frac{1}{\sigma^2}\boldsymbol{H}\boldsymbol{\Phi}_{\boldsymbol{x}}\boldsymbol{H}^{\dagger}\right|, \tag{1.18}$$

as the capacity achieved by transmitting independent complex circular Gaussian symbols along the eigenvectors of $\boldsymbol{\Phi}_{\boldsymbol{x}}$. Now the capacity of the channel (1.15) becomes a transmitter optimization problem, where, subject to the transmitter power constraint, it is required to find the optimal input covariance matrix to maximize $C(\boldsymbol{\Phi}_{\boldsymbol{x}})$:

$$C = \max_{\boldsymbol{\Phi}_{\boldsymbol{x}};\mathrm{tr}(\boldsymbol{\Phi}_{\boldsymbol{x}})\leq P_{\mathrm{T}}} C(\boldsymbol{\Phi}_{\boldsymbol{x}}). \tag{1.19}$$

1.4.2 Channel Unknown at Transmitter

When there is no feedback in the system and the channel is known at the receiver but unknown at the transmitter, it was shown in [5,7] that in i.i.d. Rayleigh fading the optimal input covariance matrix that maximizes ergodic capacity occurs for *equal power* uncorrelated sources, given by $\boldsymbol{\Phi}_{\boldsymbol{x}} = \frac{P_{\mathrm{T}}}{n_{\mathrm{T}}}\boldsymbol{I}_{n_{\mathrm{T}}}$. Therefore, the channel capacity is given by

$$C_{\mathrm{ep}} = \log\left|\boldsymbol{I}_{n_{\mathrm{R}}} + \frac{\eta}{n_{\mathrm{T}}}\boldsymbol{H}\boldsymbol{H}^{\dagger}\right|, \tag{1.20}$$

where $\eta = P_{\mathrm{T}}/\sigma^2$ is the average SNR at any receive antenna.

To emphasis the outstanding capacity growth achievable consider the singular value decomposition (SVD) of the channel matrix $\boldsymbol{H}$, where the MIMO channel can be decomposed into an equivalent system of parallel AWGN SISO channels. Let $\boldsymbol{H} = \boldsymbol{U}\boldsymbol{D}\boldsymbol{V}^{\dagger}$ be the SVD of $\boldsymbol{H}$, then $\boldsymbol{U} = [\boldsymbol{u}_1, \ldots, \boldsymbol{u}_{n_{\mathrm{R}}}] \in \mathbb{C}^{n_{\mathrm{R}}\times n_{\mathrm{R}}}$ and $\boldsymbol{V} = [\boldsymbol{v}_1, \ldots, \boldsymbol{v}_{n_{\mathrm{T}}}] \in \mathbb{C}^{n_{\mathrm{T}}\times n_{\mathrm{T}}}$ are unitary and $\boldsymbol{D} = \mathrm{diag}(\sqrt{\lambda_1}, \sqrt{\lambda_2}, \cdots, \sqrt{\lambda_N}, 0, \cdots, 0)$, where $\sqrt{\lambda_n}$, $n = \{1, \ldots, N\}$, are the singular values of the channel matrix, and $N = \mathrm{rank}(\boldsymbol{H}) \leq \min(n_{\mathrm{T}}, n_{\mathrm{R}})$. Therefore, (1.4) can be written as

$$\widetilde{\boldsymbol{y}} = \boldsymbol{D}\widetilde{\boldsymbol{x}} + \widetilde{\boldsymbol{n}}, \tag{1.21}$$

where $\widetilde{\boldsymbol{y}} = \boldsymbol{U}^{\dagger}\boldsymbol{y}$, $\widetilde{\boldsymbol{x}} = \boldsymbol{V}^{\dagger}\boldsymbol{x}$ and $\widetilde{\boldsymbol{n}} = \boldsymbol{U}^{\dagger}\boldsymbol{n}$. Therefore we have a system of N equivalent parallel SISO eigen-channels, as illustrated in Fig. 1.7, with signal powers given by the non-zero eigenvalues $\{\lambda_1, \lambda_2, \ldots, \lambda_N\}$. Hence, the channel capacity (1.20) can be expressed as the sum of the capacities of the individual subchannels:

$$C_{\mathrm{ep}} = \sum_{n=1}^{N} \log\left(1 + \frac{\eta}{n_{\mathrm{T}}}\lambda_n\right). \tag{1.22}$$

Clearly, with a reduced number of significant eigenvalues in (1.22) the capacity of the MIMO channel will be reduced because of a rank deficient channel matrix. This situation occurs when the signals become correlated due to antenna placement or scattering environment, and is the main focus of this thesis.

1.4.3 Channel Known at Transmitter

If the channel is fading slowly enough it may remain constant long enough for timely feedback of the channel state to the transmitter. In this case, when the

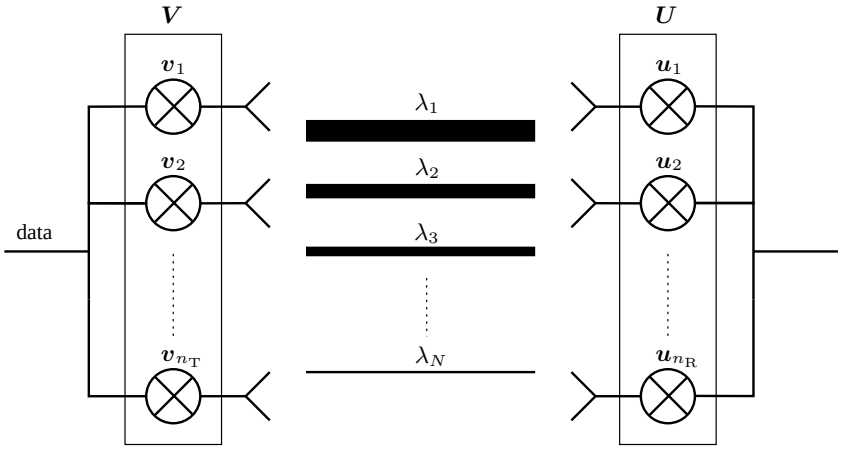

Figure 1.7: Illustration of parallel eigen-channels of a MIMO system for the singular value decomposition $\boldsymbol{H} = \boldsymbol{U}\boldsymbol{D}\boldsymbol{V}^{\dagger}$. The width of the line indicates the different eigen-channel power gains λ_n.

channel is known at the transmitter (and at the receiver) then the optimal $\boldsymbol{\Phi}_{\boldsymbol{x}}$ is called the *waterfilling* solution [7,31–33]. Here waterfilling the transmit power over the parallel SISO channels whose gains are given by the eigenvalues of the channel matrix, gives the power allocation

$$P_n = \left(\mu - \lambda_n^{-1}\right)^+, \tag{1.23}$$

to the n-th eigenmode of the channel, where μ is the waterfill level chosen such that $\sum_n P_n \leq P_{\mathrm{T}}$, and a^+ denotes $\max(a, 0)$. The channel capacity is then given by [7]

$$C_{\mathrm{wf}} = \sum_n \log(\mu\lambda_n)^+. \tag{1.24}$$

Waterfilling allocates more power to those subchannels with higher SNR $\eta\lambda_n$, with the water level μ indicating the amount of power to be poured into the channel formed by the function $\{\lambda_n^{-1}, n = 1, 2, \ldots, N\}$. Each of the sub-channels contributes $\log(\mu\lambda_n)^+$ to the total capacity. Feedback of the channel state and waterfilling provides significant capacity gains over uniform power allocation at low SNR, however, the gain margin becomes negligible as the SNR increases [34]. The intuition is that when there is low SNR, it is important to allocate the available transmit power to the strongest sub-channels, while as the SNR increases, there is sufficient power to be distributed evenly over all the sub-subchannels.

1.4.4 Partial Channel Knowledge

Along with the two cases mentioned above, namely knowledge and no knowledge of the channel at the transmitter, there has been much interest in the capacity of MIMO systems with partial channel knowledge at the transmitter, as well as partial or no knowledge at both transmitter and receiver.

In systems with channels that change rapidly, feedback of perfect channel knowledge may not be possible. However, feedback of partial knowledge may be possible using the channel distribution, such as the covariance [35–39] or the mean [35,36,40,41], which changes much more slowly than the channel itself. Here not only does the capacity increase, but this feedback allows the transmitter to identify the dominant eigen-modes of the channel and achieves higher capacity with simple coding schemes [12].

The well known linear growth in capacity with increasing antennas relies on perfect channel knowledge at the receiver [5]. However, if the channel experiences rapid fluctuations the receiver may not be able to perform reliable channel estimation. In the case of no channel knowledge at both the transmitter and receiver [42] showed a saturation point occurs in capacity growth with increasing numbers of antennas. Modelling the channel matrix components as i.i.d. complex Gaussian random variables that remain constant for a block of T symbol periods, [42] showed that the capacity does not increase after the number of antennas is increased beyond the channel coherence interval T. This result was further studied in [43] for high SNRs, where the optimal number of antennas is shown to be $\lfloor T/2 \rfloor$. Furthermore, lower capacity growths are predicted for continuous fading channels where the block fading assumption does not hold [44, 45].

Although the results for no receiver channel knowledge, presented in [42, 43], indicate limited capacity for rapidly changing channels, it may be possible for the receiver to resolve the slower varying channel distribution. Here, in contrast to the capacity saturation predicted in [42, 43] for increasing antenna numbers, recent results [46,47] indicate that additional antennas will always increase capacity provided their channel fading coefficients are spatially correlated. Thus, in contrast to results with perfect channel knowledge, these results indicate that with partial knowledge fade correlations can be beneficial. This result implies that for highly mobile, fast fading channels that cannot be accurately measured, reducing the spacing between antennas may in fact improve capacity performance [12].

It is important to also note that other propagation effects not captured in (1.4), such as multipath delay spread, may serve to reinforce the capacity gains of MIMO.

This was shown in particular in the case when the transmit channel is known [6] but also in the case when it is unknown [26].

1.4.5 Achieving Capacity: Space-Time Codes

The information theoretic analysis presented in the previous sections and throughout this thesis does not reflect the performance achieved by actual communications systems, as it is an upper bound computed without any complexity restrictions. Therefore, similar to the need of powerful error-correction codes in single-antenna systems, analogous multidimensional error-correction codes are required in multiple-antenna systems in order to approach the rates promised in [5, 7]. Such multidimensional coding procedures (i.e., codes that involve both the spatial and the temporal dimensions of the input signals) are generally referred to as "space-time codes" (STC) [21]. This thesis does not cover STC in any detail, however, for completeness we present an overview below. A more detailed summary of space-time coding can be found in [48].

One of the first space-time coding structures (known as D-BLAST) was presented in [23] and is structured in a way to avoid the exponential explosion of complexity with the number of spatial dimensions. The BLAST project showed that multipath is not as harmful as previously thought and that multiple diversity can be exploited to increase capacity even when the channel is unknown [23, 42]. Nonetheless, in practice, this scheme is still quite complex and there is a great interest in investigating the construction of much simpler alternatives for practical use [21, 48–54].

Along with coding for maximal data rates or spatial multiplexing (BLAST), there is a need to encode across the individual antennas to protect the data against errors due to channel fading. Here the goal of the coding process is to minimize the outage probability, that is, to improve the spatial diversity. The first such attempt was by Alamouti [55], where two transmit antennas where used to provide an order two diversity advantage to a receiver with a single antenna and no CSI at the transmitter. Recently, there have been several attempts at extending the work of [55] to more than two transmit antennas [56, 57]. However, in the case of a general complex symbol constellation, full-rate orthogonal codes cannot be constructed, thereby losing the simple decoding structure offered by Alamouti's scheme. Therefore there have been a number of design strategies to extend the work of [55] where either the data rate or the orthogonality of the code is sacrificed, to either preserve the simple decoding structure, or retain full data rate, respectively [22, 58, 59].

Full spatial multiplexing (BLAST) gives full independent usage of the antennas, however, it provides limited diversity and may not provide enough protection to meet the required bit error rate (BER). Therefore, it is often desirable to sacrifice some data rate for an increase in diversity, where the tradeoff between data rate and diversity is obtained via some optimization scheme [56, 60–63]. Although the data rate increases linearly with the number of antennas, the diversity effect gives diminishing returns. Therefore, with a large number of antennas it is sensible to place more emphasis on spatial multiplexing and less on diversity schemes.

1.5 Structure of this Thesis

This chapter has summarized the theoretical and practical features of single-user multiple-antenna communication systems for use in wireless networks. Information theoretic studies have predicted outstanding capacity gains for MIMO wireless links over current single antenna systems. Whether this can be achieved in practice is still to be seen, however, preliminary experiments have shown promising results [25,64].

One of the most significant factors determining the capacity of the MIMO system is that of the channel and hence it is important to have realistic channel models. However, most of the analysis of MIMO systems have been performed using rather idealistic channel models and conditions. The outstanding linear capacity growth outlined in this chapter is only valid under certain channel conditions. It was originally derived for the independent and identically distributed (i.i.d.) flat Rayleigh fading channel. However, Rayleigh fading models are inadequate in describing many fading channels encountered in practice, and the i.i.d. assumption only holds for significant scattering and sufficiently spaced antennas, which may not be feasible in many scenarios.

In this thesis, the capacity performance of MIMO systems will be examined in more physically realistic environments. By including the spatial aspects, which have been previously ignored, into the channel model, this thesis derives new bounds and fundamental limitations to MIMO capacity within general scattering environments.

1.5.1 Questions to be Answered in this Thesis

In this thesis the following open questions are addressed:

- What dictates the information theoretic capacity of a MIMO wireless channel?

- What are the key propagation conditions to achieve this capacity?
- Is there a tractable analytical model which describes the observable capacity behavior?
- Is there a more fundamental capacity between the two spatial volumes containing the antenna arrays?
- How can this continuous spatial channel be modelled?
- What factors determine the information theoretic capacity between two regions in space?
- What is the relationship between the MIMO channel and the continuous spatial channel?

1.5.2 Content and Contribution of Thesis

In the following the chapters of this thesis are outlined with emphasis on contributions made within:

Chapter 2 introduces the concept of space into the capacity calculations of MIMO systems. By exploiting the convergence of the ergodic capacity as the number transmit antennas is increased an upper bound on the ergodic capacity is derived which depends on the spatial correlation at the receiver. Using a novel channel model the separate effects of scattering environment and antenna array configuration can be seen on the spatial correlation, allowing for the capacity to be studied analytically for a wide variety of scattering environments and antenna placement. Specifically, the capacity is computed for several common scattering distributions and the uniform linear and uniform circular arrays. Most significantly, a capacity saturation is shown to occur as the number of antennas is increased for a fixed sized array, where further increases in antennas fails to give a corresponding capacity increase.

Chapter 3 further explores and quantifies the saturation observed in Chapter 2. Using the ergodic capacity bound derived in Chapter 2, the capacity of a uniform circular array is shown theoretically to have a distinct saturation point proportional to the radius of the array. This result is then extended to include arbitrary array geometries within a circular aperture and non-isotropic scattering, where the minimum number of antennas required to

achieve maximum capacity for the aperture is derived. A fixed received power concept is introduced, where regardless of the number of antennas within the receiver aperture the total received power remains constant. This physically realistic normalization shows that there is a fundamental limit to MIMO communications which is independent of the number of antennas.

Chapter 4 introduces a MIMO channel model which includes the spatial aspects of the arbitrary transmit and receive arrays, along with the spatial properties of the random scattering environment. This chapter begins by characterizing the well used plane wave for modelling wireless channels, giving a truncated modal expansion that is used throughout the rest of the thesis. Using this truncated expression, the channel is decomposed into three distinct regions of signal propagation and allows a spatial degrees of freedom (SDOF) concept to be defined. The defined SDOF gives the number of free parameters of the spatial channel, and is shown to be defined by the transmit and receive aperture size, and the scattering environment, and ultimately determines the maximum capacity achievable. Finally, the concept of spatial richness is addressed, where it is argued that the size of the apertures must be considered when defining the richness of a channel.

Chapter 5 numerically studies the MIMO model presented in Chapter 4 for a wide range of scattering, aperture and array scenarios. The theoretical results of the previous chapters are verified via simulation, including antenna saturation and the effects of angular spread. A discrete scattering model is presented, which models the scattering environment via a number of paths between the apertures. Angular spread surrounding both the transmit and receive apertures is introduced into the model under the assumption of independent local scattering. This model then allows the simulation of almost all channel scenarios previously presented in the literature, including the elusive pinhole channel.

Chapter 6 introduces the concept of an intrinsic or fundamental capacity between the apertures. The intrinsic capacity gives the maximum capacity between two circular or spherical apertures, regardless of the number of antennas, array geometry, or antenna signal processing. This capacity is shown to be dependent on the aperture size and the scattering environment. Under this framework, MIMO is shown to be an implementation issue where the continuous apertures are sampled with discrete antenna arrays. The results of the

circular and spherical apertures is extended to continuous arbitrary apertures. A novel framework is presented, where the capacity between continuous spatial apertures is developed using the general concepts of separable Hilbert Spaces.

Chapter 2

Introducing Space into MIMO Capacity Calculations

Multiple-Input Multiple-Output (MIMO) communication systems using multiple antenna arrays simultaneously during transmission and reception have generated significant interest in recent years. Theoretical work of [7] and [5] showed the potential for significant capacity increases in wireless channels utilizing spatial diversity. Consider a system employing n_{T} transmit antennas and n_{R} receive antennas in a narrowband flat fading channel. It was shown in [5] that as $\min(n_{\mathrm{T}}, n_{\mathrm{R}})$ tends to infinity then the capacity of the system grows proportionally to $\min(n_{\mathrm{T}}, n_{\mathrm{R}})$ for fixed transmit power, provided that the fading between antennas is independent and identically distributed (i.i.d.) Rayleigh. This linear capacity growth has emerged as one of the most promising solutions for overcoming the demand for higher bit rates in wireless communications. In reality, however, the capacity is significantly reduced when the fades are not independent, but correlated due to insufficient antenna separation or angular spread of the scatterers surrounding the arrays [5, 65].

A significant hurdle in analyzing the capacity of wireless fading MIMO systems is the random nature of the channel. The ergodic, or mean, capacity is often used to characterize the random channel capacity. However, the ergodic calculation requires extensive simulations which limits analysis into the physical factors determining MIMO capacity. A closed form expression for the ergodic capacity is derived in [66] for the special case of uncorrelated Rayleigh fading. However, as mentioned above, i.i.d. Rayleigh fading models an unrealistic environment not often seen in practice.

Capacity results for various correlation models using Monte Carlo simulations

are studied in [30, 65, 67–70], and asymptotic results and bounds on the effects of correlated channels are presented in [65, 67, 68, 71–73]. However, these simulations, bounds and asymptotic results have been for a limited set of channel realizations and/or antenna configurations. For single antenna systems it is sufficient to only consider received signal power and/or the time varying amplitude distribution of the channel. However, for systems employing multiple antennas, consideration must also be given to the angle of arrival (AOA) of the impinging signals as well as the spatial geometry of the array. Most channel models do not include spatial information (antenna locations and scattering environment) explicitly. Although spatial information is represented by the correlation between channel matrix elements there is no direct realizable physical representation, and, therefore does not easily lend itself to insightful capacity results. In particular, of interest is the effect on channel capacity of antenna placement, particularly in the realistic case when antenna arrays are restricted in size, along with non-isotropic scattering environments.

In contrast, in this chapter an expression for MIMO capacity is derived which overcomes these limitations, that is, with additional theory for modelling scattering environments refined here, a model is derived which can be readily reconciled with a multitude of scattering distributions and antenna configurations and allows us to derive a closed form expression for the MIMO capacity.

2.1 Convergence of Ergodic Capacity

Consider a MIMO system consisting of n_{T} transmit antenna and n_{R} receive antennas. When the transmitted signal vector is composed of statistically independent equal power components, each with a Gaussian distribution, the ergodic channel capacity was shown to be [5, 7]

$$C_{\mathrm{erg}} = E_{\boldsymbol{H}} \left\{ \log \left| \boldsymbol{I}_{n_{\mathrm{R}}} + \frac{\eta}{n_{\mathrm{T}}} \boldsymbol{H}\boldsymbol{H}^{\dagger} \right| \right\}, \tag{2.1}$$

where $\boldsymbol{H}$ is the $n_{\mathrm{R}} \times n_{\mathrm{T}}$ random flat fading channel matrix, assumed known at the receiver, and normalized such that $E\left\{|h_{rt}|^2\right\} = 1$, where h_{rt} is the channel gain from the t-th transmitter to the r-th receiver. Note that the logarithm is base 2 and gives the capacity in bits-per-second-per-Hertz (bps/Hz).

Let $\boldsymbol{H} = [\boldsymbol{h}_1\, \boldsymbol{h}_2\, \cdots\, \boldsymbol{h}_{n_{\mathrm{T}}}]$, where $\boldsymbol{h}_t$ is the $n_{\mathrm{R}} \times 1$ complex zero-mean Gaussian vector of channel gains corresponding to the t-th transmit antenna, then the cor-

relation matrix at the receiver is defined as $\boldsymbol{R} \triangleq E\left\{\boldsymbol{h}_t \boldsymbol{h}_t^{\dagger}\right\}$, where the expectation is over all transmitters and channel realizations, then

$$\boldsymbol{R} = \begin{bmatrix} \rho_{11} & \rho_{12} & \cdots & \rho_{1n_{\mathrm{R}}} \\ \rho_{21} & \rho_{22} & & \\ \vdots & & \ddots & \vdots \\ \rho_{n_{\mathrm{R}}1} & & \cdots & \rho_{n_{\mathrm{R}}n_{\mathrm{R}}} \end{bmatrix}, \tag{2.2}$$

with elements $\boldsymbol{R}|_{rr'} = \rho_{rr'}$ corresponding to the spatial correlation between two sensors r and r' at the receiver.

Consider the situation where the transmit array has uncorrelated transmit branches corresponding to independent $\boldsymbol{h}_t$ vectors. This can occur when the transmit antennas are sufficiently separated for a given angular spread of the scatterers surrounding the transmit array. For example, using the correlation expression developed in Section 2.2, a two dimensional isotropic scattering environment with antennas separated by 0.35λ gives correlation of 0.1. However, for more realistic scattering environments, when the transmitter is usually mounted high above the scatterers, the angular spread is considerably less. For angular spread of 3° the antennas must be separated by around 9λ to achieve the same level of correlation. With sufficient transmit antenna spacing the vectors $\boldsymbol{h}_t$ are independent and the sample correlation matrix, defined as

$$\widehat{\boldsymbol{R}} \triangleq \frac{1}{n_{\mathrm{T}}} \sum_{t=1}^{n_{\mathrm{T}}} \boldsymbol{h}_t \boldsymbol{h}_t^{\dagger}, \tag{2.3}$$

converges to $\boldsymbol{R}$ for large numbers of transmit antennas ($n_{\mathrm{T}} \to \infty$). Observing that the channel matrix product can be expressed as

$$\boldsymbol{H}\boldsymbol{H}^{\dagger} = \sum_{t=1}^{n_{\mathrm{T}}} \boldsymbol{h}_t \boldsymbol{h}_t^{\dagger}, \tag{2.4}$$

then for a large number of sufficiently separated transmit antennas the ergodic capacity converges to the capacity C;

$$\lim_{n_{\mathrm{T}} \to \infty} C_{\mathrm{erg}} = C \triangleq \log |\boldsymbol{I}_{n_{\mathrm{R}}} + \eta \boldsymbol{R}|. \tag{2.5}$$

The convergence error of the ergodic capacity to the expression (2.5) is shown in Fig. 2.1 for increasing numbers of uncorrelated transmit antennas and various

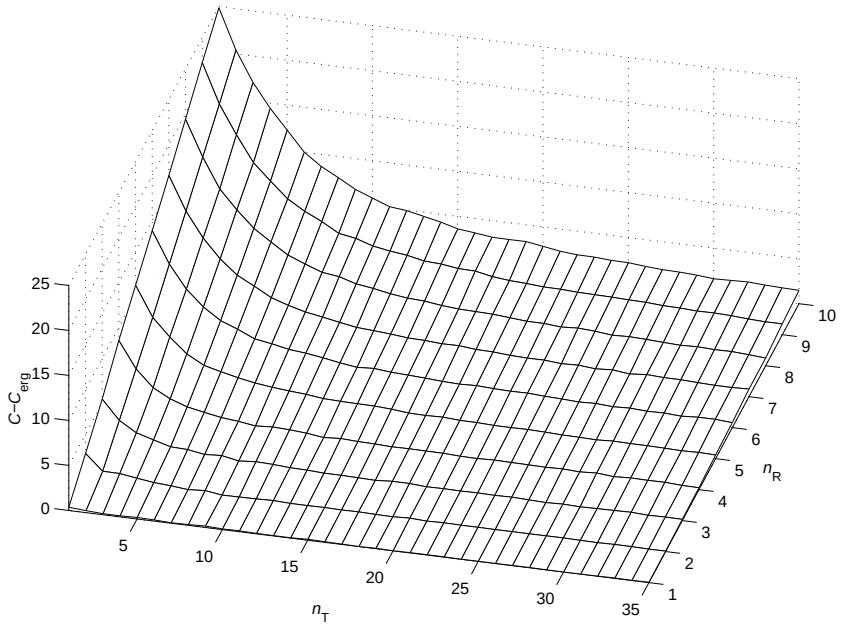

Figure 2.1: Convergence error of ergodic capacity C_{erg} (2.1) to bound C (2.5) with increasing number of transmit antennas for various numbers of receive antennas and SNR 10dB.

numbers of receiver antennas. It is important to observe that the ergodic capacity approaches the capacity C for finite numbers of transmit antennas, with faster convergence for smaller numbers of receive antennas. Therefore, the capacity expression will be accurate for many practical fixed wireless scenarios, where the receiver has a small number of antennas whilst the base station is less restricted in geometrical size and is able to provide a sufficient number of uncorrelated transmit branches. Therefore, provided the channel does not contain keyholes[1] and the transmit antennas are sufficient in number and separation, the capacity C provides a good estimate of the ergodic capacity C_{erg}. Note that a bound similar to (2.5) has also been derived in [76] to demonstrate a space-time cross-correlation model for a von-Mises scattering environment.

[1]It has been shown theoretically that some channels may exhibit low capacity even though there is no spatial correlation at the transmitter or receiver [74, 75]. However, no observations of keyhole (pinhole) degenerate channel effects from practical measurements have appeared in the literature. Therefore, this Chapter will assume non-degenerate channels only. The properties of these special channels are studied further in Chapter 5.

2.1.1 Capacity Scaling Limits

The capacity given by (2.5) is maximized when there is no correlation between the receive antennas, i.e., $\boldsymbol{R} = \boldsymbol{I}_{n_\mathrm{R}}$, giving

$$C_{\max} = n_\mathrm{R} \log(1 + \eta). \tag{2.6}$$

Therefore, in the idealistic situation of zero correlation at both transmitter and receiver arrays (corresponding to the i.i.d. case) we see the maximum capacity scaling is linear in the number of receive antennas. In this case, the system achieves the equivalent of n_R independent nonfading subchannels, each with SNR η. This result agrees with the traditional capacity formulation [66] which is widely used to advocate the use of MIMO systems.

Conversely, when each pair of antenna elements at the receiver are fully correlated, the correlation matrix becomes the $n_\mathrm{R} \times n_\mathrm{R}$ matrix of ones, $\boldsymbol{R} = \mathbf{1}_{n_\mathrm{R}}$, and the capacity of the MIMO system will be minimized to

$$C_{\min} = \log(1 + n_\mathrm{R}\eta). \tag{2.7}$$

Here the logarithmic capacity growth with increasing receiver antennas is due to an effective increase in the average SNR of the single antenna case, due to the assumption of independent noise at each receiver, and is widely known as a receiver diversity array gain effect.

The capacity (2.5) provides an expression for the ergodic capacity without the need for extensive simulations. In contrast to current simulation studies presented in the literature, which are difficult to relate to physical factors of the system, in the next section it is shown that for essentially all common scattering distributions, and any array configurations, it is possible to compute a closed form capacity expression.

2.2 Receiver Spatial Correlation for General Distributions of Farfield Scatterers

2.2.1 Channel Model

The *one-ring* model was initially proposed in [77] to model fixed wireless communications systems where the base station is elevated and not obstructed by local scattering, whilst the user is uniformly surrounded by scatterers. In [65] this model

was extended to include multiple transmit and receive antennas, and the capacity was studied for various transmit angular spreads and receive antenna geometries. Here the multipath propagation and fading correlation is modelled using a generalized 3D *one-ring* model that allows for more general scattering environments at both the transmit and receive arrays. This model allows for greater insights into the spatial factors determining channel capacity, in particular, closed-form capacity expressions can be computed for a wide range of scattering environments and antenna geometries.

Consider the narrowband transmission of n_{T} statistically independent uniform power signals $\{x_1, x_2, \ldots, x_{n_{\mathrm{T}}}\}$ through a general 3D flat fading scattering environment with scatterers assumed distributed in the farfield from the receiver antennas, as shown in Fig. 2.2, then the incoming signal from direction $\widehat{\boldsymbol{\psi}}$ at the receiver is given by

$$\Phi(\widehat{\boldsymbol{\psi}}) = \sum_{t=1}^{n_{\mathrm{T}}} x_t \, g_t(\widehat{\boldsymbol{\psi}}), \tag{2.8}$$

where $k = 2\pi/\lambda$ is the wavenumber with λ the wavelength, and $g_t(\widehat{\boldsymbol{\psi}})$ is the effective random complex gain of the scatterers for the transmitted signal x_t from the t-th transmit antenna arriving at the receiver array from direction $\widehat{\boldsymbol{\psi}}$. Since the scatterers are assumed farfield to the receiver antennas, signals impinging on the receiver array will be plane waves, therefore, the received signal at the r-th sensor located at $\boldsymbol{y}_r$ is given by

$$z_r = \int_{\mathbb{S}^2} \Phi(\widehat{\boldsymbol{\psi}}) e^{-ik\boldsymbol{y}_r \cdot \widehat{\boldsymbol{\psi}}} \, ds(\widehat{\boldsymbol{\psi}}) \tag{2.9a}$$

$$= \sum_{t=1}^{n_{\mathrm{T}}} x_t \int_{\mathbb{S}^2} g_t(\widehat{\boldsymbol{\psi}}) e^{-ik\boldsymbol{y}_r \cdot \widehat{\boldsymbol{\psi}}} \, ds(\widehat{\boldsymbol{\psi}}), \tag{2.9b}$$

where $ds(\widehat{\boldsymbol{\psi}})$ is a surface element of the unit sphere $\mathbb{S}^2$. Therefore, the channel gain h_{rt} from the t-th antenna to the r-th receiver is given by

$$h_{rt} = \int_{\mathbb{S}^2} g_t(\widehat{\boldsymbol{\psi}}) e^{-ik\boldsymbol{y}_r \cdot \widehat{\boldsymbol{\psi}}} \, ds(\widehat{\boldsymbol{\psi}}), \tag{2.10}$$

with normalized scattering gains such that

$$\int_{\mathbb{S}^2} E\left\{ \left| g_t(\widehat{\boldsymbol{\psi}}) \right|^2 \right\} ds(\widehat{\boldsymbol{\psi}}) = 1. \tag{2.11}$$

2.2.2 Correlation of the Received Complex Envelopes

Define the normalized spatial correlation function between the complex envelopes of two received signals r and r' located at positions $\boldsymbol{y}_r$ and $\boldsymbol{y}_{r'}$, respectively, as

$$\rho_{rr'} = \frac{E\left\{z_r \overline{z_{r'}}\right\}}{\sqrt{E\left\{z_r \overline{z_r}\right\} E\left\{z_{r'} \overline{z_{r'}}\right\}}}, \tag{2.12}$$

where $\overline{x}$ denotes the complex conjugate of x, and z_r denotes the noiseless received signal at receiver r.

From (2.9b) the covariance between signals at sensors r and r' is given by

$$E\left\{z_r \overline{z_{r'}}\right\} = E\left\{\sum_{t=1}^{n_{\mathrm{T}}} x_t \int_{\mathbb{S}^2} g_t(\widehat{\boldsymbol{\psi}}) e^{-ik\boldsymbol{y}_r \cdot \widehat{\ }} ds(\widehat{\boldsymbol{\psi}}) \sum_{t'=1}^{n_{\mathrm{T}}} \overline{x_{t'}} \int_{\mathbb{S}^2} \overline{g_{t'}(\widehat{\boldsymbol{\psi}}')} e^{ik\boldsymbol{y}_{r'} \cdot \widehat{\ }'} ds(\widehat{\boldsymbol{\psi}}')\right\} \tag{2.13a}$$

$$= \sigma_{\mathrm{T}}^2 \iint_{\mathbb{S}^2} \sum_{t=1}^{n_{\mathrm{T}}} E\left\{g_t(\widehat{\boldsymbol{\psi}}) \overline{g_t(\widehat{\boldsymbol{\psi}}')}\right\} e^{-ik(\boldsymbol{y}_r \cdot \widehat{\ } - \boldsymbol{y}_{r'} \cdot \widehat{\ }')} ds(\widehat{\boldsymbol{\psi}}) ds(\widehat{\boldsymbol{\psi}}'), \tag{2.13b}$$

where $\sigma_{\mathrm{T}}^2 = E\left\{|x_t|^2\right\}, \forall t$, is the transmit power for each antenna, and it is assumed the transmitted symbols are independent across antennas and independent of the scattering environment. Assuming a zero-mean uncorrelated scattering environment, the scattering channel is characterized by the second-order statistics of the scattering gain function $g_t(\widehat{\boldsymbol{\psi}})$, given by,

$$E\left\{g_t(\widehat{\boldsymbol{\psi}}) \overline{g_t(\widehat{\boldsymbol{\psi}}')}\right\} = G_t(\widehat{\boldsymbol{\psi}}) \delta(\widehat{\boldsymbol{\psi}} - \widehat{\boldsymbol{\psi}}'), \tag{2.14}$$

where $G_t(\widehat{\boldsymbol{\psi}}) = E\left\{\left|g_t(\widehat{\boldsymbol{\psi}})\right|^2\right\}$, then (2.13b) simplifies to

$$E\left\{z_r \overline{z_{r'}}\right\} = \sigma_{\mathrm{T}}^2 \int_{\mathbb{S}^2} \sum_{t=1}^{n_{\mathrm{T}}} G_t(\widehat{\boldsymbol{\psi}}) e^{-ik(\boldsymbol{y}_r - \boldsymbol{y}_{r'}) \cdot \widehat{\ }} ds(\widehat{\boldsymbol{\psi}}). \tag{2.15}$$

Substitution of (2.15) into (2.12) gives the correlation between the two receiver sensors as

$$\rho_{rr'} = \int_{\mathbb{S}^2} \mathcal{P}(\widehat{\boldsymbol{\psi}}) e^{-ik(\boldsymbol{y}_r - \boldsymbol{y}_{r'}) \cdot \widehat{\ }} ds(\widehat{\boldsymbol{\psi}}), \tag{2.16}$$

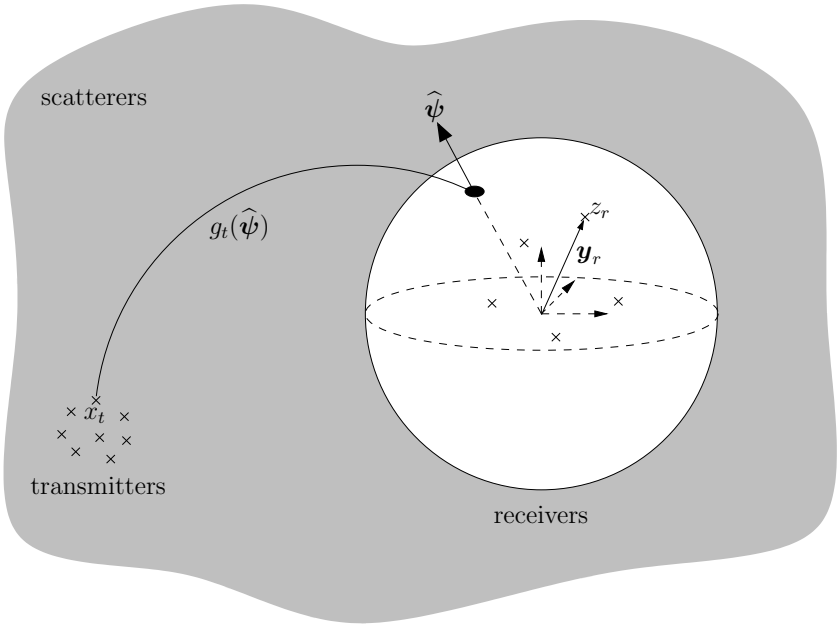

Figure 2.2: Scattering model for a flat fading MIMO system. $g_t(\widehat{\boldsymbol{\psi}})$ represents the effective random complex gain of the scatterers for transmitted signal x_t arriving at the receiver array from direction $\widehat{\boldsymbol{\psi}}$ via any number paths through the scattering environment. The sphere surrounding the receive antennas contains no scatterers and is assumed large enough that any scatterers are farfield to all receive antennas located within.

where $\mathcal{P}(\widehat{\boldsymbol{\psi}})$ is the normalized average power received from direction $\widehat{\boldsymbol{\psi}}$, defined by

$$\mathcal{P}(\widehat{\boldsymbol{\psi}}) \triangleq \frac{\sum_{t=1}^{n_{\mathrm{T}}} G_t(\widehat{\boldsymbol{\psi}})}{\int_{\mathbb{S}^2} \sum_{t=1}^{n_{\mathrm{T}}} G_t(\widehat{\boldsymbol{\psi}}) ds(\widehat{\boldsymbol{\psi}})}. \tag{2.17}$$

In two dimensional scattering environments the power distribution (2.17) is commonly known as the power azimuth spectrum (PAS) [78], or power azimuth distribution (PAD) [11].

To highlight the factors which effect spatial correlation the Jacobi-Anger plane wave expansion is employed [79],

$$e^{ik\boldsymbol{y}\cdot\widehat{\ }} = \sum_{m=0}^{\infty} i^m (2m+1) j_m(k\,\|\boldsymbol{y}\|) P_m(\cos\xi), \tag{2.18}$$

where $\xi = \angle(\boldsymbol{y}, \widehat{\boldsymbol{\psi}})$ denotes the angle between $\boldsymbol{y}$ and $\widehat{\boldsymbol{\psi}}$, $j_m(\cdot)$ are the spherical Bessel functions of the first kind, and $P_m(\cdot)$ are the Legendre polynomials of degree m. To further separate the effects of the scattering and the sensor positioning, consider the identity [80, p.694]

$$P_m(\cos\xi) = \frac{4\pi}{2m+1} \sum_{n=-m}^{m} \overline{Y_m^n(\widehat{\boldsymbol{y}})} Y_m^n(\widehat{\boldsymbol{\psi}}), \tag{2.19}$$

where $\widehat{\boldsymbol{y}} = \boldsymbol{y}/\|\boldsymbol{y}\|$ and $Y_m^n(\cdot)$ represent spherical harmonics [79, p.25], then the spatial correlation (2.16) can be expressed as

$$\rho_{rr'} = 4\pi \sum_{m=0}^{\infty} \sum_{n=-m}^{m} (-i)^m \alpha_m^n\, j_m(k\,\|\boldsymbol{y}_r - \boldsymbol{y}_{r'}\|) Y_m^n\left(\frac{\boldsymbol{y}_{r'} - \boldsymbol{y}_r}{\|\boldsymbol{y}_r - \boldsymbol{y}_{r'}\|}\right), \tag{2.20}$$

where coefficients α_m^n characterize the scattering environment,

$$\alpha_m^n = \int_{\mathbb{S}^2} \mathcal{P}(\widehat{\boldsymbol{\psi}}) \overline{Y_m^n(\widehat{\boldsymbol{\psi}})} ds(\widehat{\boldsymbol{\psi}}), \tag{2.21}$$

and are independent of the antenna positions. The spatial correlation (2.20) is now composed of a summation of terms, where each term has independent factors characterizing the scattering environment and the antenna locations. Therefore, unlike previous models, where the antenna locations and the scattering environment are coupled, the separate effects of antenna geometry and scattering environment

on the channel capacity can now be studied.

Isotropic Scattering Environment

For the special case of isotropic scattering (omnidirectional diffuse fields) the power distribution is given by the constants, $\mathcal{P}(\widehat{\boldsymbol{\psi}}) = 1/2\pi^2$ and $\mathcal{P}(\psi) = 1/2\pi$, for the 3D and 2D scattering environments respectively[2]. In this case, the summation in (2.20) reduces to a single term and the 3D and 2D spatial correlation can be shown to be:

$$\rho_{rr'}^{\mathrm{3D}} = j_0(k \left\| \boldsymbol{y}_r - \boldsymbol{y}_{r'} \right\|), \tag{2.22}$$

$$\rho_{rr'}^{\mathrm{2D}} = J_0(k \left\| \boldsymbol{y}_r - \boldsymbol{y}_{r'} \right\|), \tag{2.23}$$

which agree with the classical results [16,81], where $J_n(\cdot)$ are the Bessel functions of order n, and by definition $j_0(\cdot) = \mathrm{sinc}(\cdot)$. With these analytic forms for the spatial correlation we can compute the capacity (2.5). Figure 2.3 shows the theoretical capacity for increasing antenna numbers for a fixed aperture uniform linear (ULA) and circular (UCA) arrays in 2D and 3D isotropic scattering with SNR of 10dB. It is clear from comparison of the 2D and 3D capacities that any elevation spread has little effect on the capacity of an array in the horizontal plane. This can be seen in the insert of Fig. 2.3 where the spatial correlation for increasing spatial separation is shown for the 2D and 3D isotropic scattering environments, here the two functions $J_0(\cdot)$ and $j_0(\cdot)$ are qualitatively similar, particularly for low spatial separation. Therefore, without loss of generality, we focus on scattering environments where there is negligible power arriving from elevation angles.

2.2.3 Two Dimensional Scattering Environment

Consider a 2D scattering environment where the signals arrive only from the azimuthal plane, then $\boldsymbol{y} = (\left\| \boldsymbol{y} \right\|, \theta_y)$ and $\widehat{\boldsymbol{\psi}} = (1, \psi)$ in polar coordinates, and (2.18) can be shown to reduce to,

$$e^{ik\boldsymbol{y}\cdot\widehat{\ }} = J_0(k \left\| \boldsymbol{y} \right\|) + 2\sum_{m=1}^{\infty} i^m J_m(k \left\| \boldsymbol{y} \right\|) \cos(m\xi) \tag{2.24a}$$

$$= \sum_{m=-\infty}^{\infty} J_m(k \left\| \boldsymbol{y} \right\|) e^{-im(\theta_y - \pi/2)} e^{im\psi}. \tag{2.24b}$$

[2]The 2D scattering environment is a special case of the 3D case when the signals arrive from the azimuthal plane only.

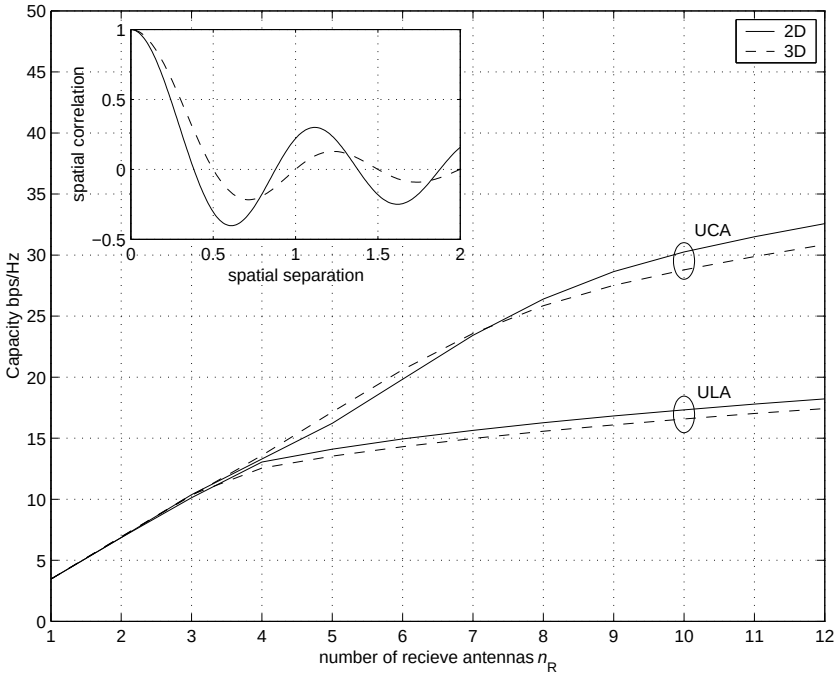

Figure 2.3: Capacity of 2D and 3D isotropic scattering environments for fixed length aperture (1λ) ULA and UCA for increasing number of receive antennas. Insert: Spatial correlation between two antennas against spatial separation for the 2D and 3D isotropic scattering environments.

Substitution of (2.24b) into (2.16) gives the spatial correlation for a 2D environment as

$$\rho_{rr'} = \sum_{m=-\infty}^{\infty} \alpha_m J_m(k \left\| \boldsymbol{y}_r - \boldsymbol{y}_{r'} \right\|) e^{im\theta_{rr'}}, \tag{2.25}$$

where $\theta_{rr'}$ is the angle of the vector connecting $\boldsymbol{y}_r$ and $\boldsymbol{y}_{r'}$. The coefficients α_m characterize any possible 2D scattering environment surrounding the receiver and are given by

$$\alpha_m = \int_{\mathbb{S}^1} \mathcal{P}(\psi) e^{-im\psi} d\psi, \tag{2.26}$$

where $\mathcal{P}(\psi)$ is the average angular power distribution over the unit circle $\mathbb{S}^1$, often referred to as the power azimuth distribution (PAD).

Bessel functions $J_n(x), |n| > 0$ exhibit spatially high pass behavior, that is, for fixed order n, $J_n(x)$ starts small and becomes significant for arguments $x \approx \mathcal{O}(n)$. Therefore, to compute the spatial correlation for points closely located in space, only a few terms in the sum (2.25) need to be evaluated in order to give a very good

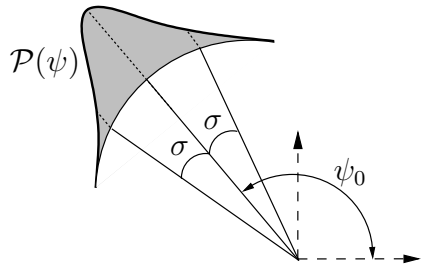

Figure 2.4: Multipath signal energy modelled as a non-isotropic scattering distribution $\mathcal{P}(\psi)$ with mean AOA ψ_0 and angular spread σ (defined as the standard deviation of the distribution).

approximation [82]. Thus, closed-form solutions for the correlation can be found provided closed-form expressions exist for the scattering coefficients (2.26). As summarized next, for many common scattering distributions, there exists closed-form expressions for the scattering coefficients α_m and thus the capacity can be computed for a wide range of realistic scattering environments.

2.2.4 Non-isotropic Scattering Environments

The spatial correlation as a function of receive antenna separation depends on the scattering distribution surrounding the receiver. One of the most commonly used distributions is the isotropic scattering model, where the power is assumed to be uniform over all AOA [16]. However, as discussed in [83–86], and verified via experimental measurement campaigns [87–92], many realistic scattering environments have nonuniform AOA distributions.

Non-isotropic scattering distributions model multipath as energy arriving from a particular direction with angular spread related to the non-isotropy parameter of the distribution, as shown in Fig. 2.4. The non-isotropic distributions are characterized by the mean AOA ψ_o and the angular spread σ, defined as the standard deviation of the distribution. Several distributions have been proposed for modelling the non-isotropic scattering environment [89, 93–97], in the following we outline several common distributions along with the scattering parameter effects on spatial correlation and capacity.

Uniform Limited Distributed Field

When the energy arrives uniformly from a restricted range of azimuth angles $\pm\Delta$ around a mean AOA, $\psi_0 \in [-\pi, \pi)$, we have the uniform limited distribution,

$$\mathcal{P}(\psi) = \begin{cases} K_{\mathrm{U}}, & |\psi - \psi_0| \leq \Delta \\ 0, & \text{elsewhere} \end{cases}, \tag{2.27}$$

where K_{U} is a normalization constant such that $\int_{\mathbb{S}^1} \mathcal{P}(\psi) d\psi = 1$. In this case $K_{\mathrm{U}} = 1/2\Delta$ and the scattering environment coefficients (2.26) are given by,

$$\alpha_m = \frac{\sin(m\Delta)}{m\Delta} e^{-im\psi_0}, \tag{2.28}$$

which gives the equivalent correlation expression to that derived in [94]. For $\Delta = \pi$ (isotropic scattering) (2.25) is given by a single term, and the correlation coefficient becomes $J_0(k \left\| \boldsymbol{y}_r - \boldsymbol{y}_{r'} \right\|)$, which agrees with earlier results.

Truncated Gaussian Distributed Field

The Gaussian distribution was proposed in [93] for modelling the distribution of scatterers as

$$\mathcal{P}(\psi) = K_{\mathrm{G}} e^{-\left(\frac{\psi - \psi_0}{\sqrt{2}\sigma_{\mathrm{G}}}\right)^2}, \qquad \psi \in [-\pi, \pi), \tag{2.29}$$

where σ_{G} is the standard deviation of the non-truncated distribution and is related to the angular spread. K_{G} is a normalization constant, which can be shown to be

$$K_{\mathrm{G}} = \frac{1}{\sqrt{2\pi}\sigma_{\mathrm{G}} \mathrm{erf}(\pi/\sqrt{2}\sigma_{\mathrm{G}})}, \tag{2.30}$$

where $\mathrm{erf}(x)$ is the error function, defined as $\mathrm{erf}(x) = \int_0^x e^{-t^2} dt$. In this case (2.26) is given by

$$\alpha_m = \frac{\Re\left\{\mathrm{erf}\left(\frac{\pi/2 + im\sigma_{\mathrm{G}}^2}{\sqrt{2}\sigma_{\mathrm{G}}}\right)\right\}}{\mathrm{erf}\left(\frac{\pi}{\sqrt{2}\sigma_{\mathrm{G}}}\right) e^{m^2\sigma_{\mathrm{G}}/2}} e^{-im\psi_0}, \tag{2.31}$$

which is well approximated by $\alpha_m \approx e^{-m^2\sigma_{\mathrm{G}}/2} e^{-im\psi_0}$ for narrow angular spread [98].

von-Mises Distributed Field

Another recently proposed non-isotropic scattering model is the von-Mises distribution [95],

$$\mathcal{P}(\psi) = K_{\mathrm{v}} e^{\kappa \cos(\psi - \psi_0)}, \qquad \psi \in [-\pi, \pi), \tag{2.32}$$

where $\kappa \geq 0$ represents the degree of non-isotropy and is related to the angular spread of the AOA. Here the normalization constant K_{v} is given by,

$$K_{\mathrm{v}} = \frac{1}{2\pi I_0(\kappa)}, \tag{2.33}$$

where $I_m(\cdot)$ is the modified Bessel function of the first kind. For $\kappa = 0$ (isotropic scattering) the distribution becomes $\mathcal{P}(\psi) = 1/2\pi$, while for small angular spread, $\kappa = \infty$, the distribution is the Dirac delta function $\mathcal{P}(\psi) = \delta(\psi - \psi_0)$. For the truncated von-Mises field the scattering environment coefficients are given by

$$\alpha_m = \frac{I_{-m}(\kappa)}{I_0(\kappa)} e^{-im\psi_0}. \tag{2.34}$$

Truncated Laplacian Distributed Field

For some scenarios the Laplacian distribution has been proposed as a good model of the scattering distribution [89, 96]. The Laplacian distribution is defined as

$$\mathcal{P}(\psi) = K_{\mathrm{L}} e^{-\sqrt{2}|\psi - \psi_0|/\sigma_{\mathrm{L}}}, \qquad \psi \in [-\pi, \pi), \tag{2.35}$$

where σ_{L} is the standard deviation of the non-truncated distribution and is related to the angular spread of the AOA, and the normalization constant K_{L} is given by

$$K_{\mathrm{L}} = \frac{1}{\sqrt{2}\sigma_{\mathrm{L}}(1 - e^{-\sqrt{2}\pi/\sigma_{\mathrm{L}}})}. \tag{2.36}$$

Here the scattering coefficients (2.26) can be expressed as [98],

$$\alpha_m = \frac{(1 - (-1)^{\lceil m/2 \rceil} e^{-\pi/\sqrt{2}\sigma_{\mathrm{L}}} F_m)}{(1 + \sigma_{\mathrm{L}}^2 m^2/2)(1 - e^{-\pi/\sqrt{2}\sigma_{\mathrm{L}}})}, \tag{2.37}$$

where $F_m = 1$ for even m, and $F_m = m\sigma/\sqrt{2}$ for odd m. In this case, the correlation agrees with the recent derivation in [99], where the spatial correlation is derived for a uniform circular array within a Laplacian distribution scattering environment.

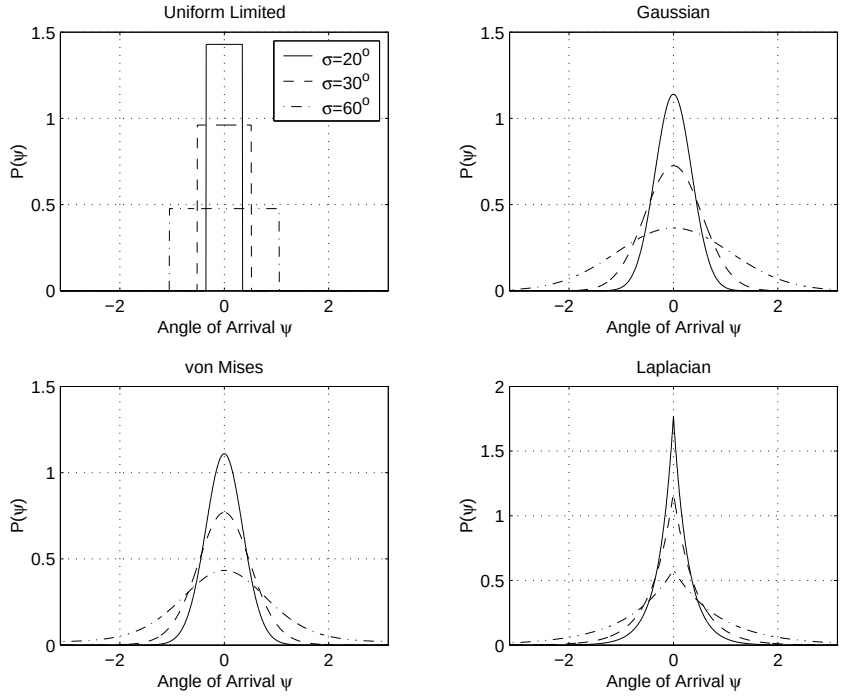

Figure 2.5: Comparison of common scattering distributions: Uniform, Gaussian, von-Mises and Laplacian, for angular spread $\sigma = \{20°, 30°, 60°\}$.

The above distributions are shown in Fig. 2.5 for various angle spreads $\sigma = \{20°, 30°, 60°\}$ about the mean AOA $\psi_0 = 0$, where the angle spread is defined as the standard deviation of the (truncated) distribution and is related to the nonisotropy parameter Δ, σ_{G}, κ, or σ_{L}.

We now explore the effects on spatial correlation of angle spread and mean AOA for the above distributions. In order to compare the spatial correlation we set the angle spread to $\sigma = \{1°, 5°, 10°\}$ for each distribution and increase the separation distance between the antennas, located on the x-axis. The spatial correlation for mean AOA $\psi_0 = 90°$ (broadside) is shown in Fig. 2.6. As shown, the spatial correlation decreases as the antenna spacing and/or the angular spread increases[3]. Here we also see that the scattering models all give similar spatial correlation for the same angular spread, particularly for small spatial separations, indicating that the choice of non-isotropic distribution is unimportant as the distribution variance dominates correlation. However, due to the higher concentration of energy about the mean for the Laplacian distribution[4], for large spatial separation the Laplacian

[3]It is important to note that the correlation does not decrease monotonically with antenna separation, therefore, in certain scenarios increasing the antenna spacing may actually increase spatial correlation.

[4]when compared with the other models for identical angular spread

model generally gives higher correlation than the other three distributions for all angular spreads considered. Finally, we observe that in all cases the von-Mises distribution gives spatial correlation nearly identical to that of the Gaussian model. This agrees with observations made in [95], where it was noted that the von-Mises distribution resembles a Gaussian pdf for large κ (small angular spread) [100, p.61].

In Fig. 2.7 the spatial correlation is shown for mean AOA $\psi_0 = 30^\circ$ (60° from broadside). Similar results are seen as for the broadside case, however, we see significant increase in spatial correlation for all angle spreads and distributions for the same spatial separation as before. Therefore, due to the reduction of resolvable angular spread at the antennas, the spatial correlation is increased as the mean AOA moves away from the broadside angle, where the broadside angle defined as the angle perpendicular to the line connecting the two antennas.

2.3 Capacity Results

In this section we study the spatial effects of non-isotropic scattering and antenna geometry on the capacity of MIMO systems. Using (2.5) and (2.25) along with the expressions for the non-isotropic scattering coefficients given in the previous section, we compute the capacity bound for a variety scattering environments for the uniform linear (ULA) and uniform circular (UCA) arrays. In particular, of interest is the notion of linear in antenna number capacity scaling widely used to advocate the use of MIMO systems [5,66], and how this is effected by non-isotropic scattering and dense array configurations. For all scenarios we consider a signal-to-noise ratio of $\eta = 10$dB. For comparison, the maximum (2.6) and minimum (2.7) capacities are also shown, corresponding to no spatial correlation and full spatial correlation capacities, respectively.

First we consider the capacity of an 8 antenna fixed aperture (length/diameter) 3.5λ array for each scattering distribution against the non-isotropy factor and for mean AOA $\psi_0 = \{0^\circ, 45^\circ, 90^\circ\}$. As shown in Fig. 2.8, the capacity increases for increasing non-isotropy factor for the uniform, Gaussian, and Laplacian distributions, corresponding to an increase in angle spread surrounding the receiver. For the von-Mises distribution, the capacity decreases as κ increases, corresponding to a reduction in angular spread at the receiver. For all distributions, the reduction in capacity with decreasing angular spread is most pronounced for the ULA when the mean AOA is inline with the array ($\psi_0 = 0^\circ$). However, for the UCA the capacity is unaffected by mean AOA, advocating the use of 2D array configurations, which

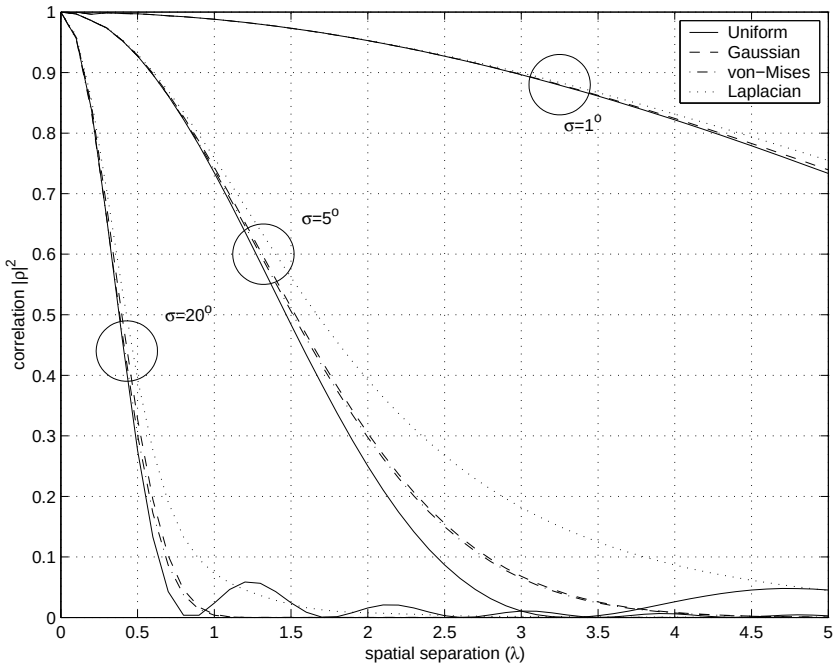

Figure 2.6: Spatial correlation between two antennas for mean AOA 90° (broadside) against spatial separation for Uniform, Gaussian, von-Mises, and Laplacian scattering distributions and angular spreads $\sigma = \{1°, 5°, 20°\}$.

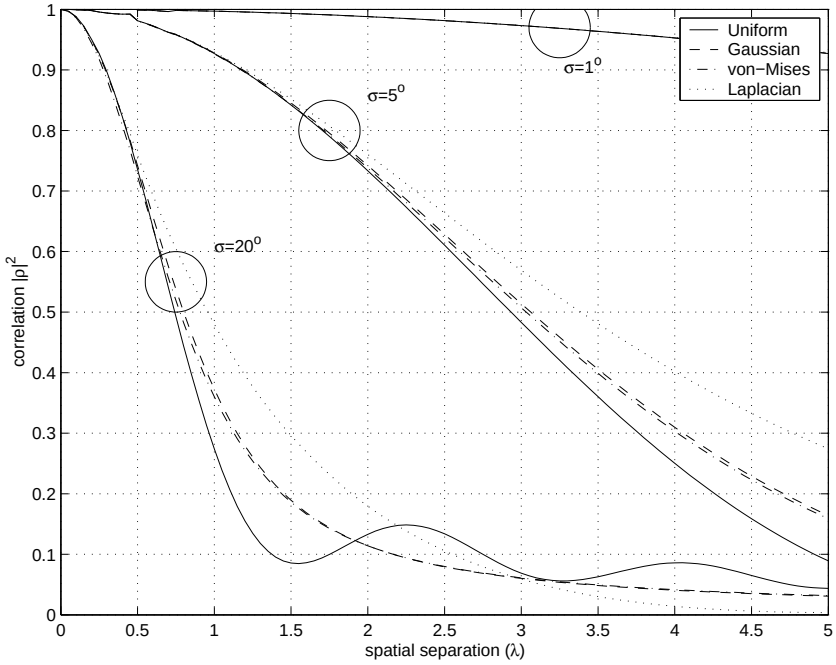

Figure 2.7: Spatial correlation between two antennas on the x-axis for mean AOA 30° (60° from broadside) against spatial separation for Uniform, Gaussian, von-Mises, and Laplacian scattering distributions and angular spreads $\sigma = \{1°, 5°, 20°\}$.

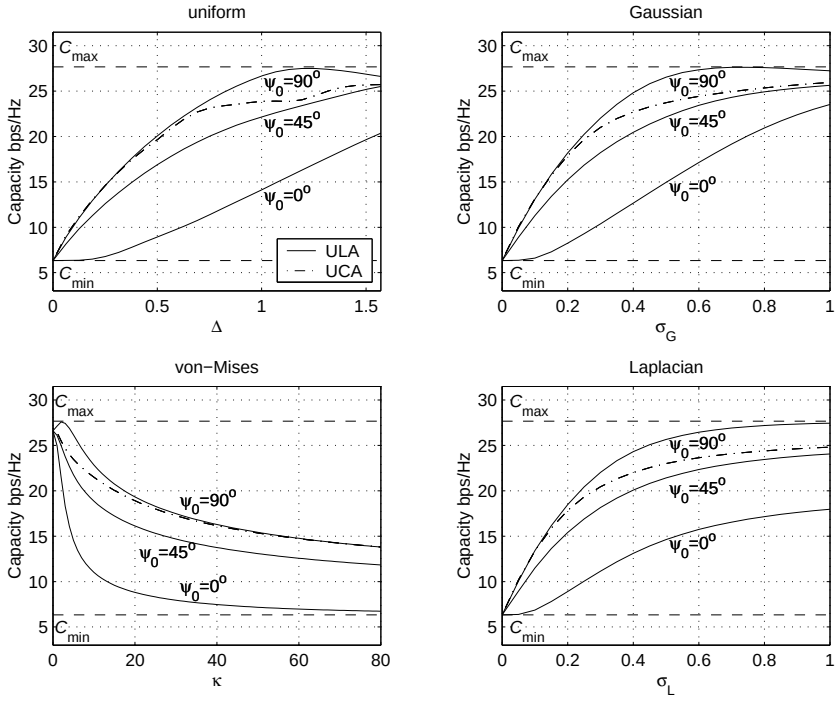

Figure 2.8: Capacity for non-isotropic distributed scattering with mean AOA $\psi_0 = \{0°, 45°, 90°\}$ and increasing nonisotropy factor, for the 8 antenna ULA and UCA of aperture width (length/diameter) 3.5λ.

are less sensitive to the mean direction of signal arrival, compared to the 1D linear arrays.

We now consider the capacity scaling of a MIMO system as the number of receive antennas increases whilst the array aperture size remains fixed. First we consider the ULA and UCA of aperture (length/diameter) $D = \{0.4\lambda, 0.6\lambda, 0.8\lambda\}$ in an isotropic scattering environment, shown in Fig. 2.9. It can be observed from Fig. 2.9 that the capacity scales almost linearly with the number of antennas before reducing to logarithmic growth after some saturation point. The saturation point is clearly related to the aperture of the array for both the ULA and UCA, where smaller apertures saturate for lower numbers of receive antennas. The capacity scaling of the ULA and UCA is shown in Fig. 2.10 and Fig. 2.11, respectively, for fixed aperture 4λ with angular spread $\sigma = \{1°, 5°, 20°\}$ of the various scattering distributions. Again, for both ULA and UCA saturation is observed in the capacity scaling, where the growth reduces from approximately linear to logarithmic after the number of antennas reaches a distinct threshold. Note that the array aperture is sufficiently large so any saturation is due to the reduction of angular spread at the receiver, which is clearly seen in both figures.

To emphasis the effects of saturation with antenna numbers seen above, we can

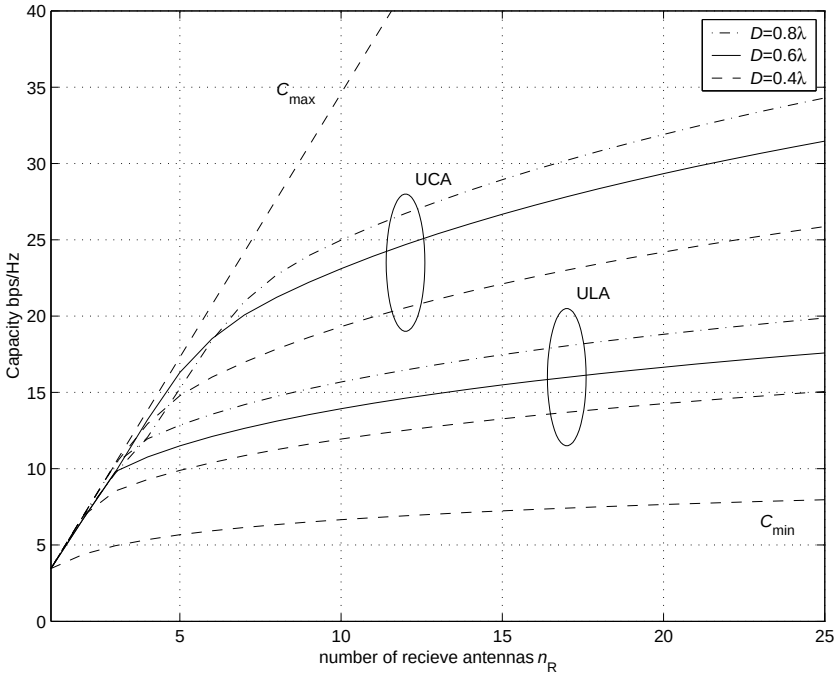

Figure 2.9: Capacity scaling of the ULA and UCA with fixed aperture (length/diameter) $D = \{0.4\lambda, 0.6\lambda, 0.8\lambda\}$ in an isotropic scattering environment.

write the capacity (2.5) as

$$C = C_{\max} + \Delta C \tag{2.38}$$

where $C_{\max}$ is the maximum antenna capacity (2.6), and $\Delta C = \log |\mathbf{\Gamma}_{\mathrm{rx}}|$, where $\mathbf{\Gamma}_{\mathrm{rx}}$ is the $n_{\mathrm{R}} \times n_{\mathrm{R}}$ matrix

$$\mathbf{\Gamma}_{\mathrm{rx}} = \begin{bmatrix} 1 & \frac{\eta}{1+\eta}\rho_{12} & \cdots & \frac{\eta}{1+\eta}\rho_{1n_{\mathrm{R}}} \\ \frac{\eta}{1+\eta}\rho_{21} & 1 & & \vdots \\ \vdots & & \ddots & \\ \frac{\eta}{1+\eta}\rho_{n_{\mathrm{R}}1} & \cdots & & 1 \end{bmatrix}. \tag{2.39}$$

Note that $\mathbf{\Gamma}_{\mathrm{rx}}$ is a positive semi-definite matrix with $0 \leq |\Gamma_{\mathrm{rx}}| \leq 1$, thus $\Delta C \leq 0$, therefore ΔC represents the loss of capacity due to antenna correlation at the receiver. The loss of capacity due to correlation is shown in Fig. 2.12 for a ULA for fixed aperture $D = \{0.5\lambda, 1.5\lambda, 2.5\lambda, 3.5\lambda, 4.5\lambda\}$ in an isotropic scattering environment. Here the distinct saturation point in antenna number is clearly visible with increasing aperture. Likewise, the loss in capacity is significant beyond an antenna saturation point for increasing angular spread as shown in Fig. 2.13 for a ULA of

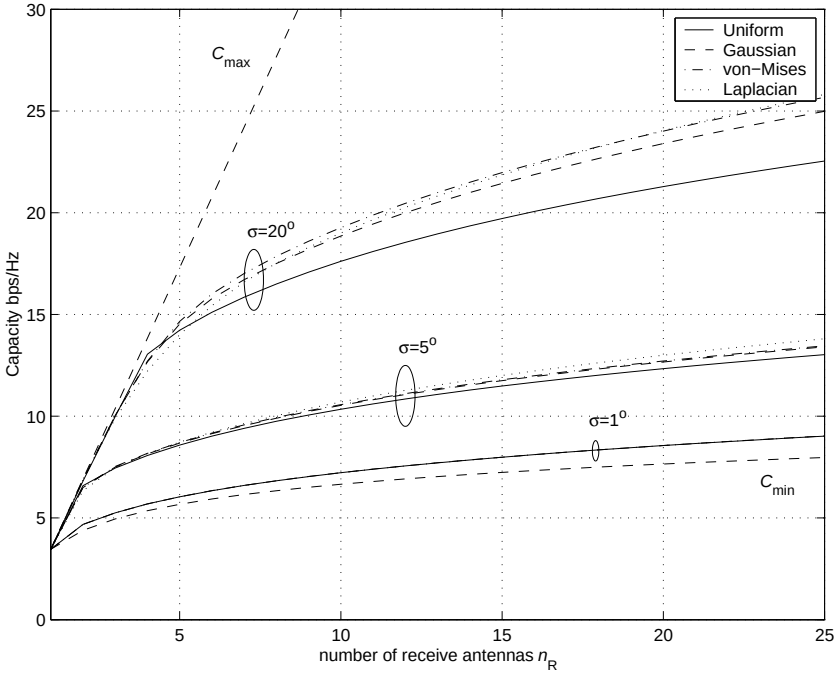

Figure 2.10: Capacity scaling of the broadside uniform linear array with fixed aperture 4λ for angular spread $\sigma = \{1°, 5°, 20°\}$ of the various scattering distributions.

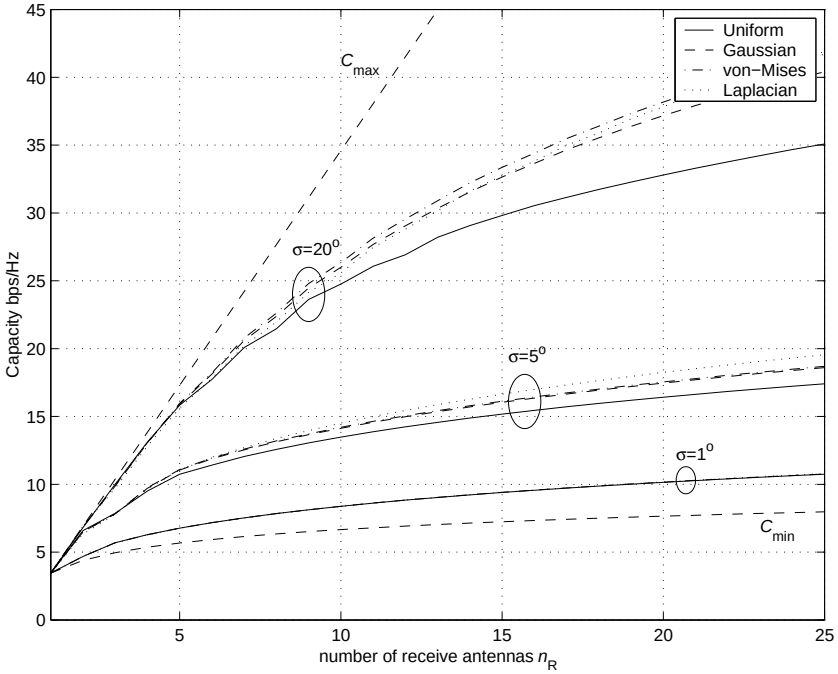

Figure 2.11: Capacity scaling of the UCA with fixed aperture 4λ for angular spread $\sigma = \{1°, 5°, 20°\}$ of the various scattering distributions.

fixed aperture 4λ.

Using a singular value decomposition of the channel matrix, the capacity of a MIMO system can be shown to be equivalent to the sum of the capacities of $\min(n_{\mathrm{T}}, n_{\mathrm{R}})$ subchannels, each with independent power gains corresponding to the eigenvalues of the channel matrix product $\boldsymbol{H}\boldsymbol{H}^{\dagger}$ [7]. The subchannel gains depend on the correlation between channel branches, and as the correlation increases some subchannels have gains too small to convey information at any significant rate [65]. Therefore, as seen here, as the number of antennas increases for a fixed aperture, or angular spread, due to increased channel branch correlation there exists a saturation point at which the subchannels generated by any addition antennas have negligible gains and do not increase the capacity, other than logarithmic array gain.

This saturation effect has significant implications for realizable MIMO systems, as the saturation point gives the optimal number of antennas required to maximize capacity, after which there are negligible gains. Asymptotic results for the fixed aperture ULA in isotropic scattering are studied in [101], with identical independent results in [102]. However, the saturation point for fixed aperture arrays has not been addressed so far, except for the special case of the UCA [103]. Promising results from a spatial model presented in [104] indicate the throughput of a MIMO system is limited by the radius of the region containing the antenna arrays, agreeing with observations in this chapter. Likewise, to the authors' knowledge, no analytical results exist for the capacity scaling saturation due to insufficient angular spreads, although the effect on capacity due to limited angular spread at the transmitter has been reported in [65], and observed elsewhere, e.g. [105], via simulation.

2.4 Summary and Contributions

In i.i.d. Rayleigh fading channels the capacity of a multi-antenna system has been shown to grow linearly with antenna numbers. However, in realistic propagation environments, the fading is correlated due to insufficient antenna spacing or angular spread, and the capacity is often significantly lower than that predicted for i.i.d. fading. This chapter has investigated the capacity of MIMO systems for realistic array sizes and scattering environments.

Some specific contributions made in this chapter are:

1. By assuming a sufficient number of sufficiently separated transmit antennas a closed-form expression for the capacity of a MIMO random fading channel

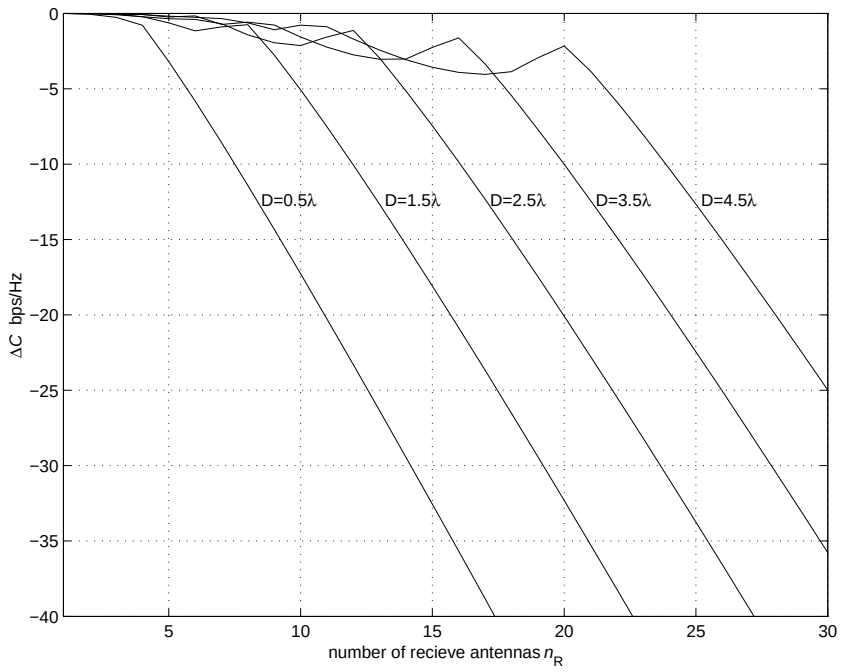

Figure 2.12: Capacity loss due to correlation of the broadside ULA for fixed aperture $D = \{0.5\lambda, 1.5\lambda, 2.5\lambda, 3.5\lambda, 4.5\lambda\}$ in an isotropic scattering environment.

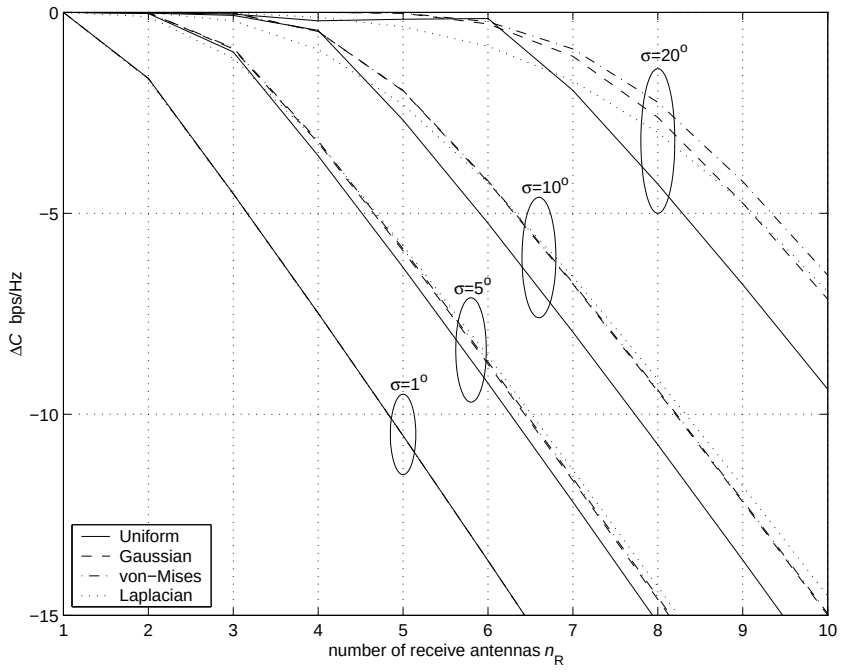

Figure 2.13: Capacity loss due to correlation of the broadside ULA of fixed aperture 4λ for angular spreads $\sigma = \{1°, 5°, 10°, 20°\}$ of the various scattering distributions.

is derived.

2. Using a novel channel model the separate effects of the scattering environment and antenna array configuration can be seen on the spatial correlation at the receiver, allowing for capacity evaluation of systems for a wide variety of scattering environments and antenna placement.

3. It is shown that the angular spread surrounding the receiver dominates the spatial correlation and thus capacity, rather than the choice of scattering distribution. However, this may not hold for multi-modal distributions which were not discussed here, but are fully captured by the analytical framework.

4. For 1D arrays it was observed that the mean AOA has a significant impact on the capacity of the system, advocating the use of 2D arrays, which are less sensitive to the mean direction of signal arrival.

5. The capacity was shown to suffer from a saturation effect in the number of antennas for a fixed angular spread or array aperture. This saturation point, at which the capacity scaling is reduced from linear to logarithmic increase with increasing antenna numbers, is an important factor in the design of practical MIMO systems and is further investigated in Chapter 3.

Chapter 3

Saturation Effects of Spatially Constrained MIMO Channels

MIMO wireless systems have recently received considerable attention, due in part to the outstanding capacity gains achievable when the channel offers independent fades between antennas. However, the capacity of a wireless fading MIMO system is significantly reduced as the channel matrix elements become correlated.

In practice, the physical size of the antenna array is limited due to physical constraints imposed by its location and application, for example, the ever decreasing size of mobile handsets places constraints on the size of the antenna array employed. This aperture constraint, along with any limited angular spread surrounding the antenna array, significantly increases the correlation between antennas as the number of antennas within the aperture is increased. Although several works have considered the impact of correlation on capacity using correlation models (e.g., [10, 65, 71, 72]), the effects of the physical constraints, such as aperture size and non-isotropic scattering, have not been explicitly addressed.

Recent work studying constrained linear arrays [101, 102, 106] has given important insights into the capacity limits for large numbers of antennas. However, from a practical perspective, it is desirable to maximize capacity for a minimum of cost, therefore the capacity behavior for a finite number of antennas is of considerable importance.

In this chapter the theoretical capacity performance of spatially constrained channels is considered for a finite number of antennas. A spatially constrained channel has physical constraints, such as aperture size and non-isotropic scattering, which limit its performance when compared to unconstrained channels, such as the i.i.d. Rayleigh fading model.

3.1 Eigen-analysis of MIMO Capacity

Consider a single-user narrowband flat fading wireless communication system, with n_{T} transmit antennas and n_{R} receive antennas. It is assumed the transmitted signal vector is composed of statistically independent equal power components, each with a Gaussian distribution, and the channel is known at the receiver. Consider the case of a large number of sufficiently separated transmit antennas, such that the transmit branches are uncorrelated[1], then the ergodic capacity of such a system is given by (2.5). Expanding the determinant by the product of its argument's eigenvalues, the capacity can be expressed as

$$C = \log |\boldsymbol{I}_{n_{\mathrm{R}}} + \eta \boldsymbol{R}| \tag{3.1a}$$

$$= \log \prod_{n=0}^{K-1} (1 + \eta \lambda_n) \tag{3.1b}$$

$$= \sum_{n=0}^{K-1} \log(1 + \eta \lambda_n), \tag{3.1c}$$

where $K = \mathrm{rank}(\boldsymbol{R}) \leq n_{\mathrm{R}}$, and λ_n are the rank and eigenvalues of the spatial correlation matrix $\boldsymbol{R}$, respectively. Since the capacity of a single-input single-output (SISO) channel is given by $\log(1+\alpha)$, where α is the SNR at the receiver, then the capacity (3.1c) is equivalent to the contribution of K parallel SISO subchannels, each with independent gain corresponding to the eigenvalues of the correlation matrix $\boldsymbol{R}$. Therefore, the properties of the set $\{\lambda_n\}$ play a vital role in the achievable capacity for a spatially constrained channel.

For n_{R} antennas $\sum_n \lambda_n = \mathrm{trace}(\boldsymbol{R}) = n_{\mathrm{R}}$, hence the maximum of (3.1c) will occur for $K = n_{\mathrm{R}}$ independent equal gain sub-channels, $\lambda_n = 1, \forall n$, giving linear growth in capacity with increasing n_{R},

$$C_{\max} = n_{\mathrm{R}} \log(1 + \eta). \tag{3.2}$$

In contrast, minimum capacity will occur when all the power is used on a single sub-channel, i.e., $\lambda_0 = n_{\mathrm{R}}$, and $\lambda_n = 0, \forall n \neq 0$, corresponding to fully correlated antennas. In this case the capacity is given by

$$C_{\min} = \log(1 + n_{\mathrm{R}} \eta), \tag{3.3}$$

[1] $E\left\{h_{rt}\overline{h_{rt'}}\right\} = 0, \forall\, t \neq t'$, where h_{rt} is the channel gain from the t-th transmit antenna to the r-th receive antenna.

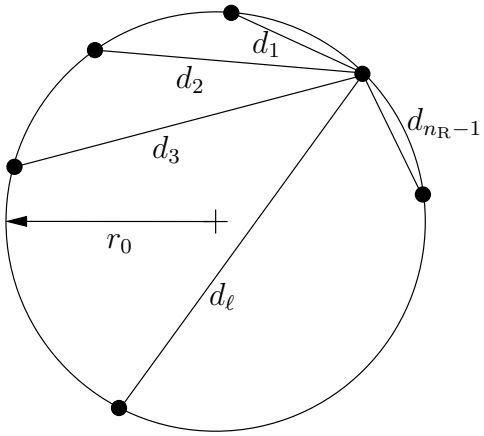

Figure 3.1: Example of a UCA of radius r_0, where d_ℓ denotes the distance between any antenna and its ℓ-th neighbor in a clockwise or anticlockwise direction.

which grows logarithmically with n_R. Therefore, the capacity still increases with antenna number even when the antennas are correlated, this array-gain effect is due to the assumption of ideal antennas and independent noise samples, and is considered in detail in Section 3.3.4.

For a spatially constrained channel, as the number of antennas is increased in a fixed aperture, with restricted scattering angular spread, the correlation between antennas will increase. This increase in spatial correlation will limit the number of significant eigenvalues, and therefore limit the otherwise linear capacity growth with increasing numbers of antennas. As more antennas are placed in the aperture, they will be highly correlated with the other antennas and therefore the logarithmic array-gain effect will dominate the capacity growth. Therefore, from a design perspective, of considerable interest is the saturation point in the number of antennas at which the capacity scaling is reduced to logarithmic with increasing number of antennas.

Section 3.2 begins by considering the simple case a UCA of fixed aperture within an isotropic scattering environment. This case provides insights into the capacity scaling of spatially constrained arrays via the nice property that the corresponding correlation matrix is symmetrically circulant, and gives closed form expressions for the eigenvalues. This result is then generalized to arbitrary arrays and general scattering environments in the remainder of the chapter.

3.2 Uniform Circular Array

Consider a UCA with radius r_0 and n_{R} antennas. Denote the set $\{d_\ell\}_{\ell=0}^{n_{\mathrm{R}}-1}$ as the distance between any antenna and the other $n_{\mathrm{R}}-1$ antennas in the array (in a clockwise or anticlockwise direction), as shown in Fig. 3.1, with $d_0 = 0$ being the distance between the antenna and itself, then

$$d_\ell = 2r_0 \sin(\pi\ell/n_{\mathrm{R}}). \tag{3.4}$$

For the special case of scattering over all angles in the plane, we have a 2D isotropic diffuse field at the receiver and the spatial correlation between any element on the UCA and its ℓ-th neighbor is given by [16]

$$\rho_\ell = J_0(k\, d_\ell), \tag{3.5}$$

where $J_0(\cdot)$ are Bessel functions of the first kind, and $k = 2\pi/\lambda$ is the wavenumber. Due to UCA symmetry, for $\ell > 0$, $\rho_\ell = \rho_{n_{\mathrm{R}}-\ell}$, and the correlation matrix becomes a $n_{\mathrm{R}} \times n_{\mathrm{R}}$ symmetric circulant matrix,

$$\boldsymbol{R} = \mathrm{Circ}\left[\rho_0, \rho_1, \ldots, \rho_{\lceil \frac{n_{\mathrm{R}}-1}{2} \rceil}, \rho_{\lfloor \frac{n_{\mathrm{R}}-1}{2} \rfloor}, \ldots, \rho_2, \rho_1\right], \tag{3.6}$$

where $\lceil\cdot\rceil$ and $\lfloor\cdot\rfloor$ are the ceiling and floor operators respectively, and

$$\mathrm{Circ}\left[x_1, x_2, \ldots, x_N\right] \triangleq \begin{bmatrix} x_1 & x_2 & \cdots & x_N \\ x_N & x_1 & \cdots & x_{N-1} \\ \vdots & \vdots & \ddots & \vdots \\ x_2 & x_3 & \cdots & x_1 \end{bmatrix}, \tag{3.7}$$

defines the circulant matrix.

3.2.1 Eigenvalues of Spatial Correlation Matrix $\boldsymbol{R}$

The eigenvalues of the symmetric circulant matrix are given by the discrete Fourier transform of the first row [107], therefore the eigenvalues of the $n_{\mathrm{R}} \times n_{\mathrm{R}}$ matrix $\boldsymbol{R}$ are given by the simple closed form expression

$$\lambda_n = \sum_{\ell=0}^{n_{\mathrm{R}}-1} \rho_\ell\, e^{i2\pi n\ell/n_{\mathrm{R}}}. \tag{3.8}$$

For a UCA in a 2D isotropic diffuse field the correlation coefficients are real and symmetric, hence (3.8) represents the Discrete Cosine Transform (DCT) of the spatial correlation coefficients,

$$\lambda_n = \sum_{\ell=0}^{n_\mathrm{R}-1} \rho_\ell \cos\left(2\pi n\ell/n_\mathrm{R}\right). \tag{3.9}$$

Since $\boldsymbol{R}$ is a positive-semidefinite Hermitian matrix and with the properties of the DCT it is easy to show the following:

$$\lambda_n \in \mathbb{R}, \tag{3.10}$$

$$\lambda_n \geq 0, \tag{3.11}$$

$$\lambda_{n_\mathrm{R}-n} = \lambda_n = \lambda_{-n}\,,\ n > 0, \tag{3.12}$$

that is, the eigenvalues are real, non-negative and symmetric.

The capacity saturation of the UCA observed in Chapter 2.3, where the capacity growth was reduced from approximately linear to logarithmic with increased antenna numbers, suggests there is fixed limit to the number of significant eigenvalues of $\boldsymbol{R}$ which is dependent on the radius of the array. Note, as discussed in Chapter 2, the Bessel function $J_0(\cdot)$ is qualitatively similar to the spherical Bessel function $j_0(\cdot) \equiv \mathrm{sinc}(\cdot)$, which has a bandlimited Fourier transform. Hence, since (3.8) is the discrete Fourier transform of the correlation function $J_0(kd_\ell)$, one would expect to observe bandlimited eigenvalues, that is, $\lambda_n \approx 0$ for $|n| \geq N$ for some integer $N < n_\mathrm{R}$. Therefore, in the following the properties of $|\lambda_n|$ are explored for increasing n.

Substitution of (3.5) and (3.4) into (3.9) gives

$$\lambda_n = \sum_{\ell=0}^{n_\mathrm{R}-1} J_0(2kr_0 \sin\left(\pi\ell/n_\mathrm{R}\right)) \cos\left(2n\pi\ell/n_\mathrm{R}\right), \tag{3.13}$$

letting $\xi = \pi\ell/n_\mathrm{R}$ and assuming a large number of antennas, we can approximate (3.13) with the integral

$$\lambda_n \approx \frac{n_\mathrm{R}}{\pi} \int_0^\pi J_0(2kr_0 \sin\xi) \cos\left(2n\xi\right) \mathrm{d}\xi, \tag{3.14}$$

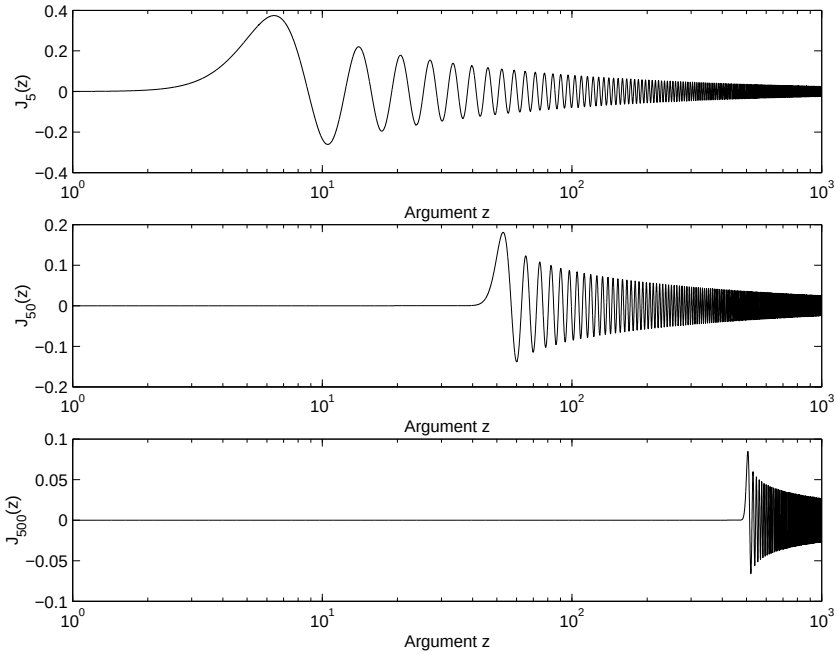

Figure 3.2: High pass nature of the Bessel functions $J_n(z)$, for $n = \{5, 50, 500\}$ versus argument z in logarithmic scale.

for $n \in [0, \lceil (n_{\mathrm{R}} - 1)/2 \rceil]$. Using the identity [108, p.32]

$$J_n^2(z) = \frac{1}{\pi} \int_0^{\pi} J_0(2z \sin\psi) \cos(2n\psi) \mathrm{d}\psi, \tag{3.15}$$

then the eigenvalues can be expressed as

$$\lambda_n \approx n_{\mathrm{R}} J_n^2(kr_0), \tag{3.16}$$

which is asymptotically equal to (3.13) with increasing antenna number.

Bessel functions $J_n(z)$, $|n| > 0$ exhibit spatially high pass behavior, that is, for fixed order n, $J_n(z)$ starts small and becomes significant for arguments $z \approx \mathcal{O}(n)$, as shown in Fig. 3.2. Therefore, for a fixed argument z, the Bessel function $J_n(z)$ is approximately zero for all but a finite set of low order $|n| \leq N$, thus, giving a finite limit to the number of significant eigenvalues (3.16). Consider the following bound [109, p.362] on the bessel functions for $z, n \geq 0$

$$|J_n(z)| \leq \frac{z^n}{2^n \Gamma(n+1)}, \tag{3.17}$$

where $\Gamma(\cdot)$ is the Gamma function, then, since $2^n\Gamma(n+1)$ increases significantly faster than the exponential z^n, (3.17) will rapidly approach 0 for some $n > 0$ for

which $2^n\Gamma(n+1) > z^n$. Using a relaxed Stirling lower bound[2] [110] for $\Gamma(n+1)$, we see that Bessel functions $J_n(z) \approx 0$ for orders $n > ez/2$.

Asserting that n must be an integer, and given the vanishing nature of the Bessel functions, define an *eigenvalue threshold*

$$N \triangleq \lceil \pi e r_0/\lambda \rceil, \tag{3.18}$$

such that the eigenvalues $\lambda_n \approx 0$ for $n > N$. Therefore, given the symmetric nature of the eigenvalues (3.12), for any number of antennas, $n_{\mathrm{R}} \geq 2N+1$, there is a finite set of $2N+1$ non-vanishing eigenvalues,

$$\boldsymbol{\lambda} = \{\lambda_{-N}, \lambda_{-N+1}, \cdots, \lambda_0, \cdots, \lambda_{N-1}, \lambda_N\}, \tag{3.19}$$

whose number of elements grows only with the radius of the array, and is independent on the number of antennas.

Therefore, for a UCA in a 2D isotropic diffuse field there is a finite set of significant spatial correlation matrix eigenvalues, where the set size increases linearly with the radius of the array and is independent of the number of antennas. Figure 3.3 shows the eigenvalues of the spatial correlation matrix $\boldsymbol{R}$ for various UCA radii in a 2D isotropic diffuse field. Shown as a solid black line, it can be seen that the theoretical eigenvalue threshold defines the boundary between the significant and vanishing eigenvalues for each array radius.

3.2.2 Capacity Scaling Limits

Due to the dependence of (3.1c) on the eigenvalues of the spatial correlation matrix $\boldsymbol{R}$ we see that the eigenvalue threshold derived in the previous section has significant implications on the capacity growth with increasing antenna numbers. In this section we show that this fixed set size of significant eigenvalues, regardless of the the number of antennas, leads to an antenna saturation effect on MIMO capacity.

Consider a UCA array with n_{R} antennas, then given the symmetric nature of the eigenvalues (3.12) the capacity (3.1c) can be written as

$$C = \sum_{n=-\lfloor (n_{\mathrm{R}}-1)/2 \rfloor}^{\lceil (n_{\mathrm{R}}-1)/2 \rceil} \log\left(1 + \eta\lambda_n\right). \tag{3.20}$$

For a UCA of radius r_0 placed in a 2D isotropic diffuse field, then from (3.19)

[2] $\Gamma(z+1) > \sqrt{2\pi z}\, z^z\, e^{-z} > z^z\, e^{-z}$, $z > 0$

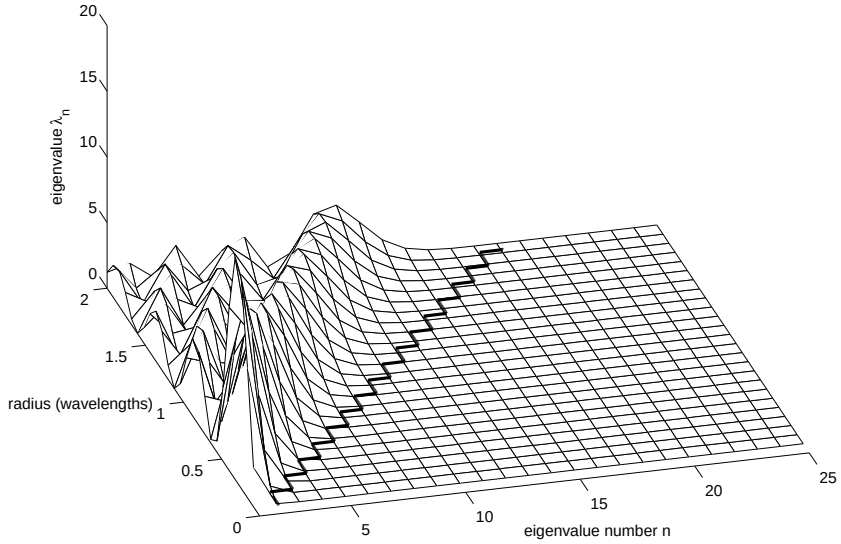

Figure 3.3: The eigenvalues of the spatial correlation matrix for various UCA radii in a 2D isotropic diffuse scattering field. The dark solid line represents the theoretical eigenvalue threshold, and clearly shows the boundary between the significant and vanishing eigenvalues of the spatial correlation matrix for each array radius.

and (3.18), for $n_{\mathrm{R}} \geq 2N+1$ the channel capacity given by (3.20) is well approximated using the set of $2N+1$ non-vanishing eigenvalues, that is,

$$C \approx \sum_{n=-N}^{N} \log\left(1+\eta\lambda_n\right). \tag{3.21}$$

Now consider two UCAs of equal radius r_0 with antenna numbers $n_{\mathrm{R}1}, n_{\mathrm{R}2} \geq 2N+1$. Denote the eigenvalues of the spatial correlation matrices of the UCAs with $n_{\mathrm{R}1}$ and $n_{\mathrm{R}2}$ antennas as $\lambda_n^{(n_{\mathrm{R}1})}$ and $\lambda_n^{(n_{\mathrm{R}2})}$, respectively, then from (3.16) we have the following relationship between the significant eigenvalues of these arrays,

$$\frac{\lambda_n^{(n_{\mathrm{R}1})}}{n_{\mathrm{R}1}} \approx \frac{\lambda_n^{(n_{\mathrm{R}2})}}{n_{\mathrm{R}2}}, \tag{3.22}$$

with the approximation asymptotically equal with the number of antennas. Define

$$n_N \triangleq 2N+1, \tag{3.23}$$

as the minimum number of antennas required to generate the full set of non-zero

eigenvalues (3.19), then letting $n_{\mathrm{R}1} = n_{\mathrm{R}}$ and $n_{\mathrm{R}2} = n_N$ we have

$$\lambda_n \approx \frac{n_{\mathrm{R}}}{n_N} \lambda_n^{(n_N)}, \tag{3.24}$$

where $\lambda_n^{(n_N)}$ are the eigenvalues of the $n_N \times n_N$ spatial correlation matrix of the n_N antenna UCA. Thus the non-vanishing eigenvalues for any UCA of radius r_0 with number of antennas $n_{\mathrm{R}} \geq n_N$ are simply scaled versions of the eigenvalues generated by an array with n_N antennas. Substituting (3.24) into (3.21) gives the capacity as

$$C \approx \sum_{n=-N}^{N} \log\left(1 + n_{\mathrm{R}}\, \eta \frac{\lambda_n^{(n_N)}}{n_N}\right), \quad n_{\mathrm{R}} \geq n_N, \tag{3.25}$$

which grows logarithmically with antenna number n_{R}. Therefore, the capacity gain is reduced to at most logarithmic growth once the number of antennas reaches a saturation point given by $n_N = 2N + 1$. Let $\widehat{\eta} = (n_{\mathrm{R}}/n_N)\eta$ be the scaled average SNR at each antenna, then (3.25) shows that the effect of any additional antennas above the saturation point is an increase in the average SNR, or in other words, an array gain effect due to the assumption of independent noise at each antenna.

Therefore, for a MIMO system with a UCA in a 2D isotropic scattering environment there exists a saturation point in the number of antennas, which is dependent only on the radius of the array, after which the addition of more antennas gives diminishing (logarithmic) capacity gains. It can be observed from Fig. 3.4 that the capacity (3.1c) does indeed increase approximately with the maximum theoretical capacity (3.2) up until the theoretical saturation point (3.23), after which logarithmic capacity scaling occurs for increasing antenna number.

The results presented in this section are of considerable importance in the design of MIMO systems, where it is desirable to maximize the capacity at a minimum cost. However, although common, the UCA is only one of many array geometries possible for a given region of space. Also of interest is the more realistic case of of non-isotropic scattering environments, which will impact on the performance of the MIMO system.

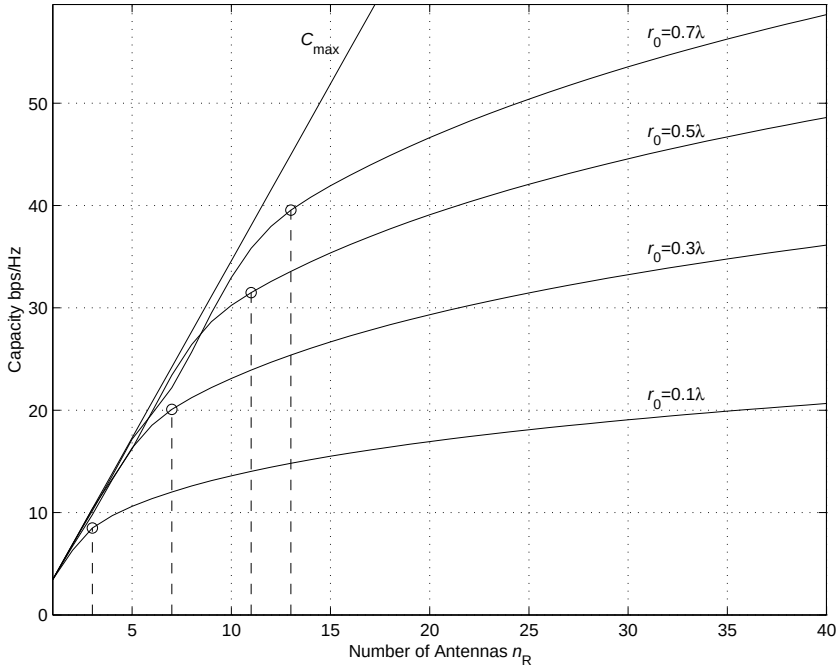

Figure 3.4: Capacity of MIMO systems for various antenna numbers of a UCA with radii $r_0 = \{0.1\lambda, 0.3\lambda, 0.5\lambda, 0.7\lambda\}$ in a 2D isotropic diffuse scattering field, along with the theoretical maximum capacity. As indicated by the dashed lines for each radii, the theoretical antenna saturation point gives a good indication where the MIMO system saturates and hence increasing antenna numbers gives only marginal capacity gain.

3.3 Arbitrary Arrays in General Scattering Environments

Consider the 2D scattering environment shown in Fig. 3.5, where n_{R} receiver antennas, located at $\boldsymbol{y}_r = (\|\boldsymbol{y}_r\|, \theta_r)$ in polar coordinates, are constrained within a circular receiver aperture of radius r_0. Let $g_t(\psi)$ represent the effective random complex gain of the scatterers for a transmitted signal x_t arriving at the receiver array from direction ψ via any number of paths through the scattering environment. The region of radius r_{S} encompassing the receiver aperture contains no scatterers and is assumed large enough such that any scatterers are farfield to all receiver antennas. The noiseless received signals at antenna r located at $\boldsymbol{y}_r$ is then given by

$$z_r = \sum_{t=1}^{n_{\mathrm{T}}} x_t \int_{\mathbb{S}^1} g_t(\widehat{\boldsymbol{\psi}}) e^{-ik\boldsymbol{y}_r \cdot \widehat{\ }} d\psi \tag{3.26a}$$

$$= \sum_{t=1}^{n_{\mathrm{T}}} h_{rt} x_t, \tag{3.26b}$$

where $\mathbb{S}^1$ the 1-sphere or unit circle, $\widehat{\boldsymbol{\psi}}$ is a unit vector in the direction ψ, and define

$$h_{rt} \triangleq \int_{\mathbb{S}^1} g_t(\widehat{\boldsymbol{\psi}}) e^{-ik\boldsymbol{y}_r \cdot \widehat{\ }} d\psi, \tag{3.27}$$

as the random complex channel gain from the t-th transmitter to the r-th receiver.

3.3.1 Spatial Correlation Matrix Decomposition

The normalized spatial correlation function between the complex envelopes of two received signals z_r and $z_{r'}$ located at positions $\boldsymbol{y}_r$ and $\boldsymbol{y}_{r'}$, respectively, was shown in Chapter 2 to be given by

$$\rho_{rr'} = \int_{\mathbb{S}^2} \mathcal{P}(\widehat{\boldsymbol{\psi}}) e^{-ik(\boldsymbol{y}_r - \boldsymbol{y}_{r'}) \cdot \widehat{\ }} ds(\widehat{\boldsymbol{\psi}}), \tag{3.28}$$

where $\mathcal{P}(\widehat{\boldsymbol{\psi}})$ is the power azimuth distribution (PAD) describing the scattering environment surrounding the receiver.

Consider the 2D Jacobi-Anger modal expansion of plane waves [79]

$$e^{ik\boldsymbol{y} \cdot \widehat{\ }} = \sum_{m=-\infty}^{\infty} J_m(k \|\boldsymbol{y}\|) e^{-im(\theta_y - \pi/2)} e^{im\psi}, \tag{3.29}$$

then the spatial correlation (3.28) can be expressed as

$$\rho_{rr'} = \sum_{m=-\infty}^{\infty} \sum_{m'=-\infty}^{\infty} \overline{\mathcal{J}_m(\boldsymbol{y}_r)} \mathcal{J}_{m'}(\boldsymbol{y}_{r'}) \int_{\mathbb{S}^1} \mathcal{P}(\psi) e^{-i(m-m')\psi} d\psi, \tag{3.30}$$

where

$$\mathcal{J}_m(\boldsymbol{y}_r) \triangleq J_m(k \|\boldsymbol{y}_r\|) e^{-im(\theta_r - \pi/2)}, \tag{3.31}$$

is the *spatial-to-mode* function, which maps the aperture sampling point $\boldsymbol{y}_r$ to the m-th mode of the expansion (3.29).

As the scattering gain function $g_t(\psi)$ is periodic with ψ, it is natural to expand

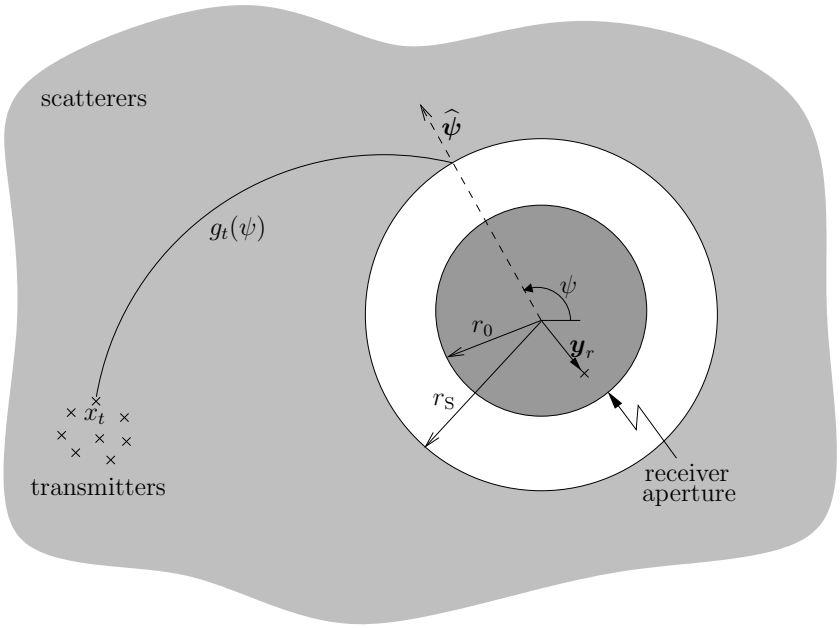

Figure 3.5: Two dimensional scattering model for a flat fading MIMO system. $g_t(\psi)$ represents the effective random complex gain of the scatterers for a transmitted signal x_t arriving at the receiver array from direction ψ via any number paths through the scattering environment. The receiver aperture of radius r_0 contains all receiver antennas, and is contained within a scatterer free region whose radius r_{S} is assumed large enough such that any scatterers are farfield to all receive antennas.

it using a modal basis function expansion

$$g_t(\psi) = \sum_{m=-\infty}^{\infty} a_{t,m}\, e^{im\psi}, \tag{3.32}$$

where the coefficients

$$a_{t,m} = \int_{\mathbb{S}^1} g_t(\psi)\, e^{-im\psi} d\psi, \tag{3.33}$$

parameterize the random scattering environment for the t-th transmitter. Define the normalized correlation between the m and m' modes at the receiver as[3]

$$\gamma_{m,m'} = \frac{\sum_{t=1}^{n_{\mathrm{T}}} E\left\{a_{t,m}\overline{a_{t,m'}}\right\}}{\sum_{t=1}^{n_{\mathrm{T}}} \sqrt{E\left\{a_{t,m}\overline{a_{t,m}}\right\} E\left\{a_{t,m'}\overline{a_{t,m'}}\right\}}}. \tag{3.34}$$

Assuming a zero-mean uncorrelated scattering environment, the covariance between receiver modes m and m' for the t-th transmitter is given by

$$E\left\{a_{t,m}\overline{a_{t,m'}}\right\} = \int_{\mathbb{S}^1} G_t(\psi)\, e^{-i(m-m')\psi} d\psi, \tag{3.35}$$

where $G_t(\psi) = E\left\{|g_t(\psi)|^2\right\}$. Therefore, the modal correlation (3.34) is given by

$$\gamma_{m,m'} = \gamma_{m-m'} = \int_{\mathbb{S}^1} \mathcal{P}(\psi) e^{-i(m-m')\psi} d\psi, \tag{3.36}$$

where $\mathcal{P}(\psi)$ is the power azimuth distribution (2.17). Note that the modal correlation expression is identical to the scattering environment coefficients α_n (2.21), for $n = m - m'$, therefore, closed-form expressions for (3.36) can be found in Section 2.2.4 for most common non-isotropic scattering distributions.

From the high-pass nature of Bessel functions discussed in the previous section, the spatial-to-mode functions $\mathcal{J}_m(\boldsymbol{y}_r) \approx 0$ for $m > \lceil \pi e \left\|\boldsymbol{y}_r\right\| / \lambda \rceil$. Therefore, given that $|\gamma_{m-m'}| \leq 1, \forall m$, we can define

$$M \triangleq \lceil \pi e r_0 / \lambda \rceil, \tag{3.37}$$

[3]It is important to note the distinction between the modal correlation $\gamma_{m,m'}$ due to scattering, and the antenna correlation $\rho_{r,r'}$ due to antenna placement and scattering.

such that the spatial correlation (3.30) is well approximated by the truncated series

$$\rho_{rr'} = \sum_{m=-M}^{M} \sum_{m'=-M}^{M} \overline{\mathcal{J}_m(\boldsymbol{y}_r)} \mathcal{J}_{m'}(\boldsymbol{y}_{r'}) \gamma_{m-m'}, \tag{3.38}$$

for every pair of antennas within the receiver aperture of radius r_0. Note that the truncation arises from a more general truncation property of the plane wave expansion (3.29) and is discussed further in Chapter 4. For now, it is sufficient to state that the truncation error is small and decreases at least exponentially as further terms are taken.

Using (3.38) the spatial correlation matrix $\boldsymbol{R}$ can now be decomposed into the matrix product

$$\boldsymbol{R} = \boldsymbol{J}\boldsymbol{\Gamma}\boldsymbol{J}^{\dagger}, \tag{3.39}$$

where $\boldsymbol{J}$ is the $n_{\mathrm{R}} \times (2M+1)$ *aperture sampling* matrix,

$$\boldsymbol{J} = \begin{bmatrix} \mathcal{J}_{-M}(\boldsymbol{y}_1) & \mathcal{J}_{-M+1}(\boldsymbol{y}_1) & \cdots & \mathcal{J}_{M}(\boldsymbol{y}_1) \\ \mathcal{J}_{-M}(\boldsymbol{y}_2) & \mathcal{J}_{-M+1}(\boldsymbol{y}_2) & \cdots & \mathcal{J}_{M}(\boldsymbol{y}_2) \\ \vdots & \vdots & \ddots & \vdots \\ \mathcal{J}_{-M}(\boldsymbol{y}_{n_{\mathrm{R}}}) & \mathcal{J}_{-M+1}(\boldsymbol{y}_{n_{\mathrm{R}}}) & \cdots & \mathcal{J}_{M}(\boldsymbol{y}_{n_{\mathrm{R}}}) \end{bmatrix}, \tag{3.40}$$

which describes the sampling of the receiver aperture by the antennas, and $\boldsymbol{\Gamma}$ is the $(2M+1) \times (2M+1)$ *modal correlation* matrix,

$$\boldsymbol{\Gamma} = \begin{bmatrix} \gamma_0 & \gamma_1 & \cdots & \gamma_{2M} \\ \gamma_{-1} & \gamma_0 & \cdots & \gamma_{2M-1} \\ \vdots & \vdots & \ddots & \vdots \\ \gamma_{-2M} & \gamma_{-2M+1} & \cdots & \gamma_0 \end{bmatrix}, \tag{3.41}$$

which characterizes the scattering environment surrounding the receiver aperture. The correlation matrix decomposition (3.39) emphases the distinct spatial effects on correlation, and ultimately capacity, of the antenna placement and the scattering environment.

The capacity (3.1a) can now written as

$$C = \log \left| \boldsymbol{I}_{n_{\mathrm{R}}} + \eta \boldsymbol{J}\boldsymbol{\Gamma}\boldsymbol{J}^{\dagger} \right| \tag{3.42a}$$

$$= \sum_{n=0}^{K-1} \log(1 + \eta\lambda_n), \tag{3.42b}$$

where λ_n and K are the eigenvalues and rank, respectively, of the spatial correlation matrix product $\boldsymbol{R} = \boldsymbol{J}\boldsymbol{\Gamma}\boldsymbol{J}^\dagger$, with

$$K = \min\{\text{rank}(\boldsymbol{J}), \text{rank}(\boldsymbol{\Gamma})\} \tag{3.43a}$$

$$\leq \min\{n_\text{R}, 2M + 1\}. \tag{3.43b}$$

Therefore, due to the linear capacity growth depending on a full rank correlation matrix, for any $n_\text{R} > K$ the capacity scaling will no longer remain linear with increasing numbers of antennas due to insufficient eigen-channels. There are two cases in which the rank of $\boldsymbol{R}$ may be reduced; a loss in rank of the aperture sampling matrix $\boldsymbol{J}$ due to the aperture size and/or antenna placement, or, a loss in modal correlation matrix $\boldsymbol{\Gamma}$ rank due to low angular spread surrounding the receiver.

3.3.2 Capacity Limits: Constrained Aperture

To isolate the effects of spatially constraining the array from those of angular spread, we assume the scatterers are uniformly distributed and generate an isotropic diffuse field (often referred to as a *rich* scattering environment) corresponding to independent modes $\gamma_{m-m'}$, with modal correlation matrix $\Gamma = \boldsymbol{I}_{2M+1}$. In this case the capacity (3.42b) is given by

$$C = \log\left|\boldsymbol{I}_{n_\text{R}} + \eta\boldsymbol{J}\boldsymbol{J}^\dagger\right|, \tag{3.44}$$

where the (r, r')-th element of the aperture sampling matrix product $\boldsymbol{J}\boldsymbol{J}^\dagger$ is given by

$$\boldsymbol{J}\boldsymbol{J}^\dagger|_{rr'} = \sum_{m=-M}^{M} \overline{\mathcal{J}_m(\boldsymbol{y}_r)}\mathcal{J}_m(\boldsymbol{y}_{r'}) \tag{3.45a}$$

$$= \sum_{m=-M}^{M} J_m(k\,\|\boldsymbol{y}_r\|)J_m(k\,\|\boldsymbol{y}_{r'}\|)e^{-im(\theta_r - \theta_{r'})} \tag{3.45b}$$

$$= J_0(k\,\|\boldsymbol{y}_r - \boldsymbol{y}_{r'}\|), \tag{3.45c}$$

where (3.45c) follows from (3.45b) from a special case of Gegenbauer's Addition Theorem [109, pp. 363]. For a rich scattering environment $J_0(k\,\|\boldsymbol{y}_r - \boldsymbol{y}_{r'}\|)$ gives the spatial correlation between the complex envelopes of the received signals at

antenna positions $\boldsymbol{y}_r$ and $\boldsymbol{y}_{r'}$ [16]. Therefore the capacity growth of (3.44) will be maximized provided all the antennas can be placed within the region such that the spatial correlation between any antenna pair is zero.

Assuming we can place all n_{R} antennas such that the spatial correlation is zero between all the antennas, then $\boldsymbol{J}\boldsymbol{J}^{\dagger} = \boldsymbol{I}_{n_{\mathrm{R}}}$ and the capacity is given by

$$C = n_{\mathrm{R}} \log(1+\eta), \tag{3.46}$$

which grows linearly with the number of antennas. However, as shown next, if $n_{\mathrm{R}} \geq \mathrm{rank}(\boldsymbol{J})$ then the capacity scaling is reduced to logarithmic growth, or an array gain effect, with increasing numbers of antennas.

Let μ_n, $n = \{0, 1, \ldots, n_{\mathrm{R}}-1\}$ denote the singular values of the aperture sampling matrix $\boldsymbol{J}$, ordered such that $\mu_n \geq \mu_{n+1}$, then we can express the capacity (3.44) as

$$C = \sum_{n=0}^{n_{\mathrm{R}}-1} \log\left(1+\eta\mu_n^2\right). \tag{3.47}$$

Consider two apertures with equal radii r_0, with antenna numbers $n_{\mathrm{R}1}, n_{\mathrm{R}2} \geq 2M+1$. Denoting $\{\mu_{n,n_{\mathrm{R}1}}\}$ and $\{\mu_{n,n_{\mathrm{R}2}}\}$ as the set of singular values of the aperture sampling matrix for each aperture, and observing that $\sum_n \mu_n^2 = \mathrm{trace}(\boldsymbol{J}\boldsymbol{J}^{\dagger}) = n_{\mathrm{R}}$, then

$$\frac{1}{n_{\mathrm{R}1}} \sum_{n=0}^{n_{\mathrm{R}1}-1} \mu_{n,n_{\mathrm{R}1}}^2 = \frac{1}{n_{\mathrm{R}2}} \sum_{n=0}^{n_{\mathrm{R}2}-1} \mu_{n,n_{\mathrm{R}2}}^2. \tag{3.48}$$

By definition, there are only $\mathrm{rank}(\boldsymbol{J})$ non-zero singular values (corresponding to the $2M+1$ independent receiver modes), therefore, assuming we can place $\mathrm{rank}(\boldsymbol{J})$ antennas within the aperture of radius r_0 such that spatial correlation between each antenna is zero, giving constant and equal non-zero singular values, we have

$$\frac{\mu_{n,n_{\mathrm{R}1}}^2}{n_{\mathrm{R}1}} = \frac{\mu_{n,n_{\mathrm{R}2}}^2}{n_{\mathrm{R}2}}, \quad n \in [0, 2M]. \tag{3.49}$$

Therefore, letting $n_{\mathrm{R}1} = n_{\mathrm{R}} \geq 2M+1$, and $n_{\mathrm{R}2} = n_M \triangleq 2M+1$, we have $\mu_{n,n_M}^2 = 1, \forall n$ and (3.47) becomes

$$C = n_M \log\left(1 + n_{\mathrm{R}}\frac{\eta}{n_M}\right), \quad n_{\mathrm{R}} \geq n_M, \tag{3.50}$$

which scales logarithmically with n_{R}, hence the maximum capacity growth is re-

duced from linear to logarithmic once the number of antennas reaches the saturation point $n_M = 2M + 1$, which scales linearly with the radius of the aperture.

Therefore, for a receiver aperture of radius r_0, define

$$n_{r_0} \triangleq 2\lceil \pi e r_0/\lambda \rceil + 1, \tag{3.51}$$

as an *aperture saturation point*, then the maximum achievable capacity for n_{R} antennas is given by

$$C_{\max}(n_{\mathrm{R}}, r_0) = \begin{cases} n_{\mathrm{R}} \log(1+\eta) & n_{\mathrm{R}} < n_{r_0} \\ n_{r_0} \log(1 + n_{\mathrm{R}}\eta/n_{r_0}) & n_{\mathrm{R}} \geq n_{r_0} \end{cases}. \tag{3.52}$$

This represents the maximum capacity for a fixed aperture region in space when the antennas (up to n_{r_0}) are placed optimally. Once the number of antennas reaches the saturation point n_{r_0}, the addition of any more antennas, regardless of their placement, provides only array gain capacity growth.

The theoretical maximum capacity $C_{\max}(n_{\mathrm{R}}, r_0)$ is shown in Fig. 3.6 for apertures of radius $r_0 = \{0.1\lambda, 0.7\lambda\}$ in an isotropic scattering environment for an increasing number of antennas. The ULA of width $2r_0$, and UCA of radius r_0, are also shown. As expected, both the ULA and UCA do not optimally place the antennas for the given aperture, and as such the capacity is lower than the theoretical maximum capacity. These array geometries do not utilize the full set of independent eigen-modes of the region, as shown by the lower saturation points and capacity.

Spatially Constrained Uniform Linear Arrays

For the special case of the commonly employed ULA, array symmetry gives $\mathcal{J}_m(\boldsymbol{y}_r) = \mathcal{J}_{-m}(\boldsymbol{y}_{r'})$, where $\boldsymbol{y}_r = (\|\boldsymbol{y}_r\|, 0)$ and $\boldsymbol{y}_{r'} = (\|\boldsymbol{y}_{r'}\|, \pi)$ are the $\lfloor n_{\mathrm{R}}/2 \rfloor$ antenna locations symmetric about the array origin. Therefore, there are at most $M + 1$ independent columns of $\boldsymbol{J}$, and hence for the ULA of length d_0 the aperture saturation point is given by

$$n_{d_0}^{\mathrm{ULA}} \triangleq \lceil \pi e d_0/2\lambda \rceil + 1. \tag{3.53}$$

It can be seen from Fig. 3.6 that the saturation point does give a good indication of where the capacity scaling of the ULA changes to logarithmic growth with increasing antenna numbers. However, (3.53) is derived under the assumption there is no

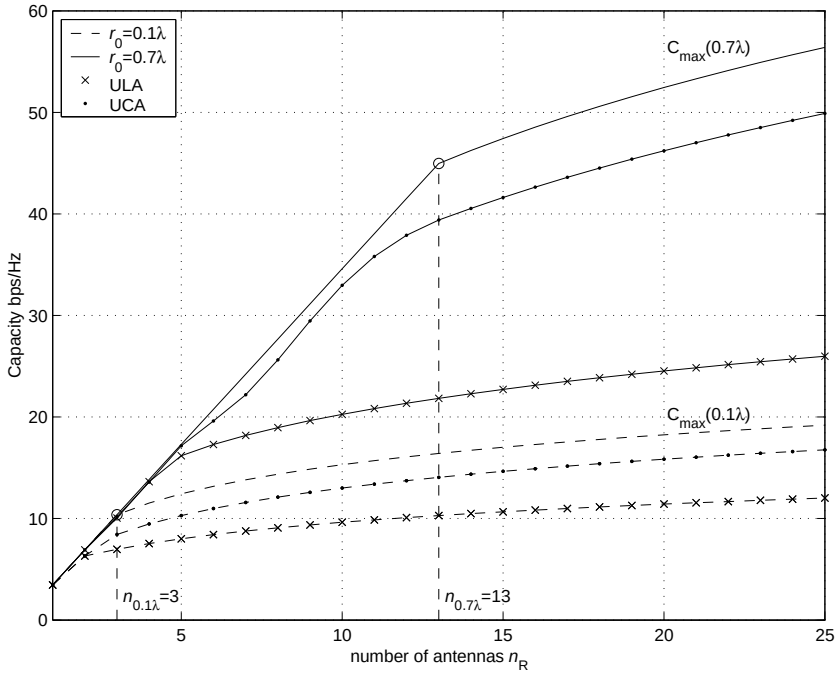

Figure 3.6: Theoretical maximum capacity $C_{\max}(n_{\mathrm{R}}, r_0)$ for apertures of radius $r_0 = \{0.1\lambda, 0.7\lambda\}$ in an isotropic scattering environment for an increasing number of antennas. Vertical dashed lines indicate the theoretical antenna saturation point for each aperture size. Shown also is the capacity of the ULA and UCA within the same sized apertures.

correlation between the antenna elements, therefore, due to spatial correlation of the antennas, the capacity growth will most likely saturate before $n_{d_0}^{\mathrm{ULA}}$. This result does however improve on the asymptotic studies of fixed aperture ULAs in [102] and [101], by giving a finite limit to number of antennas at which the addition of further antennas gives diminishing capacity gains. Note that (3.53) applied to the simulation scenarios presented in [101, 102] corresponds to the knee point in capacity growth, where the capacity growth goes from approximately linear to logarithmic with increasing numbers of antennas, which is not discussed within those references but is of considerable interest in practical MIMO systems.

3.3.3 Capacity Limits: Limited Angular Spread

To isolate the effects of scattering environment on the capacity, we assume $n_{\mathrm{R}} = 2M + 1$ antennas are optimally placed (perfect spatial to mode coupling) within the receive region of fixed radius r_0, then from the reciprocity identity $|\boldsymbol{I} + \boldsymbol{AB}| =$

$|\boldsymbol{I} + \boldsymbol{BA}|$, the capacity (3.42b) can be expressed as

$$C = \log \left| \boldsymbol{I}_{n_\mathrm{R}} + \eta \boldsymbol{J}^\dagger \boldsymbol{J} \boldsymbol{\Gamma} \right|. \tag{3.54}$$

In the case of optimal antenna placement $\boldsymbol{J}^\dagger \boldsymbol{J} = \boldsymbol{I}_{n_\mathrm{R}}$ and the aperture sampling matrix $\boldsymbol{J}$ is unitary, thus

$$C = \log |\boldsymbol{I}_{n_\mathrm{R}} + \eta \boldsymbol{\Gamma}| \tag{3.55a}$$

$$= \sum_{n=0}^{K-1} \log(1 + \eta \lambda_n), \tag{3.55b}$$

where $K = \mathrm{rank}(\Gamma) \leq n_\mathrm{R} = 2M + 1$.

With no closed-form expressions available, the analytical computation of the eigenvalue sequence $\{\lambda_n\}$ for finite numbers of antennas is difficult, other than solving the eigenvalue problem of the Toeplitz matrix $\boldsymbol{\Gamma}$. However, using the asymptotic equivalence between Toeplitz and circulant matrices [111], it can be shown that as $n_\mathrm{R} \to \infty$ then $\lambda_n / n_\mathrm{R} = \varepsilon_n$, where ε_n is a constant independent of n_R [102, 112]. Therefore, since a reduction in angular spread will decrease $\mathrm{rank}(\boldsymbol{\Gamma})$ due to increased modal correlation, for large n_R the capacity (3.55) will exhibit logarithmic growth with increasing numbers of antennas.

Figure 3.7 shows the eigenvalues of the modal correlation matrix $\boldsymbol{\Gamma}$ for various angular spread Δ of a uniform limited distributed scattering environment. As expected, there exists a definite threshold between the vanishing and significant eigenvalues for each angle spread. Shown as a solid black line, an empirically estimated linear eigenvalue threshold of $2\lceil M\Delta/\pi \rceil + 1$, gives a good estimate of the boundary between the significant and vanishing eigenvalues for each angular spread, i.e., $\lambda_n \approx 0$ for $n > 2\lceil M\Delta/\pi \rceil + 1$.

Therefore, for a receiver aperture of fixed radius R with angular spread Δ, define

$$n_\Delta \triangleq 2\lceil \Delta e R/\lambda \rceil + 1, \tag{3.56}$$

as an *angular saturation point*, then the maximum achievable capacity for n_R antennas is given by

$$C_{\max}(n_\mathrm{R}, \Delta) = \begin{cases} n_\mathrm{R} \log(1+\eta) & n_\mathrm{R} < n_\Delta \\ n_\Delta \log(1 + n_\mathrm{R}\eta/n_\Delta) & n_\mathrm{R} \geq n_\Delta \end{cases}. \tag{3.57}$$

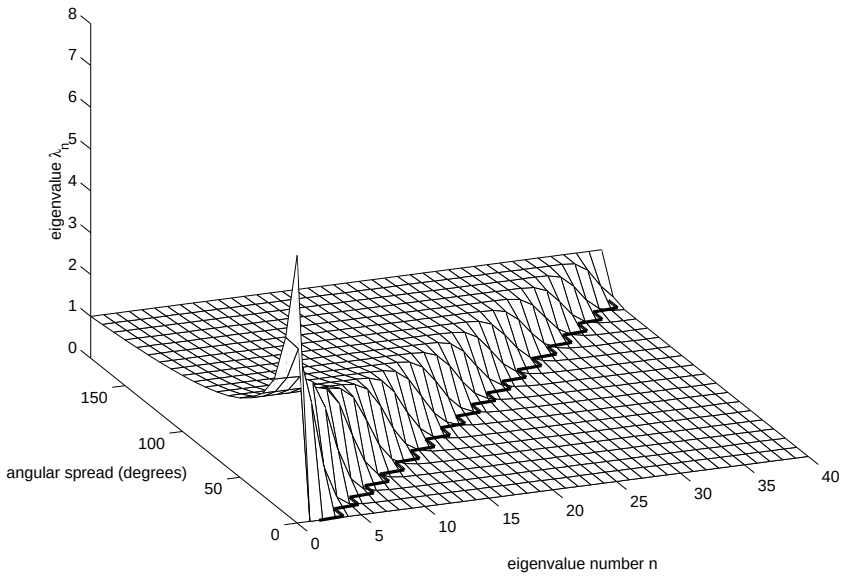

Figure 3.7: The eigenvalues of the modal correlation matrix for various angular spreads. The dark solid line represents the estimated eigenvalue threshold, and clearly shows the boundary between the significant and vanishing eigenvalues of the modal correlation matrix for each angular spread.

The theoretical maximum capacity $C_{\max}(n_{\mathrm{R}}, \Delta)$ is shown in Fig. 3.8 for aperture of fixed radius $R = 2.5\lambda$ for an increasing number of antennas. The ULA of width $2R$, and UCA of radius R, are also shown, note that the size of the aperture is large enough that any saturation effects are due only to insufficient angular spread. Again, both the ULA and UCA do not optimally place the antennas for the given aperture, and as such the capacity is lower than the theoretical maximum capacity.

Note, that if the aperture is allowed to grow with antenna number such that all n_{R} antennas can be placed optimally, then the capacity will scale linearly with increasing numbers of antennas. However, the rate of capacity increase is reduced as the angular spread is made smaller, as shown in Fig. 3.9, due to the angular saturation point being a function of both angular spread and aperture radius. This unconstrained result agrees with linear capacity scaling studied in [10] for unconstrained grid-like arrays, where instead of correlation due to reduced angular spreads, the spatial correlation due to fixed antenna placement reduces the growth rate.

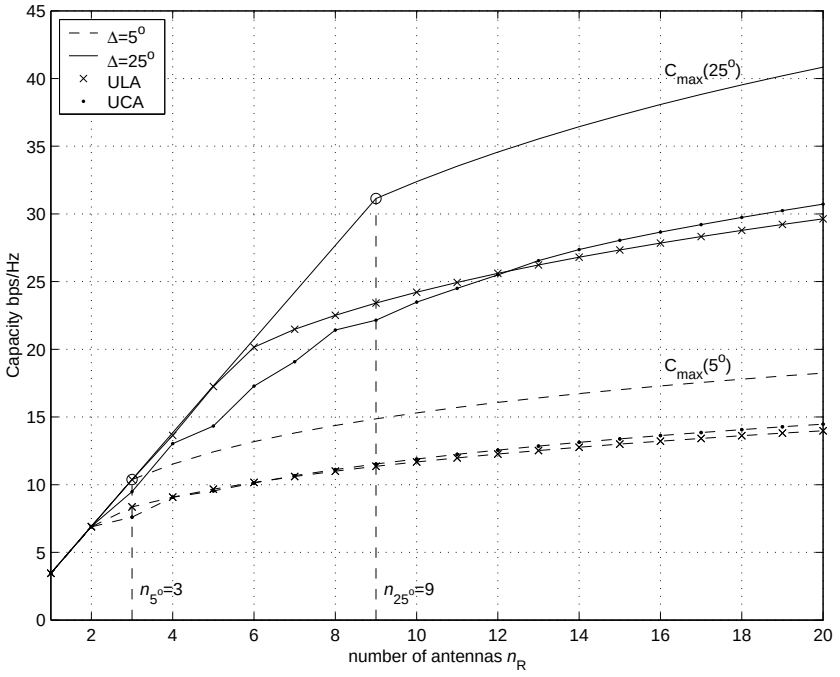

Figure 3.8: Theoretical maximum capacity $C_{\max}(n_{\mathrm{R}}, \Delta)$ for aperture of fixed radius $R = 2.5\lambda$ for an increasing number of antennas. Vertical dashed lines indicate the estimated antenna saturation point for each angular spread. Shown also is the capacity of the broadside ULA and UCA within the same size aperture.

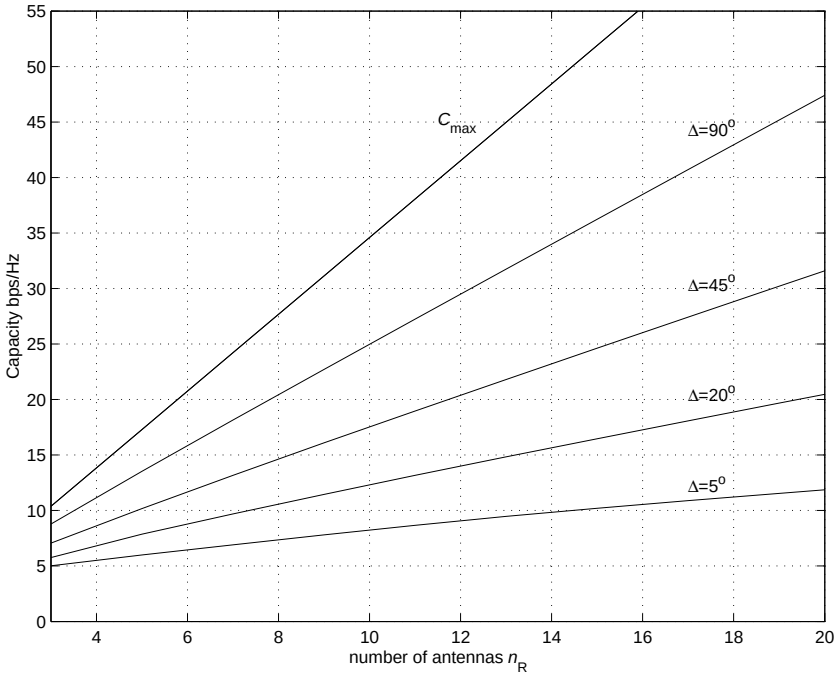

Figure 3.9: Theoretical maximum capacity of unconstrained aperture MIMO systems for various angular spreads $\Delta = \{5°, 20°, 45°, 90°\}$, along with the theoretical maximum capacity $C_{\max}$ corresponding to $\Delta = 180°$.

3.3.4 Fixed Received Power

Consider the channel model (3.26b), then the total received power is given by

$$P_{\mathrm{R}} = \sum_{r=1}^{n_{\mathrm{R}}} E\left\{|z_r|^2\right\} \tag{3.58a}$$

$$= \sum_{r=1}^{n_{\mathrm{R}}} \sum_{t=1}^{n_{\mathrm{T}}} \sigma_{\mathrm{T}}^2 \int_{\mathbb{S}^1} E\left\{|g_t(\psi)|^2\right\} d\psi \tag{3.58b}$$

$$= n_{\mathrm{R}} \sigma_H^2 P_{\mathrm{T}}, \tag{3.58c}$$

where $\sigma_{\mathrm{T}}^2 = P_{\mathrm{T}}/n_{\mathrm{T}}$ is the power per transmit antenna, and it is assumed the channel variances $\sigma_H^2 = E\left\{|h_{rt}|^2\right\} = \int_{\mathbb{S}^1} E\left\{|g_t(\psi)|^2\right\} d\psi$ are constant, usually normalized such that $\sigma_H^2 = 1$. Hence the total received power increases linearly with the number of receive antennas n_{R}, therefore giving at least logarithmic capacity growth with increasing numbers of antennas, regardless of the antenna placement within the aperture. This logarithmic capacity growth, or array-gain, with increasing numbers of antennas is plausible in the case of unconstrained arrays, where the antennas are sufficiently separated. However, if the antennas are constrained within an aperture of fixed size, then the assumption of unlimited total power is arguable.

An antenna receives power proportional to its effective area [113], therefore the total power collected by an ensemble of isolated antennas will scale linearly with the number of antennas. However, for closely spaced antennas the effective areas will overlap and the total power collected will be less than the sum of powers collected by isolated antennas.

In [106] it is proposed that the total received power should remain a constant for a given region, regardless of the number of antennas within. Therefore, by scaling the channel variances to $E\left\{|h_{rt}|^2\right\} = \sigma_H^2/n_{\mathrm{R}}$ the total received power remains bounded as the number of antennas is increased. This normalization is equivalent to scaling the transmitted power by $1/n_{\mathrm{R}}$, thus the average SNR at each receive antenna is η/n_{R}, where $\eta = P_{\mathrm{T}}/\sigma^2$ is the average SNR of the unnormalized case. The normalized capacity is then given by

$$C = \log\left|\boldsymbol{I}_{n_{\mathrm{R}}} + \frac{\eta}{n_{\mathrm{R}}} \boldsymbol{J}\boldsymbol{\Gamma}\boldsymbol{J}^{\dagger}\right| \tag{3.59a}$$

$$= \sum_{n=0}^{K-1} \log\left(1 + \frac{\eta}{n_{\mathrm{R}}}\lambda_n\right). \tag{3.59b}$$

where $K = \min\{\mathrm{rank}(\boldsymbol{J}), \mathrm{rank}(\boldsymbol{\Gamma})\}$, and $\{\lambda_n\}$ are the eigenvalues of the matrix

product $\boldsymbol{J}\boldsymbol{\Gamma}\boldsymbol{J}^{\dagger}$.

In the previous sections, it was shown that for $n_{\mathrm{R}} \to \infty$ the ratio $\lambda_n/n_{\mathrm{R}} = \varepsilon_n$, where ε_n is a constant independent of n_{R}, hence, the capacity (3.59) will converge to a constant for large n_{R}. Therefore, the capacity of this normalized system will be independent of any array gain effects, giving more realistic capacity scaling expressions for spatially constrained arrays with increasing numbers of antennas.

Fundamental Capacity Limit

For an aperture of fixed radius $r_0 = R$ there are n_{r_0} possible eigen-modes, or orthogonal sub-channels with gains large enough to convey information at a significant rate. However, since the effect of angular spread $\Delta < \pi$ is to correlate the modes, the number of orthogonal channels is reduced to $\min\{n_{r_0}, n_{\Delta}\} = n_{\Delta}$, since $n_{r_0} \geq n_{\Delta}$, with equality for $\Delta = \pi$.

Therefore, for an aperture of radius r_0 with scattering angular spread of Δ define

$$n_{\mathrm{sat}}(r_0, \Delta) \triangleq 2\lceil \Delta e r_0/\lambda \rceil + 1, \tag{3.60}$$

as the antenna saturation point, whereby further increases in the number of antennas fails to give further capacity gains. Therefore, the theoretical maximum capacity for n_{R} antennas within the aperture is given by

$$C_{\max}(n_{\mathrm{R}}, r_0, \Delta) = \begin{cases} n_{\mathrm{R}} \log(1 + \eta/n_{\mathrm{R}}) & n_{\mathrm{R}} < n_{\mathrm{sat}} \\ C_{\mathrm{sat}} & n_{\mathrm{R}} \geq n_{\mathrm{sat}} \end{cases}, \tag{3.61}$$

where

$$C_{\mathrm{sat}}(r_0, \Delta) \triangleq n_{\mathrm{sat}} \log(1 + \eta/n_{\mathrm{sat}}), \tag{3.62}$$

is the maximum capacity for an aperture of radius r_0 with scattering angular spread Δ, which in theory, can be achieved with a minimum of n_{sat} antennas. Note that $C_{\max}$ grows logarithmically with increasing numbers of antennas up to the constant C_{sat} for $n_{\mathrm{R}} = n_{\mathrm{sat}}$ antennas, where the addition of more antennas (regardless of placement) gives no further increase in capacity.

Consider the identities $\ln(1 + x) \leq x$, and $\ln(1 + x) \geq x - x^2/2$, then

$$C_{\mathrm{sat}}(r_0, \Delta) \leq \frac{\eta}{\ln 2}, \tag{3.63}$$

$$C_{\text{sat}}(r_0, \Delta) \geq \frac{\eta}{\ln 2} - \frac{1}{2 \ln 2} \left(\frac{\eta}{n_{\text{sat}}} \right)^2, \tag{3.64}$$

and hence for large radius $r_o \to \infty$ (i.e., $n_{\text{sat}} \to \infty$), the normalized capacity converges to an upper limit

$$\lim_{r_0 \to \infty} C_{\text{sat}}(r_0, \Delta) = C_{\text{limit}} \triangleq \frac{\eta}{\ln 2}. \tag{3.65}$$

Due to the assumption of optimally placed (uncorrelated) antennas within a large aperture, the capacity limit corresponds to the limit of the normalized capacity of the i.i.d. Rayleigh fading case for $n_{\text{T}}, n_{\text{R}} \to \infty$, as shown in [102]. Therefore, when the effects of array-gain are removed the normalized capacity converges to a finite limit for large numbers of uncorrelated antennas, compared to unbounded linear growth shown in Section 3.3.3 and in [5, 7] for the standard capacity. This finite limit to the normalized capacity suggests that the array-gain is a significant factor in the classical theoretical MIMO capacity scaling results, which predict capacities which cannot be achieved in practice due to antenna packing constraints.

Note that the capacity C_{sat} is identical to the capacity of n_{sat} independent equal power transmission lines ($\boldsymbol{H} = \boldsymbol{I}_{n_{\text{sat}}}$), where the total transmit power P_{T} is divided equally between the n_{sat} lines [5]. Therefore, the maximum normalized capacity for the aperture consists of n_{sat} orthogonal parallel channels each with power $P_{\text{T}}/n_{\text{sat}}$, which grows logarithmically with radius to limit $\eta / \ln 2$

The theoretical maximum capacity $C_{\max}$ is shown in Fig. 3.10 for increasing numbers of antennas within an aperture of radius $r_0 = 1\lambda$ and angular spreads of $\Delta = \{20°, 180°\}$. Again, for the given aperture and scattering environment, the ULA and UCA geometries do not couple strongly to the uncorrelated modes of the region, and therefore exhibit much less capacity than that of the theoretical maxima. The theoretical maximum capacity of an aperture of infinite radius is also shown for increasing numbers of antennas, $C_{\max}(n_{\text{R}}, r_0 = \infty)$, which converges to the upper limit $C_{\text{limit}}(n_{\text{R}} = \infty, r_0 = \infty)$, for large numbers of antennas.

For the remainder of this thesis, any reference to capacity is given with the assumption of fixed received power. Strictly speaking the capacity expression should be referred to as the *normalized capacity* (in the array-gain sense), however, in the following chapters the term capacity will be used, and it will be clearly stated when it means otherwise.

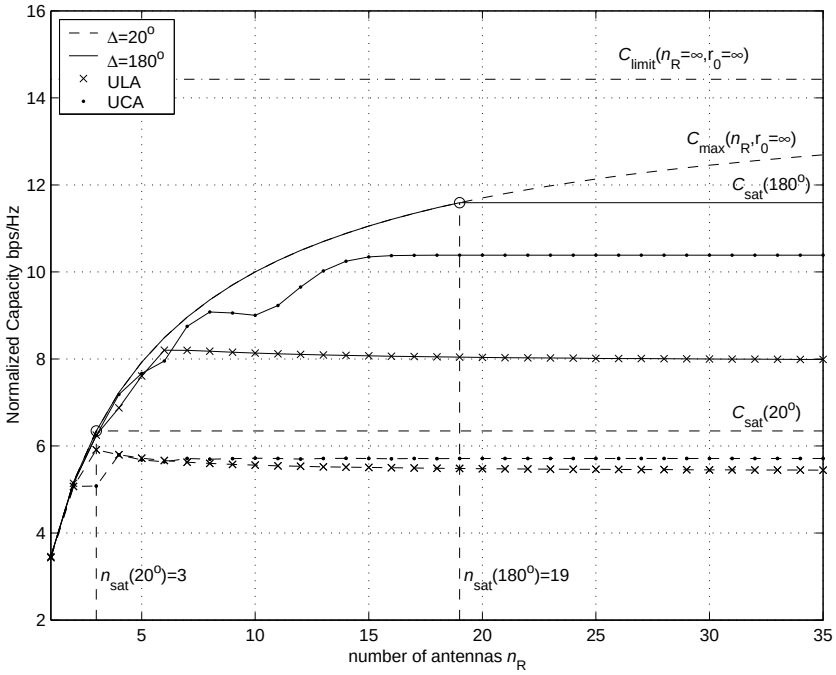

Figure 3.10: Theoretical maximum normalized capacity $C_{\max}$ of an aperture of radius $r_0 = 1\lambda$ for angular spread $\Delta = \{20°, 180°\}$ with increasing number of antennas. Vertical dashed lines indicate the theoretical antenna saturation point for each angular spread. Shown also is the normalized capacity of the ULA and UCA within the same sized apertures.

3.3.5 Constrained 3D Apertures

Consider a 3D scattering environment with the antenna array constrained within a sphere of radius r_0. Then from the 3D plane wave expansion [79]

$$e^{ik\boldsymbol{y}\cdot\widehat{\ }} = \sum_{n=0}^{\infty}\sum_{m=-n}^{n} i^n 4\pi j_n(k\,\|y\|)\overline{Y_n^m(\widehat{\boldsymbol{y}})}Y_n^m(\widehat{\boldsymbol{\psi}}), \tag{3.66}$$

then the spatial correlation between two antennas r and r' located at $\boldsymbol{y}_r$ and $\boldsymbol{y}_{r'}$, respectively, is given by,

$$\rho_{rr'} = \sum_{n=0}^{\infty}\sum_{m=-n}^{n}\sum_{n'=0}^{\infty}\sum_{m'=-n'}^{n'} \overline{\mathcal{J}_n^m(\boldsymbol{y}_r)}\mathcal{J}_{n'}^{m'}(\boldsymbol{y}_{r'})\,\gamma_{nn'}^{mm'}, \tag{3.67}$$

where

$$\mathcal{J}_n^m(\boldsymbol{y}_r) \triangleq 4\pi i^n j_n(k\,\|\boldsymbol{y}_r\|)\overline{Y_n^m(\widehat{\boldsymbol{y}}_r)}, \tag{3.68}$$

defines the 3D *spatial-to-mode* function, which maps aperture sampling point $\boldsymbol{y}_r$ to the n,m-th mode of the of the plane wave expansion (3.66), and

$$\gamma_{nn'}^{mm'} = \int_{\mathbb{S}^2} \mathcal{P}(\widehat{\boldsymbol{\psi}})\overline{Y_n^m(\widehat{\boldsymbol{\psi}})}Y_{n'}^{m'}(\widehat{\boldsymbol{\psi}})\, ds(\widehat{\boldsymbol{\psi}}), \tag{3.69}$$

is the modal correlation between the n,m and n',m' modes, and characterizes the 3D scattering environment surrounding the receiver aperture.

The order n spherical Bessel function $j_n(\cdot)$ is related to the Bessel function by

$$j_n(z) = \sqrt{\frac{\pi}{2z}} J_{n+\frac{1}{2}}(z), \tag{3.70}$$

therefore, as for Bessel functions, the spherical Bessel functions will exhibit a high-pass nature. Consider the bessel function bound [109, p.362], $|J_n(z)| \leq z^n/2^n n!$, with $n! = \Gamma(n+1)$, then the spherical Bessel functions are upper bounded by,

$$j_n(z) \leq \frac{\sqrt{\pi}}{2} \frac{(z/2)^n}{\Gamma(n+\frac{3}{2})}, \tag{3.71}$$

using the Sterling bound [110] for $\Gamma(n+3/2)$, we see that spherical Bessel functions $j_n(z) \approx 0$ for $n > (ez-1)/2$. Therefore, for a spherical aperture of radius r_0 we can define

$$M \triangleq \lceil \pi e r_0/\lambda \rceil, \tag{3.72}$$

such that the spatial correlation (3.67) is well approximated by the truncated series

$$\rho_r r' = \sum_{n=0}^{N} \sum_{m=-n}^{n} \sum_{n'=0}^{N} \sum_{m'=-n'}^{n'} \overline{\mathcal{J}_n^m(\boldsymbol{y}_r)} \mathcal{J}_{n'}^{m'}(\boldsymbol{y}_{r'})\, \gamma_{nn'}^{mm'}, \tag{3.73}$$

for every pair of antennas within the receiver aperture. As for the 2D case, we can now decompose the spatial correlation matrix as

$$\boldsymbol{R} = \boldsymbol{J}\boldsymbol{\Gamma}\boldsymbol{J}^\dagger, \tag{3.74}$$

where $\boldsymbol{J}$ is the $n_{\mathrm{R}} \times (M+1)^2$ aperture sampling matrix whose r-th row is given by

$$\boldsymbol{J}|_r = \left[\mathcal{J}_0^0(\boldsymbol{y}_r)\, \mathcal{J}_1^{-1}(\boldsymbol{y}_r) \cdots \mathcal{J}_m^m(\boldsymbol{y}_r)\, \mathcal{J}_{m+1}^{-m-1}(\boldsymbol{y}_r)\, \mathcal{J}_{m+1}^{-m}(\vec{t}y_r) \cdots \mathcal{J}_M^M(\boldsymbol{y}_r)\right], \tag{3.75}$$

and Γ is the $(M+1)^2 \times (M+1)^2$ modal correlation matrix.

Therefore, following a similar approach to the 2D case, it is possible to define aperture and angular saturation points for the capacity scaling with increasing numbers of antennas. It immediately follows from $\text{rank}(\boldsymbol{J}) \leq (M+1)^2$ that the aperture saturation point will be given by $(M+1)^2$ antennas for a spherical aperture of radius r_0, which allows for approximately $\lceil \pi e r_0/\lambda \rceil^2$ more antennas before the region saturates over the 2D aperture of the same radius. Similarly, the angular saturation point will be given by $(N+1)^2$, where $N = \lceil f(r_0, \Delta_\text{a}, \Delta_\text{e}) \rceil$ is a function of radius and the azimuth and elevation angular spreads Δ_a, Δ_e, for a uniform limited azimuth/elevation scattering distribution, where the scatterers are uniformly distributed over the sector $\{(\theta, \varphi); \theta \in [\theta_0 - \Delta_\text{a}, \theta_0 + \Delta_\text{a}], \varphi \in [\varphi_0 - \Delta_\text{e}, \varphi_0 + \Delta_\text{e}]\}$.

3.4 Summary and Contributions

This chapter has derived a theoretical maximum capacity for a fixed region of space which depends only on the radius of the region and the angular spread. An antenna saturation point has been theoretically defined at which this maximum occurs, whereby further increases in the number of antennas fails to give further capacity gains. These results have significant implications for realizable MIMO systems, simply cramming more and more antennas into a region of space does not increase the ergodic capacity. Therefore we see that space also needs to be considered for the information bearing capacity of the system, along with the usual time-frequency constraint.

Some specific contributions made in this chapter are:

1. The uniform circular array in 2D isotropic scattering was theoretically shown to suffer a capacity saturation, where further increases in antenna numbers gives no further capacity gains (other than array gain). By investigating the spectrum of the spatial correlation matrix this saturation point in the number of antennas was shown to be proportional to the array radius.

2. Using the spatial correlation expressions in Chapter 2, the spatial correlation matrix of an arbitrary array was decomposed to reveal the independent effects of antenna placement and angular spread.

3. Using this matrix decomposition the results of the UCA were extended to arbitrary arrays within a circle of fixed radius and isotropic scattering. A

maximum capacity for the circular region was derived which depends only on the radius of the region. The minimum number of antennas required to achieve maximum capacity was also derived.

4. The results of the capacity saturation for apertures in isotropic scattering were extended to scattering of limited angular spread surrounding the array.

5. A fixed received power concept was introduced, where regardless of the number of antennas the total received power remains constant. By removing the array gain effects, assuming fixed received power shows that there is a fundamental limit to MIMO communications which depends only on the SNR of the channel.

6. The circular and 2D scattering results were extended to arbitrary arrays constrained within spheres with 3D scattering. It was shown that using 3D arrays gave a significant increase in the capacity for arrays within spheres over that of the circle with the same radius.

Chapter 4

Spatial Characterization of MIMO Channels

With the recent application of antenna arrays for spatial multiplexing in MIMO systems comes the need for better understanding of the spatial properties of the wireless communications channel. As shown in the previous chapters, these spatial properties will have significant impact on the capacity of multi-antenna systems. Therefore, a good understanding of these properties is required for effective design and implementation of wireless MIMO systems.

For randomly fading channels, much of the literature is limited to the idealistic situation of independent and identically distributed (i.i.d.) Gaussian channels, where the channel gains are modelled as independent Gaussian random variables (for example see [5,7]). The i.i.d. model corresponds to sufficiently spaced antennas such that there is no spatial correlation between antenna elements at the transmit and receive arrays, along with significant scattering between arrays. However, in practice, realistic scattering environments and limited antenna separation leads to channels which exhibit correlated fades.

One approach to MIMO channel modelling for correlated fading is to measure the MIMO channel responses through field measurements. By analyzing the recorded data the significant characteristics of the MIMO channel can be obtained and the MIMO channel can be modelled to have similar characteristics [68,114–116]. Alternatively, deterministic physical models such as ray tracing [117, 118] simulate specific propagation scenarios and may be combined with Monte Carlo analysis to provide statistical channel information. Such methods give an accurate characterization of the channel, however, ray tracing modelling is computationally expensive and provides results for specific scenarios only. Finally, a statistical model can be

postulated which attempts to capture the physical channel characteristics based on the basic principles of radio propagation [65,105,119,120]. These scattering models can often be used as simple analysis tools which illustrate the essential characteristics of the MIMO channel, provided the constructed scattering environment is reasonable.

With the notable exception of [105] and [120], the statistical models mentioned above have poor physical significance. In particular, the separate effects of the scatterers and the antenna correlation are not accounted for. As outlined in [105], the models assume that only the spatial fading correlation is responsible for the rank structure of the MIMO channel. In practice, however, high rank MIMO channels correspond not only to the low fading correlation, but also to the structure of scattering in the propagation environment.

The models presented in [105,120] allow for insight into the effects of spatial correlation and scattering, however, they are unfortunately limited to particular array geometries and model the scattering environment using a discrete representation. Therefore, although offering considerable insight into the scattering characteristics of the channel they are restricted spatially, in the sense that the antenna geometry is restricted to a particular array configuration (usually linear) thus restrict the model to studying limited antenna variations (inter-element spacing), along with the ray tracing style of discrete scattering environments. From these observations, there is a need for a generalized channel model which provides insight into the spatial aspects of MIMO channels, thus giving an ideal framework to build space-time communication systems. In contrast to previous models, the contribution of this chapter is a spatial channel model which includes the physical parameters of arbitrary antenna configurations and a tractable parameterization of the complex scattering environment.

Here, it is desired to characterize the fading due to spatial effects rather than temporal, therefore the model developed in this chapter and employed throughout this thesis assumes a flat fading channel where the propagation delay is always less than the symbol period. With little effort the model can be extended to encompass frequency selective fading, however it is not reported here since, although important, it provides no further insights into the goals of this thesis.

One of the basic principles of radio propagation widely used in channel modelling is the plane wave. Before developing the general MIMO channel model, this chapter begins with a careful look at the structure of plane wave propagation and develops a truncated representation that is widely used throughout the rest of this

thesis.

4.1 Modal Truncation of Plane Waves

In the previous chapter, a critical threshold was shown to exist in the number of antennas when analyzing the behavior of the capacity for fixed apertures and angular spreads. Based on the vanishing nature of the Bessel functions, the spatial correlation expression was simplified to give rise to a spatial correlation matrix decomposition which showed the dominant factors on the capacity behavior. In this section, this simplification is shown to result from a more general truncation of plane wave expansions. This result is used extensively through out the remainder of this thesis in modelling the MIMO channel, therefore, the error associated with this truncation is of significant interest, and is studied in some depth in this section. In particular, the truncation error is shown to be small and has an exponential decrease to zero as more terms are added.

4.1.1 Plane Waves

One of the most important predictions of Maxwell's equations is the existence of electromagnetic waves which can transport energy. For a source free media, each cartesian component of the electric and magnetic fields satisfy the classical wave equation

$$\nabla^2 u(\boldsymbol{x}, t) = \mu\epsilon \frac{\partial^2 u(\boldsymbol{x}, t)}{\partial t^2}, \tag{4.1}$$

where ∇^2 is the Laplacian operator, and μ and ϵ are the permittivity and permeability of the medium, respectively, which for nondispersive media are independent of frequency.

For time-harmonic or narrowband field, the field consists of a single radial frequency ω and is and can be expressed as $u(\boldsymbol{x}, t) = u(\boldsymbol{x})e^{-i\omega t}$, for which the wave equation reduces to the Helmholtz equation

$$\nabla^2 u(\boldsymbol{x}) + k^2 u(\boldsymbol{x}) = 0, \tag{4.2}$$

where $k = \omega\sqrt{\mu\epsilon} = 2\pi/\lambda$ is the wave number, or propagation constant. The Helmholtz equation has a general solution of the exponential form $e^{i\boldsymbol{k}\cdot\boldsymbol{x}}$, therefore there is a simple set of complex travelling wave solutions to the wave equation,

given by

$$u(\boldsymbol{x}, t) = e^{i(\boldsymbol{k}\cdot\boldsymbol{x}-\omega t)}, \tag{4.3}$$

where $\boldsymbol{k} = k\widehat{\boldsymbol{k}}$. This solution is a wave 'travelling' in the direction of $\widehat{\boldsymbol{k}}$ in the sense that a point of constant phase, i.e., $\boldsymbol{k}\cdot\boldsymbol{x} - \omega t$ is constant, moves in this direction with speed $c = \omega/k$. Furthermore, the surfaces of constant phase are planes perpendicular to the direction of wave propagation $\boldsymbol{k}$, hence the solutions (4.3) are referred to as plane waves.

4.1.2 2D Plane Wave Propagation

A plane wave restricted to a 2D environment travelling in direction $\boldsymbol{k} = (k, \phi)$ can be expressed by the 2D modal[1] expansion [79]

$$e^{i\boldsymbol{k}\cdot\boldsymbol{x}} = J_0(k\,\|\boldsymbol{x}\|) + 2\sum_{n=1}^{\infty} i^n J_n(k\,\|\boldsymbol{x}\|)\cos(n(\theta_x - \phi)), \tag{4.4}$$

at some point $\boldsymbol{x} = (\|\boldsymbol{x}\|, \theta_x)$. Consider the truncation of the expansion (4.4) to $N+1$ terms, giving absolute error

$$\epsilon_N(\boldsymbol{x}) = 2\left|\sum_{n>N} i^n J_n(k\,\|\boldsymbol{x}\|)\cos(n(\theta_x - \phi))\right|. \tag{4.5}$$

Using the Bessel function bound [109, p.362],

$$|J_n(z)| \le \frac{z^n}{2^n\Gamma(n+1)} \equiv \frac{z^n}{2^n n!}, \tag{4.6}$$

for $n, z \ge 0$, the truncation error can be bounded by

$$\epsilon_N(\boldsymbol{x}) \le 2\sum_{n>N} |J_n(k\,\|\boldsymbol{x}\|)| \tag{4.7a}$$

$$\le 2\sum_{n>N} \frac{(\pi\,\|\boldsymbol{x}\|/\lambda)^n}{n!}. \tag{4.7b}$$

Letting $z \triangleq \pi\,\|\boldsymbol{x}\|/\lambda$, then the error can be written as

$$\epsilon_N(\boldsymbol{x}) \le 2\mathcal{R}_N(z), \quad z > 0, \tag{4.8}$$

[1]Each mode, indexed by n, corresponds to a different solution of the governing electromagnetic equations (Maxwell's equations) for the given boundary conditions.

where remainder

$$\mathcal{R}_N(z) \triangleq \sum_{n>N} \frac{z^n}{n!} \tag{4.9a}$$

$$= e^z - \sum_{n=0}^{N} \frac{z^n}{n!} \tag{4.9b}$$

$$= \frac{z^{N+1}}{(N+1)!} \sum_{n=0}^{\infty} \frac{(N+1)!}{(N+1+n)!} z^n, \tag{4.9c}$$

characterizes the behavior of $\epsilon_N(\boldsymbol{x})$.

First, observe that

$$\frac{(N+1)!}{(N+1+n)!} z^n \leq \left(\frac{z}{N+2}\right)^n, \tag{4.10}$$

therefore, since the sum of geometric series p^n is given by $1/(1-p)$, the remainder (4.9c) is upper bounded by

$$\mathcal{R}_N(z) \leq \frac{z^{N+1}}{(N+1)!} \left(\frac{N+2}{N+2-z}\right) \tag{4.11a}$$

$$\leq \frac{1}{\sqrt{2\pi(N+1)}} \left(\frac{N+2}{N+2-z}\right) \left(\frac{ez}{N+1}\right)^{N+1}, \tag{4.11b}$$

where the second inequality follows from the Stirling lower bound $n! > \sqrt{2\pi n} n^n e^{-n}$. Provided $N > ez - 1$ the exponential term in (4.11b) is contained, therefore giving a finite upper bound on the truncation error. Furthermore, by Taylor's theorem, for some $\eta_N \in [0, 1]$,

$$\sum_{n=0}^{\infty} \frac{(N+1)!}{(N+1+n)!} z^n = \exp(\eta_N z), \tag{4.12}$$

thus, for integer $\Delta \geq 0$, $\exp(\eta_{N+\Delta} z) \leq \exp(\eta_N z)$ and from (4.9c) the ratio

$$\frac{\mathcal{R}_{N+\Delta}(z)}{\mathcal{R}_N(z)} = \frac{z^{N+\Delta+1}}{(N+\Delta+1)!} \cdot \frac{(N+1)!}{z^{N+1}} \cdot \frac{\exp(\eta_{N+\Delta} z)}{\exp(\eta_N z)} \tag{4.13a}$$

$$\leq \frac{z^{\Delta}}{(N+2)(N+3)\cdots(N+\Delta+1)} \tag{4.13b}$$

$$\leq \left(\frac{z}{N+2}\right)^{\Delta} = \alpha^{-\Delta}|_{\alpha=(N+2)/z}. \tag{4.13c}$$

Therefore, whenever $N > z-2$ we have $\alpha > 1$ and the remainder $R_{N+\Delta}(z)$ decreases exponentially as Δ increases.

To have an effective truncation it is desirable to choose the smallest N such that the error bound is small in absolute terms as well as having exponential decay of the error as Δ increases. Therefore, motivated by (4.11b) and (4.13c) define the critical value of N as the integer function

$$\mathcal{N}_z \triangleq \lceil ez \rceil, \quad z > 0. \tag{4.14}$$

Then using inequality arguments, for $N > \mathcal{N}_z$ it can be shown that

$$\left(\frac{ez}{N+1}\right)^{N+1} \leq \frac{e^{ez}}{e^{N+1}} \leq \frac{1}{e}, \tag{4.15}$$

and

$$\left(\frac{N+2}{N+2-z}\right) \leq \frac{e}{e-1}, \tag{4.16}$$

therefore, using (4.15) and (4.16) in bound (4.11b) gives

$$\mathcal{R}_N(z) \leq \frac{(N+1)^{-1/2}}{\sqrt{2\pi}(e-1)}, \quad N > \mathcal{N}_z. \tag{4.17}$$

The piecewise nature of $\mathcal{R}_N(z)$ as a function of z, implies there are local maxima at $z \leq N/e$, therefore searching over these local maxima using the exact expression (4.9c) gives the uniform upper bound

$$R_N(z) \leq \max_N \mathcal{R}_N(N/e) = \mathcal{R}_2(2/e) \approx 0.08. \tag{4.18}$$

Futhermore, since $(N+2)/z > e$ the remainder $R_{N+\Delta}(z)$ decreases at least as fast as $\exp(-\Delta)$ as Δ increases. Therefore, from the above bound on remainder $\mathcal{R}_N(z)$, with $z \equiv \pi \|\boldsymbol{x}\| / \lambda$ then from (4.8) the truncation error is bounded by

$$\epsilon_{N+\Delta}(\boldsymbol{x}) \leq 0.16 \exp(-\Delta), \quad N > \mathcal{N}(\boldsymbol{x}),\ \Delta \in \mathbb{Z}^+, \tag{4.19}$$

where

$$\mathcal{N}(\boldsymbol{x}) \triangleq \lceil \pi e \|\boldsymbol{x}\| / \lambda \rceil, \tag{4.20}$$

that is, the truncation error in (4.4) for $\mathcal{N}(\boldsymbol{x}) + 1$ terms is small, and decreases at

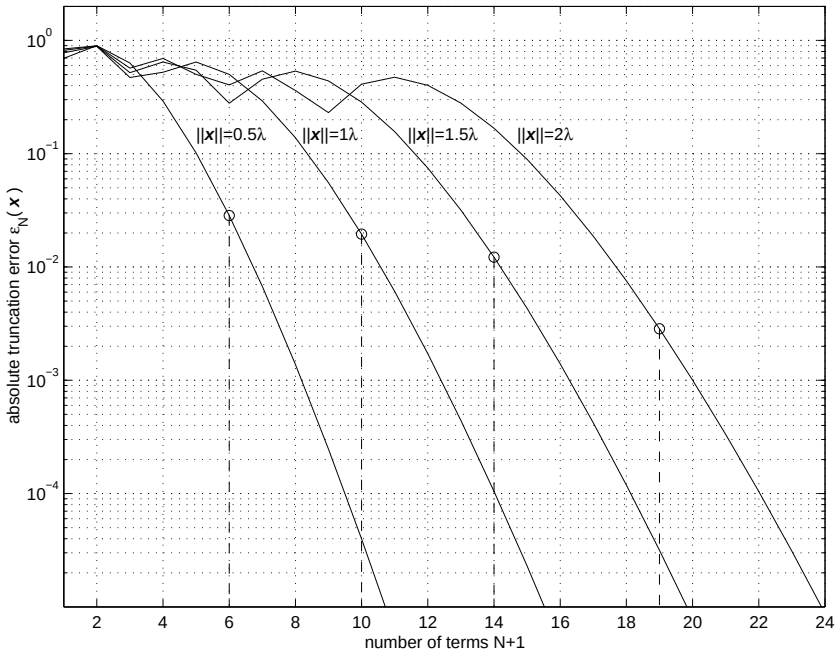

Figure 4.1: Absolute truncation error $\epsilon_N(\boldsymbol{x})$ (4.5) for increasing number of terms $N+1$ of the 2D plane wave expansion (4.4). Dashed vertical lines indicate the number of terms given by critical value $\mathcal{N}(\boldsymbol{x})+1$ for each $\boldsymbol{x}$.

least exponentially to zero as more terms are used.

The truncation error $\epsilon_N(\boldsymbol{x})$ is shown in Fig. 4.1 for increasing number of terms $N+1$ of the plane wave expansion (4.4). Shown as dashed vertical lines, the critical truncation value $\mathcal{N}(\boldsymbol{x})+1$ for each $\boldsymbol{x}$ gives a small absolute error, and as can be seen from the curves, an exponential decrease in error with any additional terms.

4.1.3 3D Plane Wave Propagation

Following a similar approach to the 2D case, the 3D plane wave can also be represented with negligible error using a finite number of terms. Consider a plane wave in a 3D environment travelling in direction $\boldsymbol{k} = k\widehat{\boldsymbol{k}}$ then it can be expressed by the 3D modal expansion [79]

$$e^{i\boldsymbol{k}\cdot\boldsymbol{x}} = \sum_{n=0}^{\infty} i^n (2n+1) j_n(k\,\|\boldsymbol{x}\|) P_n(\widehat{\boldsymbol{k}}\cdot\widehat{\boldsymbol{x}}), \tag{4.21}$$

where $P_n(\cdot)$ is the Legendre polynomial of order n. Consider the truncation of the expansion (4.21) to $N+1$ terms, giving absolute error

$$e_N(\boldsymbol{x}) = \left| \sum_{n>N} i^n (2n+1) j_n(k \|\boldsymbol{x}\|) P_n(\widehat{\boldsymbol{k}} \cdot \widehat{\boldsymbol{x}}) \right|, \tag{4.22}$$

which, given spherical Bessel function bound

$$j_n(z) \leq \frac{\sqrt{\pi}}{2} \frac{(z/2)^n}{\Gamma(n+3/2)} \equiv \frac{\sqrt{\pi}}{(2n+1)} \frac{(z/2)^n}{\Gamma(n+1/2)}, \tag{4.23}$$

and the property $\left| P_n(\widehat{\boldsymbol{k}} \cdot \widehat{\boldsymbol{x}}) \right| \leq 1$, gives the upper bound on truncation error

$$\epsilon_N(\boldsymbol{x}) \leq \sum_{n>N} (2n+1) \left| j_n(k \|\boldsymbol{x}\|) \right| \tag{4.24a}$$

$$\leq \sqrt{\pi} \sum_{n>N} \frac{(\pi \|\boldsymbol{x}\| / \lambda)^n}{\Gamma(n+1/2)}. \tag{4.24b}$$

Letting $z \triangleq \pi \|\boldsymbol{x}\| / \lambda$, then the error can be expressed as

$$\epsilon_N(\boldsymbol{x}) \leq \sqrt{\pi} \mathcal{R}_N(z), \quad z > 0, \tag{4.25}$$

where remainder

$$\mathcal{R}_N(z) \triangleq \sum_{n>N} \frac{z^n}{\Gamma(n+1/2)}, \tag{4.26}$$

characterizes the behavior of $\epsilon_N(\boldsymbol{x})$.

First, define the polynomial

$$S_N(z) = 1 + \sum_{k=1}^{\infty} \frac{z^k}{\prod_{\ell=0}^{k-1} (N+5/2+\ell)}, \tag{4.27}$$

then observe that

$$\mathcal{R}_N(z) = \frac{z^{N+1}}{\Gamma(N+3/2)} S_N(z) \tag{4.28a}$$

$$\leq \frac{z^{N+1}}{\Gamma(N+3/2)} \sum_{k=0}^{\infty} \left(\frac{z}{N+5/2} \right)^k \tag{4.28b}$$

$$\leq \frac{1}{\sqrt{2\pi e}} \left(\frac{ez}{N+1/2} \right)^{N+1} \sum_{k=0}^{\infty} \left(\frac{z}{N+5/2} \right)^k, \tag{4.28c}$$

where (4.28c) follows from (4.28b) via the Stirling bound on the Gamma function

$$\Gamma(n+3/2) \geq \sqrt{2\pi e}\left(\frac{n+1/2}{e}\right)^{n+1}. \tag{4.29}$$

Hence, provided $N > ez - 1/2$ the exponential term in (4.28c) is contained, likewise, provided $N > z - 5/2$, the geometric series converges giving

$$\mathcal{R}_N(z) \leq \frac{1}{\sqrt{2\pi e}}\left(\frac{N+5/2}{N+5/2-z}\right)\left(\frac{ez}{N+1/2}\right)^{N+1}, \tag{4.30}$$

therefore, provided N is sufficiently large a finite upper bound exists for the truncation error. Furthermore, consider the ratio

$$\frac{\mathcal{R}_{N+\Delta}(z)}{\mathcal{R}_N(z)} = \frac{z^{N+\Delta+1}}{\Gamma(N+\Delta+3/2)} \cdot \frac{\Gamma(N+3/2)}{z^{N+1}} \cdot \frac{S_{N+\Delta}(z)}{S_N(z)} \tag{4.31a}$$

$$\leq \left(\frac{z}{N+3/2}\right)^{\Delta} = \alpha^{-\Delta}|_{\alpha=(N+3/2)/z}, \tag{4.31b}$$

which for $N > z - 3/2$ gives $\alpha > 1$ and the remainder $R_{N+\Delta}(z)$ decreases exponentially as Δ increases.

To have an effective truncation it is desirable to choose the smallest N such that the error bound is small in absolute terms as well as having exponential decay of the error as Δ increases. Therefore, motivated by (4.30) and (4.31b) define the critical value of N as the integer function

$$\mathcal{N}_z \triangleq \lceil ez \rceil, \quad z > 0. \tag{4.32}$$

Then using inequality arguments, for $N > \mathcal{N}_z$ it can be shown that,

$$\frac{N+5/2}{N+5/2-z} \leq \frac{e}{e-1}, \tag{4.33}$$

and

$$\frac{ze}{N+1/2} \leq 1, \tag{4.34}$$

therefore, using (4.33) and (4.34) in bound (4.30) gives

$$\mathcal{R}_N(z) < \frac{e}{\sqrt{2\pi e}(e-1)}, \quad N > \mathcal{N}_z, \tag{4.35}$$

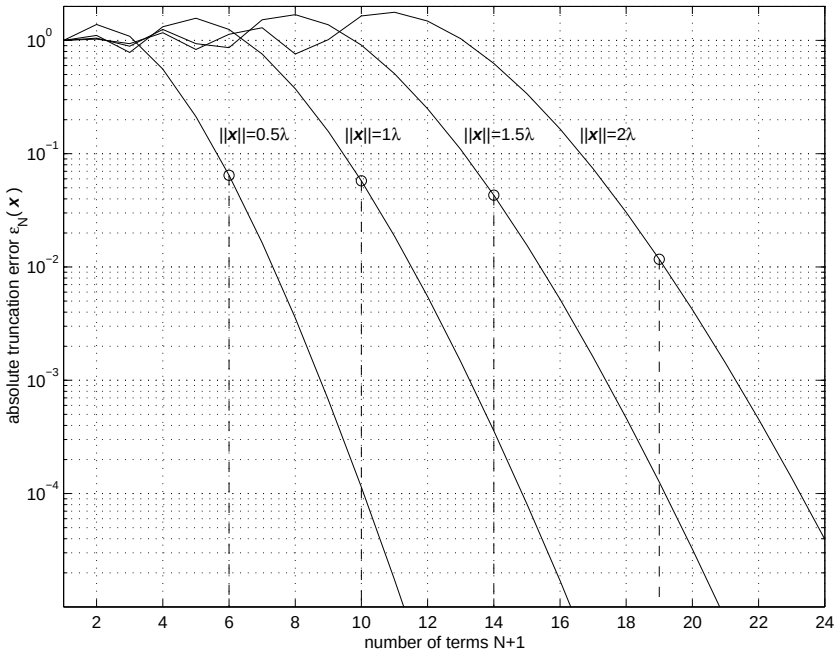

Figure 4.2: Absolute truncation error $\epsilon_N(\boldsymbol{x})$ (4.22) for increasing number of terms $N+1$ of the 3D plane wave expansion (4.21). Dashed vertical lines indicate the number of terms given by critical value $\mathcal{N}(\boldsymbol{x})+1$ for each $\boldsymbol{x}$.

which defines an explicit uniform bound. Furthermore, since $(N+3/2)/z > e$ the remainder $R_{N+\Delta}(z)$ decreases at least as fast as $\exp(-\Delta)$ as Δ increases. Therefore, from the above bound on remainder $\mathcal{R}_N(z)$, with $z \equiv \pi \|\boldsymbol{x}\|/\lambda$ then from (4.31b) the truncation error is bounded by

$$\epsilon_{N+\Delta}(\boldsymbol{x}) \leq \frac{\sqrt{e/2}}{e-1}\exp(-\Delta), \quad N > \mathcal{N}(\boldsymbol{x}),\, \Delta \in \mathbb{Z}^+, \tag{4.36}$$

where

$$\mathcal{N}(\boldsymbol{x}) \triangleq \lceil \pi e \|\boldsymbol{x}\|/\lambda \rceil, \tag{4.37}$$

that is, the truncation error in (4.21) for $\mathcal{N}(\boldsymbol{x})+1$ terms is small, and decreases at least exponentially to zero as more terms are used.

The truncation error $\epsilon_N(\boldsymbol{x})$ is shown in Fig. 4.2 for increasing number of terms $N+1$ of the plane wave expansion (4.21). Shown as dashed vertical lines, the critical truncation value $\mathcal{N}(\boldsymbol{x})+1$ for each $\boldsymbol{x}$ gives a small absolute error, and as can be seen from the curves, an exponential decrease in error with any additional terms.

4.2 2D Channel Model

Consider the 2D MIMO system shown in Fig. 4.3, where the transmitter consists of n_{T} transmit antennas located within a circular aperture of radius r_{T}. Similarly, at the receiver, there are n_{R} antennas within a circular aperture of radius r_{R}. Denote the n_{T} transmit antenna positions by $\boldsymbol{x}_t = (\|\boldsymbol{x}_t\|, \theta_t)$, $t = 1, 2, \ldots, n_{\mathrm{T}}$, in polar coordinates, relative to the origin of the transmit aperture, and the n_{R} receive antenna positions by $\boldsymbol{y}_r = (\|\boldsymbol{y}_r\|, \varphi_r)$, $r = 1, 2, \ldots, n_{\mathrm{R}}$, relative to the origin of the receive aperture. Note that all transmit and receive antennas are constrained to within the transmit and receive apertures respectively, that is,

$$\|\boldsymbol{x}_t\| \leq r_{\mathrm{T}}, \quad t = 1, 2, \ldots, n_{\mathrm{T}}, \tag{4.38}$$

$$\|\boldsymbol{y}_r\| \leq r_{\mathrm{R}}, \quad r = 1, 2, \ldots, n_{\mathrm{R}}. \tag{4.39}$$

It is also assumed that the scatterers are distributed in the farfield from all transmit and receive antennas, therefore, define circular scatterer free regions of radius $r_{\mathrm{TS}} > r_{\mathrm{T}}$, and $r_{\mathrm{RS}} > r_{\mathrm{R}}$, such that any scatterers are in the farfield to any antenna within the transmit and receive apertures, respectively. Note that for consistency, the origins of the transmit and receive apertures are required to be separated by greater than $r_{\mathrm{TS}}+r_{\mathrm{RS}}$. However, in practice the transmitter and receiver are usually separated by much larger distances.

Finally, the random scattering environment is defined by the effective random complex scattering gain $g(\phi, \psi)$ for a signal leaving from the transmit aperture at an angle ϕ, and entering the receive aperture at an angle ψ, via any number of paths through the scattering environment. One of the most physically reasonable assumptions for the modelling of signals in radio channels is the uncorrelated scatterer model, in this case the scattering channel is characterized by the second-order statistics of the scattering gain function $g(\phi, \psi)$, given by,

$$E\left\{g(\phi, \psi) g(\phi', \psi')\right\} = G(\phi, \psi)\delta(\phi - \phi')\delta(\psi - \psi'), \tag{4.40}$$

where $\delta(\cdot)$ is the Kronecker delta function, $\delta(0) = 1$ and zero elsewhere, and $G(\phi, \psi) = E\left\{|g(\phi, \psi)|^2\right\}$ represents the channel power over departure and arrival angles ϕ and ψ.

Using this model, the wireless channel has been separated into three distinct spatial regions of signal propagation, namely, the transmitter and receiver scatterer free regions which enclose the transmit and receive apertures, and the rest of space

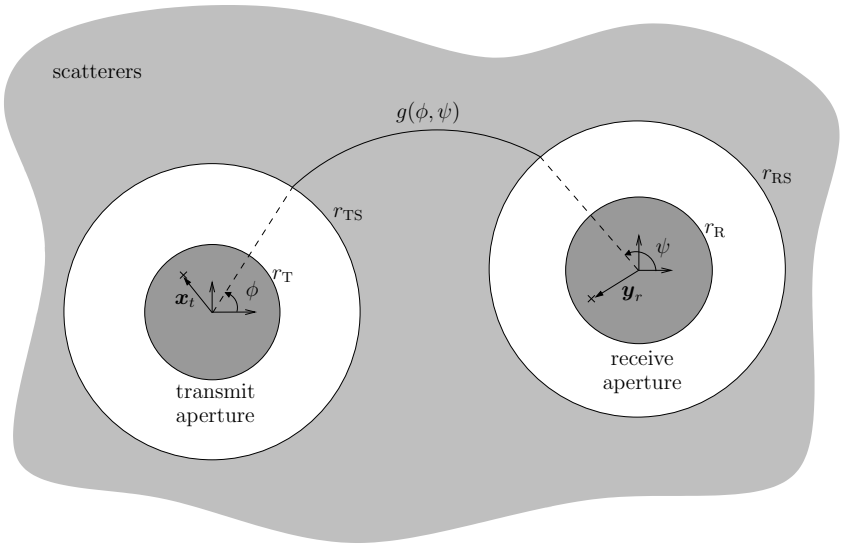

Figure 4.3: Scattering model for a 2D flat fading narrowband MIMO system. r_{T} and r_{R} are the radii of circular apertures which contain the transmit and receive antenna arrays, respectively. The radii r_{TS} and r_{RS} describe scatterer free circular regions surrounding the transmit and receive apertures, assumed large enough that any scatterer is farfield to all antennas. The scattering environment is described by $g(\phi, \psi)$ which gives the effective random complex gain for signals departing the transmit aperture from angle ϕ and arriving at the receive aperture from angle ψ, via any number of scattering paths.

assumed to be a general complex scattering media.

Consider the narrowband transmission of n_{T} baseband signals, $\{x_1, x_2, \ldots, x_{n_{\mathrm{T}}}\}$, over a single signalling interval from the n_{T} transmit antennas located within the transmit aperture. Since the region of radius r_{TS} is assumed large enough such that any point on its edge is farfield to all the transmit antennas, transmitted signals leaving this region can be considered plane waves. Therefore, the baseband signal leaving the scatterer free transmit region along direction ϕ is given by

$$\Phi(\phi) = \sum_{t=1}^{n_{\mathrm{T}}} x_t \, e^{ik\|\boldsymbol{x}_t\| \cos(\theta_t - \phi)}. \tag{4.41}$$

After the transmitted signals propagation through the scattering environment, the baseband signal entering the scatterer free receiver region along direction ψ is then given by

$$\Psi(\psi) = \int_{\mathbb{S}^1} \Phi(\phi)\, g(\phi, \psi)\, d\phi. \tag{4.42}$$

Again, given the scatterers are assumed farfield to the receive aperture, the signals impinging on the receiver array will consist of plane waves, thus the signal at $\boldsymbol{y}_r$ is given by

$$z_r = \int_{\mathbb{S}^1} \Psi(\psi) e^{-ik\|\boldsymbol{y}_r\| \cos(\varphi_r - \psi)} d\psi \tag{4.43a}$$

$$= \sum_{t=1}^{n_{\mathrm{T}}} x_t \iint_{\mathbb{S}^1} g(\phi, \psi)\, e^{ik\|\boldsymbol{x}_t\| \cos(\theta_t - \phi)}\, e^{-ik\|\boldsymbol{y}_r\| \cos(\varphi_r - \psi)}\, d\phi d\psi. \tag{4.43b}$$

Denote $\boldsymbol{x} = [x_1, x_2, \ldots, x_{n_{\mathrm{T}}}]'$ as the column vector of the transmitted signals, and $\boldsymbol{n} = [n_1, n_2, \ldots, n_{n_{\mathrm{R}}}]'$, as the noise vector where n_r is the independent additive white Gaussian noise (AWGN) at the r-th receive antenna, then the vector of received signals $\boldsymbol{y} = [y_1, y_2, \ldots, y_{n_{\mathrm{R}}}]'$ is given by

$$\boldsymbol{y} = \boldsymbol{H}\boldsymbol{x} + \boldsymbol{n}, \tag{4.44}$$

where $\boldsymbol{H}$ is the complex random channel matrix with r, t-th element

$$\boldsymbol{H}|_{r,t} = \iint_{\mathbb{S}^1} g(\phi, \psi) e^{ik\|\boldsymbol{x}_t\| \cos(\theta_t - \phi)}\, e^{-ik\|\boldsymbol{y}_r\| \cos(\varphi_r - \psi)}\, d\phi d\psi, \tag{4.45}$$

representing the channel gain between the t-th transmit antennna and the r-th receive antenna.

Equation (4.45) allows modelling of the spatial channel for any array configuration and scattering environment. However, the integral representation is not directly usable in many applications where closed-form channel gain expressions are desired. In the next section, using a modal analysis of plane waves (4.45) reduces into a form which reveals the underlying spatial structure of the channel gains, giving a decomposition of the channel matrix $\boldsymbol{H}$ which highlights the different effects of signal propagation in each spatial region.

4.2.1 Channel Matrix Modal Decomposition

Consider the 2D modal expansion of the plane wave

$$e^{ik\|\boldsymbol{x}\|\cos(\theta_x-\phi)} = J_0(k\|\boldsymbol{x}\|) + 2\sum_{n=1}^{\infty} i^n J_n(k\|\boldsymbol{x}\|)\cos(n(\theta_x-\phi)) \tag{4.46a}$$

$$= \sum_{n=-\infty}^{\infty} J_n(k\|\boldsymbol{x}\|)e^{-in(\theta_x-\phi)}, \tag{4.46b}$$

for vector $\boldsymbol{x} = (\|\boldsymbol{x}\|, \theta_x)$, then from Section 4.1.2 the plane wave is well approximated by the finite summation

$$e^{ik\|\boldsymbol{x}\|\cos(\theta_x-\phi)} \approx \sum_{n=-N}^{N} \overline{\mathcal{J}_n(\boldsymbol{x})}e^{in\phi}, \tag{4.47}$$

for $N = \lceil \pi e \|\boldsymbol{x}\| / \lambda \rceil$, where $\mathcal{J}_n(\boldsymbol{x})$ is defined as the *spatial-to-mode* function

$$\mathcal{J}_n(\boldsymbol{x}) \triangleq J_n(k\|\boldsymbol{x}\|)e^{in(\theta_x-\pi/2)}, \tag{4.48}$$

which maps the sampling point $\boldsymbol{x}$ to the n-th mode of the expansion (4.46b).

Define

$$N_{\mathrm{T}} \triangleq \lceil \pi e r_{\mathrm{T}}/\lambda \rceil, \tag{4.49}$$

$$N_{\mathrm{R}} \triangleq \lceil \pi e r_{\mathrm{R}}/\lambda \rceil, \tag{4.50}$$

then from Section 4.1.2 the truncated expansions

$$e^{ik\|\boldsymbol{x}_t\|\cos(\theta_t-\phi)} \approx \sum_{n=-N_{\mathrm{T}}}^{N_{\mathrm{T}}} \overline{\mathcal{J}_n(\boldsymbol{x}_t)}e^{in\phi}, \tag{4.51}$$

$$e^{-ik\|\boldsymbol{y}_r\|\cos(\varphi_r-\psi)} \approx \sum_{m=-N_\mathrm{R}}^{N_\mathrm{R}} \mathcal{J}_m(\boldsymbol{y}_r)e^{-in\psi}, \tag{4.52}$$

hold for every antenna within the transmit and receive apertures of radius r_T and r_R, respectively.

Substitution of (4.51) and (4.52) into (4.45), gives the closed-form expression for the channel gain between the t-th transmit antenna and r-th receive antenna as

$$\boldsymbol{H}|_{r,t} \approx \sum_{n=-N_\mathrm{T}}^{N_\mathrm{T}} \sum_{m=-N_\mathrm{R}}^{N_\mathrm{R}} \overline{\mathcal{J}_n(\boldsymbol{x}_t)}\mathcal{J}_m(\boldsymbol{y}_r) \iint_{\mathbb{S}^1} g(\phi,\psi)e^{in\phi}e^{-im\psi}d\phi d\psi. \tag{4.53}$$

Therefore, the channel matrix $\boldsymbol{H}$ can be decomposed into a product of three matrices, which correspond to the three spatial regions of signal propagation,

$$\boldsymbol{H} = \boldsymbol{J}_\mathrm{R}\boldsymbol{H}_\mathrm{S}\boldsymbol{J}_\mathrm{T}^\dagger, \tag{4.54}$$

where $\boldsymbol{J}_\mathrm{T}$ is the $n_\mathrm{T} \times (2N_\mathrm{T}+1)$ *transmit aperture sampling* matrix,

$$\boldsymbol{J}_\mathrm{T} = \begin{bmatrix} \mathcal{J}_{-N_\mathrm{T}}(\boldsymbol{x}_1) & \mathcal{J}_{-N_\mathrm{T}+1}(\boldsymbol{x}_1) & \cdots & \mathcal{J}_{N_\mathrm{T}}(\boldsymbol{x}_1) \\ \mathcal{J}_{-N_\mathrm{T}}(\boldsymbol{x}_2) & \mathcal{J}_{-N_\mathrm{T}+1}(\boldsymbol{x}_2) & \cdots & \mathcal{J}_{N_\mathrm{T}}(\boldsymbol{x}_2) \\ \vdots & \vdots & \ddots & \vdots \\ \mathcal{J}_{-N_\mathrm{T}}(\boldsymbol{x}_{n_\mathrm{T}}) & \mathcal{J}_{-N_\mathrm{T}+1}(\boldsymbol{x}_{n_\mathrm{T}}) & \cdots & \mathcal{J}_{N_\mathrm{T}}(\boldsymbol{x}_{n_\mathrm{T}}) \end{bmatrix}, \tag{4.55}$$

which describes the sampling of the transmit aperture, $\boldsymbol{J}_\mathrm{R}$ is the $n_\mathrm{R} \times (2N_\mathrm{R}+1)$ *receiver aperture sampling* matrix,

$$\boldsymbol{J}_\mathrm{R} = \begin{bmatrix} \mathcal{J}_{-N_\mathrm{R}}(\boldsymbol{y}_1) & \mathcal{J}_{-N_\mathrm{R}+1}(\boldsymbol{y}_1) & \cdots & \mathcal{J}_{N_\mathrm{R}}(\boldsymbol{y}_1) \\ \mathcal{J}_{-N_\mathrm{R}}(\boldsymbol{y}_2) & \mathcal{J}_{-N_\mathrm{R}+1}(\boldsymbol{y}_2) & \cdots & \mathcal{J}_{N_\mathrm{R}}(\boldsymbol{y}_2) \\ \vdots & \vdots & \ddots & \vdots \\ \mathcal{J}_{-N_\mathrm{R}}(\boldsymbol{y}_{n_\mathrm{R}}) & \mathcal{J}_{-N_\mathrm{R}+1}(\boldsymbol{y}_{n_\mathrm{R}}) & \cdots & \mathcal{J}_{N_\mathrm{R}}(\boldsymbol{y}_{n_\mathrm{R}}) \end{bmatrix}, \tag{4.56}$$

which describes the sampling of the receive aperture, and $\boldsymbol{H}_\mathrm{S}$ is a $(2N_\mathrm{R}+1) \times (2N_\mathrm{T}+1)$ *scattering environment* matrix, with p,q-th element

$$\boldsymbol{H}_\mathrm{S}|_{p,q} = \iint_{\mathbb{S}^1} g(\phi,\psi)\, e^{i(q-N_\mathrm{T}-1)\phi}\, e^{-i(p-N_\mathrm{R}-1)\psi}\, d\phi d\psi, \tag{4.57}$$

representing the complex gain between the $(q-N_\mathrm{T}-1)$-th mode of the transmit

aperture and the $(p - N_{\mathrm{R}} - 1)$-th mode of the receive aperture[2].

Consider the 2D Fourier series expansion of the periodic scattering function $g(\phi, \psi)$, given by

$$g(\phi, \psi) = \frac{1}{4\pi^2} \sum_{n=-\infty}^{\infty} \sum_{m=-\infty}^{\infty} \beta_m^n e^{-in\phi} e^{im\psi}, \tag{4.58}$$

with coefficients

$$\beta_m^n = \iint_{\mathbb{S}^1} g(\phi, \psi) e^{in\phi} e^{-im\psi} d\phi d\psi. \tag{4.59}$$

Therefore, letting $n = q - N_{\mathrm{T}} - 1$, and $m = p - N_{\mathrm{R}} - 1$ denote the transmitter mode and receiver mode index, respectively, the scattering environment matrix coefficients are given by

$$\boldsymbol{H}_{\mathrm{S}}|_{p,q} = \beta_{p-N_{\mathrm{R}}-1}^{q-N_{\mathrm{T}}-1} = \beta_m^n. \tag{4.60}$$

Thus the random scattering environment can be parameterized by the complex random coefficients β_m^n, $n = \{-N_{\mathrm{T}}, \ldots, N_{\mathrm{T}}\}$, $m = \{-N_{\mathrm{R}}, \ldots, N_{\mathrm{R}}\}$, giving

$$\boldsymbol{H}_{\mathrm{S}} = \begin{bmatrix} \beta_{-N_{\mathrm{R}}}^{-N_{\mathrm{T}}} & \beta_{-N_{\mathrm{R}}}^{-N_{\mathrm{T}}+1} & \cdots & \beta_{-N_{\mathrm{R}}}^{N_{\mathrm{T}}} \\ \beta_{-N_{\mathrm{R}}+1}^{-N_{\mathrm{T}}} & \beta_{-N_{\mathrm{R}}+1}^{-N_{\mathrm{T}}+1} & \cdots & \beta_{-N_{\mathrm{R}}+1}^{N_{\mathrm{T}}} \\ \vdots & \vdots & \ddots & \vdots \\ \beta_{N_{\mathrm{R}}}^{-N_{\mathrm{T}}} & \beta_{N_{\mathrm{R}}}^{-N_{\mathrm{T}}+1} & \cdots & \beta_{N_{\mathrm{R}}}^{N_{\mathrm{T}}} \end{bmatrix}. \tag{4.61}$$

Due to the similarities between the 2D and 3D channel models, comments on the significance of the model and the channel decomposition are left to after the 3D case, and can be found in Section 4.4.

4.3 3D Channel Model

Consider the 3D MIMO system shown in Fig. 4.4, where the transmitter consists of n_{T} transmit antennas located within a spherical aperture of radius r_{T}. Similarly, at the receiver, there are n_{R} antennas within a spherical aperture of radius r_{R}. Denote the n_{T} transmit antenna positions by the vectors $\boldsymbol{x}_t$, $t = 1, 2, \ldots, n_{\mathrm{T}}$, relative to the origin of the transmit aperture, and the n_{R} receive antenna positions by

[2]It is important to note the distinction between the *mode-to-mode* gains due to the scattering environment described by $\boldsymbol{H}_{\mathrm{S}}$, and the *antenna-to-antenna* channel gains described by $\boldsymbol{H}$.

$\boldsymbol{y}_r$, $r = 1, 2, \ldots, n_{\mathrm{R}}$, relative to the origin of the receive aperture. Note that all transmit and receive antennas are constrained to within the transmit and receive apertures respectively, that is,

$$\|\boldsymbol{x}_t\| \leq r_{\mathrm{T}}, \quad t = 1, 2, \ldots, n_{\mathrm{T}}, \tag{4.62}$$

$$\|\boldsymbol{y}_r\| \leq r_{\mathrm{R}}, \quad r = 1, 2, \ldots, n_{\mathrm{R}}. \tag{4.63}$$

It is also assumed that the scatterers are distributed in the farfield from all transmit and receive antennas, therefore, define spherical scatterer free regions of radius $r_{\mathrm{TS}} > r_{\mathrm{T}}$, and $r_{\mathrm{RS}} > r_{\mathrm{R}}$, such that any scatterers are in the farfield to any antenna within the transmit and receive apertures, respectively. Note that for consistency, the origins of the transmit and receive apertures are required to be separated by greater than $r_{\mathrm{TS}} + r_{\mathrm{RS}}$, however in practice the transmitter and receiver are usually separated by much larger distances.

Finally, the random scattering environment is defined by the effective random complex scattering gain $g(\widehat{\boldsymbol{\phi}}, \widehat{\boldsymbol{\psi}})$ for a signal leaving from the transmit aperture along direction $\widehat{\boldsymbol{\phi}}$, and entering the receive aperture from direction $\widehat{\boldsymbol{\psi}}$, via any number of paths through the scattering environment. Again the uncorrelated scatterer model is assumed, hence the scattering channel is characterized by the second-order statistics of the scattering gain function $g(\widehat{\boldsymbol{\phi}}, \widehat{\boldsymbol{\psi}})$, given by,

$$E\left\{g(\widehat{\boldsymbol{\phi}}, \widehat{\boldsymbol{\psi}}) g(\widehat{\boldsymbol{\phi}}', \widehat{\boldsymbol{\psi}}')\right\} = G(\widehat{\boldsymbol{\phi}}, \widehat{\boldsymbol{\psi}}) \delta(\widehat{\boldsymbol{\phi}} - \widehat{\boldsymbol{\phi}}') \delta(\widehat{\boldsymbol{\psi}} - \widehat{\boldsymbol{\psi}}'), \tag{4.64}$$

where $G(\widehat{\boldsymbol{\phi}}, \widehat{\boldsymbol{\psi}}) = E\left\{\left|g(\widehat{\boldsymbol{\phi}}, \widehat{\boldsymbol{\psi}})\right|^2\right\}$ represents the channel power over departure and arrival directions $\widehat{\boldsymbol{\phi}}$ and $\widehat{\boldsymbol{\psi}}$.

Using this 3D model a derivation similar to that of (4.43b) gives the received signal at position $\boldsymbol{y}_r$ as

$$z_r = \sum_{t=1}^{n_{\mathrm{T}}} x_t \iint_{\mathbb{S}^2} g(\widehat{\boldsymbol{\phi}}, \widehat{\boldsymbol{\psi}})\, e^{ik\boldsymbol{x}_t \cdot \widehat{\boldsymbol{\phi}}}\, e^{-ik\boldsymbol{y}_r \cdot \widehat{\boldsymbol{\phi}}}\, ds(\widehat{\boldsymbol{\phi}}) ds(\widehat{\boldsymbol{\phi}}), \tag{4.65}$$

where $ds(\widehat{\boldsymbol{\phi}})$ is a surface element of the unit sphere $\mathbb{S}^2$ with unit normal $\widehat{\boldsymbol{\phi}}$. Therefore, the vector of received signals can be expressed in matrix vector form (4.44),

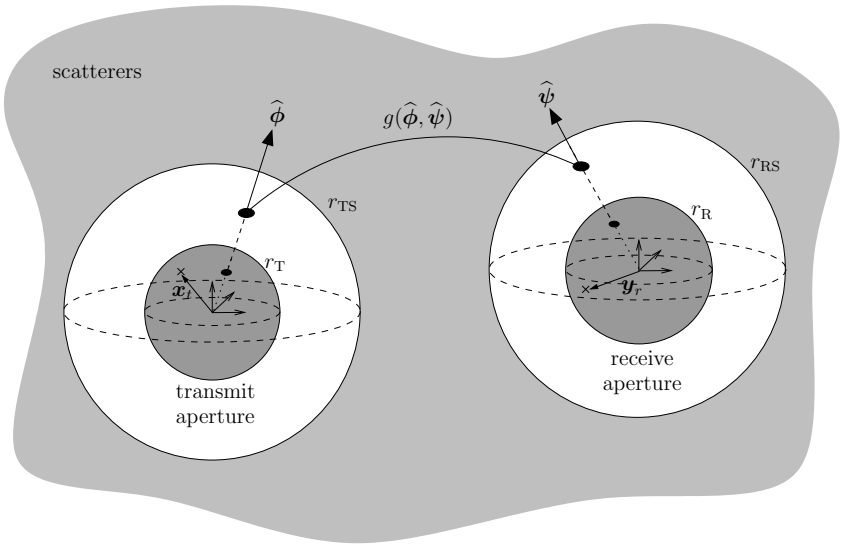

Figure 4.4: Scattering model for a 3D flat fading narrowband MIMO system. r_{T} and r_{R} are the radii of spherical apertures which contain the transmit and receive antenna arrays, respectively. The radii r_{TS} and r_{RS} describe scatterer free spherical regions surrounding the transmit and receive apertures, assumed large enough that any scatterer is farfield to all antennas. The scattering environment is described by $g(\widehat{\boldsymbol{\phi}}, \widehat{\boldsymbol{\psi}})$ which gives the effective random complex gain for signals departing the transmit aperture from direction $\widehat{\boldsymbol{\phi}}$ and arriving at the receive aperture from direction $\widehat{\boldsymbol{\psi}}$, via any number of scattering paths.

with the r,t-th element of the complex random channel matrix given by

$$\boldsymbol{H}|_{r,t} = \iint_{\mathbb{S}^2} g(\widehat{\boldsymbol{\phi}},\widehat{\boldsymbol{\psi}})\, e^{ik\boldsymbol{x}_t\cdot\widehat{\ }}\, e^{-ik\boldsymbol{y}_r\cdot\widehat{\ }}\, ds(\widehat{\boldsymbol{\phi}})ds(\widehat{\boldsymbol{\psi}}), \tag{4.66}$$

representing the channel gain between the t-th transmit antennna and the r-th receive antenna.

4.3.1 Channel Matrix Modal Decomposition

Consider the 3D modal expansion of the plane wave

$$e^{ik\boldsymbol{x}\cdot\widehat{\ }} = \sum_{n=0}^{\infty} i^n(2n+1)j_n(k\,\|\boldsymbol{x}\|)P_n(\widehat{\boldsymbol{x}}\cdot\widehat{\boldsymbol{\phi}}) \tag{4.67a}$$

$$= 4\pi\sum_{n=0}^{\infty}\sum_{m=-n}^{n} i^n j_n(k\,\|\boldsymbol{x}\|)\overline{Y_n^m(\widehat{\boldsymbol{x}})}Y_n^m(\widehat{\boldsymbol{\phi}}), \tag{4.67b}$$

where (4.67b) follows via the addition theorem [79]

$$\sum_{m=-n}^{n}\overline{Y_n^m(\widehat{\boldsymbol{x}})}Y_n^m(\widehat{\boldsymbol{\phi}}) = \frac{2n+1}{4\pi}P_n(\widehat{\boldsymbol{x}}\cdot\widehat{\boldsymbol{\phi}}), \tag{4.68}$$

then from Section 4.1.3 the plane wave is well approximated by the truncated summation

$$e^{ik\boldsymbol{x}\cdot\widehat{\ }} \approx \sum_{n=0}^{N}\sum_{m=-n}^{n}\mathcal{J}_n^m(\boldsymbol{x})Y_n^m(\widehat{\boldsymbol{\phi}}), \tag{4.69}$$

where $\mathcal{J}_n^m(\boldsymbol{x})$ is defined as the *spatial-to-mode* function

$$\mathcal{J}_n^m(\boldsymbol{x}) \triangleq 4\pi(-i)^n j_n(k\,\|\boldsymbol{x}\|)Y_n^m(\widehat{\boldsymbol{x}}), \tag{4.70}$$

which maps the sampling point $\boldsymbol{x}$ to the n,m-th mode of the expansion (4.67b).

Define

$$N_{\mathrm{T}} = \lceil \pi e r_{\mathrm{T}}/\lambda \rceil, \tag{4.71}$$

$$N_{\mathrm{R}} = \lceil \pi e r_{\mathrm{R}}/\lambda \rceil, \tag{4.72}$$

then from Section 4.1.3 the truncated expansions

$$e^{ik\boldsymbol{x}_t\cdot\widehat{\ }} \approx \sum_{n=0}^{N_\mathrm{T}} \sum_{m=-n}^{n} \overline{\mathcal{J}_n^m(\boldsymbol{x}_t)} Y_n^m(\widehat{\boldsymbol{\phi}}), \tag{4.73}$$

$$e^{-ik\boldsymbol{y}_r\cdot\widehat{\ }} \approx \sum_{n'=0}^{N_\mathrm{R}} \sum_{m'=-n'}^{n'} \mathcal{J}_{n'}^{m'}(\boldsymbol{y}_r) \overline{Y_{n'}^{m'}(\widehat{\boldsymbol{\psi}})}, \tag{4.74}$$

hold for every antenna within the transmit and receive apertures of radius r_T and r_R, respectively.

Substitution of (4.73) and (4.74) into (4.66), gives the closed-form expression for the channel gain between the t-th transmit antenna and r-th receive antenna as

$$\boldsymbol{H}|_{r,t} = \sum_{n=0}^{N_\mathrm{T}} \sum_{m=-n}^{n} \sum_{n'=0}^{N_\mathrm{R}} \sum_{m'=-n'}^{n'} \overline{\mathcal{J}_n^m(\boldsymbol{x}_t)} \mathcal{J}_{n'}^{m'}(\boldsymbol{y}_r) \beta_{n,m}^{n',m'}, \tag{4.75}$$

where

$$\beta_{n,m}^{n',m'} = \iint_{\mathbb{S}^2} g(\widehat{\boldsymbol{\phi}}, \widehat{\boldsymbol{\psi}})\, Y_n^m(\widehat{\boldsymbol{\phi}})\, \overline{Y_{n'}^{m'}(\widehat{\boldsymbol{\psi}})}\, ds(\widehat{\boldsymbol{\phi}}) ds(\widehat{\boldsymbol{\psi}}), \tag{4.76}$$

are the coefficients of the spherical harmonic basis expansion of the periodic channel gains;

$$g(\widehat{\boldsymbol{\phi}}, \widehat{\boldsymbol{\psi}}) = \sum_{n=0}^{\infty} \sum_{m=-n}^{n} \sum_{n'=0}^{\infty} \sum_{m'=-n'}^{n'} \beta_{n,m}^{n',m'} \overline{Y_n^m(\widehat{\boldsymbol{\phi}})} Y_{n'}^{m'}(\widehat{\boldsymbol{\psi}}). \tag{4.77}$$

Therefore, the channel matrix $\boldsymbol{H}$ can be decomposed into a product of three matrices, which correspond to the three spatial regions of signal propagation,

$$\boldsymbol{H} = \boldsymbol{J}_\mathrm{R} \boldsymbol{H}_\mathrm{S} \boldsymbol{J}_\mathrm{T}^\dagger, \tag{4.78}$$

where $\boldsymbol{J}_\mathrm{T}$ is the $n_\mathrm{T} \times (N_\mathrm{T}+1)^2$ *transmit aperture sampling* matrix,

$$\boldsymbol{J}_\mathrm{T} = \begin{bmatrix} \mathcal{J}_0^0(\boldsymbol{x}_1) & \mathcal{J}_1^{-1}(\boldsymbol{x}_1) & \cdots & \mathcal{J}_m^{-m}(\boldsymbol{x}_1) & \cdots & \mathcal{J}_m^m(\boldsymbol{x}_1) & \cdots & \mathcal{J}_{N_\mathrm{T}}^{N_\mathrm{T}}(\boldsymbol{x}_1) \\ \mathcal{J}_0^0(\boldsymbol{x}_2) & \mathcal{J}_1^{-1}(\boldsymbol{x}_2) & \cdots & & & & & \\ \vdots & & & & \ddots & & & \vdots \\ \mathcal{J}_0^0(\boldsymbol{x}_{n_\mathrm{T}}) & \mathcal{J}_1^{-1}(\boldsymbol{x}_{n_\mathrm{T}}) & \cdots & & & & \cdots & \mathcal{J}_{N_\mathrm{T}}^{N_\mathrm{T}}(\boldsymbol{x}_{n_\mathrm{T}}) \end{bmatrix}, \tag{4.79}$$

which describes the sampling of the transmit aperture, $\boldsymbol{J}_{\mathrm{R}}$ is the $n_{\mathrm{R}} \times (N_{\mathrm{R}}+1)^2$ *receiver aperture sampling* matrix,

$$\boldsymbol{J}_{\mathrm{R}} = \begin{bmatrix} \mathcal{J}_0^0(\boldsymbol{y}_1) & \mathcal{J}_1^{-1}(\boldsymbol{y}_1) & \cdots & \mathcal{J}_m^{-m}(\boldsymbol{y}_1) & \cdots & \mathcal{J}_m^m(\boldsymbol{y}_1) & \cdots & \mathcal{J}_{N_{\mathrm{R}}}^{N_{\mathrm{R}}}(\boldsymbol{y}_1) \\ \mathcal{J}_0^0(\boldsymbol{y}_2) & \mathcal{J}_1^{-1}(\boldsymbol{y}_2) & \cdots & & & & & \\ \vdots & & & & \ddots & & & \vdots \\ \mathcal{J}_0^0(\boldsymbol{y}_{n_{\mathrm{R}}}) & \mathcal{J}_1^{-1}(\boldsymbol{y}_{n_{\mathrm{R}}}) & \cdots & & & & \cdots & \mathcal{J}_{N_{\mathrm{R}}}^{N_{\mathrm{R}}}(\boldsymbol{y}_{n_{\mathrm{R}}}) \end{bmatrix}, \tag{4.80}$$

which describes the sampling of the receive aperture, and $\boldsymbol{H}_{\mathrm{S}}$ is a $(N_{\mathrm{R}}+1)^2 \times (N_{\mathrm{T}}+1)^2$ *scattering environment* matrix,

$$\boldsymbol{H}_{\mathrm{S}} = \begin{bmatrix} \beta_{0,0}^{0,0} & \beta_{1,-1}^{0,0} & \cdots & \beta_{N_{\mathrm{T}},N_{\mathrm{T}}}^{0,0} \\ \beta_{0,0}^{1,-1} & \beta_{1,-1}^{1,-1} & \cdots & \beta_{N_{\mathrm{T}},N_{\mathrm{T}}}^{1,-1} \\ \vdots & \vdots & \ddots & \vdots \\ \beta_{0,0}^{N_{\mathrm{R}},N_{\mathrm{R}}} & \beta_{1,-1}^{N_{\mathrm{R}},N_{\mathrm{R}}} & \cdots & \beta_{N_{\mathrm{T}},N_{\mathrm{T}}}^{N_{\mathrm{R}},N_{\mathrm{R}}} \end{bmatrix}, \tag{4.81}$$

which gives the complex gains between the m,n-th mode of the transmit aperture and the m',n'-th mode of the receive aperture, and parameterizes random scattering environment.

4.4 Comments on the Channel Model

The 2D and 3D channel matrix decompositions separates the channel into three distinct regions of signal propagation: a free-space transmitter region, a scattering environment region, and a free-space receiver region. The transmit and receive aperture sampling matrices, $\boldsymbol{J}_{\mathrm{T}}$ and $\boldsymbol{J}_{\mathrm{R}}$, describe the mapping of the transmitted signals to the transmitter modes, and the receiver modes to the receiver antenna positions, respectively. For fixed array geometries within the spatial apertures, regardless of aperture movement or scattering environment variations, the sampling matrices are constant and characterize the effects of antenna placement on the overall channel matrix $\boldsymbol{H}$. Conversely, for a random scattering environment[3] the scattering environment matrix $\boldsymbol{H}_{\mathrm{S}}$ has random elements, corresponding to random gains between the modes of the transmit and receive apertures.

In the wireless literature on MIMO systems, the elements of the channel matrix

[3]The scattering environment may be random due to random variations in the scatterers, or due moving apertures through fixed scattering, or both.

are generally modelled as random variables (with the exception of work of Gesbert et. al. [105], and Sayeed [120]). However, in this model, deterministic portions are factored out leaving only the parameters of the scattering environment to be modelled as random variables. This is a clear advantage over existing models, since one can explicitly see the role of spatially constrained arbitrary antenna configurations (not limited to specific array configurations [120], or the manifested antenna correlation as in [105]) and general scattering environments within the model.

Therefore, the model presented in this chapter is more general than previously reported models, giving a succinct representation of the continuous MIMO channel for a wide range of antenna configurations and scattering environments. In fact, as will be explored further in Chapter 5, many common models in the literature are special cases of the model presented here. Although a more general model than those previously reported, many important aspects of the channel are captured and, as shown in the next section and later chapters, give rise to valuable insights into the spatial characteristics of the channel.

4.4.1 Spatial Degrees of Freedom (SDOF)

In this section the Spatial degrees of freedom (SDOF) of a given MIMO system are quantified. In other words, how many free parameters are available when the transmit and receive antennas are contained within spatial apertures of radius r_{T} and r_{R}, respectively, within some scattering environment.

The rank of the channel matrix $\boldsymbol{H}$ determines the maximum number of parallel sub-channels between the transmitter array and the receiver array. In the literature the i.i.d. model assumes that the channel matrix has independent elements corresponding to sufficiently spaced antennas, in this case the channel rank is given by $\min\{n_{\mathrm{T}}, n_{\mathrm{R}}\}$. However, when realistic antenna configurations and scattering environments are considered, the elements of $\boldsymbol{H}$ become correlated and the number of possible parallel sub-channels is reduced. The channel decomposition presented in this chapter separates the effects of antenna configuration and the scattering environment and therefore allows us to express their independent effects on channel rank as

$$\mathrm{rank}(\boldsymbol{H}) = \min\{\mathrm{rank}(\boldsymbol{J}_{\mathrm{R}}), \mathrm{rank}(\boldsymbol{H}_{\mathrm{S}}), \mathrm{rank}(\boldsymbol{J}_{\mathrm{T}})\}. \tag{4.82}$$

Recall that the number of columns in the receive and transmit aperture sampling matrices is determined by the radii of the aperture, then for fixed sized apertures

the rank of $\boldsymbol{J}_{\mathrm{T}}$ and $\boldsymbol{J}_{\mathrm{R}}$ cannot exceed $2N_{\mathrm{T}}+1$ and $2N_{\mathrm{R}}+1$, respectively, for the 2D environment, and $(N_{\mathrm{T}}+1)^2$ and $(N_{\mathrm{R}}+1)^2$, respectively, for the 3D environment, regardless of the number of antennas contained within.

A rich scattering environment has generally been defined in the MIMO literature as one which supports $\min\{n_{\mathrm{T}}, n_{\mathrm{R}}\}$ independent sub-channels. However, if the antennas are contained within spatial apertures of finite size, the environment need only provide the maximum number of independent links between the transmit aperture modes to the receive aperture modes, which for a large number of antennas is less than $\min(n_{\mathrm{T}}, n_{\mathrm{R}})$. Therefore, denote the number of transmit modes by N and the number of receive modes by M, then define the *spatial richness factor*

$$\kappa_{\mathrm{S}} \triangleq \frac{\mathrm{rank}(\boldsymbol{H}_{\mathrm{S}})}{\min\{N, M\}} \tag{4.83}$$

where $\kappa_{\mathrm{S}} \in \mathbb{Q}^{(0,1]}$ characterizes the scattering environment. For $\kappa_{\mathrm{S}} = 1$, corresponding to a rich scattering environment, the scattering matrix $\boldsymbol{H}_{\mathrm{S}}$ is full rank with rank given by the minimum rank of the transmit and receive aperture sampling matrices. However, for $\kappa_{\mathrm{S}} < 1$ the scattering environment is not sufficiently rich to support the full set of independent modal gains, hence, the coefficients of $\boldsymbol{H}_{\mathrm{S}}$ may become correlated leading to a reduction in $\mathrm{rank}(\boldsymbol{H}_{\mathrm{S}})$.

The SDOF of the a scattering environment surrounding transmit and receive apertures of radii r_{T} and r_{R}, respectively, can now be expressed as

$$\mathrm{SDOF} = \kappa_{\mathrm{S}} \min\{N, M\}, \tag{4.84}$$

where $N = 2N_{\mathrm{T}}+1$, $M = 2N_{\mathrm{R}}+1$ for circular apertures, and $N = (N_{\mathrm{T}}+1)^2$, $M = (N_{\mathrm{R}}+1)^2$ for spherical apertures, with $N_{\mathrm{T}} = \lceil \pi e r_{\mathrm{T}}/\lambda \rceil$, $N_{\mathrm{R}} = \lceil \pi e r_{\mathrm{R}}/\lambda \rceil$, and $\kappa_{\mathrm{S}} \in (0, 1]$ is the spatial richness of the scattering environment. Note that the SDOF is independent of the number of antennas of the system, and gives the maximum number degrees of freedom available given the spatial constraints imposed by the channel. In comparison to the i.i.d. case, the maximum number of independent sub-channels of a spatially constrained MIMO system is now $\min\{n_{\mathrm{T}}, n_{\mathrm{R}}, \mathrm{SDOF}\}$.

4.5 Summary and Contributions

The previous two chapters have shown that the spatial properties of the channel will have significant impact on the capacity of multi-antenna systems. A good understanding of these properties is required for effective design and implementation of

wireless MIMO systems. Responding to this need, in this chapter a general channel model which includes the spatial aspects of a MIMO system was developed for both 2D and 3D scattering environments. The spatial channel model developed includes the physical parameters of arbitrary antenna configurations and a tractable parameterization of the complex scattering environment. Furthermore, by exploiting the properties of plane waves the channel is decomposed to emphasize the individual contributions of the arrays and the scattering environment.

Some specific contributions made in this chapter are:

1. The extensively used plane wave in channel modelling is represented as a truncated modal expansion in the 2D and 3D cases. The truncation point is shown to give a small error which exponentially decreases as more terms are added.

2. A 2D and 3D channel model is developed, which models the spatial channel for any antenna configurations within spatial apertures connected by any general scattering environment.

3. Using the plane wave truncations, the channel model is decomposed into three distinct regions of signal propagation: free-space transmitter, free-space receiver, and the scattering environment connecting them. For fixed array geometries within the transmit and receive apertures, the free-space transmitter and receiver component of the model are constant, with the random scattering component modelled by a tractable parameterization.

4. The concept of spatial degrees of freedom (SDOF) is introduced. The number of available free parameters of the spatial channel is given by the size of the transmit and receive apertures along with the scattering environment. A stricter definition of the richness of a scattering environment is defined which depends on the size of the apertures, in contrast to previous work where it has been considered independent of the antenna arrays.

Chapter 5

Capacity of Spatially Selective Channels

This chapter numerically verifies the theoretical statements made in the previous chapters. Using the model presented in Chapter 4, various aperture and scattering scenarios are explored. For simplicity, the numerical results are restricted to the 2D model. For comparison between the different numerical scenarios it is assumed $n_{\mathrm{T}} = n_{\mathrm{R}} = 6$, $r_{\mathrm{T}} = r_{\mathrm{R}} = 0.5\lambda$ and SNR is 10dB whenever these variables are not being studied.

5.1 MIMO Model and Channel Rank

Consider a MIMO system consisting of n_{T} transmit antennas and n_{R} receive antennas within circular apertures of radius r_{T} and r_{R}, respectively, along with the 2D channel model developed in Chapter 4.2. Using this model the channel matrix can be decomposed to give

$$\boldsymbol{H} = \boldsymbol{J}_{\mathrm{R}} \boldsymbol{H}_{\mathrm{S}} \boldsymbol{J}_{\mathrm{T}}^{\dagger}, \tag{5.1}$$

where $\boldsymbol{J}_{\mathrm{T}}$ is the transmit aperture sampling matrix (4.55), $\boldsymbol{J}_{\mathrm{R}}$ is the receive aperture sampling matrix (4.56), and $\boldsymbol{H}_{\mathrm{S}}$ is the scattering environment matrix.

The random complex scattering environment matrix $\boldsymbol{H}_{\mathrm{S}}$ describes the scattering environment through which the apertures communicate. The rank of $\boldsymbol{H}_{\mathrm{S}}$ gives the effective number of independent communication modes the scattering can support for given transmit and receive aperture size. Consider the elements of $\boldsymbol{H}_{\mathrm{S}}$ as zero mean i.i.d. complex Gaussian, then $\boldsymbol{H}_{\mathrm{S}}$ is a full rank matrix giving

spatial richness factor $\kappa_{\mathrm{S}} = 1$ and the maximum SDOF (4.84) for a the givien aperture sizes. This is shown pictorially in Fig. 5.1(a), where there is isotropic scattering around both apertures and throughout the rest of space. Conversely, a rank one $\boldsymbol{H}_{\mathrm{S}}$ occurs for fully correlated zero mean identically distributed complex Gaussian elements, $\boldsymbol{H}_{\mathrm{S}} \sim \mathbb{C}\mathcal{N}(\mathbf{0}, \mathbf{1})$, giving minimum spatial richness and offering only one SDOF. Figure 5.1(c)–(e) shows three possible scattering environments for rank one scattering matrices; (c) isotropic scattering surrounding both apertures, with limited scattering in between, (d) limited angular spread at one aperture, and (e) limited angular spread at both apertures. Note that channels exhibiting the scattering shown in Fig. 5.1(c) are often referred to as a pin-hole or key-hole channels, where there is only a single communication channel through the scattering environment [74, 105], these rare channels are explored further in Section 5.3.

The ergodic capacity for the two extreme scattering cases (full rank and rank 1 $\boldsymbol{H}_{\mathrm{S}}$) is shown in Fig. 5.2 for increasing SNR. The antennas $n_{\mathrm{T}} = n_{\mathrm{R}} = 6$ are arranged as UCAs constrained within the transmit and receive apertures of radius of either 0.5λ or 0.01λ. In the case of large apertures and full rank scattering the capacity is nearly that of the i.i.d. capacity shown as a dashed line. However, if either an aperture is made small, or the channel is scattering deficient the ergodic capacity is significantly reduced, with approximately the same capacity for all cases. Note that the rank of the transmit and receive sampling matrices, $\boldsymbol{J}_{\mathrm{T}}$ and $\boldsymbol{J}_{\mathrm{R}}$, respectively, is reduced to 1 for radius 0.01λ, therefore, Fig. 5.2 shows that the ergodic capacity is dominated by the overall channel rank

$$\mathrm{rank}(\boldsymbol{H}) = \min\{\mathrm{rank}(\boldsymbol{J}_{\mathrm{T}}), \mathrm{rank}(\boldsymbol{J}_{\mathrm{R}}), \mathrm{rank}(\boldsymbol{H}_{\mathrm{S}})\}, \tag{5.2}$$

or equivalently the SDOF of the spatial channel.

Although the ergodic capacity is governed by the overall rank, the outage capacity will depend on which component of the channel loses rank. The CDF of the capacity for the same scenarios as Fig. 5.2 is shown in Fig. 5.3 for SNR of 10dB. Here it can be seen that the outage capacity is governed not only by the overall channel rank loss but is also dependent on the location of the rank loss (transmitter, receiver, or scattering - see Fig. 5.1). From Fig. 5.3 it can be seen that there are three distinct causes of reduced outage capacity, (a) loss of rank in one location (receiver or scattering)[1], (b) loss in two locations (transmitter and receiver,

[1]Note that due to the reciprocity property, for the same scattering identical capacity is given regardless of whether we consider transmit or receive rank loss (i.e., $r_{\mathrm{T}} = 0.5\lambda$, $r_{\mathrm{R}} = 0.01\lambda$ or $r_{\mathrm{T}} = 0.01\lambda$, $r_{\mathrm{R}} = 0.5\lambda$). Therefore, without loss of generality we consider only the receive aperture.

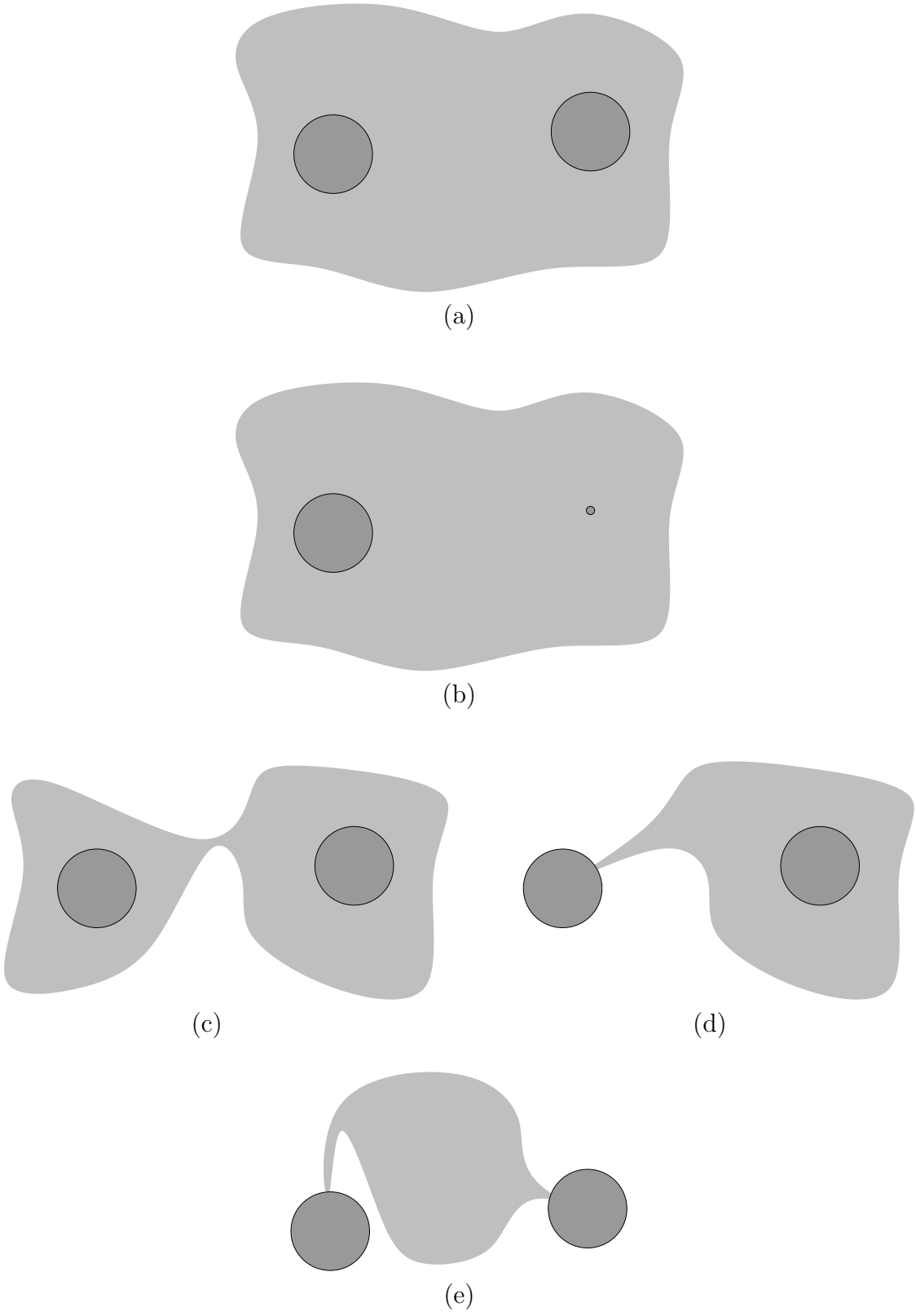

Figure 5.1: Spatial model interpretation. Dark grey circles represent apertures and light grey represents scattering: (a) full rank, (b) loss in aperture rank, (c)–(e) loss in scattering rank

or receiver and scattering), or (c) loss in three locations (transmitter, receiver and scattering). In the first two cases, a loss in scattering rank results in the lowest outage capacity for that case, due to a loss of scattering diversity (increased fading correlation) resulting in lower diversity for the overall channel. The worst capacity occurs for (c) where there is no diversity provided by either transmitter or receiver array and insufficient scattering gives correlated fading.

Similar results regarding the outage capacity behavior have been presented in [121] using a discrete scattering model described in [105]. As antennas constrained within a very small aperture will be highly correlated, it is straightforward to see how these two models give rise to identical results. In fact, with some limiting assumptions on the scattering environment, the channel model presented in [105] can be shown to be a special case of the model developed in Chapter 4. This connection is made more apparent with the work in Section 5.3.

These results indicate that the spatial constraints imposed by the scattering and apertures effects the ergodic and outage capacity differently. Therefore, in the following sections these constraints are further studied independently.

5.2 Capacity - Aperture Effects

In this section the effects of antenna geometry and aperture size on capacity are studied. To remove any scattering effects the scattering environment is assumed rich in all cases, e.g., $\kappa_{\mathrm{S}} = 1$. The effects of the scattering environment on capacity can be found in Section 5.3.

5.2.1 Antenna Saturation

In Chapter 3 an antenna saturation effect was shown for spatially constrained arrays at one end of the communication link, with the other end assumed unrestricted. In this section the capacity of a MIMO system for increasing numbers of antennas is investigated for both transmit and receive arrays constrained within separate apertures of finite size.

Figure 5.4 shows the capacity growth with increasing numbers $n_{\mathrm{T}} = n_{\mathrm{R}}$ of antennas within transmit and receive apertures of radius $r_{\mathrm{T}} = r_{\mathrm{R}} = 0.5\lambda$, for the ULA and UCA. As was shown in Chapter 3, the capacity suffers a saturation in the number of antennas whereby further antennas fail to give further capacity gain. Also shown is the antenna saturation when the receive aperture radius is reduced to $r_{\mathrm{R}} = 0.25\lambda$ for the same size transmit aperture $r_{\mathrm{T}} = 0.5\lambda$. In this case the saturated

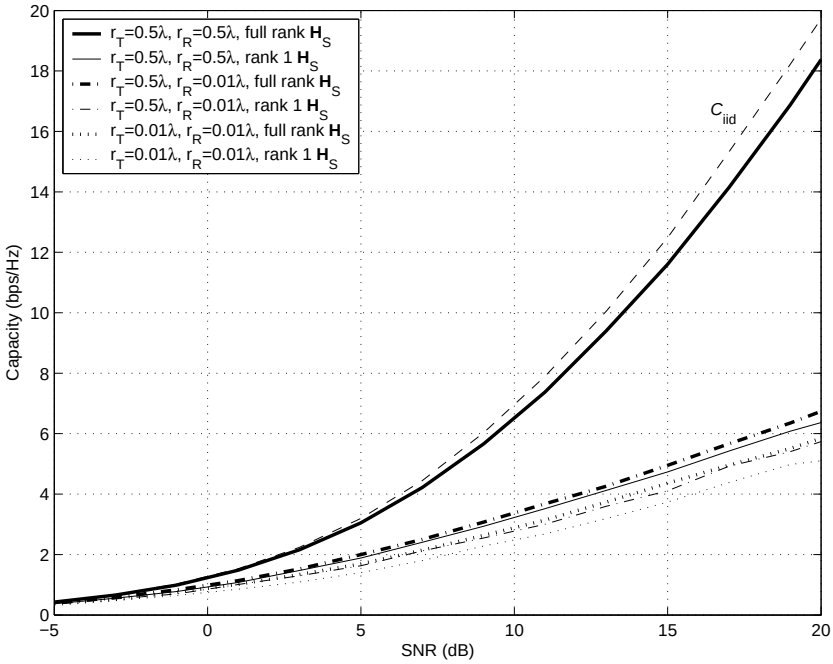

Figure 5.2: Ergodic capacity with increasing SNR for various channel scenarios for 6 antenna UCAs.

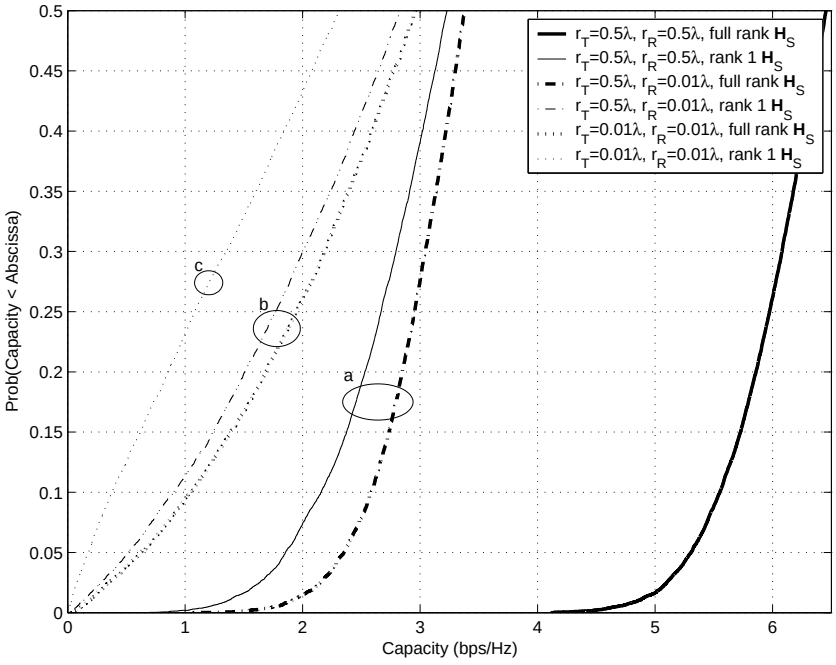

Figure 5.3: CDF of channel capacity for various channel scenarios for 6 antenna UCAs with SNR 10dB.

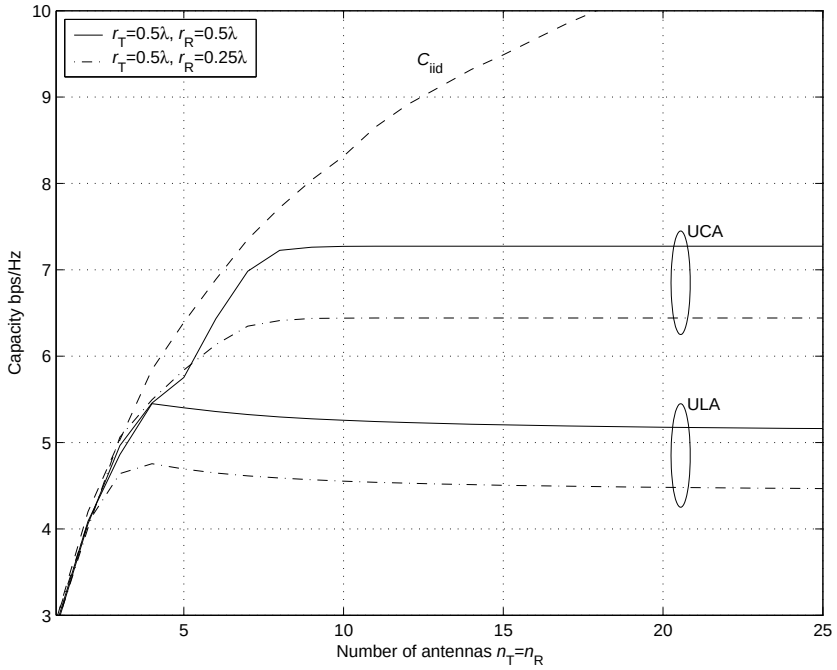

Figure 5.4: Antenna saturation of capacity for the ULA and UCAs constrained within transmit and receiver apertures of radius r_{T} and r_{R}, respectively. The scattering environment is modelled as isotropic and the received SNR is 10dB. Also shown is the unconstrained aperture capacity corresponding to i.i.d. channel gains.

capacity for both array types is lower, as expected, since the SDOF of the channel will be reduced. For this example $r_{\mathrm{T}} = r_{\mathrm{R}} = 0.5\lambda$, $\kappa_{\mathrm{S}} = 1$ giving SDOF = 11, whereas $r_{\mathrm{T}} = 0.5\lambda$, $r_{\mathrm{R}} = 0.25\lambda$, $\kappa_{\mathrm{S}} = 1$ gives SDOF = 7. Hence the capacity of the system is upper bounded by the smallest 'communications pipe', that is, even if the scattering and transmit aperture can offer significant throughput, the capacity of the system will be limited by the low throughout of the receiver aperture. Hence an upper bound on capacity can be given by the compound bound

$$C_{\max} = \min\{C_{\mathrm{sat}}(r_{\mathrm{T}}), C_{\mathrm{sat}}(r_{\mathrm{R}}), C_{\mathrm{S}}(\kappa_{\mathrm{S}})\}, \tag{5.3}$$

where $C_{\mathrm{sat}}(r_{\mathrm{T}})$ and $C_{\mathrm{sat}}(r_{\mathrm{R}})$ are the saturated capacity bounds derived in Chapter 3.3.2 for the transmit and receive apertures, respectively, and $C_{\mathrm{S}}(\kappa_{\mathrm{S}})$ is the maximum throughput of the scattering environment parameterized by the spatial richness factor κ_{S}. Similar arguments are proposed in [72] for an upper bound on ergodic capacity using a compound bound based on the individual transmit and receive branch correlations, however, as mentioned previously these provide little physical intuition into the aspects affecting capacity.

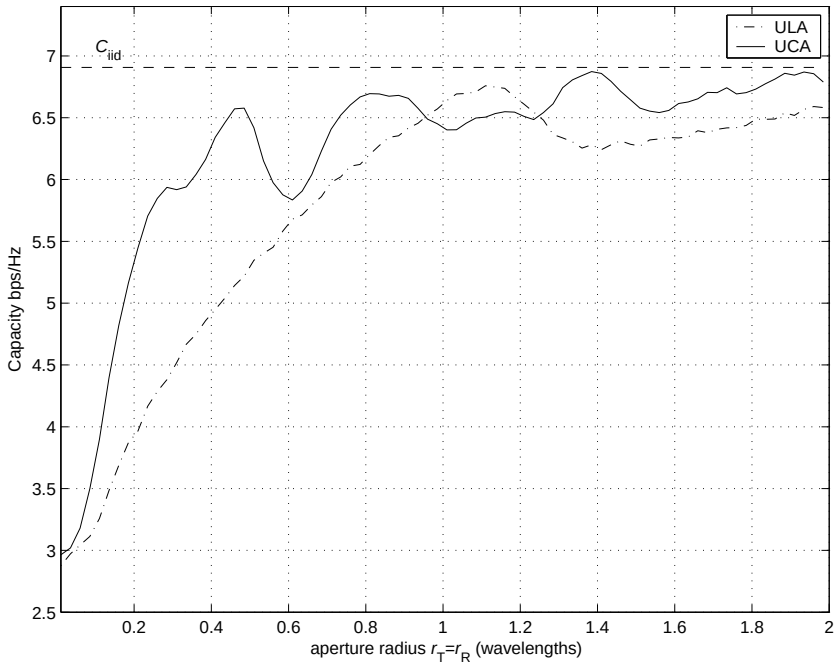

Figure 5.5: Capacity growth with increasing aperture size for 6 antenna ULA and UCAs in isotropic scattering and SNR 10dB.

5.2.2 Aperture Size

From the previous arguments and from the results of Chapter 3, the aperture size plays a dominant role in the capacity of a MIMO system. Consider 6 antenna arrays within transmit and receive apertures of radius r_{T} and r_{R} with an isotropic scattering environment, $\kappa_{\mathrm{S}} = 1$. The capacity growth of this scenario with increasing aperture radii $r_{\mathrm{T}} = r_{\mathrm{R}}$ is shown in Fig. 5.5 for the ULA and UCA arrays. As the apertures are made larger, both the ULA and UCA capacities approach that of the 6×6 i.i.d. case shown as a dashed horizontal line. Note that, as observed in Chapter 2, the spatial correlation between antennas does not decrease monotonically with antenna separation, therefore, in certain scenarios increasing the aperture radius may actually increase the spatial correlation leading to a reduction in capacity. The capacity growth as the aperture radius is increased is due to an increase in the SDOF of the channel, due to an increase in the effective parallel sub-channels between the arrays. This is best observed by considering the singular values of the channel matrix $\boldsymbol{H}$.

Figures 5.6 and 5.7 show the probability distributions (PDF's)[2] of the ordered singular values of the channel matrix $\boldsymbol{H}$ for the ULA and UCA, respectively. As

[2]Generated from 10,000 realizations of the random channel matrix $\boldsymbol{H}$ and scaled for display purposes.

the radius of the apertures are increased it can be observed that the median of the dominant singular value μ_1 is decreased, conversely, the medians of μ_k, $k > 1$ increase. Also observe that the separation of the singular values or difference between μ_k and μ_{k+1} decreases for all k as the aperture size is increased. Therefore the growth in capacity seen in Fig. 5.5 is due to the decrease in statistical disparity among the singular values, i.e., the disparity among the subchannels decreases giving a larger set of significant subchannels which to communicate on.

The convergence of the singular values is shown in Figures 5.8 and 5.9 for the ULA and UCA, respectively. Here as the radii are increased the medians of the singular values μ_k, $k > 1$ monotonically increase towards 1, whilst the median of the dominant singular value μ_1 decreases towards 1.

Note that the capacity difference between the ULA and UCA for increasing radii can be seen in the pdf's of the singular values of $\boldsymbol{H}$. Observe that in Fig. 5.6(b) there are less singular values with median over 0dB than the UCA case shown in Fig. 5.7(b) for the same radii. Hence the ULA has less subchannels with significant gain than a UCA within the same aperture size, thereby resulting in lower capacity. This clearly seen in Figures 5.8 and 5.9 by observing the curves of the median eigenvalues of the two arrays for the same aperture radii (note the radius scale is not the same for both the ULA and UCA). The effects of array geometry on capacity are discussed in detail in Chapter 6.2.

5.3 Capacity - Scattering effects

In this section the effects of the scattering environment on the capacity is studied. To compare environments, $n_{\mathrm{T}} = n_{\mathrm{R}} = 6$ antennas are fixed within apertures of radius $r_{\mathrm{T}} = r_{\mathrm{R}} = 0.5\lambda$ for all simulations.

5.3.1 Discrete Channel Representation

Consider the physical finite scatterers model, where each path is indexed by s and has a defined AOD ϕ_s and AOA ψ_s along with a complex random path gain g_s due to the scatterers. For n_{S} paths, the scattering channel is given by the discrete representation

$$g(\phi, \psi) = \sum_{s=1}^{n_{\mathrm{S}}} g_s \, \delta(\phi - \phi_s) \, \delta(\psi - \psi_s). \tag{5.4}$$

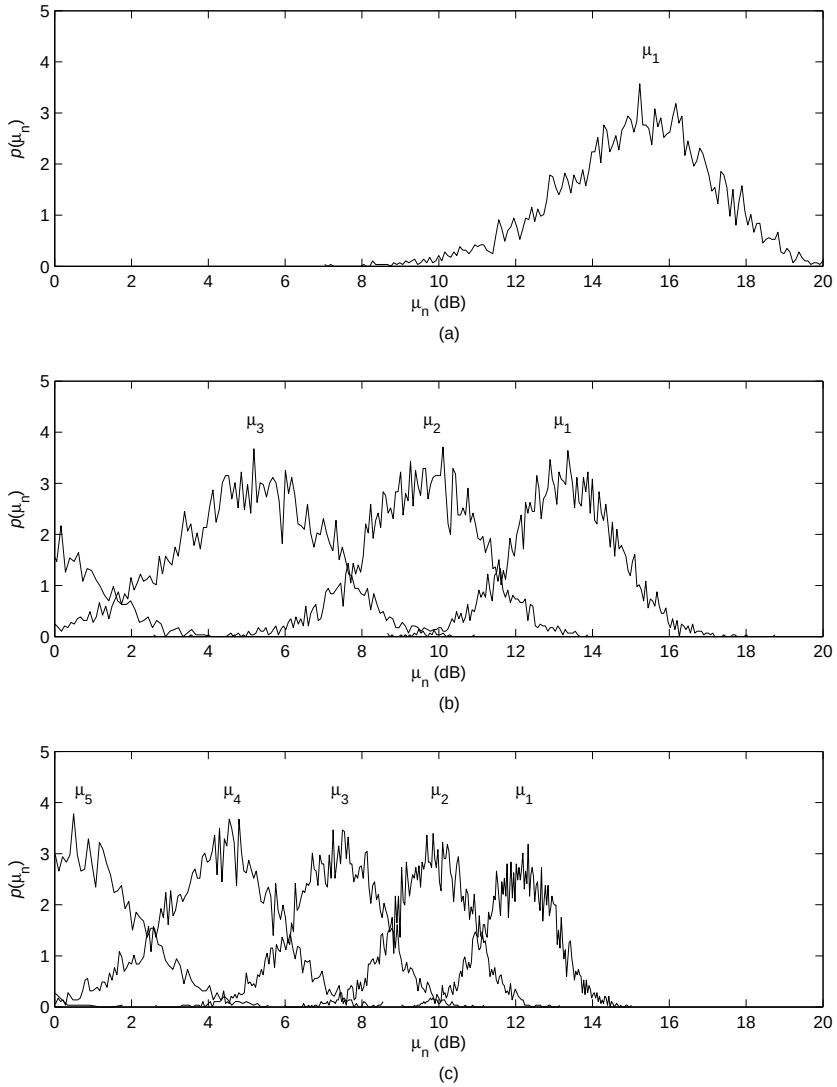

Figure 5.6: PDF's of the ordered singular values of $\boldsymbol{H}$ for $n_{\mathrm{T}} = n_{\mathrm{R}} = 6$ antenna ULAs within fixed radius apertures within isotropic scattering. μ_k represents the k-th largest singular value represented in dB. (a) $r_{\mathrm{T}} = r_{\mathrm{R}} = 0.01\lambda$. (b) $r_{\mathrm{T}} = r_{\mathrm{R}} = 0.5\lambda$. (c) i.i.d. channel, $r_{\mathrm{T}} = r_{\mathrm{R}} = \infty$.

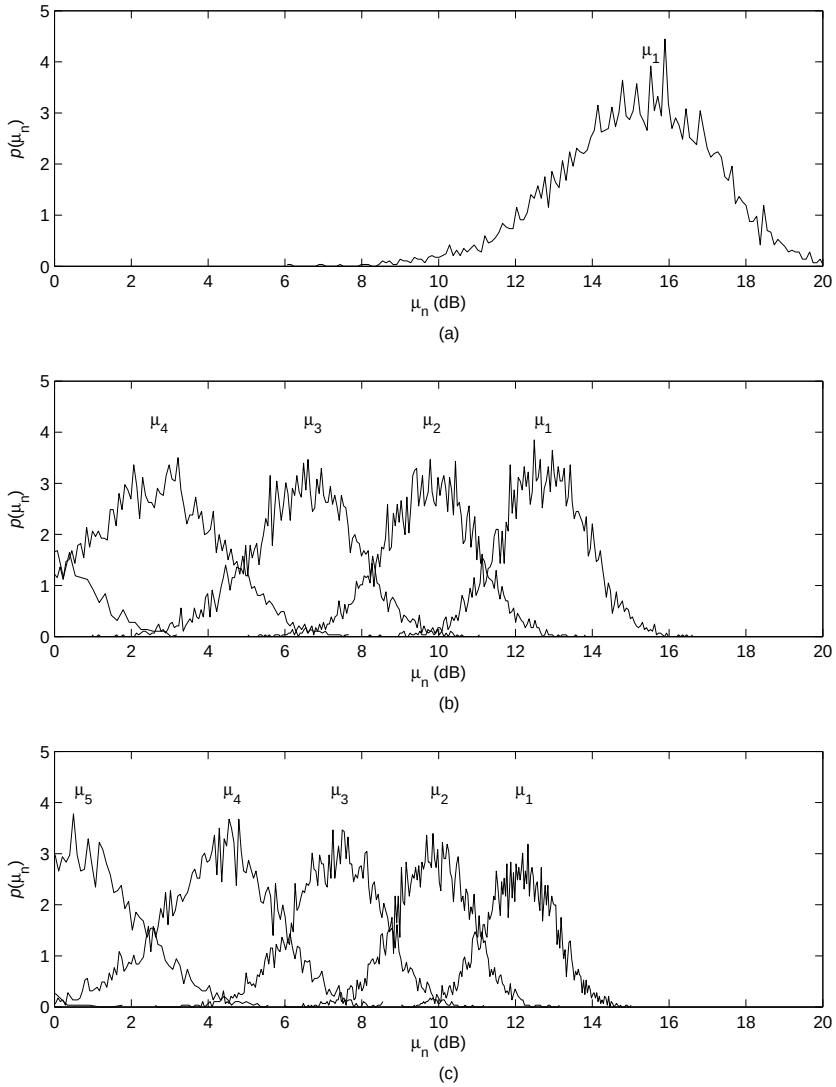

Figure 5.7: PDF's of the ordered singular values of $\boldsymbol{H}$ for $n_{\mathrm{T}} = n_{\mathrm{R}} = 6$ antenna UCAs within fixed radius apertures within isotropic scattering. μ_k represents the k-th largest singular value represented in dB. (a) $r_{\mathrm{T}} = r_{\mathrm{R}} = 0.01\lambda$. (b) $r_{\mathrm{T}} = r_{\mathrm{R}} = 0.5\lambda$. (c) i.i.d. channel, $r_{\mathrm{T}} = r_{\mathrm{R}} = \infty$.

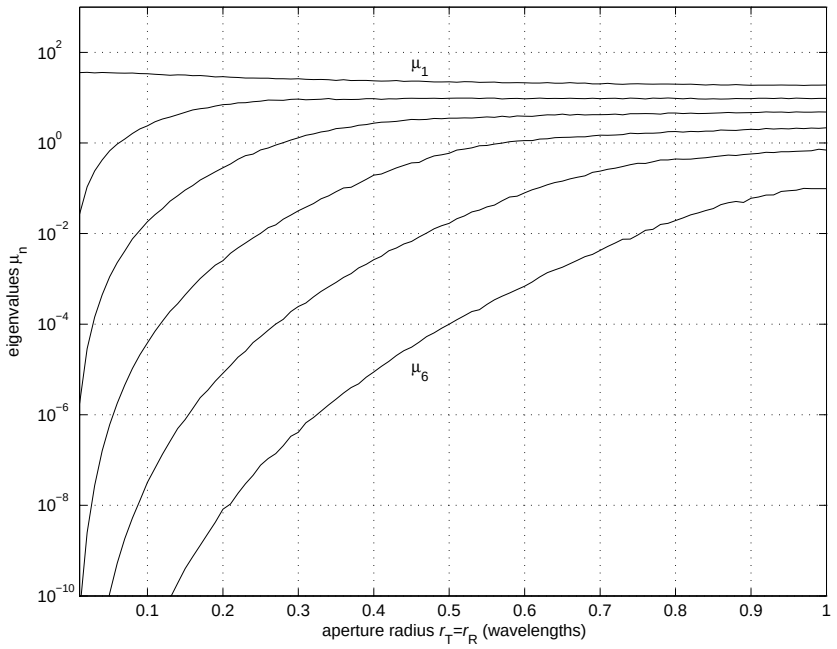

Figure 5.8: Mean of the ordered singular values of $\boldsymbol{H}$ for $n_{\mathrm{T}} = n_{\mathrm{R}} = 6$ antenna ULAs for increasing radius apertures within isotropic scattering.

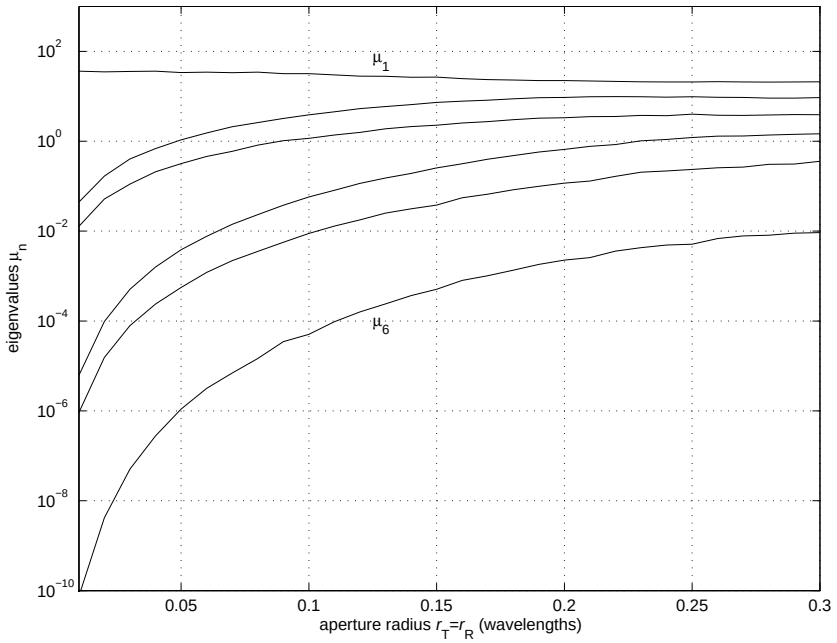

Figure 5.9: Mean of the ordered singular values of $\boldsymbol{H}$ for $n_{\mathrm{T}} = n_{\mathrm{R}} = 6$ antenna UCAs for increasing radius apertures within isotropic scattering.

Using this discrete channel the p,q-th element of the scattering environment matrix becomes

$$\boldsymbol{H}_{\mathrm{S}}|_{p,q} = \iint_{\mathbb{S}^1} g(\phi,\psi)\, e^{i(q-N_{\mathrm{T}}-1)\phi}\, e^{-i(p-N_{\mathrm{R}}-1)\psi} d\phi d\psi \tag{5.5a}$$

$$= \sum_{s=1}^{n_{\mathrm{S}}} g_s \int_{\mathbb{S}^1} \delta(\phi-\phi_s) e^{i(q-N_{\mathrm{T}}-1)\phi} d\phi \int_{\mathbb{S}^1} \delta(\psi-\psi_s) e^{-i(p-N_{\mathrm{R}}-1)\psi} d\psi \tag{5.5b}$$

$$= \sum_{s=1}^{n_{\mathrm{S}}} g_s e^{i(q-N_{\mathrm{T}}-1)\phi_s} e^{-i(p-N_{\mathrm{R}}-1)\psi_s}, \tag{5.5c}$$

which gives the discrete scattering environment matrix decomposition

$$\boldsymbol{H}_{\mathrm{S}} = \boldsymbol{\Phi}\boldsymbol{\Lambda}_{\mathrm{S}}\boldsymbol{\Psi}^{\dagger}, \tag{5.6}$$

where $\boldsymbol{\Psi}$ is the $(2N_{\mathrm{T}}+1)\times n_{\mathrm{S}}$ matrix

$$\boldsymbol{\Psi} = \begin{bmatrix} e^{iN_{\mathrm{T}}\phi_1} & e^{iN_{\mathrm{T}}\phi_2} & \dots & e^{iN_{\mathrm{T}}\phi_{n_{\mathrm{S}}}} \\ e^{i(N_{\mathrm{T}}-1)\phi_1} & e^{i(N_{\mathrm{T}}-1)\phi_2} & \dots & e^{i(N_{\mathrm{T}}-1)\phi_{n_{\mathrm{S}}}} \\ \vdots & \vdots & \ddots & \vdots \\ e^{-iN_{\mathrm{T}}\phi_1} & e^{-iN_{\mathrm{T}}\phi_2} & \dots & e^{-iN_{\mathrm{T}}\phi_{n_{\mathrm{S}}}} \end{bmatrix}, \tag{5.7}$$

$\boldsymbol{\Phi}$ is the $(2N_{\mathrm{R}}+1)\times n_{\mathrm{S}}$ matrix

$$\boldsymbol{\Psi} = \begin{bmatrix} e^{iN_{\mathrm{R}}\psi_1} & e^{iN_{\mathrm{R}}\psi_2} & \dots & e^{iN_{\mathrm{R}}\psi_{n_{\mathrm{S}}}} \\ e^{i(N_{\mathrm{R}}-1)\psi_1} & e^{i(N_{\mathrm{R}}-1)\psi_2} & \dots & e^{i(N_{\mathrm{R}}-1)\psi_{n_{\mathrm{S}}}} \\ \vdots & \vdots & \ddots & \vdots \\ e^{-iN_{\mathrm{R}}\psi_1} & e^{-iN_{\mathrm{R}}\psi_2} & \dots & e^{-iN_{\mathrm{R}}\psi_{n_{\mathrm{S}}}} \end{bmatrix}, \tag{5.8}$$

and $\boldsymbol{\Lambda}_{\mathrm{S}}$ is a $n_{\mathrm{S}}\times n_{\mathrm{S}}$ diagonal matrix

$$\boldsymbol{\Lambda}_{\mathrm{S}} = \mathrm{diag}\left([g_1, g_2, \dots, g_{n_{\mathrm{S}}}]\right). \tag{5.9}$$

It is further assumed that the path gains $\{g_s\}_{s=1}^{n_{\mathrm{S}}}$ are independent complex Gaussian variables, i.e., the scatterers model an independent Rayleigh multipath environment. As with previous chapters the channel gains are normalized such that

$$\iint_{\mathbb{S}^1} G(\phi,\psi)\, d\phi\, d\psi = 1, \tag{5.10}$$

where $G(\phi,\psi) = E\left\{|g(\phi,\psi)|^2\right\}$, which for the discrete channel representation gives

$$\iint_{\mathbb{S}^1} G(\phi,\psi)\,d\phi\,d\psi = \iint_{\mathbb{S}^1} \sum_{s=1}^{n_\mathrm{S}} E\left\{|g_s|^2\right\}\delta(\phi-\phi_s)\,\delta(\psi-\psi_s)\,d\phi\,d\psi \tag{5.11a}$$

$$= \sum_{s=1}^{n_\mathrm{S}} E\left\{|g_s|^2\right\}. \tag{5.11b}$$

Assuming on average all paths have the same gain, the equivalent discrete normalization to the continuous case (5.10) gives path gains

$$E\left\{|g_s|^2\right\} = \frac{1}{n_\mathrm{S}}. \tag{5.12}$$

The capacity of 6 antenna ULA and UCAs within apertures of radius $r_\mathrm{T} = r_\mathrm{R} = 0.5\lambda$ are shown in Fig. 5.10 for increasing n_S. As the number of paths is increased, the capacity approaches that of the infinite paths case, given by the continuous $g(\phi,\psi)$, shown as horizontal lines on the graph. Observe that the significant growth in capacity occurs for increasing number of paths up until $n_\mathrm{S} = 11$, which corresponds to the SDOF for this scenario. This is better observed by considering the ordered singular values of the scattering environment matrix $\boldsymbol{H}_\mathrm{S}$ (5.6) shown in Fig. 5.11. Here the effect of increasing capacity with the number of paths is clearly reflected in a corresponding increase in the number of significant singular values for the channel. Every significant singular value represents an available parallel sub-channel through the scattering environment with associated gain μ_n^2.

5.3.2 Angular Spread

In the previous section the scattering was modelled using discrete scatterers, here a statistical model of the scattering environment is employed. Consider a modal fading model with the following properties:

1. The correlation between the fading from transmit modes n and n' to the same receive mode m does not depend on the receive mode.

2. Similarly, the correlation between the fading from a transmit mode n to receive modes m and m' does not depend on the transmit mode.

3. The correlation between the fading of two distinct mode pairs is the product of the corresponding transmit mode correlation and receive mode correlation.

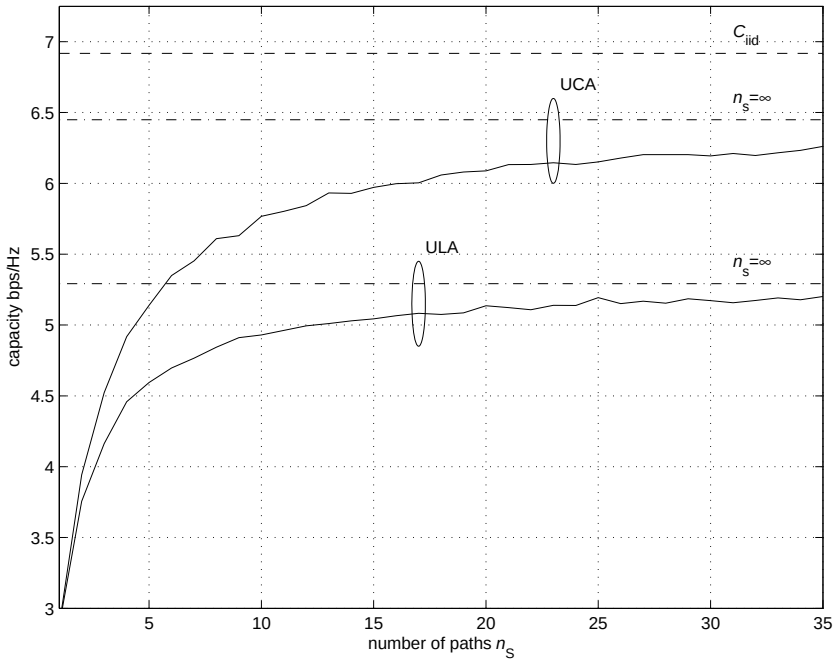

Figure 5.10: Capacity of 6 antenna ULA and UCA within apertures of radius $r_{\mathrm{T}} = r_{\mathrm{R}} = 0.5\lambda$ for increasing number of multipaths n_{S}, with SNR 10dB.

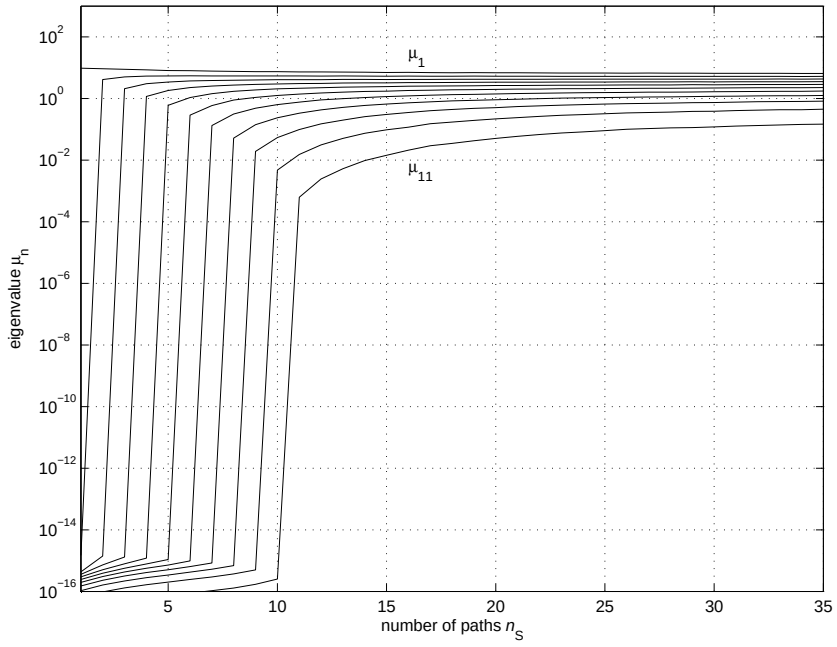

Figure 5.11: Mean ordered singular values of scattering environment matrix $\boldsymbol{H}_{\mathrm{S}}$ for increasing number of multipaths n_{S}, for apertures $r_{\mathrm{T}} = r_{\mathrm{R}} = 0.5\lambda$.

Assumptions 1 and 2 are usually quite accurate when the apertures are well separated with sufficient local scattering at each aperture. The final assumption can be thought of as a first-order approximation of the correlation structure when the fading from two transmit modes to the same receive mode and the fading from two receive modes to the same transmit mode is much more correlated than that between two distinct mode pairs [10].

Consider zero mean identically distributed Gaussian elements $\beta_m^n \in \mathcal{N}(0,1)$ of the scattering matrix $\boldsymbol{H}_{\mathrm{S}}$, then following the above fading assumptions the cross correlation may be expressed as

$$E\left\{\beta_m^n \overline{\beta_{m'}^{n'}}\right\} \triangleq \gamma_{n,n',m,m'} \tag{5.13a}$$

$$= \gamma_{n-n'}^{\mathrm{T}} \gamma_{m-m'}^{\mathrm{R}}, \tag{5.13b}$$

where $\gamma_{n-n'}^{\mathrm{T}}$ is the transmit aperture modal correlation between modes n and n', and $\gamma_{m-m'}^{\mathrm{R}}$ is the receive aperture modal correlation between modes m and m'. The scattering channel matrix $\boldsymbol{H}_{\mathrm{S}}$ can now be decomposed as

$$\boldsymbol{H}_{\mathrm{S}} = \boldsymbol{\Gamma}_{\mathrm{R}}^{1/2} \boldsymbol{H}_0 \boldsymbol{\Gamma}_{\mathrm{T}}^{1/2}, \tag{5.14}$$

where $\boldsymbol{\Gamma}_{\mathrm{T}}$ is the $(N \times N)$ transmit modal correlation matrix

$$\boldsymbol{\Gamma}_{\mathrm{T}} = \begin{bmatrix} \gamma_0^{\mathrm{T}} & \gamma_1^{\mathrm{T}} & \cdots & \gamma_{2N_{\mathrm{T}}}^{\mathrm{T}} \\ \gamma_{-1}^{\mathrm{T}} & \gamma_0^{\mathrm{T}} & \cdots & \gamma_{2N_{\mathrm{T}}-1}^{\mathrm{T}} \\ \vdots & \vdots & \ddots & \vdots \\ \gamma_{-2N_{\mathrm{T}}}^{\mathrm{T}} & \gamma_{-2N_{\mathrm{T}}+1}^{\mathrm{T}} & \cdots & \gamma_0^{\mathrm{T}} \end{bmatrix}, \tag{5.15}$$

and $\boldsymbol{\Gamma}_{\mathrm{R}}$ is the $(M \times M)$ receive modal correlation matrix

$$\boldsymbol{\Gamma}_{\mathrm{R}} = \begin{bmatrix} \gamma_0^{\mathrm{R}} & \gamma_1^{\mathrm{R}} & \cdots & \gamma_{2N_{\mathrm{R}}}^{\mathrm{R}} \\ \gamma_{-1}^{\mathrm{R}} & \gamma_0^{\mathrm{R}} & \cdots & \gamma_{2N_{\mathrm{R}}-1}^{\mathrm{R}} \\ \vdots & \vdots & \ddots & \vdots \\ \gamma_{-2N_{\mathrm{R}}}^{\mathrm{R}} & \gamma_{-2N_{\mathrm{R}}+1}^{\mathrm{R}} & \cdots & \gamma_0^{\mathrm{R}} \end{bmatrix}, \tag{5.16}$$

and $\boldsymbol{H}_0$ is a $(M \times N)$ matrix with identically distributed complex Gaussian entries. Note that $\boldsymbol{\Gamma}_{\mathrm{T}}^{1/2}$ is the principle square root of matrix $\boldsymbol{\Gamma}_{\mathrm{T}}$, such that $\boldsymbol{\Gamma}_{\mathrm{T}}^{1/2}\boldsymbol{\Gamma}_{\mathrm{T}}^{1/2} = \boldsymbol{\Gamma}_{\mathrm{T}}$. Depending on the angular spread the modal correlation matrices ranges between the two extreme cases of the rank one all ones matrix (narrow angular spread) and the full rank identity matrix (wide angular spread).

The channel matrix product (5.1) can now be expressed as

$$\boldsymbol{H} = \boldsymbol{J}_{\mathrm{R}} \boldsymbol{\Gamma}_{\mathrm{R}}^{1/2} \boldsymbol{H}_0 \boldsymbol{\Gamma}_{\mathrm{T}}^{1/2} \boldsymbol{J}_{\mathrm{T}}^{\dagger}, \tag{5.17}$$

which shows the independent effects of antenna placement and aperture size ($\boldsymbol{J}_{\mathrm{T}}$ and $\boldsymbol{J}_{\mathrm{R}}$), angular spread around the apertures ($\boldsymbol{\Gamma}_{\mathrm{T}}^{1/2}$ and $\boldsymbol{\Gamma}_{\mathrm{R}}^{1/2}$), and the rest of the scattering environment ($\boldsymbol{H}_0$). Note the spatial richness of the channel κ_{S} is now governed by angular spread at each aperture and the scattering throughout the rest of the channel.

Using this model a wide range of scattering scenarios can be considered:

1. Full diversity (full rank $\boldsymbol{\Gamma}_{\mathrm{T}}, \boldsymbol{\Gamma}_{\mathrm{R}}$, and $\boldsymbol{H}_0$): this channel is shown in Fig. 5.1(a) and corresponds to a sufficiently rich scattering environment, full rank $\boldsymbol{H}_0 \sim \mathbb{C}\mathcal{N}(\boldsymbol{0}, \boldsymbol{I})$, with isotropic scattering surrounding both the transmit and receive apertures, $\boldsymbol{\Gamma}_{\mathrm{T}} = \boldsymbol{I}$, $\boldsymbol{\Gamma}_{\mathrm{R}} = \boldsymbol{I}$.

2. Pin-hole (full rank $\boldsymbol{\Gamma}_{\mathrm{T}}, \boldsymbol{\Gamma}_{\mathrm{R}}$, rank one $\boldsymbol{H}_0$): this channel is shown in Fig. 5.1(c), where there is isotropic scattering surrounding both the transmit and receive apertures, however there is only a single communication channel between the local scatterers at each end of the link, $\boldsymbol{H}_0 \sim \mathbb{C}\mathcal{N}(\boldsymbol{0}, \boldsymbol{1})$. Such channels have been shown to exist for large separation between transmit and receive arrays [30, 65]. In [122] it was shown that these degenerate channels may arise from diffraction effects of buildings. However, although pin-hole channels have been shown to exist in theory, to the author's knowledge no observations of these degenerate channel effects from practical measurements have appeared in the literature.

3. Small Angular Spread (full rank $\boldsymbol{H}_0$, rank one $\boldsymbol{\Gamma}_{\mathrm{T}}$ or $\boldsymbol{\Gamma}_{\mathrm{R}}$): this channel corresponds to Fig. 5.1(d) where there is low angular spread at one aperture, $\boldsymbol{\Gamma}_{\mathrm{T}} = \boldsymbol{1}$, with isotropic local scattering at the other, $\boldsymbol{\Gamma}_{\mathrm{R}} = \boldsymbol{I}$, and sufficient global scattering. This channel is the most common channel in mobile systems, where the base station is mounted high above the scattering environment and has low angular spread, whilst the user is surrounded by dense scattering at street level. Note if both apertures experience low angular spread, Fig. 5.1(e), the channel is another case of a low diversity channel.

4. Low Diversity (rank one $\boldsymbol{H}_0$, rank one $\boldsymbol{\Gamma}_{\mathrm{T}}$ or $\boldsymbol{\Gamma}_{\mathrm{R}}$ or both): these channels are pin-hole channels with low angular spread at either or both apertures, given by Fig. 5.1(c) in combination with Fig. 5.1(d) or Fig. 5.1(e). This channel

represents the worst possible channel for MIMO systems, providing ergodic capacity of a SISO system and giving no diversity gains (low outage capacity).

The ergodic and outage capacity for $n_{\mathrm{T}} = n_{\mathrm{R}} = 6$ antenna UCAs within apertures of radius $r_{\mathrm{T}} = r_{\mathrm{R}} = 0.5\lambda$ and the various scattering scenarios are shown in Fig. 5.12 and Fig. 5.13, respectively. As with the results in Section 5.1, the ergodic capacity is invariant to the matrix or matrices which lose rank. However, the outage capacity strongly depends on where the channel is degenerate. Not surprisingly, the outage capacity curves are very similar to those in Fig. 5.3, since small angular spread is equivalent to decreasing the aperture size, as both increase the branch correlation, thereby reducing the number of significant subchannels between the arrays.

Finally, the capacity for angular spreading within the extreme examples shown above is considered. Figure 5.14 shows the ergodic capacity of UCAs within apertures $r_{\mathrm{T}} = r_{\mathrm{R}} = 0.5\lambda$ for increasing angular spread at the transmitter Δ_{T} for various receiver angular spreads Δ_{R}, for uniform limited scattering fields and full rank $\boldsymbol{H}_0$. As with the capacity for various apertures sizes, it can be seen that the capacity is limited by the aperture with the smaller angular spread. Figure 5.15 shows the CDF of the capacity for the pin-hole channel for the same angular spreading at the receiver Δ_{R} as in Fig. 5.14 for small angular spread, $\Delta_{\mathrm{T}} = 10°$, and isotropic scattering $\Delta_{\mathrm{T}} = 180°$, at the transmitter. It can clearly be seen that regardless of the angle spread at the receiver, the overall channel provides no diversity for small transmit angular spreads.

5.4 Summary and Contributions

In this chapter, the MIMO model developed in Chapter 4 was simulated for a wide range of apertures and scattering environments. Many of the scenarios studied were chosen to verify the theoretical results of previous chapters. However, almost all scattering and array geometries can be studied in depth using this model. As we have seen, the model can represent practically all scattering environments and antenna array geometries presented in the literature in a simple tractable form. Furthermore, unlike many other models, significant theoretical insights into the capacity of a spatially constrained systems can be obtained without the need for extensive simulations, as seen in Chapter 3, and to follow in Chapter 6.

Some specific contributions made in this chapter are:

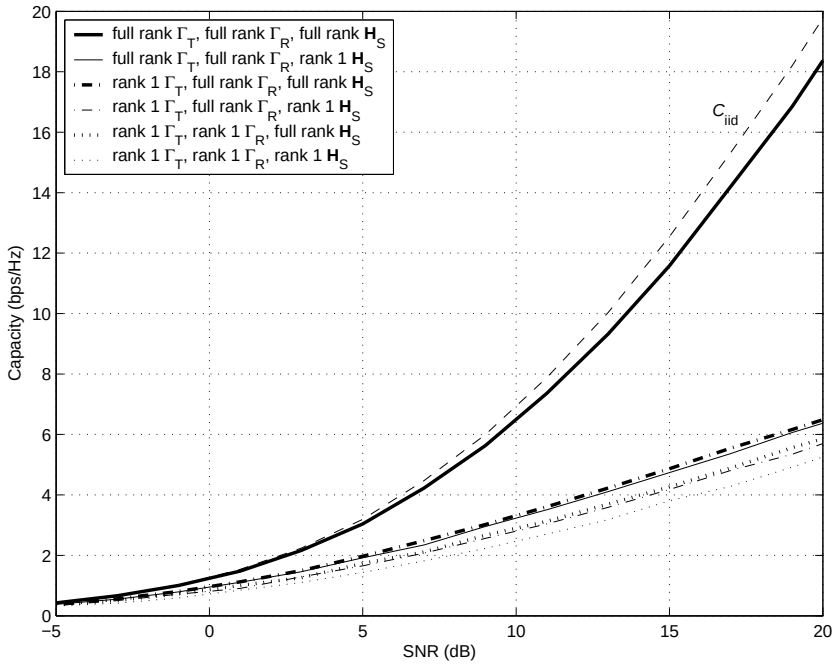

Figure 5.12: Ergodic capacity with increasing SNR for scattering scenarios for 6 antenna UCAs within apertures of radius $r_{\mathrm{T}} = r_{\mathrm{R}} = 0.5\lambda$.

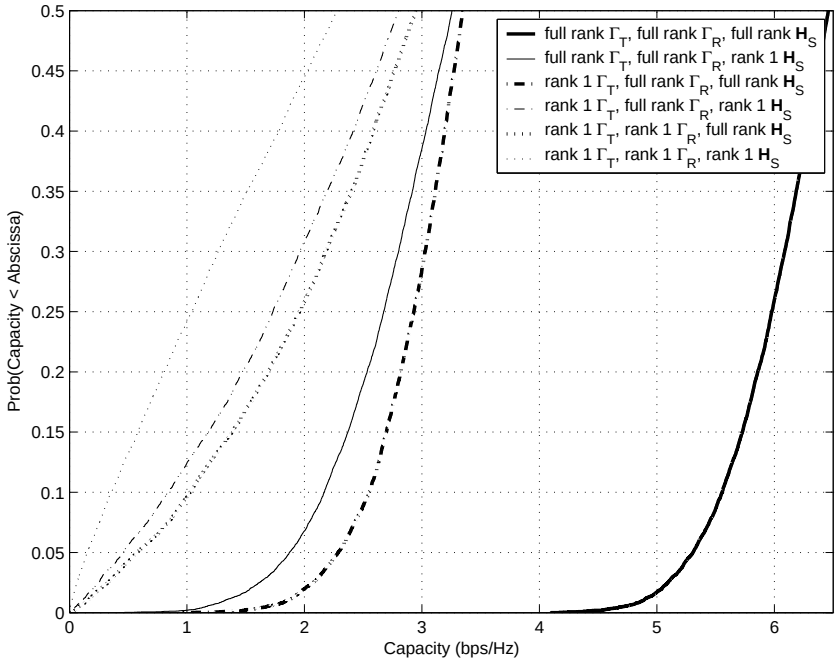

Figure 5.13: CDF of channel capacity for various scattering scenarios for 6 antenna UCAs within apertures of radius $r_{\mathrm{T}} = r_{\mathrm{R}} = 0.5\lambda$ with SNR 10dB.

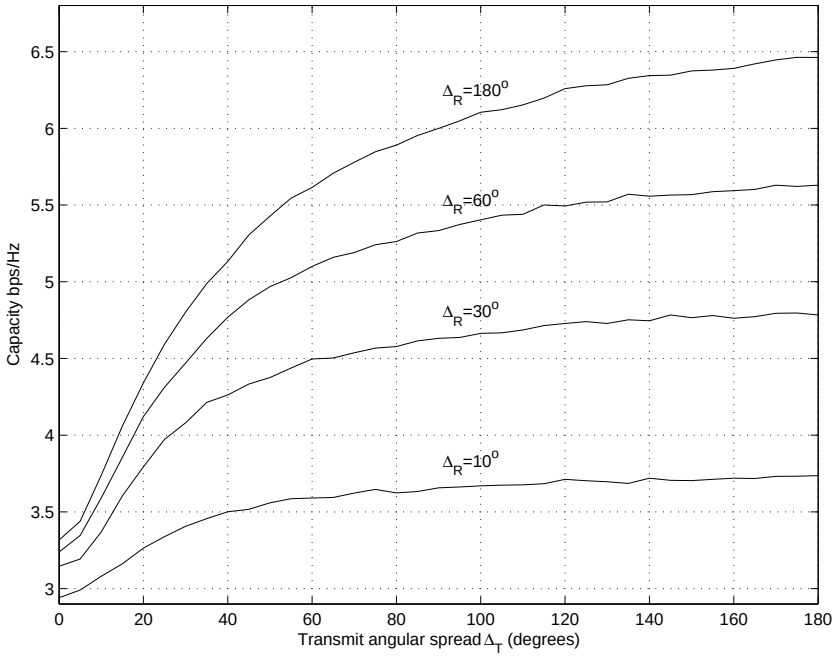

Figure 5.14: Capacity of 6 antenna UCAs in apertures $r_{\mathrm{T}} = r_{\mathrm{R}} = 0.5\lambda$ for increasing transmitter angular spread Δ_{T} for various receiver angular spread Δ_{R}, and SNR 10dB. Scattering is modelled by uniform limited field and full rank $\boldsymbol{H}_0$.

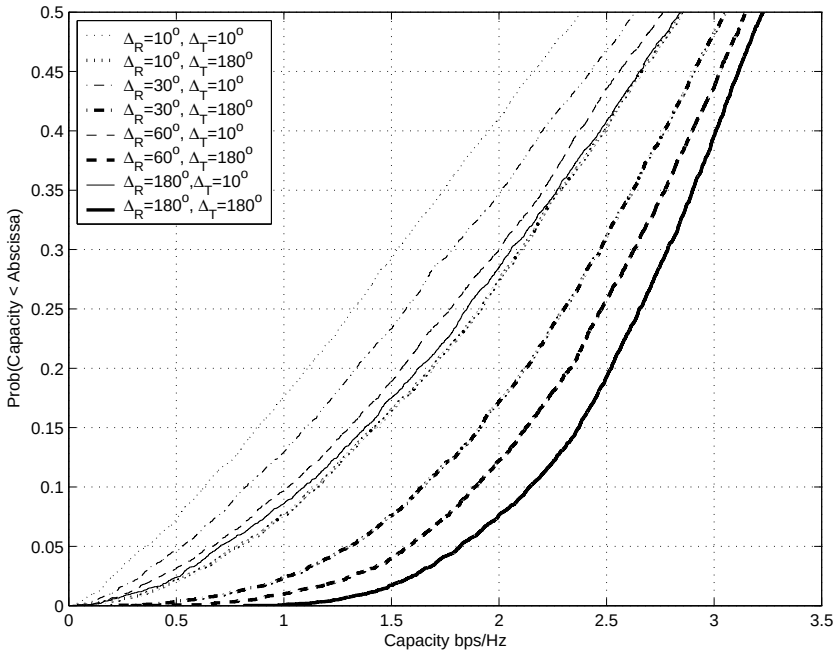

Figure 5.15: CDF of channel capacity for various angular spreading at the transmitter Δ_{T} and receiver Δ_{R} for the same scenario as Fig. 5.14 with rank one $\boldsymbol{H}_0$.

1. The ergodic and outage capacity were shown to have different responses to the loss in channel rank. Whilst small apertures at the transmit or receiver, or a low scattering richness factor gives approximately the same reduction of the ergodic capacity from that of a full diversity system, the outage capacity was shown to be highly dependent on where the channel was degenerate. In particular, a loss in spatial richness impacted the outage capacity the most.

2. The effects of increasing the numbers of antennas within constrained apertures at both ends of the channel were considered. Similar to the results in Chapter 3, the capacity suffered a saturation in the number of antennas, where more antennas failed to give further capacity gains. It was shown that the smallest aperture limits the overall capacity of the channel.

3. The singular values of the channel matrix were shown to have less disparity as the apertures were increased in size, for fixed numbers of antennas. This leads to a lowering of the disparity amongst the subchannels giving a larger set of significant subchannels which to communicate on and hence an increase in capacity.

4. A discrete scattering model was developed, where the scattering environment was modelled by a distinct number of paths between the apertures. Simulations showed that as the number of paths (i.e., scatterers) is increased the capacity converged to the continuous model case, supporting the spatial richness proposition in Chapter 4, where it is argued that sufficient channel 'richness' is related to the aperture size.

5. Angular spread surrounding both the transmitter and receiver was introduced into the model under the assumption of independent local scattering. Angular spread is shown to increase the modal correlation at each end of the communications link, thereby reducing the capacity. Using the angular spread model, many scattering scenarios are studied, and the generic nature of the model is revealed.

Chapter 6

Intrinsic Capacity of Continuous Space Channels

The previous chapters have shown that there is a limit to communication when the antennas are restricted to within spatially constrained apertures. This limit has been shown to be independent of the number of antennas and relates only to the characteristics of the spatial channel, that is, the size of the apertures and the scattering environment.

In this chapter a new framework is developed for computing the capacity of spatially constrained channels which is independent of the transmit and receive antenna configuration and signal processing. This capacity represents the fundamental or intrinsic capacity between two continuous apertures in space, and MIMO can be considered as an implementation, where the apertures are sampled such that the discrete system approaches the limits of the continuous space channel.

6.1 Mode-to-Mode Communication

In the previous chapters it has been shown that the rank of the channel matrix $\boldsymbol{H}$ gives the effective number of independent parallel channels between the transmit and receive antenna arrays, and thus determines the capacity of the system. For the channel matrix decomposition derived in Chapter 4, $\boldsymbol{H} = \boldsymbol{J}_{\mathrm{R}}\boldsymbol{H}_{\mathrm{S}}\boldsymbol{J}_{\mathrm{T}}^{\dagger}$, the channel rank is given by

$$\begin{aligned} \mathrm{rank}(\boldsymbol{H}) &= \min\{\mathrm{rank}(\boldsymbol{J}_{\mathrm{T}}), \mathrm{rank}(\boldsymbol{J}_{\mathrm{R}}), \mathrm{rank}(\boldsymbol{H}_{\mathrm{S}})\} && \text{(6.1a)} \\ &\leq \mathrm{rank}(\boldsymbol{H}_{\mathrm{S}}). && \text{(6.1b)} \end{aligned}$$

Let N and M denote number of significant transmit and receive aperture modes, respectively[1], then equality in (6.1b) is achieved for $n_{\mathrm{T}} \geq N$, $n_{\mathrm{R}} \geq M$. Therefore, as discussed in Chapter 4 and verified in Chapter 5, the number of available modes for the transmit and receive apertures, determined by the size of the apertures, and any possible modal correlation or key-hole effects [74], limit the capacity of the system, regardless of how many antennas are packed into the apertures.

From (6.1b) and assuming no array gain effects, the maximum mutual information between the two apertures can be achieved with a minimum of N and M antennas within the transmit and receive apertures, respectively. Therefore, assume $n_{\mathrm{T}} = N$ and $n_{\mathrm{R}} = M$ antennas can be optimally placed[2] within the transmit and receive apertures of radius r_{T} and r_{R}, respectively. In this situation $\boldsymbol{J}_{\mathrm{T}}^{\dagger}\boldsymbol{J}_{\mathrm{T}} = \boldsymbol{I}$ and $\boldsymbol{J}_{\mathrm{R}}^{\dagger}\boldsymbol{J}_{\mathrm{R}} = \boldsymbol{I}$, hence the transmit and receive aperture sampling matrices are unitary and $\boldsymbol{H}_{\mathrm{S}}$ is then unitarily equivalent to $\boldsymbol{H}$. The instantaneous normalized channel capacity is then given by

$$C = \log \left| \boldsymbol{I}_{n_{\mathrm{R}}} + \frac{\eta}{n_{\mathrm{T}} n_{\mathrm{R}}} \boldsymbol{H}\boldsymbol{H}^{\dagger} \right| \tag{6.2a}$$

$$= \log \left| \boldsymbol{I}_{M} + \frac{\eta}{NM} \boldsymbol{H}_{\mathrm{S}}\boldsymbol{H}_{\mathrm{S}}^{\dagger} \right|, \tag{6.2b}$$

where η is the average SNR at any antenna within the receive aperture.

The mode-to-mode capacity (6.2b) represents the intrinsic capacity for communication between two spatial apertures, giving the maximum capacity for all possible array configurations and array signal processing. For the circular and spherical apertures we have $N_{\mathrm{T}} = \lceil \pi e r_{\mathrm{T}}/\lambda \rceil$ and $N_{\mathrm{R}} = \lceil \pi e r_{\mathrm{R}}/\lambda \rceil$ (see Chapter 4), and it can be seen that the intrinsic capacity is limited by the size of the apertures containing the antenna arrays (number of available modes), and the statistics of the scattering channel matrix $\boldsymbol{H}_{\mathrm{S}}$ (modal correlation).

The CDF of the mode-to-mode capacity (6.2b) is shown for increasing aperture radius $r = r_{\mathrm{T}} = r_{\mathrm{R}}$ in Fig. 6.1 and Fig. 6.2 for the circular and spherical apertures, respectively, within an isotropic scattering environment. Both the outage and mean capacity increase for increasing radii (increased number of modes).

Consider an increasing transmit aperture ($r_{\mathrm{T}} \to \infty$), then by the law of large numbers $\frac{1}{N}\boldsymbol{H}_{\mathrm{S}}\boldsymbol{H}_{\mathrm{S}}^{\dagger} \to \boldsymbol{I}_{M}$ almost surely as N gets large. Thus the capacity (6.2b)

[1] e.g., for circular apertures $N = 2N_{\mathrm{T}} + 1$, $M = 2N_{\mathrm{R}} + 1$, and for spherical apertures $N = (N_{\mathrm{T}} + 1)^2$, $M = (N_{\mathrm{R}} + 1)^2$.

[2] For now, it is sufficient to consider optimally placed antennas as array geometries within the aperture such that the array excites N (resp. M) uncorrelated modes, this is discussed in more detail in Section 6.2

for large r_{T} is given by

$$\lim_{r_{\mathrm{T}}\to\infty} C = M\log(1+\frac{\eta}{M}), \tag{6.3}$$

which, as shown in Chapter 3.3.4, for large r_{R} converges to

$$\lim_{r_{\mathrm{T}},r_{\mathrm{R}}\to\infty} C = C_{\mathrm{limit}} \triangleq \frac{\eta}{\ln 2}, \tag{6.4}$$

giving the upper limit on capacity for all communication schemes in AWGN channels. The capacity limit $C_{\mathrm{limit}} \approx 14.47$bps/Hz for 10dB SNR is shown as a dashed line in the capacity curves of Fig. 6.1 and Fig. 6.4, and is approached as the size of the apertures increases. It is interesting to note that a spherical aperture of radius 1.5λ is within 10% of the upper limit on capacity, whereas the circular aperture requires a radius of over 10λ to achieve the same capacity, clearly showing the capacity gains due to an increase in SDOF for higher dimensional apertures.

Figures 6.3 and 6.4 show the ergodic mode-to-mode capacity of the circular and spherical apertures, respectively, for increasing spatial richness κ_S (4.83) of various array radii $r = r_{\mathrm{T}} = r_{\mathrm{R}}$. As expected, for an increase in spatial richness the capacity of the system grows as the scattering environment can support more parallel sub-channels. For small a spatial richness factor, $\kappa_S \to 0$, the scattering environment is sparse and only a single sub-channel is available for communication, hence the capacity converges to that of a SISO system, i.e.,

$$\lim_{\kappa_S\to 0} C = \log(1+\eta), \tag{6.5}$$

which for SNR 10dB is approximately 3.45bps/Hz.

6.1.1 Mode Excitation

Although the modes considered here are generated from spatially constrained antenna arrays, recent advances in multi-mode antennas allow for the excitation of several modes of the same frequency on a single antenna. From electromagnetic antenna theory, several modes or solutions can exist at the same time on the same structure. In fact, it is possible to excite several modes at the same temporal frequency on the one antenna, and regard these as separate antenna elements. However, utilizing the higher order modes of antennas have not received much attention. For microstrip antennas, the fundamental mode has dominated the literature, however, higher order modes have been considered in a limited number of

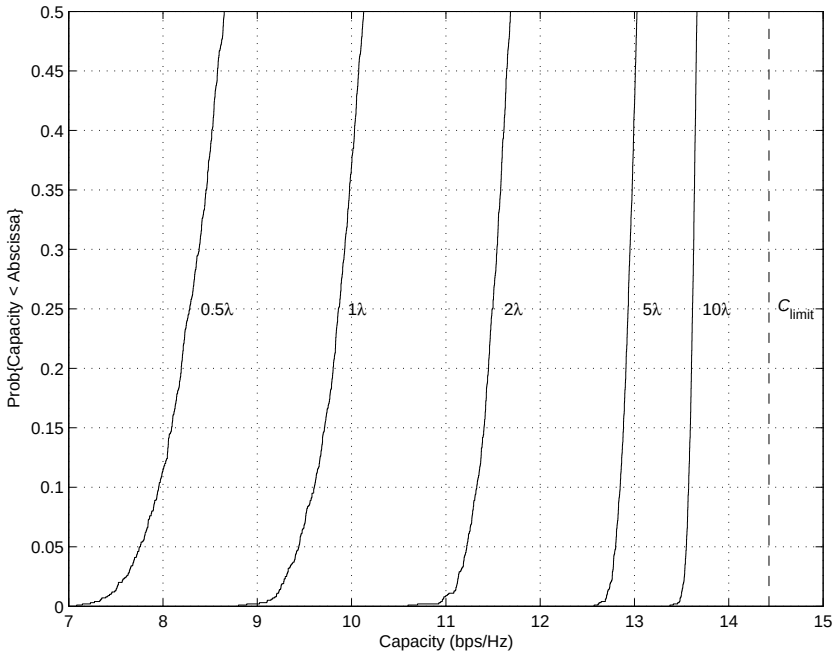

Figure 6.1: CDF of capacity for mode-to-mode communication for circular apertures of increasing radius $r = r_{\mathrm{T}} = r_{\mathrm{R}}$ with SNR 10dB.

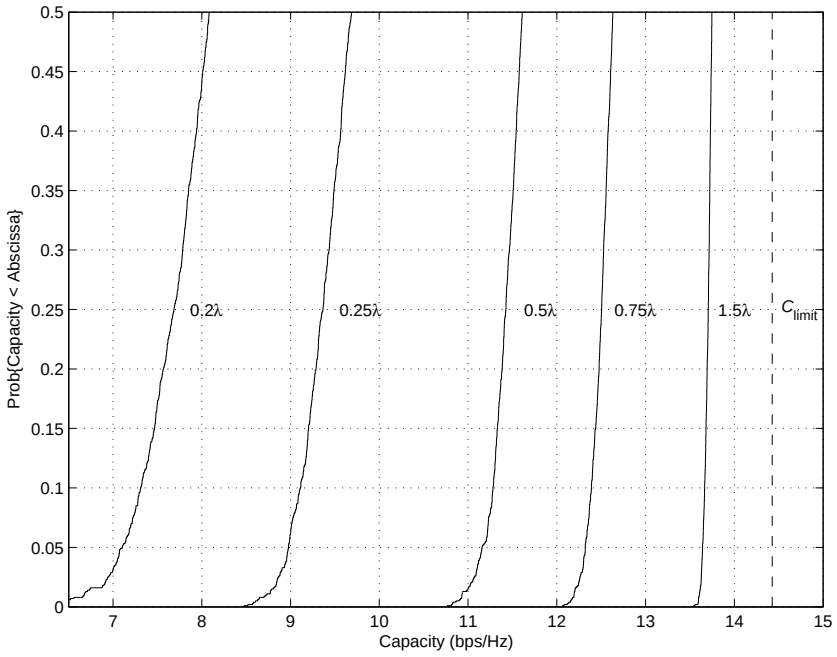

Figure 6.2: CDF of capacity for mode-to-mode communication for spherical apertures of increasing radius $r = r_{\mathrm{T}} = r_{\mathrm{R}}$ with SNR 10dB.

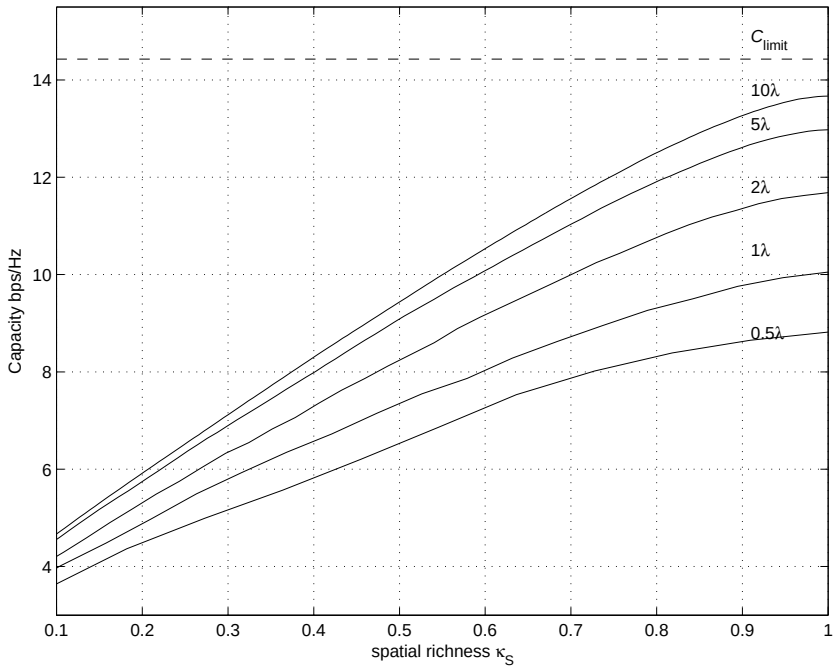

Figure 6.3: Ergodic capacity for mode-to-mode communication for circular apertures of various radii $r = r_{\mathrm{T}} = r_{\mathrm{R}}$ with increasing spatial richness κ_S and SNR 10dB.

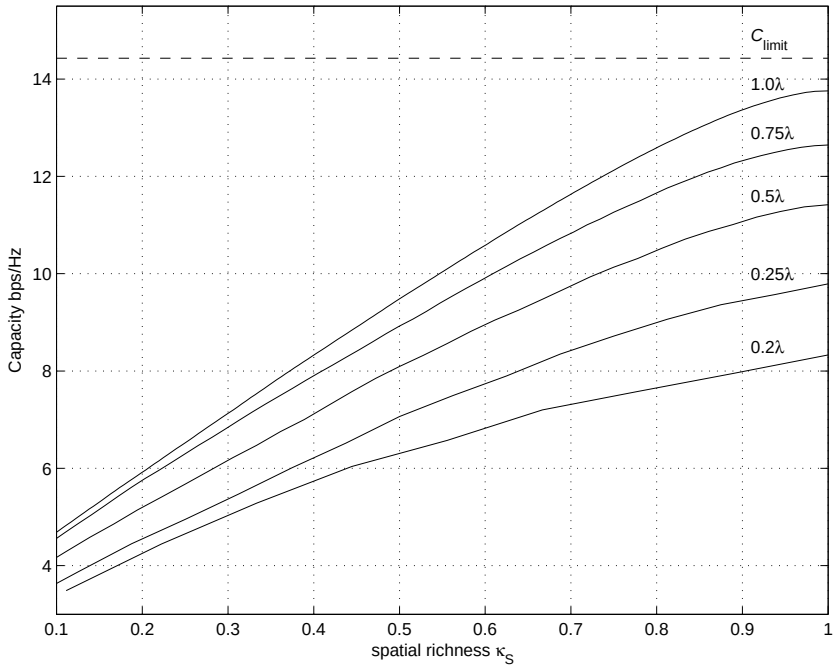

Figure 6.4: Ergodic capacity for mode-to-mode communication for circular apertures of various radii $r = r_{\mathrm{T}} = r_{\mathrm{R}}$ with increasing spatial richness κ_S and SNR 10dB.

publications (e.g., [123–126]). Subsequently, in [127], a circular microstrip antenna employing higher order modes, was designed based on an element figure of merit that was introduced in [128]. More recently, a modified biconical antenna employing several modes to form directional beams was developed in [129]. Currently, the microstrip and biconical elements appear to be the only antennas that have been used to excite multiple modes in the context of beamforming and diversity. These two antenna structures have recently been shown to offer MIMO capacity gains similar to that of an antenna array [130], and show significant promise for future MIMO implementation.

Regardless of the method of excitation, the number of effective modes will be restricted by the geometrical properties of the antenna(s), and the capacity of the system limited by the statistics of the mode-to-mode channel matrix $\boldsymbol{H}_{\mathrm{S}}$. Therefore, the mode-to-mode capacity (6.2b) represents an intrinsic, or fundamental capacity for spatially constrained MIMO systems.

The radiation pattern of the first 6 modes of the circular and spherical apertures are shown in Fig. 6.5 and Fig. 6.6, respectively. Due to the orthogonality of the basis functions, each mode has a unique radiation pattern, therefore, mode-to-mode communication is effectively a pattern diversity scheme [97], where the signals obtained by different modes may be combined to yield a diversity gain. However, the level of diversity achieved (and subsequently the multiplexing gain) depends on the correlation between the modes and is strongly dependent on the scattering environment, as shown in the following section.

6.1.2 Properties and Statistics of Scattering Channel Matrix $\boldsymbol{H}_{\mathrm{S}}$

Consider a 2D scattering environment, where the 2D Fourier series expansion of the periodic scattering gain function $g(\phi, \psi)$ is given by

$$g(\phi,\psi) = \frac{1}{4\pi^2} \sum_{n=-\infty}^{\infty} \sum_{m=-\infty}^{\infty} \beta_m^n e^{-in\phi} e^{im\psi}, \tag{6.6}$$

with coefficients

$$\beta_m^n = \iint_{\mathbb{S}^1} g(\phi,\psi) e^{in\phi} e^{-im\psi} d\phi d\psi. \tag{6.7}$$

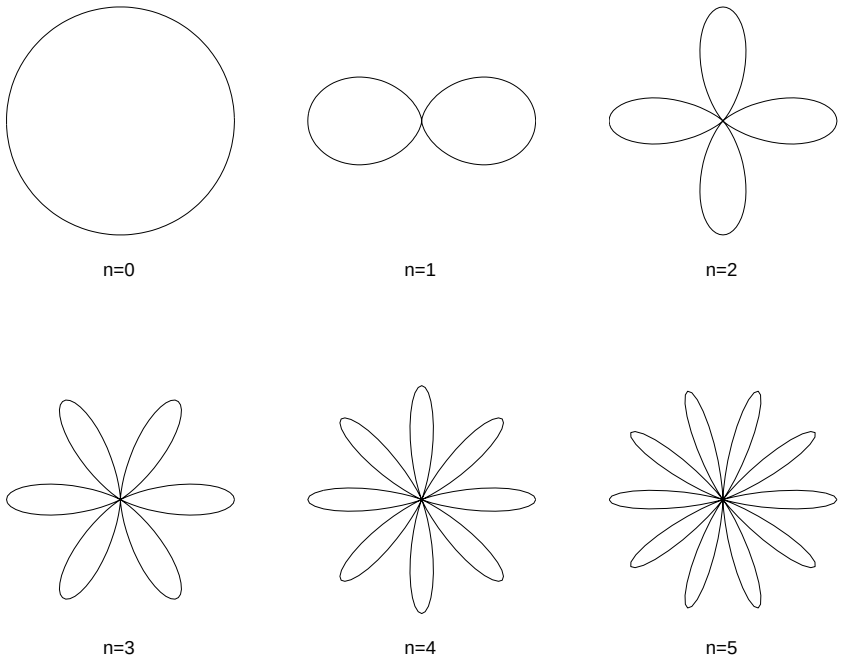

Figure 6.5: Radiation patterns of the first six modes of a circular aperture, $\Re\{e^{in\phi}\}^2$.

Let $n = q - N_{\mathrm{T}} - 1$, and $m = p - N_{\mathrm{R}} - 1$ denote the transmitter mode and receiver mode index, respectively, then the scattering environment matrix coefficients are given by

$$\boldsymbol{H}_{\mathrm{S}}|_{p,q} = \beta^{q-N_{\mathrm{T}}-1}_{p-N_{\mathrm{R}}-1} = \beta^{n}_{m}. \tag{6.8}$$

Thus the random scattering environment can be parameterized by the complex random coefficients β^n_m, $n \in \{-N_{\mathrm{T}}, \ldots, N_{\mathrm{T}}\}$, $m \in \{-N_{\mathrm{R}}, \ldots, N_{\mathrm{R}}\}$, which gives the scattering gain between the n-th transmit mode and the m-th receive mode, and $\boldsymbol{H}_{\mathrm{S}}$ becomes

$$\boldsymbol{H}_{\mathrm{S}} = \begin{bmatrix} \beta^{-N_{\mathrm{T}}}_{-N_{\mathrm{R}}} & \cdots & \beta^{N_{\mathrm{T}}}_{-N_{\mathrm{R}}} \\ \beta^{-N_{\mathrm{T}}}_{-N_{\mathrm{R}}+1} & \cdots & \beta^{N_{\mathrm{T}}}_{-N_{\mathrm{R}}+1} \\ \vdots & \ddots & \vdots \\ \beta^{-N_{\mathrm{T}}}_{N_{\mathrm{R}}} & \cdots & \beta^{N_{\mathrm{T}}}_{N_{\mathrm{R}}} \end{bmatrix}. \tag{6.9}$$

Assuming a zero-mean uncorrelated scattering environment (Rayleigh), the scattering channel is characterized by the second-order statistics of the scatter-

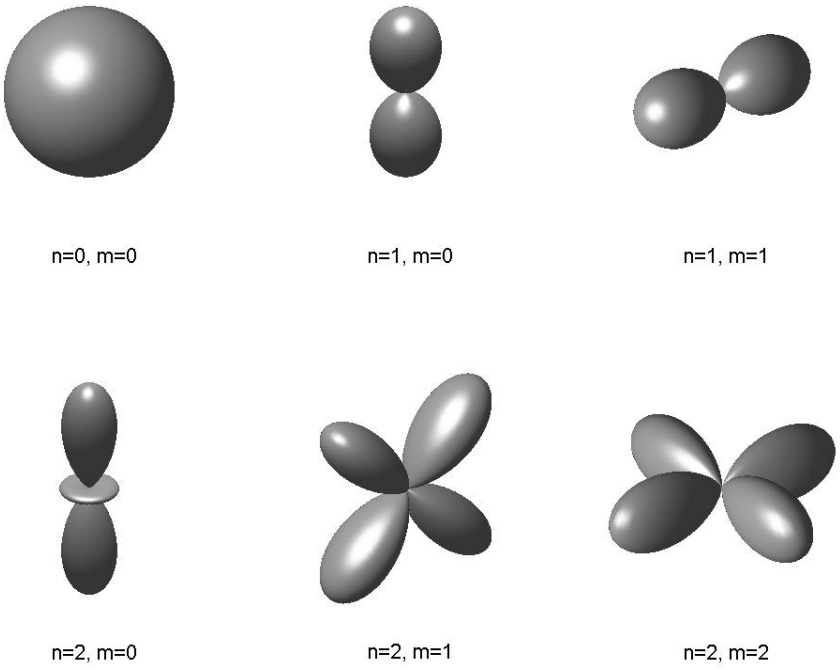

Figure 6.6: Radiation patterns of the first six modes of a spherical aperture $\Re\{Y_n^m(\widehat{\boldsymbol{\phi}})\}^2$.

ing gain function $g(\phi, \psi)$,

$$E\left\{g(\phi,\psi)\overline{g(\phi',\psi')}\right\} = G(\phi,\psi)\delta(\phi-\phi')\delta(\psi-\psi'), \tag{6.10}$$

where $\delta(\cdot)$ is the Kronecker delta function, and $G(\phi,\psi) = E\left\{|g(\phi,\psi)|^2\right\}$ is the 2D power spectral density (PSD) of the modal correlation function,

$$\begin{aligned}\gamma_{n-n',m-m'} &\triangleq E\left\{\beta_m^n\overline{\beta_{m'}^{n'}}\right\} \\ &= \iint_{\mathbb{S}^1} G(\phi,\psi)e^{i(n-n')\phi}e^{-i(m-m')\psi}d\phi d\psi,\end{aligned} \tag{6.11}$$

and represents the scattering channel power over departure and arrival angles ϕ and ψ, normalized such that the total scattering channel power

$$\sigma^2_{\boldsymbol{H}_{\mathrm{S}}} = \iint_{\mathbb{S}^1} G(\phi,\psi)d\phi d\psi = 1. \tag{6.12}$$

For the special case of uniform PSD, $G(\phi,\psi) = 1/4\pi^2$, the modal correlation

becomes

$$\gamma_{n-n',m-m'} = \gamma_{0,0}\,\delta(n-n')\delta(m-m'), \tag{6.13}$$

corresponding to the i.i.d $\{\beta_n^m\}$ case.

6.1.3 Modal Correlation in General Scattering Environments

Define $\mathcal{P}(\psi)$ as the average power density of the scatterers surrounding the receiver, given by the marginalized PSD

$$\mathcal{P}(\psi) \triangleq \int_{\mathbb{S}^1} G(\phi,\psi)\,d\phi, \tag{6.14}$$

then, from (6.11) the modal correlation between the m and m' communication modes at the receiver is given by

$$\gamma^{\mathrm{R}}_{m-m'} = \int_{\mathbb{S}^1} \mathcal{P}(\psi) e^{-i(m-m')\psi} d\psi, \tag{6.15}$$

which gives the modal correlation for all common power distributions $\mathcal{P}(\psi)$: von-Mises, gaussian, truncated gaussian, uniform, Laplacian, piecewise constant, polynomial, Fourier series expansion, etc. Similarly, defining $\mathcal{P}(\phi)$ as the power density of the scatterers surrounding the transmitter, we have the modal branch correlation at the transmitter

$$\gamma^{\mathrm{T}}_{n-n'} = \int_{\mathbb{S}^1} \mathcal{P}(\phi) e^{i(n-n')\phi} d\phi. \tag{6.16}$$

As shown in Chapter 2 there is very little variation in the correlation due to the various non-isotropic distributions mentioned above, therefore without loss of generality, consider the case of energy arriving uniformly over limited angular spread Δ around mean ψ_0, i.e., $(\psi_0-\Delta, \psi_0+\Delta)$. In this case the modal correlation is given by

$$\gamma^{\mathrm{R}}_{m-m'} = \mathrm{sinc}((m-m')\Delta) e^{-i(m-m')\psi_0}, \tag{6.17}$$

which is shown in Fig. 6.7 for various modes and angular spread. As one would expect, for increasing angular spread there is a decrease in modal correlation, with more rapid reduction for well separated mode orders, e.g., large $m-m'$. For the

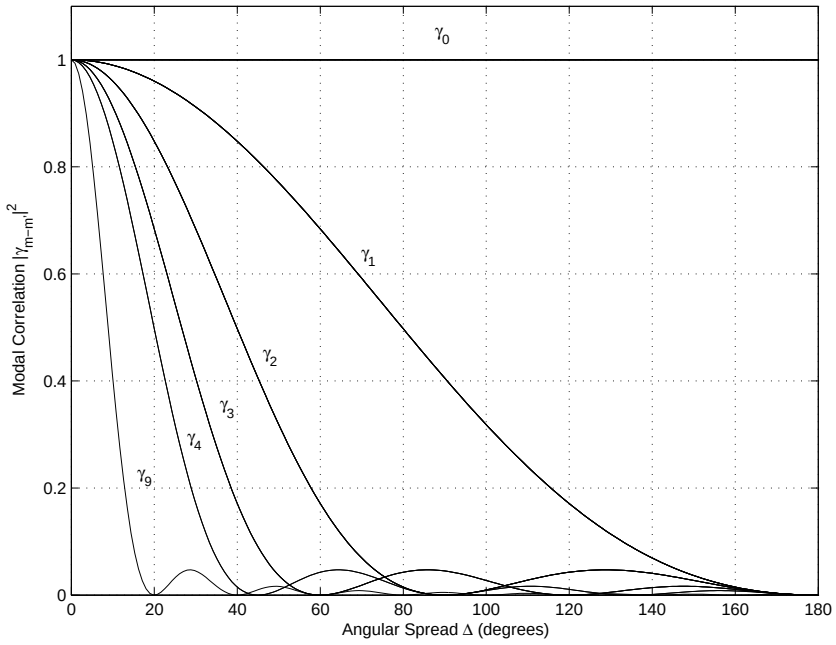

Figure 6.7: Modal correlation versus angular spread Δ of a uniform limited power density surrounding the aperture.

special case of a uniform isotropic scattering environment, $\Delta = \pi$, there is zero correlation between all modes, e.g., $\gamma^{\mathrm{R}}_{m-m'} = \delta(m - m')$.

Figure 6.8 shows the impact of modal correlation on the ergodic mode-to-mode capacity for increasing angular spread at the transmitter and isotropic scattering at the receiver[3] for 10dB SNR. The transmit and receive apertures are of radius 0.8λ, corresponding to $2\lceil \pi e 0.8 \rceil + 1 = 15$ modes at each aperture. For comparison, also shown is the capacity for an 15 antenna uniform linear (ULA), uniform circular (UCA), and uniform grid (UGA) arrays, contained within the same aperture size. Also shown is the 15×15 antenna i.i.d. case, corresponding to the rich scattering environment with no restrictions on the antenna placement, i.e., $r_{\mathrm{T}}, r_{\mathrm{R}} \to \infty$.

The mode-to-mode capacity is the maximum achievable capacity between the two apertures, and represents the upper bound on capacity for any antenna array geometry or multi-mode antennas constrained within those apertures. All four cases show no capacity growth for angular spread greater than approximately 60°, which corresponds to low modal correlations ($\ll 0.5$) for the majority of modes, as seen in Fig. 6.7.

Figure 6.9 shows ergodic capacity as the mean angle of departure ϕ_0 is varied from 0 to 90° with transmit angular spread of 20°, and the same scenario as

[3]This models a typical mobile communication scenario, where the receiver is usually surrounded by scatterers, and the base station is mounted high above the scattering environment.

in Fig. 6.8. It can be seen that the mode-to-mode, UCA, and UGA are invariant to mean departure angle. However, due to the linear array sampling along one dimension, the capacity of the ULA decreases as ϕ_0 approaches the inline case ($\phi_0 = 0°$), where the antenna array offers little diversity.

In this section the properties of the scattering channel matrix for 2D scattering environments where explored. Similar, albeit more tedious, expressions for the 3D case can also be derived, however, no further insights are gained and they are therefore not presented here.

6.2 Sampling Effects on Capacity

Implementation of a MIMO system requires sampling of the transmit and receive apertures by antenna arrays. The mode-to-mode capacity is the maximum capacity between the two apertures, however, the ULA, UCA and UGA give significantly lower capacity due to poor spatial-to-mode coupling for the given aperture. To observe this, consider the signal transmitted by the n-th mode generated by n_T antennas contained within an aperture of radius r_T

$$\widetilde{x}_n = \sum_{t=1}^{n_\mathrm{T}} x_t \overline{\mathcal{J}_n(\boldsymbol{x}_t)}. \tag{6.18}$$

Note that (6.18) represents both the $2D$ and $3D$ cases, as the 3D spatial-to-mode function (4.70) can be expressed as $\mathcal{J}_p(\boldsymbol{x}) \equiv \mathcal{J}_n^m(\boldsymbol{x})$ where $p = n(n+1)+m$ with inverse $n = \lfloor\sqrt{p}\rfloor$ and $m = p - \lfloor\sqrt{p}\rfloor(\lfloor\sqrt{p}\rfloor + 1)$, e.g., $p = 10$ gives $n = 3$ and $m = -2$, i.e., $\mathcal{J}_{10}(\boldsymbol{x}) = \mathcal{J}_2^{-3}(\boldsymbol{x})$.

The power radiated by the n-th mode is then

$$\sigma_n^2 = E\left\{|\widetilde{x}_n|^2\right\} \tag{6.19a}$$

$$= \sum_{t=1}^{n_\mathrm{T}} \sum_{t'=1}^{n_\mathrm{T}} E\left\{x_t \overline{x_{t'}}\right\} \overline{\mathcal{J}_n(\boldsymbol{x}_t)} \mathcal{J}_n(\boldsymbol{x}_{t'}) \tag{6.19b}$$

$$= \frac{P_\mathrm{T}}{n_\mathrm{T}} \sum_{t=1}^{n_\mathrm{T}} \left|\mathcal{J}_n(\boldsymbol{x}_t)\right|^2, \tag{6.19c}$$

where (6.19c) follows from the assumption of transmit antennas with statistically independent equal power transmit signals, with total power P_T, i.e., $E\left\{|x_t|^2\right\} = P_\mathrm{T}/n_\mathrm{T}$. Note that, since the spatial-to-mode function $\mathcal{J}_n(\boldsymbol{x}_t) \approx 0$ for all but the first N terms, only the first N modes have sufficient power to convey information at

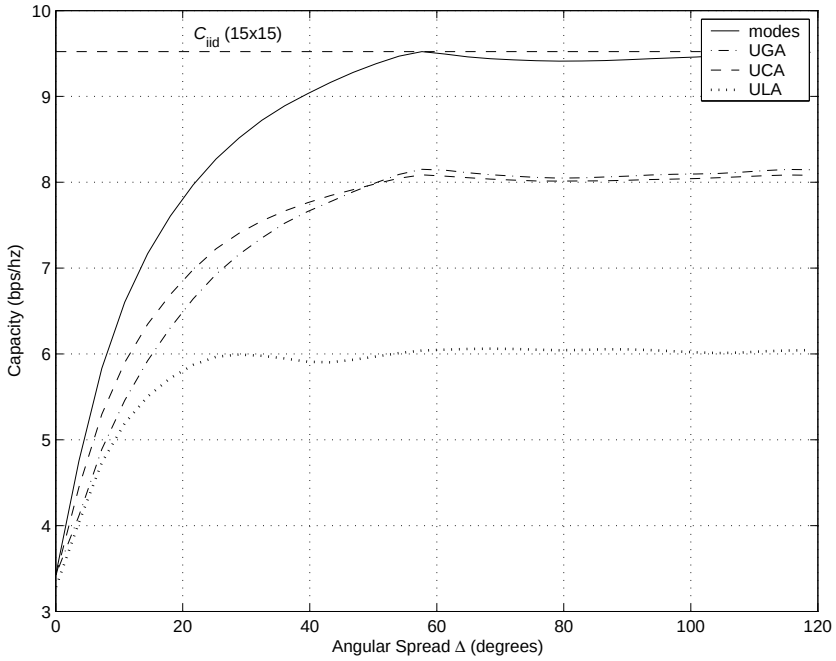

Figure 6.8: Capacity versus angular spread at the transmitter for mode-to-mode communication (modes), uniform linear array (ULA), uniform circular array (UCA), and uniform grid array (UGA), within spatial regions of radius 0.8λ and isotropic receiver scattering.

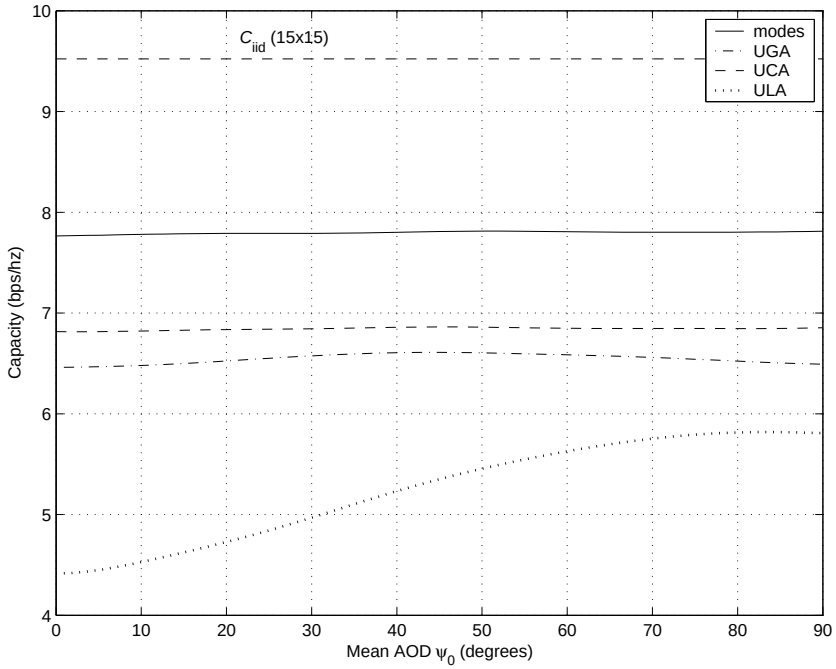

Figure 6.9: Capacity versus mean angle of departure for 20° spread at the transmitter for mode-to-mode communication (modes), uniform linear array (ULA), uniform circular array (UCA), and uniform grid array (UGA), within spatial regions of radius 0.8λ and isotropic receiver scattering.

any significant rate. Therefore, the antenna array excites N modes of the aperture with the power allocated to each mode given by (6.19c). The reception of energy at the receiver uses the same kind of structure as excitation, and is just the reverse process. The antenna array within the receive aperture combines the signals on the M modes with weighting

$$\sigma_m^2 = \frac{P_{\mathrm{R}}}{n_{\mathrm{R}}} \sum_{r=1}^{n_{\mathrm{R}}} \left| \mathcal{J}_m(\boldsymbol{y}_r) \right|^2 , \tag{6.20}$$

given to the m-th mode, where P_{R} is the total received power.

In MIMO systems, maximum diversity occurs when there are independent transmit and receive branches, therefore, the maximum capacity will occur for equal power allocation to the full set of uncorrelated modes available for the given aperture size. That is, for arrays within fixed apertures, ideal spatial-to-mode coupling occurs for antenna array geometries such that they excite N and M independent modes with uniform power allocation given by $\sigma_n^2 = P_{\mathrm{T}}/N$ and $\sigma_m^2 = P_{\mathrm{R}}/M$, at the transmit and receive apertures, respectively.

Fig. 6.10 shows the power allocation to each mode by the three array geometries considered in the previous section, relative to uniform power allocation of 0dB to each mode for ideal spatial-to-mode coupling in a 2D aperture. Recall from Chapter 3.3.2 that due to symmetry a fixed linear aperture (e.g., sampling along a line of length $2r_{\mathrm{T}}$) can only excite $N_{\mathrm{T}} + 1$ independent modes, therefore the ULA only allocates power to the $n = \{0, \ldots, N_{\mathrm{T}}\}$ modes, giving the poor capacity performance seen in Fig. 6.8. From the UCA and UGA distributions one would expect the UGA to perform better than the UCA, however, although the UCA is less uniform at the lower order modes, it has 5-10dB more power allocated to the higher order modes than that of the UGA. As shown in Section 6.1.3, well separated modal orders have lower correlation than small modal separation at small angular spreads, hence the UCA distribution predicts better capacity performance for low angular spread, as seen in Fig. 6.8.

Note that the nulls in the power allocation for the UCA at modes $|n| = 2$ is an artifact of placing the circular array on the boundary of the aperture. The power allocation to each mode for the UCA of smaller radii than the aperture using the same number of antennas is shown in Fig. 6.11. It can be seen that as the UCA is made smaller, the lower order modes become more uniform. However, the power at the higher order modes is reduced, therefore one would expect little capacity improvement, as can be seen in Fig. 6.12, where the capacity for the various UCA

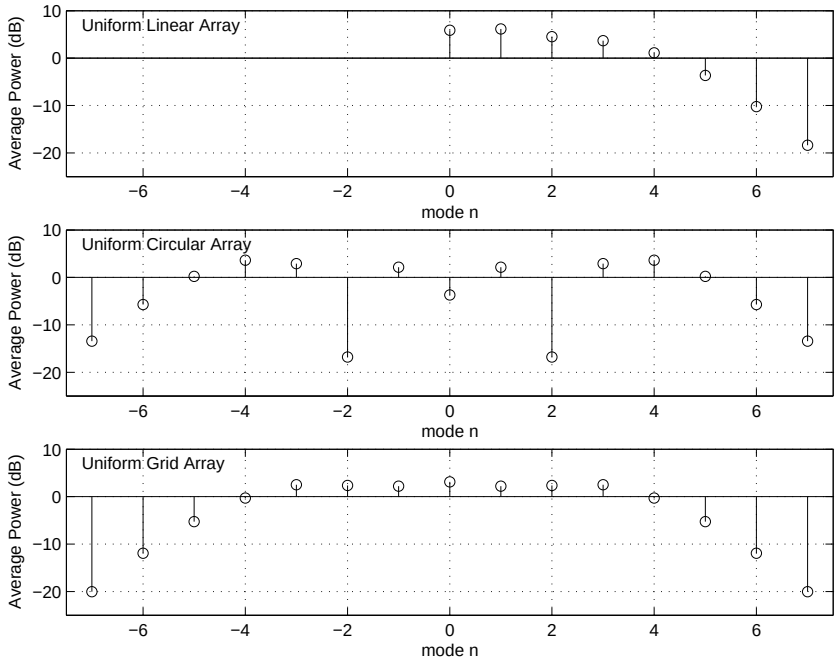

Figure 6.10: Average power assigned to each mode for the ULA, UCA, and UGA, within an aperture of 0.8λ, relative to 0dB in each mode for ideal spatial-to-mode coupling.

radii are nearly identical.

The roll off of power at the higher order modes shown for all array geometries indicates the difficulty using constrained antenna arrays to excite the modes of the aperture. As can be seen, the higher order modes receive very little power and contribute little to the capacity of the system. Therefore, it is important to note that achieving ideal spatial-to-mode coupling, where N uncorrelated modes are excited with equal power, may not be possible using antenna arrays. Consider a densely sampled circular aperture such that the spatial-to-mode functions are continuous, then the n, n'-th element of matrix product $\boldsymbol{J}_{\mathrm{T}}^{\dagger}\boldsymbol{J}_{\mathrm{T}}$ is given by

$$\boldsymbol{J}_{\mathrm{T}}^{\dagger}\boldsymbol{J}_{\mathrm{T}}|_{n,n'} = \sum_{t=1}^{n_{\mathrm{T}}} \overline{\mathcal{J}_n(\boldsymbol{x}_t)}\mathcal{J}_{n'}(\boldsymbol{x}_t) \tag{6.21a}$$

$$= i^{n-n'} \sum_{t=1}^{n_{\mathrm{T}}} J_n(k\,\|\boldsymbol{x}_t\|)J_{n'}(k\,\|\boldsymbol{x}_t\|)e^{-i(n-n')\theta_x} \tag{6.21b}$$

$$\approx \frac{n_{\mathrm{T}}}{\pi {r_{\mathrm{T}}}^2}\, i^{n-n'} \iint_{\mathbb{S}^1} J_n(kr)J_{n'}(kr)e^{-i(n-n')\theta} r\,dr\,d\theta \tag{6.21c}$$

$$= \frac{n_{\mathrm{T}}}{\pi {r_{\mathrm{T}}}^2}\, i^{n-n'} \int_0^{r_{\mathrm{T}}} J_n(kr)J_{n'}(kr)r\,dr \int_0^{2\pi} e^{-i(n-n')\theta} d\theta. \tag{6.21d}$$

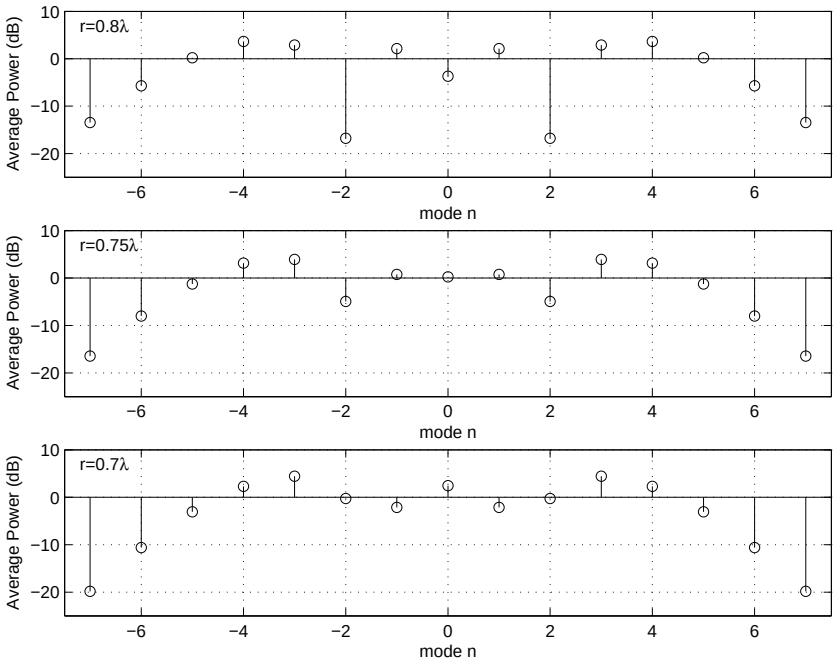

Figure 6.11: Average power assigned to each mode for the UCA of radii $r = \{0.8\lambda, 0.75\lambda, 0.7\lambda\}$, within an aperture of 0.8λ, relative to 0dB in each mode for ideal spatial-to-mode coupling.

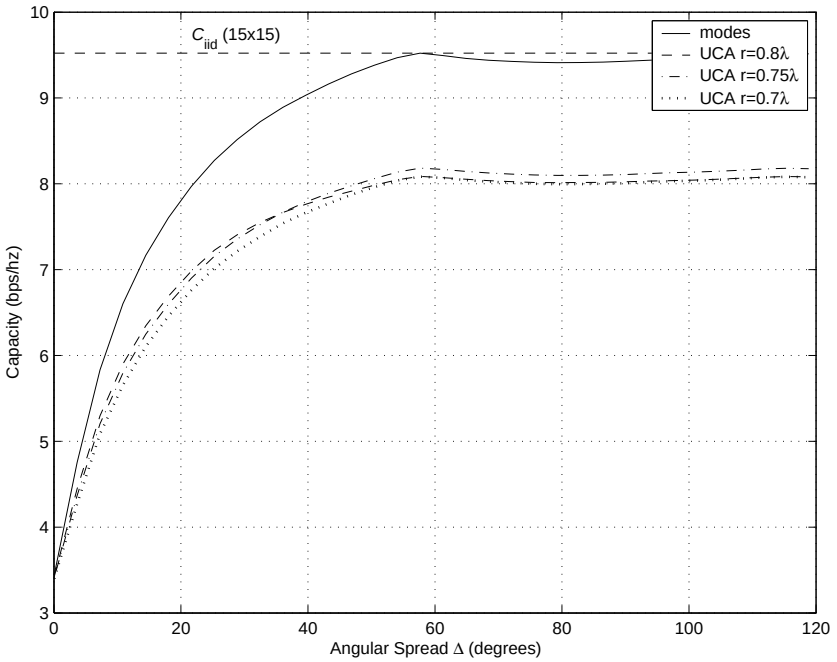

Figure 6.12: Capacity versus angular spread at the transmitter for mode-to-mode communication (modes), and a uniform circular array (UCA) of radii $r = r_{\mathrm{T}} = r_{\mathrm{R}} = \{0.8\lambda, 0.75\lambda, 0.7\lambda\}$, within spatial regions of radius 0.8λ and isotropic receiver scattering.

From the last term in (6.21d), the matrix product $\boldsymbol{J}_{\mathrm{T}}^{\dagger}\boldsymbol{J}_{\mathrm{T}}$ is zero for all $n \neq n'$, thus $\boldsymbol{J}_{\mathrm{T}}^{\dagger}\boldsymbol{J}_{\mathrm{T}}$ is a diagonal matrix with diagonal entries

$$\boldsymbol{J}_{\mathrm{T}}^{\dagger}\boldsymbol{J}_{\mathrm{T}}|_{n,n} = \frac{2n_{\mathrm{T}}}{{r_{\mathrm{T}}}^2}\int_0^{r_{\mathrm{T}}} r J_n^2(kr)\, dr \tag{6.22a}$$

$$= n_{\mathrm{T}} J_{n+1}^2(kr_{\mathrm{T}}), \tag{6.22b}$$

where (6.22b) follows from the identity $\int_0^1 z J_n^2(\alpha z)dz = J_{n+1}^2(\alpha)/2$ [131, p.658]. Note that the separation of radial and angular variables in (6.21d) also occurs in the 3D case, where the orthogonality of the spherical harmonics $Y_n^m(\theta,\phi)$ gives a diagonal matrix with non-unity diagonal terms for the matrix product $\boldsymbol{J}_{\mathrm{T}}^{\dagger}\boldsymbol{J}_{\mathrm{T}}$. Therefore, the assumption of semi-unitary matrix $\boldsymbol{J}_{\mathrm{T}}$ (i.e. $\boldsymbol{J}_{\mathrm{T}}^{\dagger}\boldsymbol{J}_{\mathrm{T}} = \alpha \boldsymbol{I}_N$, $\alpha \in \mathbb{R}$) indicating ideal spatial-to-mode coupling, cannot be achieved even with a large number of antennas uniformly sampling the aperture. Note that the diagonal structure of $\boldsymbol{J}_{\mathrm{T}}^{\dagger}\boldsymbol{J}_{\mathrm{T}}$ indicates the antennas generate N independent modes, however, the total power is not uniformly distributed across the modes. Identical expressions hold for the receiver matrix product $\boldsymbol{J}_{\mathrm{R}}^{\dagger}\boldsymbol{J}_{\mathrm{R}}$.

Further insight into the relationship between antenna placement and modal correlation can be shown by considering the cross correlation of the channel branches. Denote h_{rt} as the random complex channel gain between the t-th transmit antenna and the r-th receive antenna within circular apertures, given by (4.53), then the cross correlation between the communication links h_{rt} and $h_{r',t'}$ can be expressed as

$$\rho_{tt',rr'} \triangleq E\left\{h_{rt}\overline{h_{r't'}}\right\} \tag{6.23a}$$

$$= \sum_{n,n'}\sum_{m,m'}\iint_{\mathbb{S}^1} G(\phi,\psi)\,\overline{F_n^{n'}(\boldsymbol{x}_t,\boldsymbol{x}_{t'})}\, e^{i(n-n')\phi} F_m^{m'}(\boldsymbol{y}_r,\boldsymbol{y}_{r'}) e^{-i(m-m')\psi} d\phi d\psi \tag{6.23b}$$

$$= \sum_{n,n'}\overline{F_n^{n'}(\boldsymbol{x}_t,\boldsymbol{x}_{t'})}\sum_{m,m'} F_m^{m'}(\boldsymbol{y}_r,\boldsymbol{y}_{r'})\iint_{\mathbb{S}^1} G(\phi,\psi)\, e^{i(n-n')\phi}\, e^{-i(m-m')\psi}\, d\phi d\psi \tag{6.23c}$$

$$= \sum_{n,n'}\overline{F_n^{n'}(\boldsymbol{x}_t,\boldsymbol{x}_{t'})}\sum_{m,m'} F_m^{m'}(\boldsymbol{y}_r,\boldsymbol{y}_{r'})\,\gamma_{n-n',m-m'}, \tag{6.23d}$$

where

$$F_n^{n'}(\boldsymbol{x}_t,\boldsymbol{x}_{t'}) \triangleq \mathcal{J}_n(\boldsymbol{x}_t)\overline{\mathcal{J}_{n'}(\boldsymbol{x}_{t'})}, \tag{6.24}$$

with notation $\sum_{n,n'} \triangleq \sum_{n=-N_{\mathrm{T}}}^{N_{\mathrm{T}}} \sum_{n'=-N_{\mathrm{T}}}^{N_{\mathrm{T}}}$, and $\gamma_{n-n',m-m'}$ is the modal correlation (6.11). Equation (6.23d) shows the separate effects of the number of possible modes, modal correlation, and antenna placement on channel branch cross-correlation for spatially constrained antenna arrays.

Consider the transmit branch correlation between two antennas t and t', given by (6.23d) with $r = r'$,

$$\rho_{tt'} = \sum_{n,n'} \overline{\mathcal{J}_n(\boldsymbol{x}_t)} \mathcal{J}_{n'}(\boldsymbol{x}_{t'}) \gamma^{\mathrm{T}}_{n-n'}, \tag{6.25}$$

where $\gamma^{\mathrm{T}}_{n-n'}$ is the modal correlation (6.16) between the n and n'-th mode of the transmit aperture. Assuming uncorrelated modes at the transmitter, then $\gamma^{\mathrm{T}}_{n-n'} = \delta(n - n')$ and

$$\rho_{tt'} = \sum_{n} \mathcal{J}_n(\boldsymbol{x}_t) \overline{\mathcal{J}_n(\boldsymbol{x}_{t'})} \tag{6.26a}$$

$$= J_0(k \left\| \boldsymbol{x}_t - \boldsymbol{x}_{t'} \right\|), \tag{6.26b}$$

where (6.26b) follows from a special case of Gegenbauer's Addition Theorem [109, pp. 363]. From (6.26b), for a minimum $n_{\mathrm{T}} = N$ antennas, perfect spatial-to-mode coupling occurs when the antennas are placed within the aperture such that the scaled separation, $k \left\| \boldsymbol{x}_t - \boldsymbol{x}_{t'} \right\|$, between each and every pair of antennas is a zero of the Bessel function of zero order. Note that (6.26b) is the spatial correlation expression for 2D rich scattering [16], therefore, achieving ideal spatial-to-mode coupling is equivalent to finding the set of points within the aperture which are uncorrelated for an isotropic diffuse scattering environment.

6.3 Communication Between Arbitrarily Shaped Apertures

In the previous sections, multiple antenna systems are shown to be a particular choice of implementation for a more fundamental spatial signal processing underlying communication between two apertures in space. In this section communication in a continuous spatial channel is considered, where an arbitrarily shaped continuous aperture transmits signals which, after propagation through a general scattering environment, are received via a second arbitrarily shaped continuous receive aperture.

Consider the continuous spatial channel shown in Fig. 6.13. The source or transmit aperture[4], denoted Ω_{T}, is excited by some means and radiates signals into the surrounding scattering environment. After propagation through the complex scattering media, the transmitted signals arrive at the receive aperture, denoted Ω_{R}. Note, both transmit and receive apertures are assumed finite and starlike [79][5].

Denote $\Phi(\widehat{\boldsymbol{\phi}})$ as the source signal radiating in direction $\widehat{\boldsymbol{\phi}}$ from the surface $\partial\Omega_{\mathrm{T}}$ of the transmit aperture Ω_{T}. Let $\Psi(\widehat{\boldsymbol{\psi}})$ denote the signal received from direction $\widehat{\boldsymbol{\psi}}$ on the surface $\partial\Omega_{\mathrm{R}}$ of the receive aperture Ω_{R}, generated due to the transmitted signals, given by

$$\Psi(\widehat{\boldsymbol{\psi}}) = \int_{\Omega_{\mathrm{T}}} g(\widehat{\boldsymbol{\phi}}, \widehat{\boldsymbol{\psi}})\, \Phi(\widehat{\boldsymbol{\phi}})\, ds(\widehat{\boldsymbol{\phi}}), \tag{6.27}$$

where $ds(\widehat{\boldsymbol{\phi}})$ is a surface element of transmit aperture Ω_{T} with unit normal $\widehat{\boldsymbol{\phi}}$, and $g(\widehat{\boldsymbol{\phi}}, \widehat{\boldsymbol{\psi}})$ is the effective complex random scattering gain of the scattering environment for signals leaving the transmit aperture in direction $\widehat{\boldsymbol{\phi}}$ and arriving at the receive aperture along $\widehat{\boldsymbol{\psi}}$.

To describe the source function $\Phi(\widehat{\boldsymbol{\phi}})$ consider a complete orthonormal basis set of functions defined on $\partial\Omega_{\mathrm{T}}$, namely, $\{\phi_1(\widehat{\boldsymbol{\phi}}), \phi_2(\widehat{\boldsymbol{\phi}}), \ldots\}$. Note that at this stage it is not important to know what the set of functions, $\{\phi_n(\widehat{\boldsymbol{\phi}})\}$, are as long as they are complete orthonormal basis sets on $\partial\Omega_{\mathrm{T}}$. The orthonormality of the functions is with respect to the natural inner product

$$\langle f, h \rangle_{\Omega} \triangleq \int_{\Omega} f(\widehat{\boldsymbol{\varphi}}) \overline{h(\widehat{\boldsymbol{\varphi}})}\, ds(\widehat{\boldsymbol{\varphi}}), \tag{6.28}$$

where $ds(\widehat{\boldsymbol{\varphi}})$ is a surface element of $\Omega \in [\Omega_{\mathrm{T}}, \Omega_{\mathrm{R}}]$ with norm $\widehat{\boldsymbol{\varphi}}$, that is,

$$\Big\langle \phi_n(\widehat{\boldsymbol{\phi}}), \phi_{n'}(\widehat{\boldsymbol{\phi}}) \Big\rangle_{\Omega_{\mathrm{T}}} \equiv \int_{\Omega_{\mathrm{T}}} \phi_n(\widehat{\boldsymbol{\phi}}) \overline{\phi_{n'}(\widehat{\boldsymbol{\phi}})}\, ds(\widehat{\boldsymbol{\phi}}) = \delta(n - n'). \tag{6.29}$$

The source function $\Phi(\widehat{\boldsymbol{\phi}})$ can be represented by this basis set to obtain

$$\Phi(\widehat{\boldsymbol{\phi}}) = \sum_{n} \widetilde{x}_n \phi_n(\widehat{\boldsymbol{\phi}}), \tag{6.30}$$

[4]Strictly speaking, in the following Ω_{T} and Ω_{R} no longer denote apertures, rather volumes, however for simplicity we will retain the notation.

[5]This restriction is relaxed in Chapter 6.4 where a more generalized model is presented.

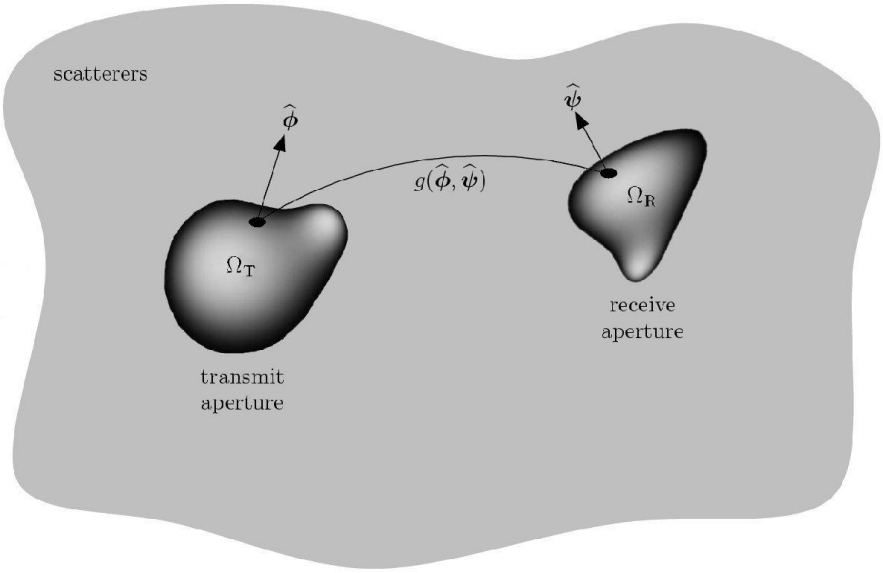

Figure 6.13: Continuous spatial channel model for communication between two arbitrary apertures. $g(\widehat{\boldsymbol{\phi}}, \widehat{\boldsymbol{\psi}})$ is the effective complex random scattering gain of the scattering environment for signals leaving the transmit aperture Ω_{T} in direction $\widehat{\boldsymbol{\phi}}$ and arriving at the receive aperture Ω_{R} along $\widehat{\boldsymbol{\psi}}$. All scatterers are considered external to apertures and exist in $\mathbb{R}^3 \setminus \{\Omega_{\mathrm{T}}, \Omega_{\mathrm{R}}\}$.

where $\widetilde{x}_n$ are the Fourier coefficients given by the projection of ϕ_n on Φ;

$$\widetilde{x}_n = \left\langle \Phi(\widehat{\boldsymbol{\phi}}), \phi_n(\widehat{\boldsymbol{\phi}}) \right\rangle_{\Omega_\mathrm{T}}. \tag{6.31}$$

Similarly, to describe the stimulated function $\Psi(\widehat{\boldsymbol{\psi}})$ on the surface Ω_R consider a second complete orthonormal basis set of functions, denoted $\{\psi_1(\widehat{\boldsymbol{\psi}}), \psi_2(\widehat{\boldsymbol{\psi}}), \ldots\}$, with orthonormality

$$\left\langle \psi_m(\widehat{\boldsymbol{\psi}}), \psi_{m'}(\widehat{\boldsymbol{\psi}}) \right\rangle_{\Omega_\mathrm{R}} \equiv \int_{\Omega_\mathrm{R}} \psi_m(\widehat{\boldsymbol{\psi}}) \overline{\psi_{m'}(\widehat{\boldsymbol{\psi}})}\, ds(\widehat{\boldsymbol{\psi}}) = \delta(m - m'). \tag{6.32}$$

Using this basis set, the function $\Psi(\widehat{\boldsymbol{\psi}})$ can be expressed as

$$\Psi(\widehat{\boldsymbol{\psi}}) = \sum_m \widetilde{z}_m \psi_m(\widehat{\boldsymbol{\psi}}), \tag{6.33}$$

where $\widetilde{z}_m$ are the Fourier coefficients given by the projection of ψ_m on Ψ;

$$\widetilde{z}_m = \left\langle \Psi(\widehat{\boldsymbol{\psi}}), \psi_m(\widehat{\boldsymbol{\psi}}) \right\rangle_{\Omega_\mathrm{R}}. \tag{6.34}$$

The coefficients $\widetilde{x}_n$ (6.31) and $\widetilde{z}_m$ (6.34) correspond to the signals transmitted and received on the n-th and m-th modes of the expansions (6.30) and (6.33), respectively. To compute the intrinsic capacity for the continuous channel, the relationship between the transmitted and received modes due to the scattering environment is required. Consider the received signal from direction $\widehat{\boldsymbol{\psi}}$ due to transmitted signal $\widetilde{x}_n$ on the n-th transmit mode,

$$\Psi_n(\widehat{\boldsymbol{\psi}}) = \widetilde{x}_n \int_{\Omega_\mathrm{T}} g(\widehat{\boldsymbol{\phi}}, \widehat{\boldsymbol{\psi}}) \phi_n(\widehat{\boldsymbol{\phi}}) ds(\widehat{\boldsymbol{\phi}}), \tag{6.35}$$

with the total received signal given by the sum over all transmit modes,

$$\Psi(\widehat{\boldsymbol{\psi}}) = \sum_n \Psi_n(\widehat{\boldsymbol{\psi}}). \tag{6.36}$$

From (6.34), (6.35), and (6.36), the relationship between the received signal $\widetilde{z}_m$ on the m-th mode due to the signal $\widetilde{x}_n$ transmitted on the n-th mode is given by

$$\widetilde{z}_m = \sum_n \left\langle \Psi_n(\widehat{\boldsymbol{\psi}}), \psi_m(\widehat{\boldsymbol{\psi}}) \right\rangle_{\Omega_\mathrm{R}} \tag{6.37a}$$

$$= \sum_n \beta_m^n \widetilde{x}_n, \tag{6.37b}$$

where

$$\beta_m^n \triangleq \left\langle \left\langle g(\widehat{\boldsymbol{\phi}}, \widehat{\boldsymbol{\psi}}), \overline{\phi_n(\widehat{\boldsymbol{\phi}})} \right\rangle_{\Omega_\mathrm{T}}, \psi_m(\widehat{\boldsymbol{\psi}}) \right\rangle_{\Omega_\mathrm{R}} \tag{6.38a}$$

$$= \int_{\Omega_\mathrm{R}} \int_{\Omega_\mathrm{T}} g(\widehat{\boldsymbol{\phi}}, \widehat{\boldsymbol{\psi}})\, \phi_n(\widehat{\boldsymbol{\phi}})\, \overline{\psi_m(\widehat{\boldsymbol{\psi}})}\, ds(\widehat{\boldsymbol{\phi}}) ds(\widehat{\boldsymbol{\psi}}), \tag{6.38b}$$

are the complex gains of the scattering environment for transmission from mode n of Ω_T and reception by mode m of Ω_R.

There are an infinite number of modes for each aperture, however, in terms of practical systems with finite transmit power and channel gains along with noise at the receiver there is very little energy associated with the higher order modes. Similar to the sampling of a frequency band-limited signal, where there is a threshold of sampling in the time domain at which any further sampling gives no further increase in information, for sampled spatial apertures in the presence of finite precision or noise there will be a fundamental limit to the information content that the spatial aperture can bear. For the circular and spherical apertures this manifested in the number of significant coefficients in the wavefield expansions and could be shown analytically. However, for arbitrary apertures finding the significant modes or dominant eigenfunctions poses a much harder problem[6].

Therefore, from a communications point of view, the higher order modes contribute little to the capacity of the system. With this in mind, the infinite channel representation may be truncated to a finite set of appropriately chosen transmit modes (cardinality N), and receive modes (cardinality M) to give the finite matrix representation

$$\widetilde{\boldsymbol{z}} = \boldsymbol{H}_\mathrm{S}\, \widetilde{\boldsymbol{x}}, \tag{6.39}$$

where $\widetilde{\boldsymbol{z}}$ and $\widetilde{\boldsymbol{x}}$ are the column vectors of the N transmit mode signals $\{\widetilde{x}_n\}_{n=1}^N$, and M receive mode signals $\{\widetilde{z}_m\}_{m=1}^M$, respectively, and $\boldsymbol{H}_\mathrm{S}$ is the $(M \times N)$ scattering environment matrix, with m, n-th element given by (6.38b).

From (6.39) the intrinsic capacity is limited by the geometry of the apertures (number of significant modes), and the scattering channel matrix $\boldsymbol{H}_\mathrm{S}$ (coupling between transmit and receive modes). Larger apertures enable the excitation of a larger number of modes, analogous to the well studied waveguide, where for a fixed frequency the number propagation modes of significant energy is proportional to

[6]Note that, since every finite aperture can be enclosed within a finite sphere it is possible to find an upper limit to the number of modes using the results from Chapter 4.

the waveguide dimensions. The amount of information available on these modes at the receiver is limited by correlation between the modal gains β_m^n and is strongly dependent on the scattering environment described by $g(\widehat{\boldsymbol{\phi}}, \widehat{\boldsymbol{\psi}})$. Therefore, for analysis of communication over continuous spatial channels it is necessary to study the properties of the basis functions of the apertures and the connection between them due to scattering.

A natural arena to study such properties is that of the Hilbert Spaces $L^2(\Omega_{\mathrm{T}})$ and $L^2(\Omega_{\mathrm{R}})$ with associated inner products on Ω_{T} and Ω_{R}. Therefore in the following, the above formulation is recast under a more general framework of compact linear operators in Hilbert Spaces, which not only encompasses the previous chapters on continuous spacially constrained channels, but provides a more general principle that includes, for example, the time- and band-limited channel communication formulations. A complete treaty would easily fill a second Ph.D. thesis, hence in the following few specifics are given, rather an overview of a more general approach to communication between two arbitrary volumes is presented, with an emphasis on highlighting the key points for future investigation.

6.4 Spatial Information and Communication

Consider two non-intersecting finite size apertures Ω_{T} and Ω_{R}, shown in Fig. 6.14, with source $\{u \equiv u(\boldsymbol{x}) \in L^2(\Omega_{\mathrm{T}})\}$, and generated $\{v \equiv v(\boldsymbol{y}) \in L^2(\Omega_{\mathrm{R}})\}$, complex separable Hilbert Spaces respectively, with the natural inner product

$$\langle f, g \rangle_{\Omega} \triangleq \int_{\Omega} f(\boldsymbol{x}) \overline{g(\boldsymbol{x})} d\Omega(\boldsymbol{x}), \tag{6.40}$$

and induced norm

$$\|f\|_{\Omega}^2 \triangleq \int_{\Omega} |f(\boldsymbol{x})|^2 \, d\Omega(\boldsymbol{x}), \tag{6.41}$$

where $d\Omega(\boldsymbol{x})$ is a volume element of Ω at $\boldsymbol{x}$.

Define the linear integral operator $\mathcal{L} : L^2(\Omega_{\mathrm{T}}) \to L^2(\Omega_{\mathrm{R}})$ by

$$v = \mathcal{L}\, u, \tag{6.42}$$

where

$$v(\boldsymbol{y}) = \int_{\Omega_{\mathrm{T}}} g(\boldsymbol{x}, \boldsymbol{y})\, u(\boldsymbol{x})\, d\Omega_{\mathrm{T}}(\boldsymbol{x}), \tag{6.43}$$

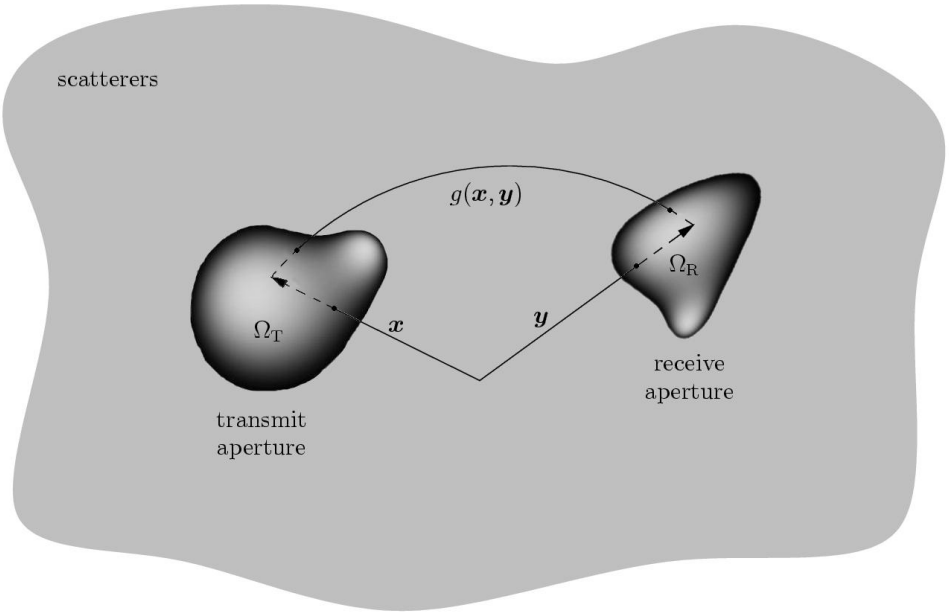

Figure 6.14: Generalized continuous spatial channel model for communication between two arbitrary apertures. $g(\boldsymbol{x}, \boldsymbol{y})$ is the resultant function generated at $\boldsymbol{y} \in \Omega_{\mathrm{R}}$ due to the source function $u(\boldsymbol{x})$, $\boldsymbol{x} \in \Omega_{\mathrm{T}}$. All scatterers are considered external to apertures and exist in $\mathbb{R}^3 \setminus \{\Omega_{\mathrm{T}}, \Omega_{\mathrm{R}}\}$.

with $d\Omega_{\mathrm{T}}(\boldsymbol{x})$ a volume element of Ω_{T} at $\boldsymbol{x}$. The kernel of the operator, $g(\boldsymbol{x},\boldsymbol{y})$, describes the channel, giving the resultant function generated at $\boldsymbol{y} \in \Omega_{\mathrm{R}}$ due to the source function $u(\boldsymbol{x})$, $\boldsymbol{x} \in \Omega_{\mathrm{T}}$. Note, that in the absence of scatterers the kernel is given by [79]

$$g(\boldsymbol{x},\boldsymbol{y}) = \frac{e^{-ik\|\boldsymbol{x}-\boldsymbol{y}\|}}{4\pi\,\|\boldsymbol{x}-\boldsymbol{y}\|}, \tag{6.44}$$

which is the fundamental solution to the Helmholtz equation for a point source at $\boldsymbol{x}$. However, in the following it is assumed the environment contains scatterers giving much more complicated expression for the channel $g(\boldsymbol{x},\boldsymbol{y})$ than (6.44).

Consider two sets of functions $\{\phi_n(\boldsymbol{x})\}$ and $\{\psi_m(\boldsymbol{y})\}$ orthonormal and complete in Hilbert Spaces $L^2(\Omega_{\mathrm{T}})$ and $L^2(\Omega_{\mathrm{R}})$, respectively. The source and receive functions may be expressed as

$$u = \sum_n \langle u, \phi_n \rangle_{\Omega_{\mathrm{T}}}\, \phi_n, \tag{6.45}$$

$$v = \sum_m \langle v, \psi_m \rangle_{\Omega_{\mathrm{R}}}\, \psi_m. \tag{6.46}$$

Denote the Fourier coefficients $\alpha_n = \langle u, \phi_n \rangle_{\Omega_{\mathrm{T}}}$ and $\beta_m = \langle v, \psi_m \rangle_{\Omega_{\mathrm{R}}}$ of the expansions (6.45) and (6.46) in the transmit and receive apertures, respectively, then following the approach in the previous section it immediately follows that,

$$\beta_m = \sum_n \gamma_m^n\, \alpha_n, \tag{6.47}$$

where

$$\gamma_m^n = \int_{\Omega_{\mathrm{R}}} \int_{\Omega_{\mathrm{T}}} g(\boldsymbol{x},\boldsymbol{y})\, \phi_n(\boldsymbol{x})\, \overline{\psi_m(\boldsymbol{y})}\, d\Omega_{\mathrm{T}}(\boldsymbol{x})\, d\Omega_{\mathrm{R}}(\boldsymbol{y}). \tag{6.48}$$

The variables γ_m^n can be thought of as coupling coefficients between the transmission from mode n in Ω_{T} and the reception by mode m in Ω_{R}, giving the amplitude of the function ψ_m in Ω_{R} that results from source ϕ_n in Ω_{T}. Note that (6.47) is equivalent to (6.43) (via the representations (6.45) and (6.46)), where the basis functions are parameterized by the coefficients $\{\alpha_n\}$ and $\{\beta_m\}$, and the channel by $\{\gamma_m^n\}$.

As discussed in the previous section, the infinite dimensional representation (6.47) can be reduced to a finite dimensional matrix form by considering that in the presence of noise there is a limit to the information content of a spatially-constrained aperture. That is, for given apertures, the information bearing functions u and v

can be essentially reconstructed using a finite set of coefficients $\{\alpha_n\}$ and $\{\beta_m\}$, respectively. Therefore, the dimensionality of the apertures and communication strengths between the apertures gives a fundamental limit to spatial communication.

6.4.1 Dimensionality of Spatial Apertures

Consider a source free finite sized aperture $\Omega \in \mathbb{R}^3$, for which we wish to determine the complete subspace of solutions $f \equiv f(\boldsymbol{x}), \boldsymbol{x} \in \Omega$ to the homogenous Helmoltz equation

$$\triangle f + k^2 f = 0, \tag{6.49}$$

describing wavefields f in Ω due to sources in $\mathbb{R}^3 \setminus \Omega$.

With respect to the inner product (6.40), the set of functions satisfying $\|f\|_\Omega^2 < \infty$ is a separable Hilbert Space, and solutions to (6.49) are a strict subspace. Since the Hilbert Space $\{f \in L^2(\Omega) : \triangle f + k^2 f = 0\}$ is separable, the functions f can be expressed by the complete (in the Hilbert Space) orthonormal sequence $\{\varphi_p\}$,

$$f = \sum_p \langle f, \varphi_p \rangle_\Omega \, \varphi_p. \tag{6.50}$$

Under this Hilbert Space setting, finite dimensional approximations to the infinite dimensional wavefield $f(\boldsymbol{x})$ in Ω give rise to a essential dimensionality of the wavefields. The essential dimensionality refers to a well-defined threshold in dimension, beyond which the best finite dimensional approximation achieves a high relative precision [132]. That is, one wishes to find the best finite dimensional approximation to (6.50) of the form

$$f_P = \sum_{p \in \mathcal{P}} \langle f, \varphi_p \rangle_\Omega \, \varphi_p, \tag{6.51}$$

where $\mathcal{P}$ is a finite index set with cardinality $|\mathcal{P}| = P < \infty$, and $\{\varphi_p\}_{p \in \mathcal{P}}$ is a finite, incomplete, orthonormal basis function set within Ω. Clearly, the metric to determine the degree of approximation should be the induced norm (6.41). Hence, to obtain the best approximation f_P to f an orthonormal set $\{\varphi_p\}_{p \in \mathcal{P}}$ along with an index set $\mathcal{P}$ must be determined satisfying

$$\min_{\{\varphi_p\}_{p \in \mathcal{P}}} \|f - f_P\|_\Omega^2 . \tag{6.52}$$

Determination of the best approximation $f_P(\boldsymbol{x})$ of a given dimension P to represent the wavefield $f(\boldsymbol{x})$ in an arbitrary aperture Ω is non-trivial, made more difficult when the source field generating f is not specified.

Using an appropriately normalized orthogonal basis set for spherical apertures developed in [133, 134], the optimization problem (6.52) is approached in [132] by considering a larger aperture $\Omega_{\mathrm{S}} \in \mathbb{R}^3$ encompassing the aperture of interest, i.e., $\Omega \subset \Omega_{\mathrm{S}}$, where the larger aperture contains no sources. Using this model, the approximation is then closely related to a spatial concentration problem where one wishes to determine the finite dimensional approximation to the wavefield in sphere Ω_{S} that best captures the energy of that wavefield in the inner sphere Ω.

It is interesting to note that using this method, with outer sphere Ω_{S} assumed large enough such that any source in $\mathbb{R}^3 \setminus \Omega_{\mathrm{S}}$ is farfield to the surface of the inner sphere Ω, gives (within an appropriate normalization) identical field representations to those developed in Chapter 4. That is, the choice of truncation and plane wave expansion used in Chapter 4 is the optimal in the sense of (6.52).

Extension to non-spherical regions is non-trivial and requires the spectral properties of linear integral and truncation operators, and has strong parallels with the time-frequency concentration and associated dimensionality of time- and band-limited signals [135–137]. However, regardless of the difficulties in determining the basis set $\{\varphi_p\}_{p\in\mathcal{P}}$, it has been shown that it is possible to define a threshold where including more basis functions provides limited reduction in the error of the approximation. This implies that in the presence of noise or finite precision, the wavefield can be reconstructed using a finite number of coefficients, hence the infinite dimensional operator can be represented by a finite matrix representation, which surplants the standard MIMO matrix.

Note that the most spatially concentrated wave-field for a spherical aperture is given by the an isotropic source field, generated by uniformly distributed sources in all directions [132]. Therefore, the solutions to the approximation problem in the absence of source knowledge will in general be for isotropic scattering. That is, solving (6.52) without source knowledge will give the supremum essential dimensionality of the aperture. Thus the choice of $\mathcal{P}$ may not be optimal in the sense of communication between two apertures in a arbitrary scattering environment, and as such the connection between basis functions within the apertures must also be considered.

6.4.2 Communication Strengths Between Apertures

Consider $g(\boldsymbol{x},\boldsymbol{y}) \in L^2(\Omega_{\mathrm{T}} \times \Omega_{\mathrm{R}})$ corresponding to source free physically realistic scattering environments, then,

$$\int_{\Omega_{\mathrm{T}}} \int_{\Omega_{\mathrm{R}}} |g(\boldsymbol{x},\boldsymbol{y})|^2 \, d\Omega_{\mathrm{R}}(\boldsymbol{y}) d\Omega_{\mathrm{T}}(\boldsymbol{x}) = G_{\Omega_{\mathrm{T}},\Omega_{\mathrm{R}}} < \infty, \tag{6.53}$$

in which case $\mathcal{L}$ is a compact linear operator (self-adjoint Hilbert-Schmidt operator), therefore there exists infinitely many eigenvalues λ_j and eigenfunctions φ_j such that $\mathcal{L}\varphi_j = \lambda_j \varphi_j$.

Applying Parseval's theorem, it is straight forward to show that

$$\sum_{n,m} |\gamma_m^n|^2 = G_{\Omega_{\mathrm{T}},\Omega_{\mathrm{R}}}, \tag{6.54}$$

that is, since $G_{\Omega_{\mathrm{T}},\Omega_{\mathrm{R}}}$ is finite the total strength of the coupling between apertures is bounded, hence the strength of the interconnections $|\gamma_m^n|$ is negligible[7] for all but a finite set of couplings. Therefore, although there are infinitely many connections between apertures, the number of practical channels in the presence of noise or finite precision is finite. In effect, weakly connected communications channels (vanishingly small $|\gamma_m^n|$) will lead to vanishingly small received basis functions which become insignificant in the presence of noise.

Note that the total connection strength $G_{\Omega_{\mathrm{T}},\Omega_{\mathrm{R}}}$ is computed by the evaluation of the kernel $g(\boldsymbol{x},\boldsymbol{y})$ over the apertures Ω_{T} and Ω_{R}, therefore, both the geometry of the apertures and the scattering environment determine the possible limits to communication between the apertures. In the special case of no scattering, from (6.44) $G_{\Omega_{\mathrm{T}},\Omega_{\mathrm{R}}}$ depends only on the geometry of the apertures and their relative positions. Also observe that the value of $G_{\Omega_{\mathrm{T}},\Omega_{\mathrm{R}}}$ is invariant to the choice of basis functions, however, it is possible to choose these basis sets such that the number of channels with connection strengths above the threshold imposed by noise is maximized.

The optimal set of basis functions would be the one that maximizes the connection strengths, i.e., the best choice of (normalized) transmit function $\phi(\boldsymbol{x})$ would be the one that gives the maximum value of $|\gamma|^2 = \int_{\Omega_{\mathrm{R}}} |\psi(\boldsymbol{y})|^2 \, d\Omega_{\mathrm{R}}(\boldsymbol{y})$. Substitution of (6.43) leads to maximization of

$$|\gamma|^2 = \iint_{\Omega_{\mathrm{T}}} G_{\Omega_{\mathrm{R}}}(\boldsymbol{x},\boldsymbol{x}')\phi(\boldsymbol{x})\overline{\phi(\boldsymbol{x}')} \, d\Omega_{\mathrm{T}}(\boldsymbol{x}) \, d\Omega_{\mathrm{T}}(\boldsymbol{x}'), \tag{6.55}$$

[7] i.e., there exists some M and N such that $|\gamma_m^n| \leq \epsilon$ for $m > M$, $n > N$ and small ϵ.

where

$$G_{\Omega_{\mathrm{R}}}(\boldsymbol{x},\boldsymbol{x}') = \int_{\Omega_{\mathrm{R}}} g(\boldsymbol{x},\boldsymbol{y})\overline{g(\boldsymbol{x}',\boldsymbol{y})}\, d\Omega_{\mathrm{R}}(\boldsymbol{y}). \tag{6.56}$$

Note that the kernel $G_{\Omega_{\mathrm{R}}}(\boldsymbol{x},\boldsymbol{x}')$ is continuous finite Hermitian function in Ω_{T} and Ω_{R}, therefore (6.55) is maximized when ϕ is an eigenfunction of $G_{\Omega_{\mathrm{R}}}$, i.e., finding eigenfunction ϕ such that eigenvalue $|\gamma|^2$ is maximized for

$$|\gamma|^2 \phi(\boldsymbol{x}') = \int_{\Omega_{\mathrm{T}}} G_{\Omega_{\mathrm{R}}}(\boldsymbol{x},\boldsymbol{x}')\phi(\boldsymbol{x}) d\Omega_{\mathrm{T}}(\boldsymbol{x}). \tag{6.57}$$

Hence, the set of orthonormal basis functions with the largest successive values of $|\gamma|$ is the set $\{\phi_j\}$ where ϕ_j is the j-th normalized eigenfunction in descending order of their eigenvalues $\lambda_j = |\gamma_j|^2$.

For each normalized source eigenfunction ϕ_j there is a normalized receiver function ψ_j for which

$$\lambda_j \psi_j = \mathcal{L}\phi_j. \tag{6.58}$$

Similar to the source functions, the ψ_j are the solutions of the eigenfunction problem

$$|\gamma_j|^2 \psi_j(\boldsymbol{y}) = \int_{\Omega_{\mathrm{R}}} G_{\Omega_{\mathrm{T}}}(\boldsymbol{y},\boldsymbol{y}')\psi_j(\boldsymbol{y}')\, d\Omega_{\mathrm{R}}(\boldsymbol{y}'), \tag{6.59}$$

where

$$G_{\Omega_{\mathrm{T}}}(\boldsymbol{y},\boldsymbol{y}') = \int_{\Omega_{\mathrm{T}}} g(\boldsymbol{x},\boldsymbol{y})\overline{g(\boldsymbol{x},\boldsymbol{y}')}\, d\Omega_{\mathrm{T}}(\boldsymbol{x}). \tag{6.60}$$

Therefore, for any two arbitrary apertures, there is a set of communications modes that are pairs of eigenfunctions (ϕ_j, ψ_j) which correspond to the best coupled functions between the two apertures with the same eigenvalue λ_j. The total strength of the coupling between apertures can now be expressed in terms of the eigenvalues, which are the coupling strengths for the optimal choice of eigenfunctions in Ω_{T} and Ω_{R},

$$G_{\Omega_{\mathrm{T}},\Omega_{\mathrm{R}}} = \sum_{n,m} |\gamma_m^n|^2 = \sum_j \lambda_j, \tag{6.61}$$

where λ_j are the eigenvalues of the operator $\mathcal{L}$, with optimal eigenfunctions ϕ_j and ψ_j. Therefore, the optimal choice of basis functions corresponds to a set of parallel

communication channels, i.e., activation of a given source function results in the excitation of the corresponding receiving function and to a null excitation of the rest of the receiving functions.

By defining a dimensionality threshold similar to that in section 6.4.1 (in fact, given the preceding arguments a sensible choice of dimensionality would be $\min\{N, M\}$, where N and M correspond to the dimensionality of the transmit and receive apertures, respectively), the infinite dimensional operator describing the communication between the two apertures can now be expressed by the finite dimensional matrix equation

$$\boldsymbol{\beta} = \boldsymbol{\Gamma}\boldsymbol{\alpha}, \tag{6.62}$$

where $\boldsymbol{\Gamma}$ is a diagonal matrix with the diagonal terms given by the significant eigenvalues of the spectrum of the bounded linear operator $\mathcal{L}$, and $\boldsymbol{\alpha}, \boldsymbol{\beta}$ are the vectors of transmit and receive aperture Fourier coefficients respectively.

As in section 6.4.1, analysis of communication between arbitrary apertures in an arbitrary scattering environment reduces to the spectral properties of a linear operator, and is in general a non-trivial problem. The communication modes between two rectangular prism volumes in free space is analyzed in [138] where the eigenfunctions separates into prolate spheroidal wavefunctions for each dimension. However, extension to volumes that do not give rise to separable eigenfunctions are much more difficult and will in general require the use of numerical techniques, since there is no general analytical solution for the corresponding eigenvalue problem. In [139] the free space analysis of [138] was extended to include scattering. Using a numerical algorithm, the connection strengths between the two prisms for a finite set of randomly located scatterers was investigated.

Intrinsic Capacity

A more general result of intrinsic capacity than that of (6.2b) can now be defined. The intrinsic capacity between two arbitrary apertures Ω_{T} and Ω_{R} is defined as the maximum mutual information of the vectors $\boldsymbol{\beta}$ and $\boldsymbol{\alpha}$ over all possible basis functions for the transmit aperture $\{\phi_n\}_{n\in\mathcal{N}}$ and receive aperture $\{\psi_m\}_{m\in\mathcal{M}}$;

$$C = \max_{\substack{\{\phi_n\}_{n\in\mathcal{N}} \\ \{\psi_m\}_{m\in\mathcal{M}}}} I(\boldsymbol{\beta}; \boldsymbol{\alpha} \mid g(\boldsymbol{x}, \boldsymbol{y})), \tag{6.63}$$

with transmit and receive sets of finite cardinality, e.g., $|\mathcal{N}| \leq \infty$ and $|\mathcal{M}| \leq \infty$, respectively. Maximization of (6.63) occurs for basis functions chosen as the associated eigenfunctions for the eigenvalues λ_j of the linear operator $\mathcal{L}$, giving the instantaneous capacity

$$C = \sum_{j=1}^{K} \log\left(1 + \frac{\eta}{K}\lambda_j^2\right), \tag{6.64}$$

where $K \leq \min\{N, M\}$ denotes the number of significant eigenvalues of the operator, and is closely related to the spatial richness factor defined in Chapter 4. Observe that K represents the number of eigen-modes between the two apertures and is defined by the size of the transmit and receive apertures along with the properties of the scattering environment.

In the case of isotropic scattering, from Section 6.4.1, $K = \min\{N, M\}$ and $\lambda_j^2 \approx 1, j = \{1, \ldots, K\}$ giving the maximum capacity between the two apertures as $K\log(1+\eta/K)$, which gives an absolute limit for spatial communication of $\eta/\ln 2$ for large apertures, i.e., $K \to \infty$.

6.5 Summary and Contributions

This chapter has shown that the antenna elements are not the limiting factor in the capacity of MIMO systems. Antenna arrays are simply one choice of implementation of a more general spatial processing underlying all wireless communication systems. This chapter has shown that there is a fundamental limit to communication between two continuous apertures in space, and MIMO is an implementation requiring sampling of the apertures such that the discrete system approaches the limits of the spatial channel.

Some specific contributions made in this chapter are:

1. A mode-to-mode capacity was introduced, which gives the maximum capacity between two circular or spherical apertures regardless of the numbers of antennas or array geometry. This capacity was shown to be dependent on the aperture size and the scattering environment.

2. It was shown that the MIMO implementation of sampling the apertures with antenna elements is a form of mode excitation, where each mode of the transmit aperture is coupled via the scattering environment to a receiver mode.

The use of uniform linear and uniform circular arrays of antennas to excite the modes was shown to give significantly lower capacities than that achievable by the apertures (mode-to-mode capacity), due to poor mode excitation by those arrays.

3. The results of the circular and spherical apertures was extended to continuous arbitrary shaped apertures. A novel framework for studying the capacity between continuous spatial apertures is developed using the general concepts of separable Hilbert Spaces.

4. The capacity for communication between arbitrary apertures is shown to be determined by the eigenvalues and eigenfunctions of a compact linear operator. Using dimensionality results analogous to that for the circular and spherical regions in Chapter 4, the linear operator can be shown to have a finite matrix representation in the presence of noise, therefore tools from well known spectral analysis can be applied to calculate the best choice of excitation and receiver functions within the apertures to maximize capacity.

Chapter 7

Conclusions and Future Research

This chapter states the conclusions drawn from this thesis. The summary of contributions can be found at the end of each chapter and are not repeated here. Following this, some possible future research directions are proposed.

7.1 Conclusions

This thesis has been concerned with the information theoretic capacity of a single-user, narrowband wireless communications link utilizing multiple-antennas at the transmitter and receiver. Motivated by the linear growth in capacity with increasing numbers of antennas shown to be possible for i.i.d. Rayleigh fading channels, this thesis investigated the capacity for more physically realistic environments, where both the antenna arrays and scattering are constrained.

By introducing the previously ignored spatial aspects, namely the antenna array geometry and the scattering distribution, into the channel model new bounds and fundamental limitations to MIMO capacity were derived for spatially constrained, or spatially selective, channels. The most significant result was the concept that the volumes containing the antenna arrays had an intrinsic capacity, which is an upper limit to communication between the volumes that could not be increased with increasing numbers of antennas within. The intrinsic capacity was shown to be determined by the aperture shape, size and orientation, along with the richness of the scattering environment, and is independent of the number of antennas and their geometry.

With respect to practical systems, MIMO was shown to be an implementation of a more fundamental communication over a continuous spatial channel, where the discrete antennas sample the continuous apertures such that the discrete system

approaches the limits of the spatial channel.

This thesis has shown there is a fundamental limit to the communication between two continuous volumes in space, where using antenna arrays is simply one choice of implementation of a more general spatial signal processing underlying all wireless communication systems.

7.2 Future Directions of Research

Although this thesis has given valuable insights into the limitations of wireless communication systems, there are many more research directions one could follow to further broaden the understanding and implementation of such systems. Outlined below is a small subset of a much larger group of possible research projects pertinent to this thesis.

Spatial signal processing theory: As outlined in Chapter 6 communication in continuous spatial channels requires the development of a spatial signal processing theory, analogous to the time- and band-limited channel formulations. Some foundations have been laid in Chapter 6 using the Hilbert Space setting and linear operator theory, however, there is a significant amount of work required to fully develop the theory.

Channel modelling and validation: Although the channel model presented in this thesis gives theoretical insights into the factors determining capacity, the emphasis has been on statistical based models. To fully understand and exploit all the properties wireless channels offer, there is a need to further extend the modelling of scattering environments along with experimental validation to reconcile with results presented here.

Wideband and multiuser systems: This thesis has focused on single-user narrowband channels, an obvious extension is to include wideband channels as well as multiuser schemes. Some results have appeared in the literature. However, these generally assume the i.i.d. Rayleigh fading channel and need to be re-evaluated given the conclusions of this thesis.

Implementation: As discussed above, implementation using multiple-antennas is one of several options to communication between spatial volumes. However, in the foreseeable future it is the most likely scheme to be incorporated widely in wireless systems. Therefore, to achieve the capacities predicted in

this thesis coding schemes which approach the limits imposed by the spatial channels are required. Space-time codes have been developed for MIMO systems, however to date these have optimized capacity for the i.i.d. Rayleigh fading channel and have therefore ignored the spatial component inherent in realistic channels. Therefore, a true *space*-time coding scheme is required, where the codes are optimized over space and time, that is, given a fixed aperture in which to place the antenna elements, what is the optimal antenna placement and coding scheme with respect to the capacity or diversity performance.

Bibliography

[1] T. Cover and J. Thomas, *Elements of Information Theory*, Wiley, New York, 1991.

[2] A. Goldsmith, "Smart antennas," *IEEE Personal Communications*, vol. 5, no. 1, pp. 9, 1998.

[3] A. Paulraj and C. B. Papadias, "Space-time processing for wireless communications," *IEEE Signal Processing Magazine*, vol. 14, pp. 49–83, 1997.

[4] D.C. Cox, "Universal digital portable radio communications," *Proceedings of the IEEE*, vol. 75, no. 4, pp. 436–477, 1987.

[5] G. J. Foschini and M. J. Gans, "On limits of wireless communications in a fading environment when using multiple antennas," *Wireless Personal Communications*, vol. 6, no. 3, pp. 311–335, 1998.

[6] G. Raleigh and J. Cioffi, "Spatial-temporal coding for wireless communications," *IEEE Transactions on Communications*, vol. 46, no. 3, pp. 357–366, 1998.

[7] E. Telatar, "Capacity of multi-antenna gaussian channels," Tech. Rep., ATT Bell Labs, 1995.

[8] A. Paulraj and T. Kailath, "Increasing capacity in wireless broadcast systems using distributed transmission/directional reception," 1994, U.S. Patent no. 5,345,599.

[9] J.H. Winters, "On the capacity of radio communication systems with diversity in a rayleigh fading environment," *IEEE Journal on Selected Areas in Communications*, vol. 5, no. 5, pp. 871–878, 1987.

[10] C.N. Chuah, D.N.C. Tse, J.M. Kahn, and R.A. Valenzuela, "Capacity scaling in MIMO wireless systems under correlated fading," *IEEE Transactions on Information Theory*, vol. 48, no. 3, pp. 637–650, 2002.

[11] D. Gesbert, M. Shafi, D.S. Shiu, P. Smith, and A. Naguib, "From theory to practice: An overview of MIMO space-time coded wireless systems," *IEEE Journal on Selected Areas in Communications, Special Issue on MIMO Systems*, vol. 21, no. 3, pp. 281–302, 2003.

[12] A.J. Goldsmith, S.A. Jafar, N. Jindal, and S. Vishwanath, "Capacity limits of MIMO channels," *IEEE Journal on Selected Areas in Communications, Special Issue on MIMO Systems*, vol. 21, no. 5, pp. 684–702, 2003.

[13] J.F. Lemieux, M. Tanany, and H.M. Hafez, "Experimental evaluation of space/frequency/polarization diversity in the indoor wireless channel," *IEEE Transactions on Vehicular Technology*, vol. 40, no. 3, pp. 569–574, 1991.

[14] B. LeFloch, M. Alard, and C. Berrou, "Coded orthogonal frequency division multiplex," *IEEE Proceedings*, vol. 83, pp. 982–996, 1995.

[15] W.C.Y. Lee and S.Y. Yeh, "Polarization diversity system for mobile radio," *IEEE Transactions on Communications*, vol. 20, pp. 912–922, 1972.

[16] W.C. Jakes, *Microwave Mobile Communications*, John Wiley, New York, 1974.

[17] R. Steele, *Mobile Radio Communications*, IEEE Press, New York, 1992.

[18] A. Wittneben, "Base station modulation diversity for digital SIMULCAST," in *IEEE Vehicular Technology Conference*, 1993, pp. 505–511.

[19] N. Seshadri and J.H. Winters, "Two signalling schemes for improving the error performance frequency-division-duplex (FDD) transmission systems using transmitter antenna diversity," *International Journal on Wireless Information Networks*, vol. 1, no. 1, pp. 49–60, 1994.

[20] J. Guey, M.P. Fitz, M. Bell, and W. Kuo, "Signal design for transmitter diversity wireless communication systems over Rayleigh fading channels," in *IEEE Vehicular Technology Conference*, Atlanta, Georgia, USA., 1996, pp. 136–140.

[21] V. Tarokh, N. Seshadri, and A.R. Calderbank, "Space-time codes for high data rate wireless communication: Performance criterion and code construction," *IEEE Transactions on Information Theory*, vol. 44, pp. 744–765, 1998.

[22] V. Tarokh, H. Jafarhani, and A.R. Calderbank, "Space-time block codes from orthogonal designs," *IEEE Transactions on Information Theory*, vol. 45, pp. 1456–1467, 1999.

[23] G.J. Foschini, "Layered space-time architecture for wireless communication in a fading environment when using multi-element antennas," *Bell Labs Technical Journal*, vol. 1, no. 2, pp. 41–59, 1996.

[24] J.G. Proakis, *Digital Communications*, McGraw-Hill, 3rd edition, 1995.

[25] A.F. Molish, M. Stienbauer, M. Toeltsch, E. Bonek, and R.S. Thoma, "Capacity of MIMO systems based on measured wireless channels," *IEEE Journal on Selected Areas of Communications*, vol. 20, no. 3, pp. 561–569, 2002.

[26] H. Bölcskei, D. Gesbert, and A. Paulraj, "On the capacity of ODFM-based spatial multiplexing systems," *IEEE Transactions on Communications*, vol. 50, no. 2, pp. 225–234, 2002.

[27] C.E. Shannon, "A mathematical theory of communication," *The Bell Systems Technical Journal*, vol. 27, no. July, pp. 379–423, 1948.

[28] P.B. Rapajic and D. Popescu, "Information capacity of a random signature multiple-input multiple-output channel," *IEEE Transactions on Communications*, vol. 48, no. 8, pp. 1245–1248, 2000.

[29] A. Lozano, F.R. Farrokhi, and R.A. Valenzuela, "Lifting the limits on high speed wireless data access using antenna arrays," *IEEE Communications Magazine*, vol. 39, no. 9, pp. 156–162, 2001.

[30] P.F. Driessen and G.J. Foschini, "On the capacity formula for multiple-input multiple-output wireless channels: a geometric interpretation," *IEEE Transactions on Communications*, vol. 47, no. 2, pp. 173–176, 1999.

[31] F.R. Farrokhi, G.J. Foschini, A. Lozano, and R.A. Valenzuela, "Link-optimal space-time processing with multiple transmit and receive antennas," *IEEE Communications Letters*, vol. 5, no. 3, pp. 85–87, 2001.

[32] D.S. Shiu, *Wireless communication using dual antenna arrays*, Kluwer Internation Series in Engineering and Computer Science. Kluwer Academic, 1999.

[33] D.N. Viswanath, D.N.C. Tse, and V. Anantharam, "Asymptotically optimal water-filling in vector multiple-access channels," *IEEE Transactions on Information Theory*, vol. 47, no. 1, pp. 241–267, 2001.

[34] D.W. Bliss, K.W. Forsythe, A.O. Hero, and A.F. Yegulalp, "Environmental issues for MIMO capacity," *IEEE Transactions on Signal Processing*, vol. 50, no. 9, pp. 2128–2142, 2002.

[35] E. Visotsky and U. Madhow, "Space-time transmit precoding with imperfect feedback," *IEEE Transactions on Information Theory*, vol. 47, pp. 2632–2639, 2001.

[36] S.A. Jafar and A.J. Goldsmith, "On optimality of beamforming for multiple antenna systems with imperfect feedback," in *Internation Symposium on Information Theory*, 2001, p. 321.

[37] S.A. Jafar, S. Vishwanath, and A.J. Goldsmith, "Channel capacity and beamforming for multiple transmit and receive antennas with covariance feedback," in *IEEE Internation Conference on Communications*, 2001, vol. 7, pp. 2266–2270.

[38] E. Jorswieck and H. Boche, "Optimal transmission with imperfect channel state information at the transmit antenna array," *Submitted to Wireless Personal Communications, March 2002.*

[39] E. Jorswieck and H. Boche, "Channel capacity and capacity-range of beamforming in MIMO wireless systems under correlated fading with covariance feedback," *Submitted to IEEE Transactions on Wireless Communications, March 2002.*

[40] A. Narula, M.J. Lopez, M.D. Trott, and G.W. Wornell, "Efficient use of side information in multiple antenna data transmission over fading channels," *IEEE Journal on Selected Areas in Communications*, vol. 16, no. 8, 1998.

[41] S. Jafar and A.J. Goldsmith, "Transmitter optimization and optimality of beamforming for multiple antenna systems with imperfect feedback," *submitted to IEEE Transactions on Wireless Communications.*

[42] T.L. Marzetta and B.M. Hochwald, "Capacity of a mobile multiple-antenna communication link in rayleigh flat fading," *IEEE Transactions on Information Theory*, vol. 45, no. 1, pp. 139–157, 1999.

[43] L. Zheng and D.N.C. Tse, "Packing spheres in the grassmann manifold: A geometric approach to the non-coherent multiple antenna channel," in *Allerton Conference on Communication, Control, and Computing*, Monticello, Illinois, 1999.

[44] T.L. Marzetta and B.M. Hochwald, "Unitary space-time modulation for multiple-antenna communications in rayleigh fading," *IEEE Transactions on Information Theory*, vol. 46, no. 2, pp. 543–564, 2000.

[45] A. Lapidoth and S.M. Moser, "Capacity bounds via duality with applications to multi-antenna systems on flat fading channels," *to appear in IEEE Transactions on Information Theory.*

[46] S.A. Jafar and A.J. Goldsmith, "Multiple-antenna capacity in correlated rayleigh fading with no side information," *Preprint (available at http://wsl.stanford.edu/publications.html).*

[47] M.T. Ivrlac, T.P. Kurpjuhn, C. Brunner, and W. Utschick, "Efficient use of fading correlations in MIMO systems," in *IEEE Vechicular Technology Conference*, Rhodes Island, Greece, 2001, vol. 4, pp. 2763 –2767.

[48] A.F. Naguib, N. Seshadri, and A.R. Calderbank, "Increasing data rate over wireless channels," *IEEE Signal Processing Magazine*, vol. 17, no. 3, pp. 76–92, 2000.

[49] C.B. Papadias and G.J. Foschini, "Capacity-approaching space-time codes for systems employing four transmitter antennas," *IEEE Transactions on Information Theory*, vol. 49, no. 3, pp. 726– 732, 2003.

[50] S.L. Ariyavisitakul, "Turbo space-time processing to improve wireless channel capacity," *IEEE Communications Magazine*, vol. 48, no. 8, pp. 1347–1359, 2000.

[51] B.L. Hughes, "Differential space-time modulation," *IEEE Transactions on Information Theory*, vol. 46, no. 7, pp. 2567–2578, 2000.

[52] B.M. Hochwald and T.L. Marzetta, "Unitary space-time modulation for multiple-antenna communications in Rayleigh flat fading," *IEEE Transactions on Information Theory*, vol. 46, no. 2, pp. 543–564, 2000.

[53] A.O. Hero and T.L. Marzetta, "Cutoff rate and signal design for the quasi-static rayleigh-fading space-time channel," *IEEE Transactions on Information Theory*, vol. 47, no. 6, pp. 2400–2416, 2001.

[54] V. Tarokh, A.F. Naguib, N. Seshadri, and A.R. Calderbank, "Space-time codes for high data rate wireless communication: Performance criteria in the presence of channel estimation errors and mobility and multiple paths," *IEEE Transactions on Information Theory*, vol. 47, no. 2, pp. 199–207, 1999.

[55] S. Alamouti, "A simple transmitter diversity scheme for wireless communications," *IEEE Journal in Selected Areas of Communications*, vol. 16, pp. 1451–1458, 1998.

[56] V. Tarokh, H. Jafarkhani, and A.R. Calderbank, "Space-time block codes for wireless communications: Performance results," *IEEE Journal on Selected Areas in Communications*, vol. 17, no. 3, pp. 451–460, 1999.

[57] G. Ganesan and P. Stoica, "Space-time diversity using orthogonal and amicable orthogonal designs," *Wireless Personal Communications*, vol. 18, pp. 165–178, 2001.

[58] H. Jafarkhani, "A quasi-orthogonal space-time block code," *IEEE Transactions on Communications*, vol. 49, pp. 1–4, 2001.

[59] O. Tirkkonen, A. Boariu, and A. Hottinen, "Minimal non-orthogonality rate 1 space-time block code for 3+ tx antennas," in *IEEE International Symposium on Spread Spectrum Technology*, Parsippany, 2000.

[60] L. Zheng and D.N.C. Tse, "Diversity and multiplexing: a fundamental tradeoff in multiple-antenna channels," *IEEE Transactions on Information Theory*, vol. 49, no. 5, pp. 1073–1096, 2003.

[61] B. Hassibi and B.M. Hochwald, "High-rate codes that are linear in space and time," *IEEE Transactions on Information Theory*, vol. 48, no. 7, pp. 1804–1824, 2002.

[62] M.O. Damen, A. Tewfik, and J.C. Belfiore, "A construction of a space-time code based on number theory," *IEEE Transactions on Information Theory*, vol. 48, no. 3, pp. 753–760, 2002.

[63] S. Sandhu and A. Paulraj, "Unified design of linear space-time block-codes," in *IEEE Globe Communications Conference*, San Antonio, TX., 2001.

[64] M.J. Gans, N. Amitay, S.Y. Yeh, H. Xu, T.C. Damen, R.A. Valenzuela, T. Sizer, R. Storz, D. Taylor, W.M. MacDonald, C. Tran, and A. Adamiecki, "Outdoor BLAST measurement system at 2.44 GHz: calibration and initial results," *IEEE Journal on Selected Areas in Communications*, vol. 20, no. 3, pp. 570–581, 2002.

[65] Da-Shan Shiu, G.J. Foschini, M.J. Gans, and J.M. Kahn, "Fading correlation and its effect on the capacity of multielement antenna systems," *IEEE Transactions on Communications*, vol. 48, no. 3, pp. 502–513, 2000.

[66] E. Telatar, "Capacity of multi-antenna Gaussian channels," *European Transactions on Telecommunications*, vol. 10, no. 6, pp. 585–596, 1999.

[67] A. Gorokhov, "Transmit diversity versus SDMA: analytic and numerical comparisons," in *IEEE International Conference on Communications*, New Orleans, LA, 2000, pp. 1020–1024.

[68] K.I. Pedersen, J.B. Anderson, J.P. Kermoal, and P.E. Mogensen, "A stochastic multiple-input multiple-output radio channel model for evaluation of space-time coding algorithms," in *IEEE Vehicular Technology Conference*, Boston, MA, 2000, pp. 893–897.

[69] C.N. Chuah, J.M. Kahn, and D.N.C. Tse, "Capacity of multi-antenna arrays systems in indoor wireless environment," in *IEEE Global Telecommunications Conference*, Sydney, Australia, 1998, pp. 1894–1899.

[70] D. Chizhik, F. Rashid-Farrokhi, J. Ling, and A. Lozano, "Effect of antenna separation on the capacity of BLAST in correlated channels," *IEEE Communications Letters*, vol. 4, no. 11, pp. 337–339, 2000.

[71] C. Chen-Nee, D.N.C. Tse, J.M. Kahn, and R.A. Valenzuela, "Capacity scaling in MIMO wireless systems under correlated fading," *IEEE Transactions on Information Theory*, vol. 48, no. 3, pp. 637–650, 2002.

[72] S. Loyka and A. Kouki, "New compound upper bound on MIMO channel capacity," *IEEE Communications Letters*, vol. 6, no. 3, pp. 96–98, 2002.

[73] A.M. Sengupta and P.P. Mitra, "Capacity of multivariate channels with multiplicative noise: I. random matrix techniques and large-n expansions fo full transfer matrices," Tech. Rep., ATT Bell Labs, 2000.

[74] D. Chizhik, G.J. Foschini, M.J. Gans, and J.M. Kahn, "Capacities of multi-antenna transmit and receive antennas: correlation and keyholes," *Electronic Letters*, vol. 36, no. 13, pp. 1099–1100, 2000.

[75] D. Gesbert, H. Bolcskei, D. Gore, and A. Paulraj., "MIMO wireless channels: Capacity and performance prediction," in *IEEE Global Communications Conference*, San Francisco, USA, 2000.

[76] A. Abdi and M. Kaveh, "A space-time correlation model for multielement antenna systems in mobile fading channels," *IEEE Journal on Selected Areas in Communications*, vol. 20, no. 3, pp. 550–560, 2002.

[77] W.C.Y. Lee, "Effects on correlation between two mobile radio base-station antennas," *IEEE Transactions on Vehicular Technology*, vol. 22, no. 4, pp. 130–140, 1973.

[78] J.P. Kermoal, L. Schumacher, K.I. Pedersen, P.E. Mogensen, and F. Frederiksen, "A stochastic MIMO radio channel model with experimental validation," *IEEE Journal on Selected Areas in Communications*, vol. 20, no. 6, pp. 1211–1226, 2002.

[79] D. Colton and R. Kress, *Inverse acoustic and elctromagnetic scattering theory*, Springer-Verlag, Berlin, 1992.

[80] G.B. Arfken, Ed., *Mathematical Methods for Physics*, Academic Press, Orlando, FL, 3rd edition, 1985.

[81] R.K. Cook, R.V. Waterhouse, R.D. Berendt, S. Edelman, and J.R. Thompson, "Measurement of correlation coefficients in reverberant sound fields," *Journal of the Acoustical Society of America*, vol. 27, no. 6, pp. 1072–1077, 1955.

[82] H.M. Jones, R.A. Kennedy, and T.D. Abhayapala, "On dimensonality of multipath fields: spatial extent and richness," in *IEEE International Conference on Acoustics, Speech and Signal Processing*, Orlando, Florida, 2002.

[83] W.R. Braun and U. Dersch, "A physical mobile radio channel model," *IEEE Transactions on Vehicular Technology*, vol. 40, pp. 472–482, 1991.

[84] M. Patzold, U. Killat, Y. Li, and F. Laue, "Modeling, analysis, and simulation of nonfrequency-selective mobile radio channels with asymmetrical doppler power spectral density shapes," *IEEE Transactions on Vehicular Technology*, vol. 46, no. 2, pp. 494–507, 1997.

[85] M. Patzold, L. Yingchun, and F. Laue, "A study of a land mobile satellite channel model with asymmetrical doppler power spectrum and lognormally distributed line-of-sight component," *IEEE Transactions on Vehicular Technology*, vol. 47, no. 1, pp. 297–310, 1998.

[86] J.S. Sadowsky and V. Katedziski, "On the correlation and scattering functions of the WSSUS channel for mobile communications," *IEEE Transactions on Vehicular Technology*, vol. 47, no. 1, pp. 270–282, 1998.

[87] J.P. Rossi, J.P. Barbot, and A.J. Levy, "Theory and measurement of the angle of arrival and time delay of UHF radiowaves using a ring array," *IEEE Transactions on Antennas and Propagation*, vol. 45, no. 5, pp. 876–884, 1997.

[88] J. Fuhl, J.P. Rossi, and E. Bonek, "High resolution 3-D direction-of-arrival determination for urban mobile radio," *IEEE Transactions on Antennas and Propagation*, vol. 45, pp. 672–682, 1997.

[89] Q. Spencer, M. Rice, B. Jeffs, and S.H. Jensen, "A statistical model for angle of arrival in indoor multipath propagation," in *IEEE Vehicular Technology Conference*, Phoenix, AZ, 1997, pp. 1415–1419.

[90] J.G. Wang, A.S. Mohan, and T.A. Aubrey, "Angles-of-arrival of multipath signals in indoor environments," in *IEEE Vehicular Technology Conference*, Atlanta, GA, 1996, pp. 155–159.

[91] T. Lo and J. Litva, "Angles of arrival of indoor multipath," *Electronic Letters*, vol. 28, pp. 1687–1689, 1992.

[92] W.C.Y. Lee, "Finding the approximate angular probability density function of wave arrival by using a directional antenna," *IEEE Transactions on Antennas and Propagation*, vol. 21, pp. 328–334, 1973.

[93] M. Kalkan and R.H. Clarke, "Prediction of the space-frequency correlation function for base station diversity reception," *IEEE Transactions on Vehicular Technology*, vol. 46, pp. 176–184, 1997.

[94] J. Salz and J.H. Winters, "Effect of fading correlation on adaptive arrays in digital mobile radio," *IEEE Transactions on Vehicular Technology*, vol. 43, no. 4, pp. 1049–1057, 1994.

[95] A. Abdi, J.A Barger, and M. Kaveh, "A parametric model for the distribution of the angle of arrival and the associated correlation function and power spectrum at the mobile station," *IEEE Transactions on Vehicular Technology*, vol. 51, no. 3, pp. 425–434, 2002.

[96] K.I. Pedersen, P.E. Mogensen, and B.H Fleury, "Power azimuth spectrum in outdoor environment," *IEE Electronic Letters*, vol. 33, no. 18, pp. 1583–1584, 1997.

[97] R.G. Vaughan, "Pattern translation and rotation in uncorrelated source distributions," *IEEE Transactions on Antennas and Propagation*, vol. 46, no. 7, pp. 982–990, 1998.

[98] P.D. Teal, T.D. Abhayapala, and R.A. Kennedy, "Spatial correlation for general distributions of scatterers," *IEEE Signal Processing Letters*, vol. 9, no. 10, pp. 305–308, 2002.

[99] J.A. Tsai, R.M. Buehrer, and B.D. Woerner, "Spatial fading correlation function of circular antenna arrays with laplacian energy distribution," *IEEE Communications Letters*, vol. 6, no. 5, pp. 178–180, 2002.

[100] K.V. Mardia, *Statistics of Directional Data*, Academic Publishers, London, U.K., 1972.

[101] S. Wei, D. Goeckel, and R. Janaswamy, "On the capacity of fixed length antenna arrays under bandlimited correlated fading," in *Conference on Information Sciences and Systems*, Princeton, 2002, pp. 1088–1093.

[102] D. Gesbert, T. Ekman, and N. Christophersen, "Capacity limits of dense palm-sized MIMO arrays," in *IEEE Global Communications Conference*, Taipei, Taiwan, 2002.

[103] T.S. Pollock, T.D. Abhayapala, and R.A. Kennedy, "Antenna saturation effects on dense array MIMO capacity," in *IEEE International Conference on Acoustics, Speech and Signal Processing*, Hong Kong, 2003, pp. 361–364.

[104] T.D. Abhayapala, T.S. Pollock, and R.A. Kennedy, "Spatial decomposition of MIMO wireless channels," in *Seventh International Symposium on Signal Processing and its Applications*, Paris, France, 2003.

[105] D. Gesbert, H. Bolcskei, D. Gore, and A. Paulraj, "Outdoor MIMO wireless channels: Models and performance prediction," *IEEE Transactions on Communications*, vol. 50, no. 12, pp. 1926–1934, 2002.

[106] N. Chiurtu, B. Rimoldi, and I.E. Telatar, "Dense multiple antenna systems," in *IEEE Information Theory Workshop*, Cairns, Australia, 2001.

[107] P.J. Davis, *Circulant Matrices*, Wiley, New York, 1979.

[108] G.N. Watson, *Theory of Bessel Functions*, Cambridge University Press, 2nd edition, 1958.

[109] M. Abramowitz and I.A. Stegun, *Handbook of Mathematical Functions*, Dover Publications, Inc., New York, 1972.

[110] E. Kreyszig, *Advanced Engineering Mathematics*, John Wiley and Sons, New York, 7th edition, 1993.

[111] R.M. Gray, "On the asymptotic eigenvalue distribution of toeplitz matrices," *IEEE Transactions on Information Theory*, vol. 18, no. 6, pp. 725–730, 1972.

[112] P. Stoica and T. Söderström, "Eigenelement statistics of sample covariance matrix in the correlated data case," *Digital Signal Processing*, vol. 7, pp. 136–143, 1997.

[113] C.A. Balanis, *Antenna Theory: Analysis and Design*, John Wiley and Sons, New York, 2nd edition, 1997.

[114] J.P. Kermoal, P.E. Mogensen, S.H. Jensen, J.B. Anderson, F. Frederiksen, T.B. Sorensen, and K.I. Pedersen, "Experimental investigation of multipath richness for multi-element transmit and receive antenna arrays," in *IEEE Vehicular Technology Conference*, Tokyo, Japan, 2000, pp. 2004–2008.

[115] W. Yu, M. Bengtsson, B. Ottersten, D.P. McNamara, P. Karlsson, and M.A. Beach, "A wideband statisitical model for NLOS indoor wireless MIMO channels," in *IEEE Vehicular Technology Conference (Spring)*, Birmingham, Al, 2002.

[116] J.W. Wallace and M.A. Jensen, "Spatial characteristics of the MIMO wireless channel: experimental data acquisition and analysis," in *IEEE International Conference on Acoustics, Speech and Signal Processing*, Salt Lake City, Utah, 2001, pp. 2497–2500.

[117] G. Athanasiadou, A. Nix, and J. McGeehan, "A microcellular ray-tracing propagation model and evaluation of its narrow-band and wide-band predictions," *IEEE Journal on Selected Areas in Communications*, vol. 18, pp. 322–335, 2000.

[118] G. German, Q. Spencer, A. Swindlehurst, and R. Valenzuela, "Wireless indoor channel modeling: statistical agreement of ray tracing simulations and channel sounding measurements," in *IEEE International Conference on Acoustics, Speech, and Signal Processing*, Salt Lake City, UT, 2001, vol. 4, pp. 778–781.

[119] J.W. Wallace and M.A. Jensen, "Modeling the indoor MIMO wireless channel," *IEEE Transactions on Antennas and Propagation*, vol. 50, no. 2, pp. 591–599, 2002.

[120] A.M. Sayeed, "Deconstructing multi-antenna fading channels," *IEEE Transactions on Signal Processing*, vol. 50, no. 10, pp. 2563–2579, 2002.

[121] D. Gesbert, H. Bolcskei, D. Gore, and A. Paulraj, "Performance evaluation for scattering MIMO channel models," in *34th Asilomar conference on signals systems and computers*, Pacific Grove, CA, 2000.

[122] D. Chizhik, G. Foschini, M. Gans, and R. Valenzuela, "Keyholes, correlations, and capacities of multielement transmit and receive antennas," *IEEE Transaction on Wireless Communications*, vol. 1, no. 2, pp. 361–368, 2002.

[123] A. Derneryd, "Analysis of the microstrip disc element," *IEEE Transactions on Antennas and Propagation*, vol. 27, no. 5, pp. 660–664, 1979.

[124] J. Huang, "Circularly polarized conical patterns from circular microstrip antennas," *IEEE Transactions on Antennas and Propagation*, vol. 27, pp. 137–145, 1984.

[125] J.Q. Howell, "Microstrip antennas," *IEEE Transactions on Antennas and Propagation*, vol. 23, pp. 90–93, 1975.

[126] Y.T. Lo, D. Solomon, and W.F. Richards, "Theory and experiment in microstrip antennas," *IEEE Transactions in Antennas and Propagation*, vol. 27, pp. 137–145, 1979.

[127] R.G. Vaughan, "Two-port higher mode circular microstrip antennas," *IEEE Transactions on Antennas and Propagation*, vol. 36, no. 3, pp. 309–321, 1988.

[128] R.G. Vaughan, "Signals in mobile communications," *IEEE Transactions on Vehicular Technology*, vol. 35, pp. 133–145, 1986.

[129] F. Demmerle and W. Wiesbeck, "A biconical multibeam antenna for space-division multiple access," *IEEE Transactions on Antennas and Propagation*, vol. 46, no. 6, pp. 782–787, 1998.

[130] T. Svantesson, "Correlation and channel capacity of MIMO systems employing multimode antennas," *IEEE Transactions on Vehicular Technology*, vol. 51, no. 6, pp. 1304–1312, 2002.

[131] I.S. Gradshetyn and I.M. Ryzhik, *Tables of Integrals, Series, and Products*, Academic Press, San Diego, sixth edition, 2000.

[132] R.A. Kennedy and T.D. Abhayapala, "Spatial concentration of wave-fields: towards spatial information content in arbitary multipath scattering," in *Australian Communications Theory Workshop*, Melbourne, Australia, 2003, pp. 38–45.

[133] R.A. Kennedy, T.D. Abhayapala, and T.S. Pollock, "Modeling multipath scattering environments using generalized Herglotz wave functions," in *Australian Communications Theory Workshop*, Canberra, Australia, 2003, pp. 87–92.

[134] R.A. Kennedy, T.D. Abhayapala, and T.S. Pollock, "Generalized Herglotz wave functions for modeling wireless nearfield multipath scattering environments," in *International Conference on Acoustics, Speech, and Signal Processing*, Hong Kong, 2003, vol. IV, pp. 660–663.

[135] D. Slepian and H.O. Pollack, "Prolate spheriodal wave functions, Fourier analysis and uncertainty - I," *Bell Systems Technical Journal*, vol. 40, pp. 43–63, 1961.

[136] H.J. Landua and H.O. Pollack, "Prolate spheriodal wave functions, Fourier analysis and uncertainty - II," *Bell System Technical Journal*, vol. 40, pp. 65–84, 1961.

[137] H.J. Landua and H.O. Pollack, "Prolate spheriodal wave functions, Fourier analysis and uncertainty - III: the dimension of space of essentially time- and band-limted signals," *Bell System Technical Journal*, vol. 41, pp. 1295–1336, 1962.

[138] D. A. B. Miller, "Communicating with waves between volumes: evaluating orthogonal spatial channels and limits on coupling strengths," *Applied Optics*, vol. 39, no. 11, pp. 1681–1699, 2000.

[139] L. Hanlen and M. Fu, "Wireless communications with spatial diversity: A volumetric approach," in *International Communications Conference*, Anchorage, Alaska, 2003, pp. 3001–3005.